PL-TR-96-2103

DEVELOPMENT OF EXPERIMENTAL PROTOCOLS FOR THE CALIBRATION OF SSM/T-2 MILLIMETER WAVE MOISTURE SOUNDER DATA

John D. Pickle
Ronald G. Isaacs
Charles P. Sarkisian
Jean-Luc Moncet
Vida Jakabhazy
Brian T. Pearson

Atmospheric and Environmental Research, Inc.
840 Memorial Drive
Cambridge, MA 02139-3794

24 May 1996

Final Report
25 March 1992 - 24 May 1996

Approved for public release; distribution unlimited

PHILLIPS LABORATORY
Directorate of Geophysics
AIR FORCE MATERIEL COMMAND
HANSCOM AIR FORCE BASE, MA 01731-3010

"This technical report has been reviewed and is approved for publication."

VINCENT J. FALCONE
Contract Manager

DONALD A. CHISHOLM
Chief, Remote Sensing Applications Branch
Optical Effects Division

WILLIAM A. M. BLUMBERG, Director
Optical Effects Division

This report has been reviewed by the ESC Public Affairs Office (PA) and is releasable to the National Technical Information Service (NTIS).

Qualified requestors may obtain additional copies from the Defense Technical Information Center (DTIC). All others should apply to the National Technical Information Service (NTIS).

If your address has changed, or if you wish to be removed from the mailing list, or if the addressee is no longer employed by your organization, please notify PL/IM, 29 Randolph Road, Hanscom AFB, MA 01731-3010. This will assist us in maintaining a current mailing list.

Do not return copies of this report unless contractual obligations or notices on a specific document requires that it be returned.

REPORT DOCUMENTATION PAGE

Form Approved
OMB No. 0704-0188

1. AGENCY USE ONLY (Leave blank)	2. REPORT DATE	3. REPORT TYPE AND DATES COVERED
	May 24, 1996	Final Report 25 March 1992 - 24 May 1996

4. TITLE AND SUBTITLE
Development of Experimental Protocols for the Calibration of SSM/T-2 Millimeter Wave Moisture Sounder Data

5. FUNDING NUMBERS
PE 35106F
PR 6670 TA G2 WU AA

F19628-92-C-0054

6. AUTHOR(S)
John D. Pickle
Charles P. Sarkisian
Vida Jakabhazy
Ronald G. Isaacs
Jean-Luc Moncet
Brian T. Pearson

7. PERFORMING ORGANIZATION NAME(S) AND ADDRESS(ES)
Atmospheric and Environmental Research, Inc.
840 Memorial Drive
Cambridge, MA 02139-3794

8. PERFORMING ORGANIZATION REPORT NUMBER

9. SPONSORING/MONITORING AGENCY NAME(S) AND ADDRESS(ES)
Phillips Laboratory
29 Randolph Road
Hanscom AFB, MA 01731-3010
Contract Manager: Vincent Falcone/GPAB

10. SPONSORING/MONITORING AGENCY REPORT NUMBER
PL-TR-96-2103

11. SUPPLEMENTARY NOTES

12a. DISTRIBUTION/AVAILABILITY STATEMENT
Approved for public release; distribution unlimited

12b. DISTRIBUTION CODE

13. ABSTRACT *(Maximum 200 words)*

This report summarizes four years of the Phillips Laboratory and AER, Inc.'s efforts in the calibration of the DMSP SSM/T-2 millimeter wave moisture sounder. Thirteen underflights of the T-2 were made by the NASA ER-2 research aircraft which carried the MIR, an instrument similar to the T-2. Comparisons of the 183 GHz measurements over water FOVs displayed RMS differences of 0.9 to 1.6 K, roughly within the accuracy limits of the calibrating MIR instrument. The overall conclusion was that the T-2 suffered no significant bias in its calibration.

An additional focus was to examine the T-2 sensitivity to the variability of the atmosphere: temperature and moisture profiles, surface temperature and emissivity, satellite viewing angle, clouds and precipitation. Also, with the failure of the 150 GHz channel on F-11 in June 1993, an additional challenge was to synthesize 150 GHz T_bs by a multiple regression method.

This work highlighted the necessity of aircraft in the calibration of satellite sensors. In addition, the wealth of information collected during a calibration effort provided invaluable understanding of the sensor behavior and limitations, both essential to users of the satellite information.

14. SUBJECT TERMS	15. NUMBER OF PAGES
SSM/T-2 DMSP Calibration Microwave Millimeter Sensitivity Satellite Water Vapor Profiles Sounder	184
	16. PRICE CODE

17. SECURITY CLASSIFICATION OF REPORT	18. SECURITY CLASSIFICATION OF THIS PAGE	19. SECURITY CLASSIFICATION OF ABSTRACT	20. LIMITATION OF ABSTRACT
Unclassified	Unclassified	Unclassified	SAR

Table of Contents

		Page
Forward		xv
1.	Introduction	1
2.	Aircraft Calibration	2
2.1	West Coast 1992 Campaign	2
2.2	East Coast 1992 Campaign	2
2.3	TOGA-COARE 1993 Campaign	5
2.4	CAMEX 1993 Campaign	5
2.5	F-12 West Coast 1994 Campaign	5
2.6	East Coast 1995 Campaign	5
2.7	Calibration Results	12
2.8	Variation T_bs	16
2.8.1	Variation of Co-located MIR T_bs	16
2.8.2	T_b Anomalies across Scans	16
2.8.2.1	AFGWC Collected T_bs	16
2.8.2.2	PL/GPA Direct-Readout T_bs	21
2.8.2.3	MIR T_bs	21
2.9	Climatology of Data Bases	30
2.10	Effects of Clouds and Precipitation on the Calibration	34
2.11	Representativeness of the Calibration Results	38
2.12	Comparison of Co-located SSM/T-2 and SSM/I Results	41
3.	Radiosonde Calibration Results	43
4.	Radiative Transfer Modeling of T_b Sensitivity	47
4.1	T_b Sensitivity to Atmospheric Water Vapor	47
4.1.1	Relating SSM/T-2 T_b Limits to Moisture Retrieval Accuracy	51
4.2	T_b Sensitivity to Atmospheric Temperature	57
4.3	T_b Sensitivity to Satellite Viewing Angle	57
4.3.1	High Incidence Angle Results	71
4.4	T_b Sensitivity to Ground Temperature	82
4.5	T_b Sensitivity to Surface Emissivity	82
4.6	Surface Emissivity Retrievals	82
4.6.1	General Procedure for Calculating Surface Emissivity	82
4.6.2	General Distribution of Retrieved Surface Emissivities	97
4.6.3	Reproducibility of Retrieved Surface Emissivities	97
4.6.4	Effect of Clouds and Precipitation	99
4.6.5	Effect of Satellite Viewing Angle	103

Table of Contents (continued)

Page

4. Radiative Transfer Modeling of T_b Sensitivity (continued)

4.6.6 Effect of Total Precipitable Water 104
4.6.7 Effect of Moisture Profile Uncertainty 104
4.6.8 Effect of Temperature Profile Uncertainty 104
4.6.9 Effect of Ground Temperature Uncertainty 104
4.6.10 Effect of SDR T_b Uncertainty 104
4.6.11 Surface Emissivity Retrieval Conclusions 109
4.7 Climatology of Atmospheric and Surface Contributions and Weighting Functions 110

5. Synthesis of 150 GHz Brightness Temperatures 110

5.1 Synthesis of 150 GHz T_bs Results 114

6. SSM/T-2 T_b Signatures 114

6.1 SSM/T-2 T_b Signatures: Effects of Clouds over Water 115
6.2 SSM/T-2 T_b Signatures: Effects of Rain over Water 118
6.3 SSM/T-2 T_b Signatures: Effects of Clouds over Land 118
6.4 SSM/T-2 T_b Signatures: Effects of Rain over Land 118
6.5 SSM/T-2 T_b Signatures: Effects of Surface Ice 118

7. Effects of Clouds and Precipitation 118

8. Upper Tropospheric Humidity Fields 125

9. AMPR Data Analysis 131

10. High Incidence Angle Viewing 150

11. Summary 150

12. Conclusions 158

13. References 158

Appendix A Meetings Attended 161

Appendix B Papers Presented 166

List of Figures

Figure		Page
1	NASA ER-2 flight tracks for the west coast campaign in May, 1992. The F-11 subtrack for the two days that the aircraft was flown are shown.	3
2	NASA ER-2 flight tracks for the east coast campaign in July and August, 1992. The F-11 subtrack for the three days that the aircraft was flown are shown.	4
3	Positions of the morning descending subtrack of the DMSP F-11 satellite over the western tropical Pacific Ocean on February 4 and 10, 1993.	6
4	Flight path of NASA's ER-2 aircraft which carried the MIR sensor along the east coast of the United States on September 30, 1993.	7
5	Flight path of NASA's ER-2 aircraft which carried the MIR sensor along the east coast of the United States on October 5, 1993.	8
6	Flight path of NASA's ER-2 aircraft which carried the MIR sensor along the west coast of the United States on December 9, 1994.	9
7	Flight path of NASA's ER-2 aircraft which carried the MIR sensor along the west coast of the United States on December 10, 1994.	10
8	Flight path of NASA's ER-2 aircraft which carried the MIR sensor along the west coast of the United States on December 9, 1994.	11
9	The 183±3 T_bs of the same scan indices of the first 300 MIR swaths when the aircraft was at 19 km altitude are connected for the F-12 December 1989 flights and the later F-12 calibration flight (August 1995).	15
10	Graph of the average T_bs for the T-2 channels as a function of scan position. Averages were taken over 32 full earth orbits acquired by AFGWC for the CALVAL experiment over the time period from March to August, 1992.	18
11	Graph of the average T_bs for the 183±7 and 183±3 GHz channels as a function of scan position.	19
12	Plots of the average T_bs for four T-2 channels a function of scan position. Averages were taken over 23 passes collected by the PL/GPA DMSP direct readout satellite ingest station.	22

List of Figures (continued)

Figure		Page
13	Graphs of the average T_bs for the 91, 183±7 and 183±3 GHz channels as a function of scan position.	23
14	Plots of the average T_bs for MIR channels as a function of scan position for each CALVAL aircraft campaign.	26
15	Graphs of the average T_bs for the 183±3 GHz channel on the MIR for all four CALVAL aircraft campaigns as a function of scan position.	31
16	Plots of the average T_bs for the 183±3 and 183±7 GHz channels on the MIR for the East Coast CALVAL aircraft campaign as a function of scan position.	32
17	The effect of fractional precipitation on the range of the MIR T_bs for the T-2 channels.	36
18	The effect of fractional precipitation on the difference between co-located mean MIR and T-2 T_bs for the T-2 channels.	37
19	The effect of fractional non-precipitating cloud cover on the range of the MIR T_bs for the T-2 channels.	39
20	The effect of fractional non-precipitating cloud cover on the difference between co-located mean MIR and T-2 T_bs for the T-2 channels.	40
21	T-2 - radiosonde co-location processing flowchart.	45
22	The change in T_b for the T-2 channels as the moisture profile was modified in the RT band model. The original profile had a TPW of 7.8 kg/m^2.	48
23	The amount of moisture profile modification required to change the forward-calculated 183±3 GHz T_b by ±1 K.	49
24	The change in T_b for the T-2 channels as the moisture profile was modified in the RT band model. The original profile had a TPW of 56.3 kg/m^2.	50
25	The change in T_b and its three dominant components for the T-2 channels as the moisture profile was modified by ±10%.	52
26	The change in T_b for the T-2 channels as the temperature profile was modified in the RT band model. The profile had a TPW of 7.8 kg/m^2.	58

List of Figures (continued)

Figure		Page
27	The change in T_b for the T-2 channels as the temperature profile was modified in the RT band model. The profile had a TPW of 56.3 kg/m^2.	59
28	The change in T_b and its three dominant components for the T-2 channels as the temperature profile was modified by ±1 K.	60
29	Relationship between atmospheric path length (normalized to one atmosphere thickness) and satellite viewing angle and local incidence angle.	65
30	Change in T_b for the T-2 channels as the satellite viewing angle was modified from 0° to 40.5° in the RT band model. The profile had a TPW of 7.8 kg/m^2.	66
31	Change in T_b for the T-2 channels as the satellite viewing angle was modified from 0° to 40.5° in the RT band model. The profile had a TPW of 56.3 kg/m^2.	67
32	Change in the pressure levels of the peak of the weighting functions for the T-2 channel frequencies as the satellite viewing angle increased from 0° to 40.5°.	69
33	Change in the pressure levels of the median of the weighting functions for the T-2 channel frequencies as the satellite viewing angle increased from 0° to 40.5°.	70
34	Changes in T_b and its three dominant components for the T-2 channels as the scan angle was modified from 0° to 40.5°.	72
35	MIR T_bs plotted versus scan angles across the 50 km swath during the TOGA-COARE flight of February 4, 1993. Only data were used when the aircraft banked at least 20° and when the average T_b across the swath was greater than 255 K.	77
36	MIR T_bs plotted versus scan angles across the 50 km swath during the TOGA-COARE flight of February 10, 1993. Only data were used when the aircraft banked at least 20° and when the average T_b across the swath was greater than 255 K.	78

List of Figures (continued)

Figure		Page
37	MIR T_bs plotted versus scan angles across the 50 km swath during the three east coast MIR flights of the summer, 1992. Only data were used when the aircraft banked at least 20° and when the average T_b across the swath was greater than 255 K.	79
38	MIR T_bs plotted versus scan angles across the 50 km swath during the two west coast MIR flights of the summer, 1992. Only data were used when the aircraft banked at least 20° and when the average T_b across the swath was greater than 255 K.	80
39	Locations of limb-warming and limb-cooling during level flight along the west coast during the two CALVAL flights of 1992.	81
40	The change in T_b for the T-2 channels as the ground temperature was modified from 295 to 285 K in the RT band model. The profile had a TPW of 7.8 kg/m^2.	83
41	The change in T_b for the T-2 channels as the ground temperature was modified from 295 to 285 K in the RT band model. The profile had a TPW of 56.3 kg/m^2.	84
42	The change in T_b and its three dominant components for the T-2 channels as the ground temperature was modified from 295 to 285 K.	85
43	The change in T_b for the T-2 channels as the surface emissivity was modified from 0.95 to 0.85 in the RT band model. The profile had a TPW of 7.8 kg/m^2.	90
44	The change in T_b for the T-2 channels as the surface emissivity was modified from 0.95 to 0.85 in the RT band model. The profile had a TPW of 56.3 kg/m^2.	91
45	The change in T_b and its three dominant components for the T-2 channels as the surface emissivity was modified from 0.95 to 0.85.	92
46	Distribution of retrieved surface emissivities for the 91, 150 and 183±7 GHz channels. Only unsaturated soundings over land were used.	98

List of Figures (continued)

Figure		Page
47	Differences between the mean surface emissivity retrieved from a radiosonde station with at least 3 cases of unsaturated profiles and surface emissivities retrieved soundings with varying thickness of saturation present. Only profiles measured at low-lying (0-200 m elevation) land stations during late spring and summer, 1992 were used.	102
48	Change in retrieved surface emissivities for the 91 and 150 GHz channel as the RH was varied from 90% to 110% of the original profile values.	105
49	Change in retrieved surface emissivities for the 91 and 150 GHz channels as the temperature profile was increased from -1 K of the original value to +1 K.	106
50	Change in retrieved surface emissivities for the 91 and 150 GHz channels as the ground temperature was increased from -5 K of the closest near-surface atmospheric temperature to +5 K.	107
51	Change in retrieved surface emissivities for the 91 and 150 GHz channel as the satellite Tb was increased from -1 K of the original value to +1 K.	108
52	T-2 T_b cloud signatures over water surfaces. Data were limited to TPW ranging from 10 to 20 kg/m^2 with varying amounts of non-precipitating clouds in the FOV.	116
53	T-2 T_b cloud signatures over water surfaces. Data were not limited by TPW and were categorized by the amount of non-precipitating clouds in the FOV.	117
54	T-2 T_b rain signatures over land surfaces. Data included all rain intensity levels.	119
55	T-2 T_b rain signatures over water surfaces. Data were limited to light rain rates (0 to 2 mm/hr) with varying amounts of precipitation in the FOV.	120
56	T-2 T_b rain signatures over water surfaces. Data were limited to FOVs that are 100% precipitation and were categorized by the average rain intensity within the FOV.	121
57	T-2 T_b cloud signatures over land. Data were limited to TPW ranging from 10 to 20 kg/m^2 with varying amounts of non-precipitating clouds in the FOV. Data were not screened for satellite viewing angle.	122

List of Figures (continued)

Figure		Page
58	T-2 T_b signatures for FOV over land. Data did not have saturated layers in the radiosonde profiles and were categorized by TPW. Data were not screened for satellite viewing angle.	123
59	Plots of precipitation identification technique based on thresholds of T-2 T_bs and gradients of T_bs (Threshold), stepwise logistic regression scheme (Regression), SSM/I rain algorithm, MDR data and combined coverage of SSM/I-identified rain and MDR data for 1037 UTC on July 29, 1992.	126
60	Plots of precipitation identification technique based on thresholds of T-2 T_bs and gradients of T_bs (Threshold), stepwise logistic regression scheme (Regression), SSM/I rain algorithm, MDR data and combined coverage of SSM/I-identified rain and MDR data for 1219 UTC on July 29, 1992.	127
61	Flow diagram of the technique to calculate UTH from the 183±1 GHz T_b.	128
62	Plots of T-2 183±1 GHz T_b, OLS visible imagery, MDR data and UTH values for 1428 UTC on November 29, 1994.	129
63	Plots of T-2 183±1 GHz T_b, OLS visible imagery, MDR data and UTH values for 0156 UTC on November 30, 1994.	130
64	Two of the Stokes parameters ([V+H]/2 and [V-H]/2) for the AMPR data taken during the CAMEX and TOGA-COARE flights. Three of the AMPR channels are displayed: 19, 37 and 85 GHz.	132
65	Two of the Stokes parameters ([V+H]/2 and [V-H]/2) for the SSM/I data observed within the region of the aircraft flights during the CAMEX and TOGA-COARE experiments. Three pairs of the SSM/I channels are displayed: 19, 37 and 85 GHz.	135
66	Two of the Stokes parameters ([V+H]/2 and [V-H]/2) for the AMPR data measured over water taken during the CAMEX and TOGA-COARE flights. Three of the AMPR channels are displayed: 19, 37 and 85 GHz.	138

List of Figures (continued)

Figure		Page
67	Two of the Stokes parameters ([V+H]/2 and [V-H]/2) for the AMPR data measured over land taken during the CAMEX and TOGA-COARE flights. Three of the AMPR channels are displayed: 19, 37 and 85 GHz.	141
68	Two of the Stokes parameters ([V+H]/2 and [V-H]/2) for the SSM/I data over water observed within the region of the aircraft flights during the CAMEX and TOGA-COARE experiments. Three pairs of the SSM/I channels are displayed: 19, 37 and 85 GHz.	144
69	Two of the Stokes parameters ([V+H]/2 and [V-H]/2) for the SSM/I data over land observed within the region of the aircraft flights during the CAMEX and TOGA-COARE experiments. Three pairs of the SSM/I channels are displayed: 19, 37 and 85 GHz.	147
70	AMPR T_bs plotted versus scan angles across the 50 km swath during the CAMEX September 30, 1993 east coast where the aircraft performed a figure eight maneuver.	151

List of Tables

Table		Page
1	RMS difference and bias between the mean of the co-located MIR and T-2 T_bs at the T-2 channels for the 5 aircraft underflights during 1992. The scan angle of the MIR data matched that of the co-located T-2 FOV. The time between the T-2 and the MIR measurements was ±1 hour.	12
2	Average RMS between T-2 and mean MIR T_bs measured on February 4 and 10, 1993.	13
3	RMS between T-2 and mean MIR T_bs measured on September 30 and October 5, 1993.	14
4	RMS between F-12 T-2 and mean MIR T_bs measured on December 9 and 10, 1994.	14
5	RMS between F-11 and F-12 T-2 and mean MIR T_bs measured on August 25, 1995 along the east coast of the United States.	16
6	Mean, standard deviation and maximum and minimum values of the range of MIR T_bs within SSM/T-2 FOVs that had less than 20% non-precipitating clouds in the view. Each case had at least 10 MIR T_bs within the FOV, and each MIR T_b had the same viewing angle as the satellite.	17
7	Mean, standard deviation and range of T-2 T_bs sampled by the co-located MIR data set, the co-located radiosonde data set, and a set of 5 orbits of the satellite.	30
8	Latitudinal mean and standard deviation of the mixing ratio and relative humidity at 6 mandatory pressure levels based on the global set of co-located radiosondes used in the T-2 calibration study.	33
9	Latitudinal average of the peak pressures of the weighting functions for the T-2 channels. Units are hPa.	33
10	Instrument beam characteristics for the microwave sensors on board the F-11 satellite.	35
11	RMS difference and bias between the mean of the co-located MIR T_bs and the observed T-2 T_bs from the TOGA-COARE flights.	35

List of Tables (continued)

Table		Page
12	RMS differences for the co-located mean MIR and T-2 T_b measurements given for topographic type, T-2 channel and flight.	38
13	Mean, standard deviation and range of T-2 T_bs sampled by the co-located MIR data set, the co-located radiosonde data set, and a set of 7 orbits of the satellite.	41
14	RMS difference, bias and standard deviation between TPW values determined using SSM/I and T-2 data.	42
15	RMS difference, bias and standard deviation between TPW values calculated using co-located radiosonde profiles and SSM/I and T-2 T_bs.	42
16	Global average of the peak pressures of the weighting functions for the T-2 channels.	43
17	The latitudinal mean ± standard deviation of the mixing ratio and relative humidity at 6 mandatory pressure levels based on the global set of radiosondes used in the T-2 calibration study.	44
18	RMS difference and bias between the calculated T_bs generated by the Eyre RT simulation model using a global set of radiosondes and co-located T-2 T_bs at the T-2 channels. Bias was based on T-2 T_bs - co-located Eyre-calculated T_bs. Co-location criteria were ±1 hour and ±100 km.	46
19	Values used to examine the sensitivities of the parameters. When a parameter was varied, the other parameters were kept at these constant values.	47
20	Mean, median and standard deviation of the absolute values of moisture modification required to change the 183±3 GHz T_b by ±1 K.	57
21	Change in total T-2 T_b and the atmospheric emission, surface emission and surface reflectance contributions as the viewing angle increased from 0° to 40.5°.	68
22	Distribution of retrieved surface emissivities for the 91 and 150 GHz channels.	97

List of Tables (continued)

Table		Page
23	Statistical distribution of the standard deviation for series of retrieved surface emissivities for individual land locations. Each series was required to have at least 5 unsaturated to thinly saturated (saturation thickness less than 50 hPa) radiosonde profiles. Data was collected during the late spring and summer months of 1992.	99
24	Distribution of retrieved surface emissivities for the 91 and 150 GHz channels for saturated profiles over low-lying land (0-200 m) only.	100
25	Distribution of retrieved surface emissivities for one location under various thicknesses of saturation.	101
26	Distribution of retrieved surface emissivities for one location at various times of the year and saturation conditions.	101
27	Distribution of retrieved surface emissivities for the 91 and 150 GHz channels with respect to satellite viewing angle. Only unsaturated profiles with TPW less than 30 kg/m^2 were used.	103
28	Sensitivity of the retrieved surface emissivity for 91 and 150 GHz to various atmospheric and surface parameters.	109
29	Mean pressure levels of statistical features of the weighting functions with respect to TPW for each of the T-2 channels.	111
30	Mean percent contributions of the three dominant components of the brightness temperature with respect to TPW.	112
31	Mean T_bs for the T-2 channels using seven revolutions of data from late winter and mid-summer, 1992 and winter, 1993. This data were used as the training data in the multiple regression technique.	113
32	Mean, standard deviation, maximum and minimum differences between the actual 150 GHz T_b minus the synthesized 150 GHz T_b for the 5 terrain classifications and 4 latitude categories. Results were based on the independent data set.	115
33	Characteristics of the AMPR sensor that was flown on board NASA's ER-2.	131

FOREWORD

The Defense Meteorological Satellite Program (DMSP) F-11 satellite was launched 28 November 1991. This satellite carried the first 183 GHz microwave water vapor sounder, the Special Sensor Microwave Water Vapor Sounder (SSM/T-2). Volume I of the Calibration/ Validation effort (Falcone et al., 1992) was directed toward determining the accuracy of the engineering and science behind the SSM/T-2, i.e. did the instrument perform on orbit as it was calibrated on earth and was the water vapor product from Air Force Global Weather Central (AFGWC) within contract specifications. Volume I showed that the SSM/T-2 on orbit performance exceeded specifications. The water vapor products were most uncertain in very moist atmospheres, but still were within contract specifications. It was decided to engage in a calibration/validation effort specifically for moist atmospheres, i.e. the tropics. An opportunity was presented in the Tropical Ocean Global Atmosphere Coupled Ocean Atmosphere Response Experiment (TOGA-COARE) during January-February, 1993, and the Convective and Moisture Experiment (CAMEX) during September-October, 1993. These flights allowed for further study of the accuracy of the instrument under extreme atmospheric conditions.

1. INTRODUCTION

This report summarizes almost four years of the Phillips Laboratory and AER, Inc.'s efforts in the calibration of the millimeter wave sounder data from the DMSP SSM/T-2 instrument (henceforth referred to as the T-2). Of primary importance to the success of any satellite instrument is its calibration. Without a fully calibrated instrument there is no way to guarantee that the operational product is accurate. The ground calibration performed by Aerojet showed that the instrument performed as contracted, i.e., within design specifications. On orbit, that calibration was checked to insure that the instrument did not change due to launch forces or mechanical/electronic problems. A major focus of the calibration effort was aircraft flight planning, data base development, and calibration data analysis.

Two independent approaches were taken to calibrate the T-2: satellite-measured brightness temperature (T_b) data were compared with (a) contemporaneous NASA Millimeter-wave Imaging Radiometer (MIR) data from NASA ER-2 underflights, and (b) outgoing microwave radiances calculated from radiative transfer (RT) models using co-located upper-air temperature and moisture profile data (radiosondes) (Falcone et al., 1992). Underflight data analysis included co-location and comparison of F-11 T-2 measurements with 2 cases of MIR data on the West coast (May, 1992), 3 cases along the East Coast (July and August, 1992), 2 cases associated with the Tropical Ocean Global Atmosphere Coupled Ocean-Atmosphere Response Experiment (TOGA-COARE) in the western Pacific Ocean (February, 1993) (Falcone et al., 1996), 2 cases associated with the Convection and Moisture Experiment (CAMEX) along the East Coast (September, 1993), and one case along the East Coast (August, 1995). A second T-2 sensor onboard the F-12 satellite was calibrated with 2 underflights along the West Coast (December, 1994) and one along the East Coast (August, 1995).

As large data sets of T-2, aircraft and radiosonde measurements were acquired, an additional focus was to study the sensitivity of the instrument to the variability of the atmosphere. Also, with the failure of the 150 GHz channel on F-11 in June 1993, an additional challenge was to synthesize 150 GHz T_bs by a multiple regression method.

The first annual report (Pickle et al., 1993) summarized the progress in developing experimental protocols for the calibration of millimeter wave sounder data from the DMSP SSM/T-2 instrument. The second annual report (Pickle and Isaacs, 1994) focused on two general topics: continued calibration of the instrument and the sensitivity of the instrument to the variability of the atmosphere. The third annual report (Pickle and Isaacs, 1995) documented the long-term calibration of the F-11 sensor; initial calibration of the F-12 sensor; examination of the effects of clouds and precipitation; development of a technique to calculate upper-tropospheric humidity fields (UTH) using the 183±1 GHz and radiosonde profiles along the east coast of the United States; analysis of colocated AMPR data (an aircraft-flown microwave sensor similar to the SSM/I); and the effects of high incidence angle viewing. This final report summarizes the efforts during the past 4 years.

2. AIRCRAFT CALIBRATION

2.1 West Coast 1992 Campaign

The proposed flight path of the ER-2 along the west coast of California was to traverse as much dissimilar terrain over land as possible in order to gather data from a wide variety of atmospheric paths and underlying surfaces yet still fly over water. Roughly one-half the time airborne was spent over the water due to the belief that the best initial calibration was over ocean surfaces. Also, in order to test the time variance of water vapor at a specific location, the flight path was to have overlapping segments over both land and ocean. The path was chosen to pass near a number of radiosonde launch sites which were coordinated with the T-2 overpass. In particular, Vandenberg AFB, Point Magu and San Nicolas Island radiosonde stations provided additional non-synoptic soundings during the two days that the ER-2 flew. The flight paths flown are shown in Figure 1.

The ER-2 flights were made on May 14 and 15 (NOTE: the dates May 14 and 15 are based on local time, roughly 1700 local time; in universal time, the flights were made on May 15 and 16 at roughly 0050 UTC. For the purposes of this report, unless UTC is specified, the dates will refer to local time), with the only deviation from the above flight path arising from restricted airspace clearance not being given for a second overpass of China Lake NAS on 14 May, forcing the ER-2 to turn towards Los Angeles before reaching Bakersfield. On both days, low, thin stratus were located off the California coast, with some clear patches over water and clear over land.

2.2 East Coast 1992 Campaign

The two months separation between the west coast and east coast flights allowed time for some analysis of the May data set. The preliminary analysis of the west coast flights showed excellent agreement between the two instruments (T-2 and MIR) over water (~1 K). Data recorded by Aerospace concerning T-2 stability showed the T-2 to be very stable.

The early positive results allowed greater flexibility in the choice of aircraft flights on the east coast. The ER-2 flight paths of 29 and 30 July and 6 August were chosen to fly over varied earth surfaces (land, ocean and coast) with emphasis on ocean surface temperature variations from 285 K in the Gulf of Maine to 297 K off Cape Hatteras and crossing the Gulf Stream. As with the west coast flights, the flight paths were to have overlapping segments in order to test the time variance of water vapor at given locations.

The only difference between the flight paths during each day of flying was the timing of the ER-2 with respect to that day's F-11 overpass. The ER-2 aircraft was required to be at roughly the halfway point of the flight (based on the total estimated flight time) at the time of the F-11 overpass. Figure 2 shows the ER-2 flight paths and T-2 subtrack for July 29 and 30 and August 6, 1992, respectively.

During the early morning hours of July 29, weak high pressure over the mid-Atlantic states resulted in mostly clear skies from New England to Cape Hatteras. On July 30, a cold front had passed through New England overnight and was located just offshore at daybreak. Extensive stratocumulus clouds and fog were located over coastal sections with light rain showers just offshore. Broken clouds were present over inland sections of New England. The front was stalled along the mid-Atlantic coast where broken clouds and scattered thunderstorms were present. On August 6, high pressure was building into the New England and mid-Atlantic states, scattered clouds were present over inland areas from Maine southwestward to Maryland. Overcast skies and scattered showers were observed in Virginia and North Carolina. Broken clouds were present offshore from Maine to North Carolina.

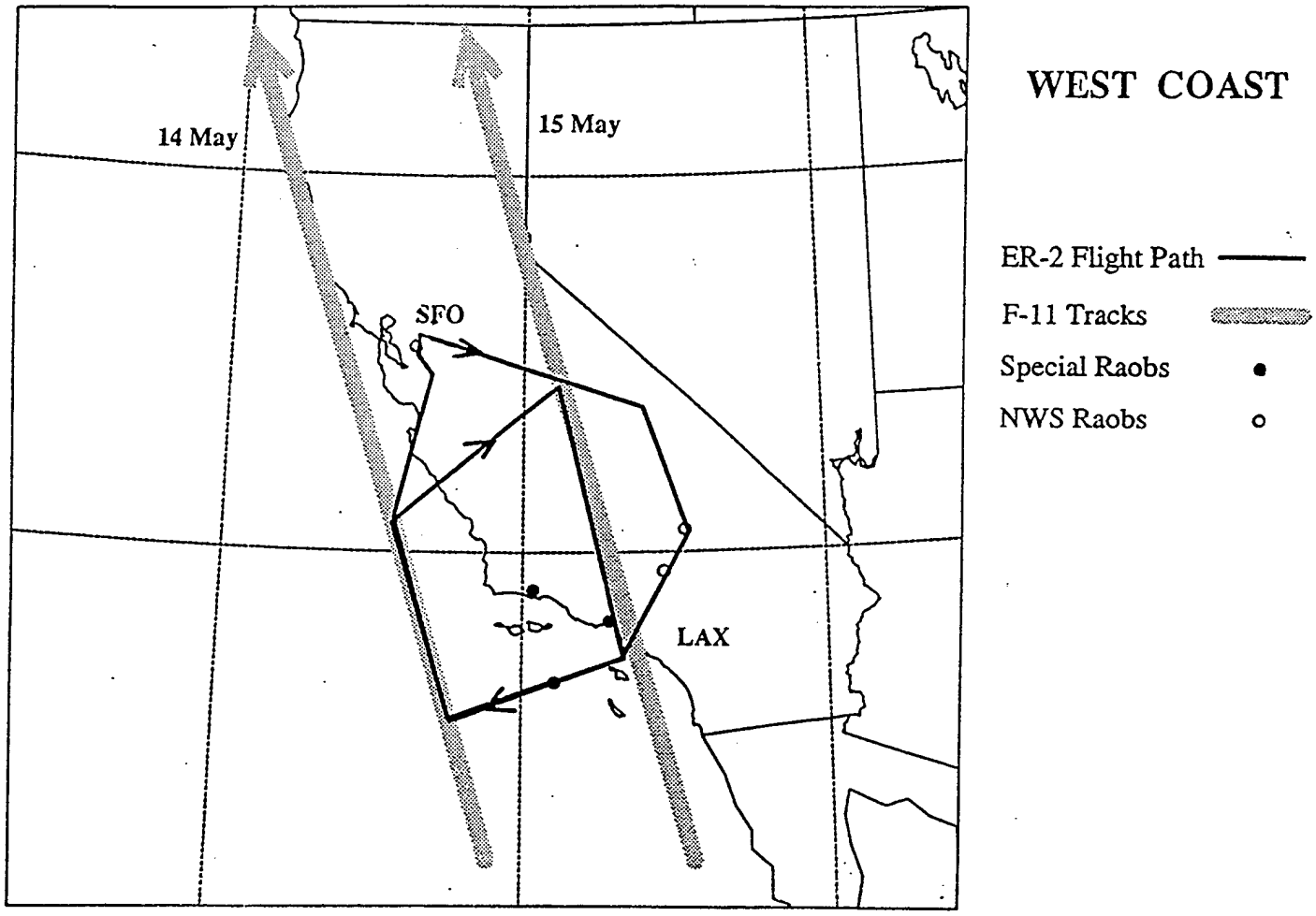

Figure 1. NASA ER-2 flight tracks for the west coast campaign in May, 1992. The F-11 subtrack for the two days that the aircraft was flown are shown.

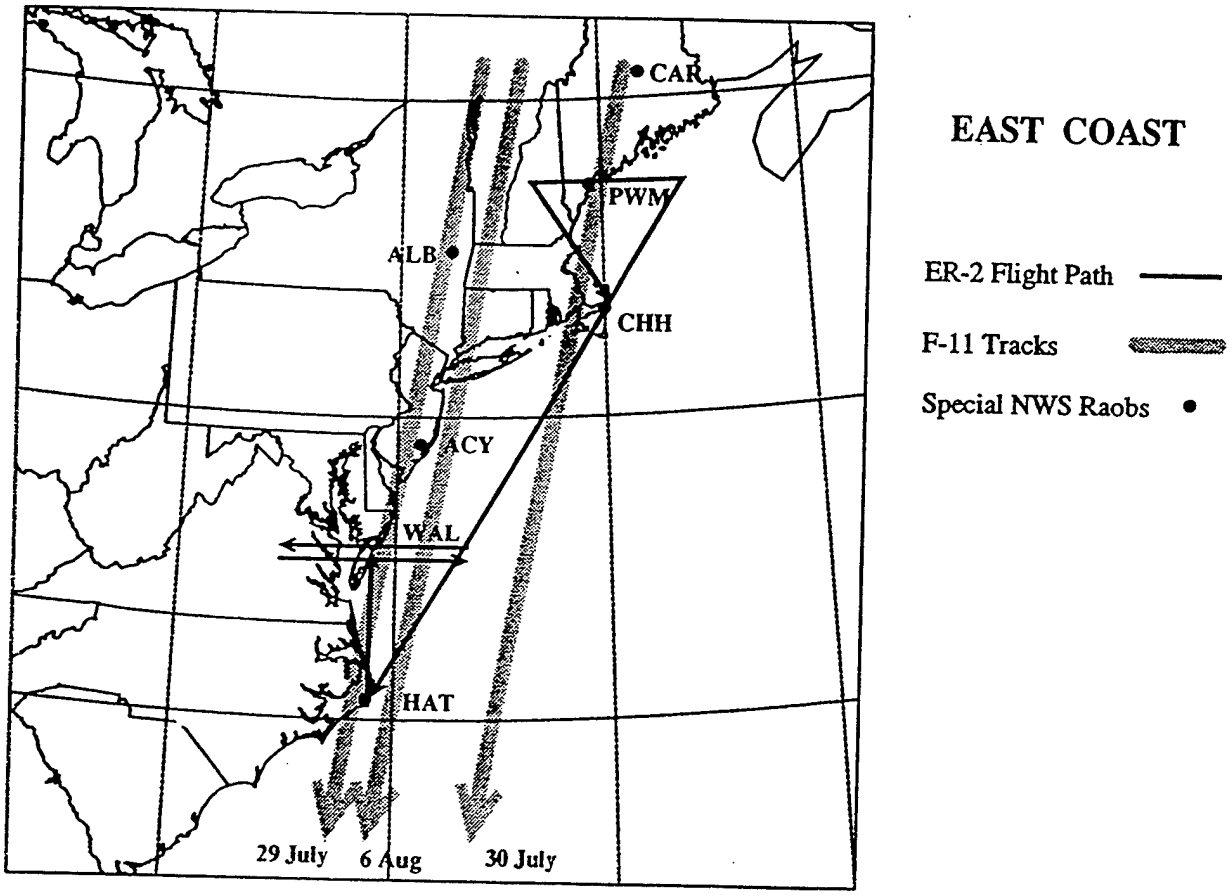

Figure 2. NASA ER-2 flight tracks for the east coast campaign in July and August, 1992. The F-11 subtrack for the three days that the aircraft was flown are shown.

2.3 TOGA-COARE 1993 Campaign

An air campaign was planned during the Tropical Ocean Global Atmosphere (TOGA) Coupled Ocean-Atmosphere Response Experiment (COARE) in the western tropical Pacific Ocean during February, 1993. The goal of this campaign was to examine the calibration and performance of the T-2 in moist tropical environments. During both flight days, February 4th and 10th, the F-11 spacecraft was on a descending track (Figure 3) over the region at the time of the aircraft flights. The NASA ER-2 aircraft was based in Townsville, on the northeast coast of Australia, and flew predominantly over tropical ocean with the exception of a few islands. On the first flight day, the majority of the ER-2 flight was spent over the deep convection of a tropical cyclone (Typhoon Oliver). During the second flight, only scattered tropical convection was present along the flight track.

2.4 CAMEX 1993 Campaign

An air campaign to examine the long term calibration of the F-11 sensor was planned during the autumn of 1993 along the east coast of the United States. The measurements were to be made during a NASA experiment called CAMEX (Convection and Moisture Experiment). Two flights were completed: September 30th and October 5th. During the first flight (Figure 4), the aircraft left Wallops Island, Virginia in the afternoon (1600 local) and flew northeastward, just south of Long Island and the New England coast. When in the Gulf of Maine, the aircraft turned and flew to Cape Hatteras, North Carolina; while enroute, the aircraft performed a near constant roll figure-eight, which provided information on increased satellite viewing angles. After crossing Cape Hatteras, the aircraft flew along the South Carolina coast and returned to Wallops Island by flying over land. The second flight flew southwestward from Wallops Island to the tip of Florida in order to observe deep, sub-tropical convection (Figure 5). On both flights, the aircraft underflew ascending F-11 orbits and was out over the ocean during the satellite overpasses (22:17 UTC on September 30 and 22:51 UTC on October 5).

2.5 F-12 West Coast 1994 Campaign

An air campaign to examine the initial calibration of the F-12 sensor was planned to take place during the winter of 1994 along the west coast of the United States. Two flights were flown on December 9 and 10. The basic flight path was to provide complete MIR coverage of several 91 GHz FOVs, which are quite large and have not been completely covered during previous CALVAL flights of the F-11 sensor. The aircraft flew parallel to the ascending F-12 subtrack in a series of tracks offset by roughly 45 km over the ocean. After these tracks were flown, the aircraft flew back to Ames, near Oakland, over land. The larger viewing angles of the T-2 were calibrated during this part of the flight. The flight paths for both days are shown in Figures 6 and 7. Both flights were flown over predominantly clear skies.

2.6 East Coast 1995 Campaign

Due to MIR instrument problems with the initial calibration of the F-12 T-2 along the west coast, an additional air campaign was planned to take place during the summer of 1995 along the east coast of the United States. One flight was flown on August 25, 1995 (see Figure 8 for the flight path). Again, the basic flight path was to provide complete MIR coverage of several 91 GHz FOVs. In addition, the calibration of the F-11 sensor was accomplished with this flight path, allowing for additional long-term calibration of this sensor.

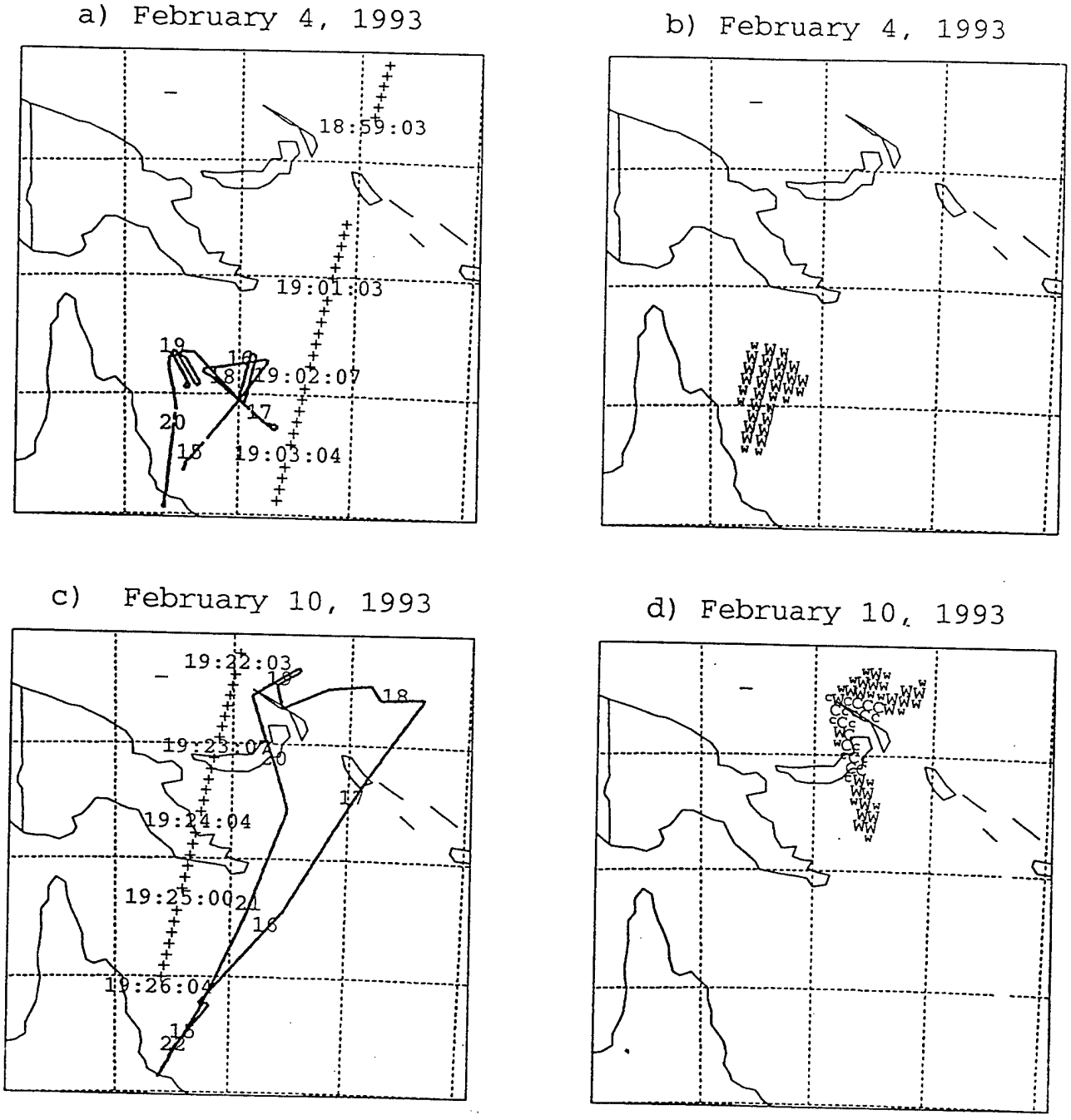

Figure 3. Positions of the morning descending subtrack of the DMSP F-11 satellite (+) over the western tropical Pacific Ocean on February 4 and 10, 1993. Superimposed on the tracks are the overpass hour (UTC) every 40 seconds. Also shown are the NASA ER-2 flight paths (solid line) and the hourly times (UTC) of the flights. The positions and topographic background classifications of the T-2 FOVs that have co-located MIR data (i.e., within ± 1 hour from the satellite over pass) are listed as W for water and C for coastal FOVs. The size of the letters represents which of the T-2 FOVs had co-located MIR data: the largest letters have data for the 91, 150 and 183 GHz FOVs; the smallest have data only for the 91 GHz FOV. For each map, the location of the upper-right corner is 0°N, 160°E and the lower-left corner is 20°S, 140°E.

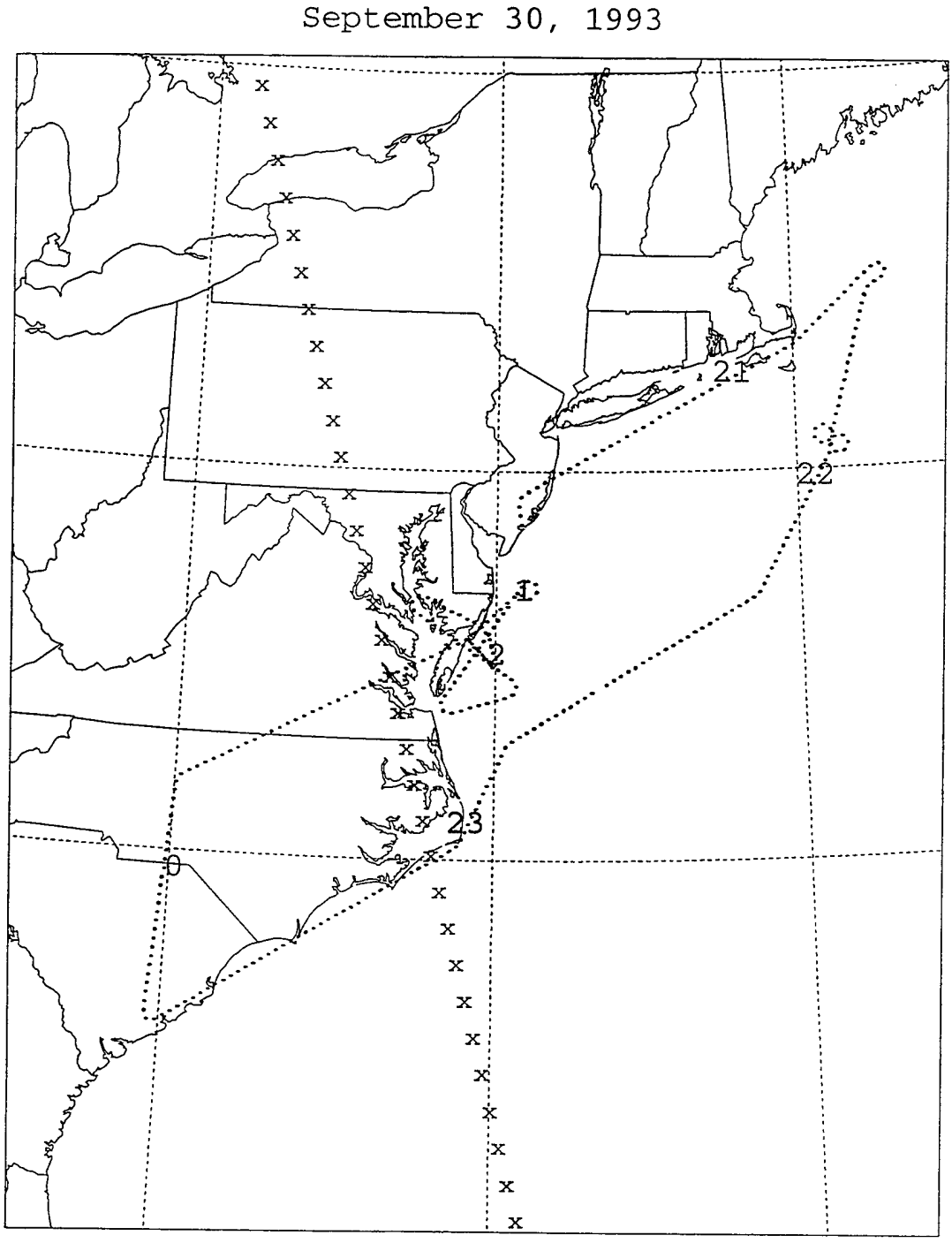

Figure 4. Flight path of NASA's ER-2 aircraft which carried the MIR sensor along the east coast of the United States on September 30, 1993. Superimposed on the track is the hour (UTC). The F-11 subtrack is shown (x).

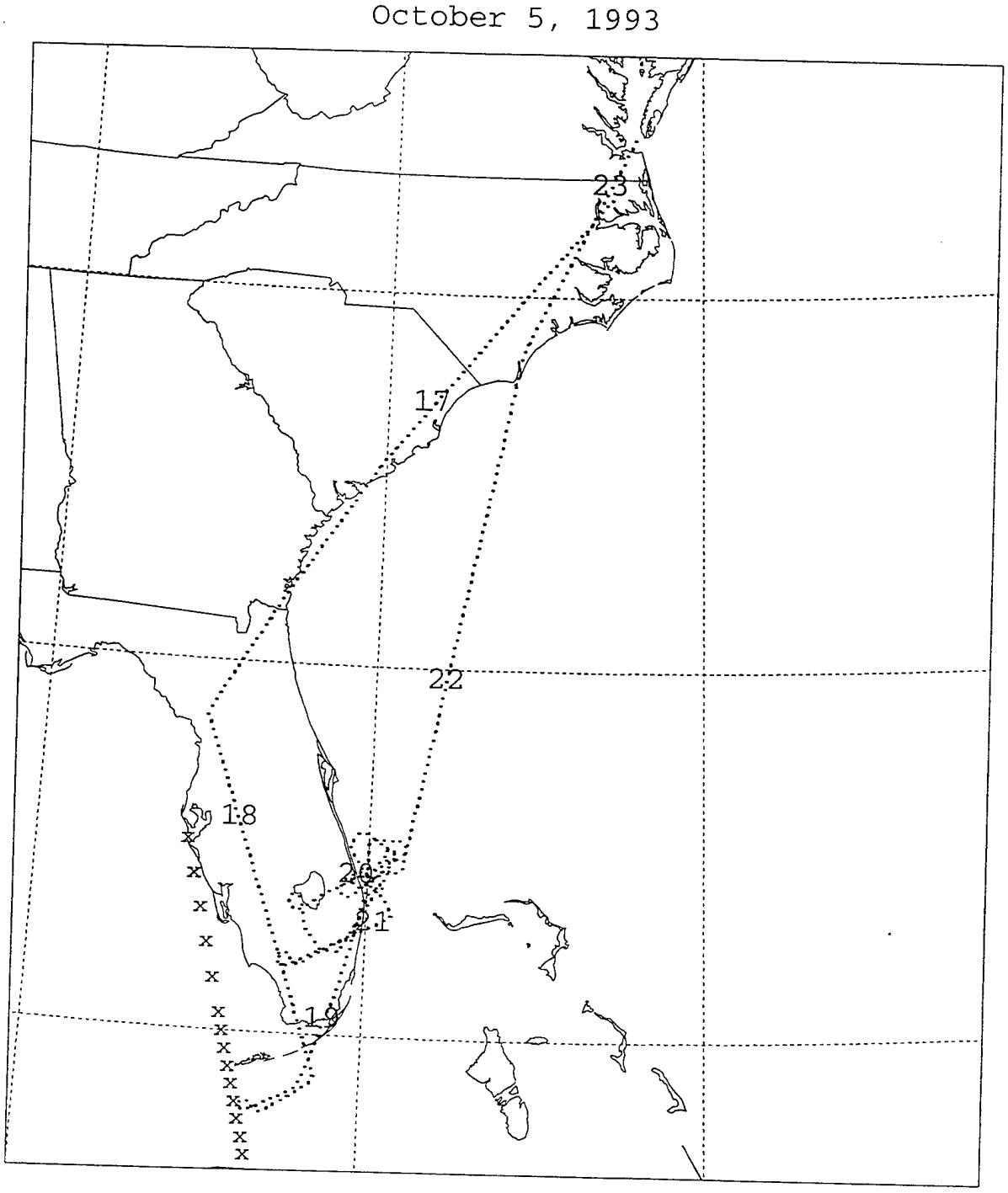

Figure 5. Flight path of NASA's ER-2 aircraft which carried the MIR sensor along the east coast of the United States on October 5, 1993. Superimposed on the track is the hour (UTC). The F-11 subtrack is shown (x).

December 9, 1994

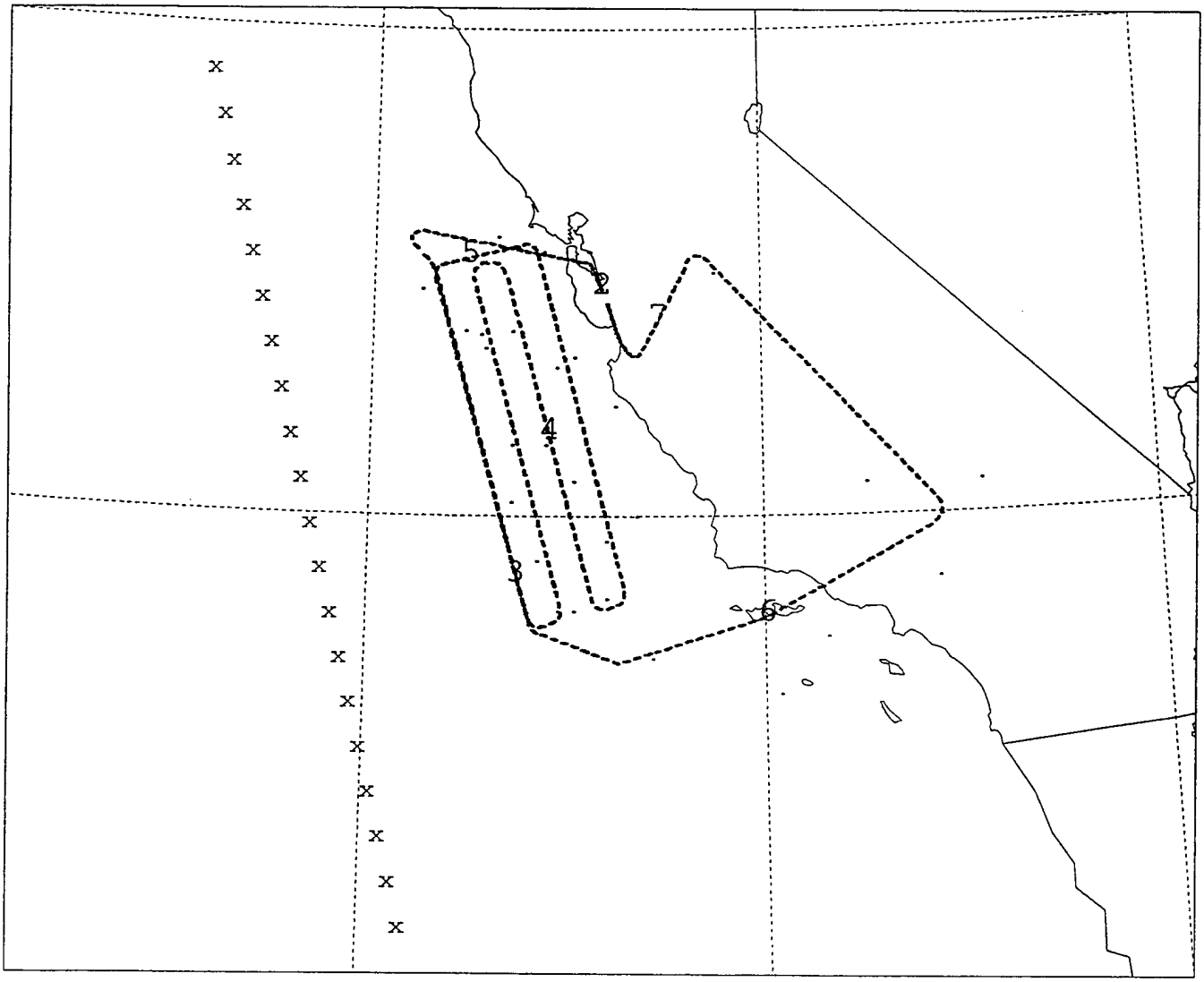

Figure 6. Flight path of NASA's ER-2 aircraft which carried the MIR sensor along the west coast of the United States on December 9, 1994. The F-12 subtrack is shown (x).

December 10, 1994

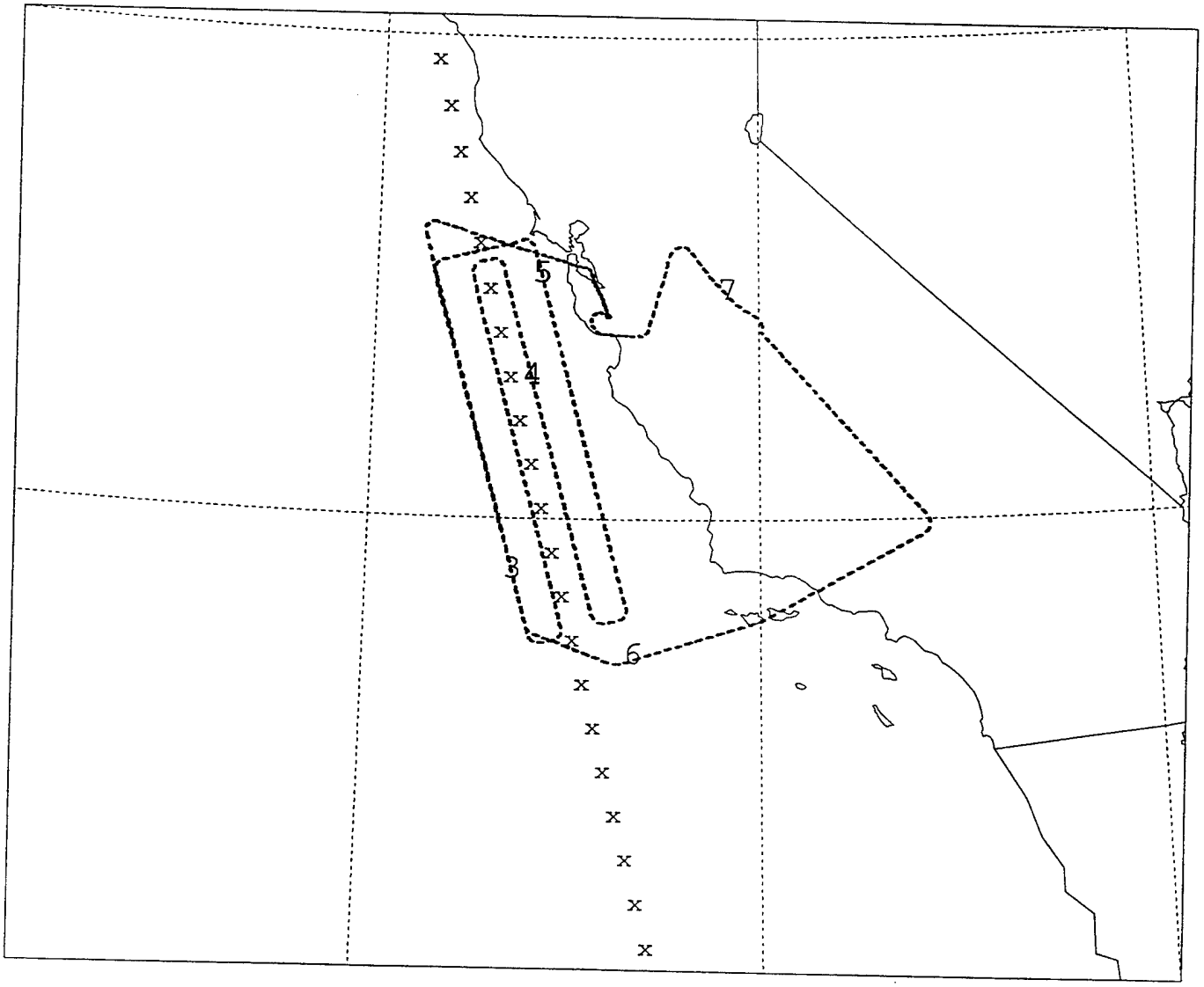

Figure 7. Flight path of NASA's ER-2 aircraft which carried the MIR sensor along the west coast of the United States on December 10, 1994. The F-12 subtrack is shown (x).

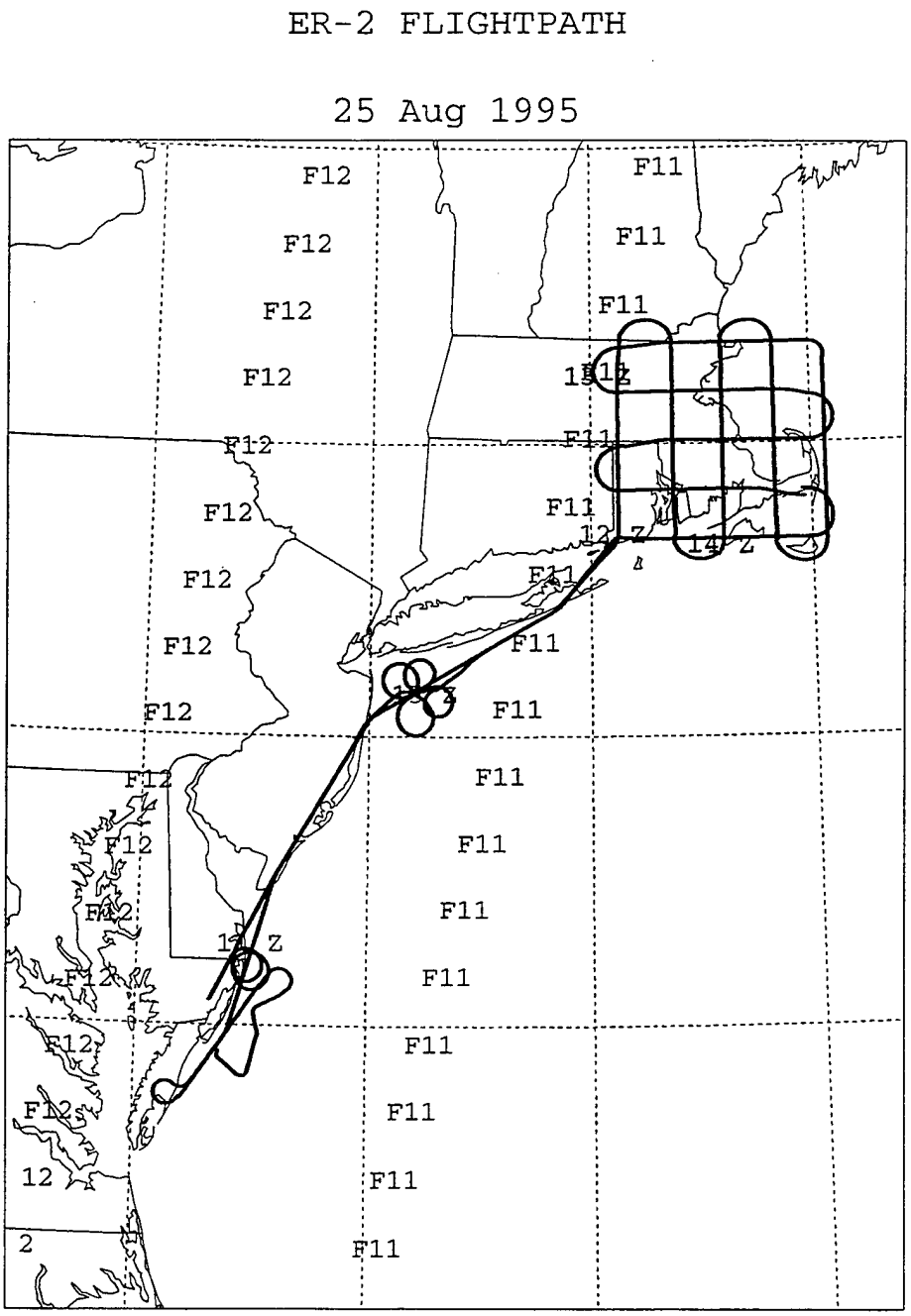

Figure 8. Flight path of NASA's ER-2 aircraft which carried the MIR sensor along the west coast of the United States on December 9, 1994. The subtracks of the F-11 and F-12 overpasses are shown.

2.7 Calibration Results

The MIR has four channels in common with the T-2 (150, 183±7, ±3, ±1 GHz) and a fifth channel at 89 GHz which differs slightly from the T-2 91.655 GHz channel. The small frequency difference between 89 and 91.655 GHz did not appreciably effect their comparison since the atmospheric and earth surface properties vary little over this frequency range.

Co-locations of T-2 and MIR measurements were determined by calculating the distance between the center of the MIR FOV and the center of the T-2 FOV. Co-location thresholds were defined for each channel frequency based on its beamwidth. There was an adjustment made for the elliptical deformation of the FOV away from the T-2 subtrack. In order to minimize atmospheric path length effects on the MIR T_b and ensure accuracy in the location of the MIR FOV, data were used only if the aircraft was at an altitude greater than 19 km with an aircraft pitch and roll less than 3°. The T-2 data were limited to scan angles less than 28.5° due to operational processing of the SSM/T-1 and T-2 data at AFGWC. This limitation was imposed on the MIR data so that all scan angles greater than 28.5° were not used in this study.

For the aircraft underflights in 1992 along the west and east coast of the United States, aircraft MIR - T-2 comparisons were stratified according to background (land, ocean, coast) and RMS differences and biases were computed (Table 1). Terrain classifications of land (L), water (W) and coast (C) are determined from the AFGWC fixed field data base (XFIX64), an eighth-mesh (48 km) gridded database (Kiess and Cox, 1988). Weather during the west coast aircraft campaign was characterized by stable atmospheric conditions; whereas, weather during the east coast campaign ranged from clear to frontal conditions. The window channels (e.g. 91 and 150 GHz) showed large RMS, especially for the coastal FOVs. This increased RMS was caused by large variation in surface emissivity within the T-2 FOV which was less well represented by the limited area scanned by the MIR. Over the ocean, the surface emissivity was more homogeneous, allowing the MIR's smaller areal measurement to be more representative of the average surface emissivity affecting the T-2's FOV. The RMS difference for the window channels for the east coast data were roughly comparable in magnitude to the west coast data.

Table 1. RMS difference and bias between the mean of the co-located MIR and T-2 T_bs at the T-2 channels for the 5 aircraft underflights during 1992. The scan angle of the MIR data matched that of the co-located T-2 FOV. The time between the T-2 and the MIR measurements was ±1 hour.

T-2 FOV TOPO	91 GHz	150 GHz	183±7GHz	183±3GHz	183±1GHz
		WEST COAST FLIGHTS			
WATER	3.4 / -1.5	2.4 / 0.5	0.7 / -0.3	0.8 / 0.2	1.3 / 0.7
LAND	3.5 / 0.5	4.3 / 1.1	3.8 / -0.1	2.9 / 1.5	3.2 / 2.1
COAST	9.1 / 4.1	3.8 / 1.5	1.2 / 0.0	1.1 / 0.2	1.7 / 0.0
		EAST COAST FLIGHTS			
WATER	3.7 / 0.2	3.6 / 2.7	1.2 / -0.6	2.1 / -1.8	1.2 / 0.2
LAND	4.7 / -1.1	2.6 / 1.2	1.9 / -1.4	2.6 / -2.5	1.2 / -0.5
COAST	10.9 / -1.2	4.5 / 1.2	1.6 / -0.8	2.4 / -1.9	1.8 / 0.3

For the west coast data, water vapor absorption line (i.e., 183.3 GHz) channels over water surfaces produced T-2 - mean MIR RMS differences of 0.7 - 1.3 K with biases of a few (up to 0.7 K) tenths of a degree. The RMS for these channels was larger for coastal FOVs (up to 1.7 K) with the largest difference for land FOVs (up to 3.8 K). The RMS differences were slightly greater for the three 183 GHz channels over the Atlantic Ocean. Comparisons of the T-2 and MIR 183 GHz measurements over water provided the best estimate of instrument performance, and overall, RMS differences ranged between 0.9 to 1.6 K.

For the 1992 west coast data, the effects of variations in the scan angle and viewing direction (east or west) of the T-2 sensor on the difference between T-2 and mean co-located MIR T_bs for the channels were examined. Only T-2 FOVs classified as water were used in the directional study. The MIR data were limited to ±1 hour from the time of the T-2 observations and to only those which had the same scan angle as the co-located T-2 data. There were no systematic variation between T-2 and MIR measurements with scan angle or direction. This implied that the two independent sensors were not biased by atmospheric path or scan angle; however, since T-2 data was recorded by AFGWC only for angles between ±28.5°, surface polarization effects were not investigated. Since the east coast weather conditions were such that strong predominant winds were not present over water, the effects of scan direction and angle on the east coast data were not examined.

For the TOGA-COARE 1993 underflights, the calibration results showed a dramatic increase in the RMS difference between T-2 and mean MIR T_bs compared to the earlier east and west coast CALVAL flights. This was due to measurements taken over a tropical cyclone on February 4. Table 2 shows that the average differences between T-2 and mean MIR T_bs during February 4 and 10, 1993. The large errors occurred predominantly on February 4th.

Table 2. Average RMS between T-2 and mean MIR T_bs measured on February 4 and 10, 1993. Topographic classifications of the T-2 FOVs are represented by W (Water) and C (Coast).

	Mean RMS between T-2 and MIR T_bs									
	91 GHz		150 GHz		183±7 GHz		183±3 GHz		183±1 GHz	
Flight	W	C	W	C	W	C	W	C	W	C
Feb 4	12.6	-	24.5	-	23.6	-	20.7	-	15.1	-
Feb 10	5.6	5.7	8.1	6.0	9.7	3.2	6.6	1.6	3.0	1.0
Both	9.6	5.7	19.0	6.0	18.4	3.2	15.7	1.6	11.2	1.0

The long-term calibration of the F-11 sensor made during September, 1993 showed a slight increase in the RMS difference between T-2 and mean MIR T_bs compared to the east and west coast CALVAL flights (Falcone et al., 1992) and TOGA-COARE flights (non-precipitating FOVs). Table 3 shows that the average differences between T-2 and mean MIR T_bs during the two flights are negligible.

Table 3. RMS between T-2 and mean MIR T_bs measured on September 30 and October 5, 1993. Topographic classifications of the T-2 FOVs are represented by W (Water) and C (Coast).

	Mean RMS between T-2 and MIR T_bs									
	91 GHz		150 GHz		183±7 GHz		183±3 GHz		183±1 GHz	
Flight	W	C	W	C	W	C	W	C	W	C
Sep 30	6.7	20.1	6.0	11.0	2.5	1.9	2.2	2.3	1.6	2.0
Oct 5	7.7	20.9	7.9	9.0	3.0	1.5	1.8	1.5	1.2	2.6
Both	7.1	20.4	6.7	10.0	2.7	1.7	2.1	1.9	1.5	2.4

Initial calibration of the F-12 sensor made during December, 1994 showed very poor agreement between T-2 and mean MIR T_bs compared to the F-11 calibration results (Table 4). Figure 9 shows that the increased error was a result of an inadequately performing MIR sensor. The 183±3 T_bs of the same scan indices of the first 300 MIR swaths when the aircraft was at 19 km altitude were connected for the December flights and the later F-12 calibration flight. The later MIR data showed a chaotic variation of T_bs across the swath with time, with a rough limit in variation of 10 K.

The MIR data during the F-12 calibration flights show a systematic variation across the swath with time, and the order of magnitude of these variations is several orders of magnitude greater than earlier flights.

Calibration of the F-11 and F-12 sensors made during August 25, 1995 along the east coast showed reasonable agreement between T-2 and mean MIR T_bs (Table 5) compared to the F-11 calibration results, similar to those observed in the early calibration results of the F-11 sensor.

Table 4. RMS between F-12 T-2 and mean MIR T_bs measured on December 9 and 10, 1994. Topographic classifications of the T-2 FOVs are represented by W (Water) and C (Coast).

	Mean RMS between T-2 and MIR T_bs									
	91 GHz		150 GHz		183±7 GHz		183±3 GHz		183±1 GHz	
Flight	W	C	W	C	W	C	W	C	W	C
Dec 9	5.4	12.9	4.2	8.9	1.7	3.3	2.4	2.2	1.9	2.0
Dec 10	1.5	11.1	3.4	7.4	8.7	6.3	8.5	6.2	10.6	8.4
Both	3.9	12.2	3.6	8.5	6.3	4.5	6.3	4.0	7.7	5.0

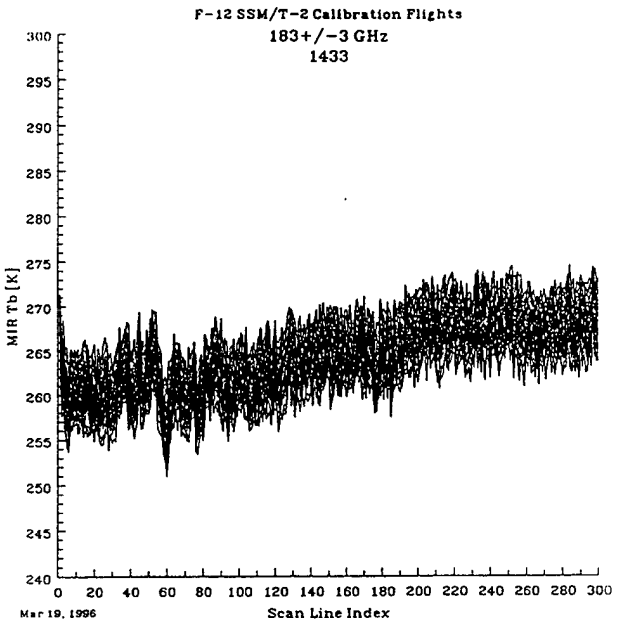

(a)

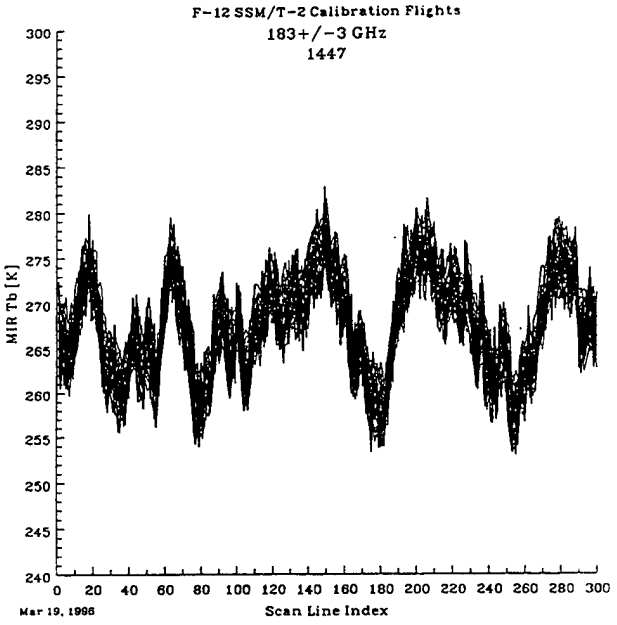

(b)

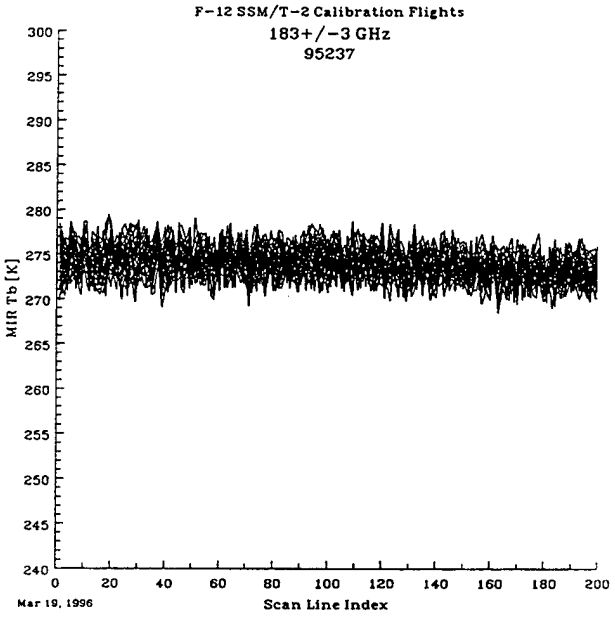

(c)

Figure 9. The 183±3 T_bs of the same scan indices of the first 300 MIR swaths when the aircraft was at 19 km altitude are connected for the F-12 December 1989 flights: (a) flight number 1443, December 9th; (b) flight number 1447, December 10th; and (c) the later F-12 calibration flight, August, 1995. Time plots of continuous sequences of MIR T_bs (no banking and an altitude of at least 19 km) for both flight days Same scan indices are connected with lines (there are 57 scan indices ranging from ±49°).

Table 5. RMS between F-11 and F-12 T-2 and mean MIR T_bs measured on August 25, 1995 along the east coast of the United States.

	Mean RMS between T-2 and MIR T_bs									
	91 GHz		150 GHz		183±7 GHz		183±3 GHz		183±1 GHz	
Flight	F-11	F-12	F-11	F-12	F-11	F-12	F-11	F-12	F-11	F-12
Aug 25	10.3	12.9	-	5.5	0.9	0.7	1.2	1.6	0.9	1.2

2.8. Variation of T_bs

2.8.1 Variation of Co-located MIR T_bs

The variation and range of MIR T_bs within each of the co-located T-2 FOVs were a result of the variation of moisture, temperature, ground temperature, surface emissivity, viewing angle and the presence of cloud and precipitation. If the atmospheric channels that are unlikely to sense a significant surface contribution (i.e., the 183±3 and 1 GHz) are studied for clear cases, the scale of the variability of atmospheric moisture can be examined. The effects of clouds and precipitation are examined in following sections. The average, standard deviation and maximum and minimum values of the range of MIR T_bs within each T-2 FOV with less than 20% cloud cover are presented in Table 6 for the 183±3 and 1 GHz channels. The average range of MIR T_bs within the T-2 FOVs was greater for 183±1 GHz than for 183±3 GHz. Both frequencies displayed quite a large average T_b range within the 183 GHz FOV which suggested that using the point-values of a radiosonde to calibrate and validate satellite sensors that have relatively large volume or areal sensing dimensions were quite limited.

2.8.2 T_b Anomalies Across Scans

With the premature loss of the 150 GHz channel in the summer of 1993, the T-2 instrument went under increased scrutiny. While the CALVAL study (Falcone et al., 1992) showed the instrument to be operating well within specifications, certain aspects of the T_bs were not explicitly studied. The sensitivity of the T_b to scan angle was examined on a scanline by scanline scale with no apparent anomalies. Long term averages of the T_bs at each of the 28 beam positions were not computed however. Subsequently, Kleespies (personal communication) at NOAA/NESDIS found that cross-track anomalies existed for the 183±3 GHz channel at specific beam positions. This was confirmed at PL/GPA and was found to occur as far back as the earliest available T-2 data. There should be no noticeable impact of these anomalies on the final water vapor retrievals since the magnitudes were on the order of 0.5 K at beam positions 14 and 16 (smaller deviations at other beam positions). These anomalies are below the determined 1 K accuracy limit of the T-2 channels (Falcone et al., 1992).

2.8.2.1 AFGWC Collected T_bs

In support of the CALVAL experiment, data was acquired and archived over a period of seven months at AFGWC. A subset of 32 full earth-orbits of the F-11 spacecraft was analyzed. These passes occurred over the period from March to August 1992 with the majority collected during March and April. On all but a few of the passes, data were missing at the outermost 4 beam positions (1-4 and 25-28) due to the influence of the glare obstructing panel (GLOB) on the SSM/T-1 measurements near the edge of swath on the sunside of the orbit. Beam positions 1-4 opposite the sunside were not processed initially because of software problems in the operational code. Changes were implemented in the summer of 1992.

Table 6. Mean, standard deviation and maximum and minimum values of the range of MIR T_bs within SSM/T-2 FOVs that had less than 20% non-precipitating clouds in the view. Each case had at least 10 MIR T_bs within the FOV, and each MIR T_b had the same viewing angle as the satellite.

Viewing Angle or Topography	Average Range	Standard Deviation	Maximum Range	Minimum Range	Number of Cases
			183±3 GHz		
1.5°	5.35	1.48	6.4	4.3	2
4.5°	4.95	1.45	6.5	3.0	4
7.5°	5.25	0.39	5.8	4.9	4
10.5°	5.06	1.28	6.9	3.5	5
13.5°	4.80	0.70	6.0	3.8	13
16.5°	5.65	1.74	9.0	3.4	13
19.5°	5.91	1.27	8.1	4.3	9
22.5°	5.28	0.99	7.5	4.4	9
25.5°	4.53	0.96	5.4	3.5	3
Water	4.79	0.68	6.1	3.5	18
Land	5.10	1.07	6.5	3.0	7
Coast	5.54	1.39	9.0	3.4	37
			183±1 GHz		
1.5°	8.65	0.35	8.9	8.4	2
4.5°	6.60	1.71	8.7	4.7	4
7.5°	6.77	0.52	7.5	6.4	4
10.5°	6.78	0.89	7.5	5.3	5
13.5°	6.43	1.71	9.6	3.9	13
16.5°	7.19	1.76	10.7	4.4	13
19.5°	7.77	1.25	10.6	6.2	9
22.5°	7.00	1.23	8.9	5.7	9
25.5°	5.70	0.52	6.3	5.4	3
Water	6.26	1.36	9.6	3.9	18
Land	6.40	0.91	7.5	4.7	7
Coast	7.41	1.46	10.7	4.4	37

The orbits were divided into both ascending and descending half-orbits and further subdivided into northern and southern hemispheric quarter orbits. Averages were computed for each beam position (5-24) corresponding to a scan width of ±28°. Figure 10 displays all T-2 channel average T_bs as a function of beam position. Each average represented over 24,000 individual measurements. This approach averaged out most if not all of the extraneous effects of the atmosphere and surface. The anomalies for the 183±3 GHz channel at beam positions 14 and 16 were clear. All other channels displayed expected results except for 183±7 GHz which had a noticeable decrease in T_b on the sunside of the scan. Figures 11a,b show enlarged plots of the 183±7 and 183±3 GHz channel averages, respectively. The channel anomalies were plainly visible at beam positions 14 and 16 and to a lesser degree at 6, 9, 11 and 21. The maximum deviation from the perceived normal value at these beam positions was approximately 0.5-0.8 K. These peaks were found at all orbital locations (ascending, descending) and at all latitudes and over all surface types.

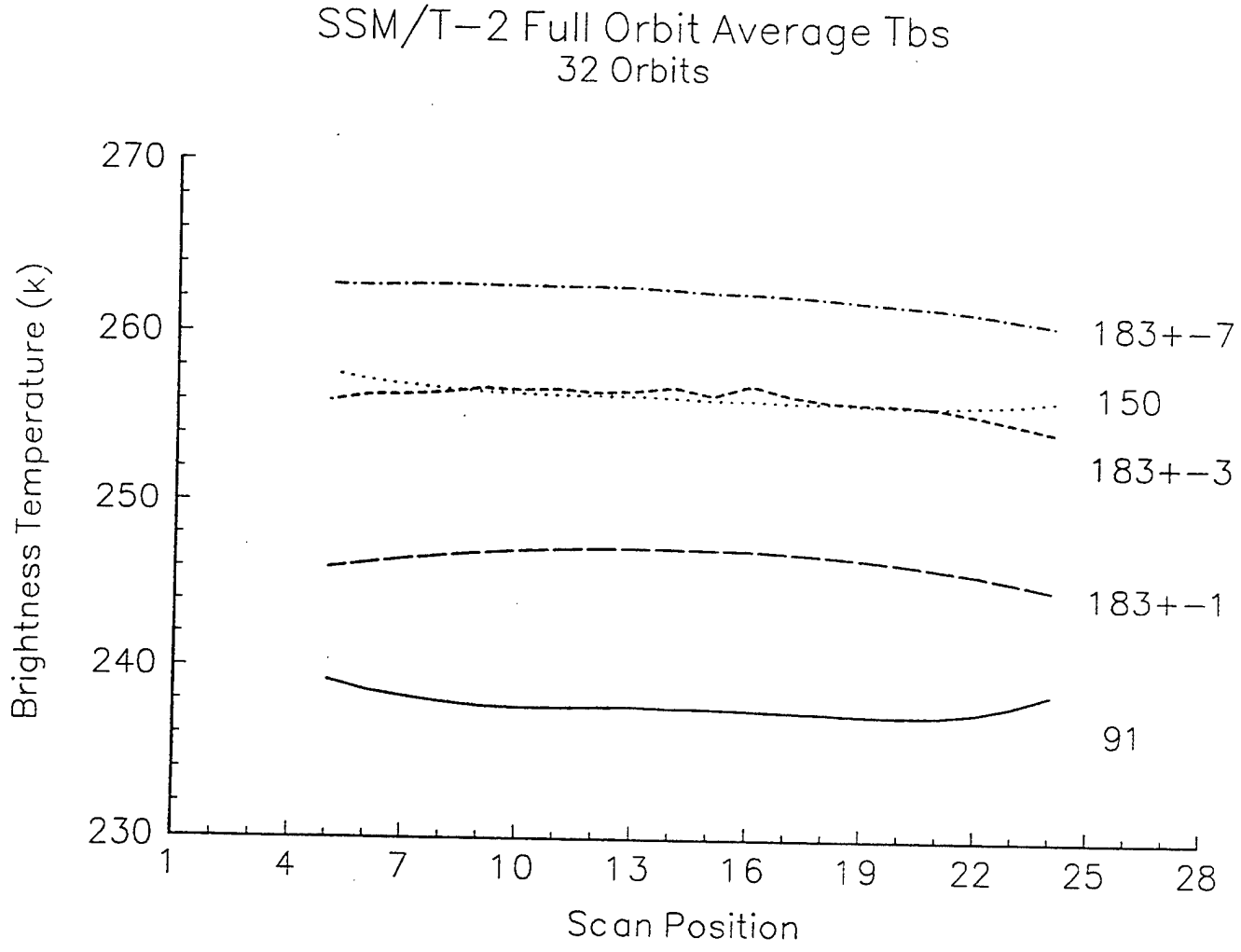

Figure10. Graph of the average T_bs for the T-2 channels as a function of scan position. Averages were taken over 32 full earth orbits acquired by AFGWC for the CALVAL experiment over the time period from March to August, 1992. Each average represented over 24,000 individual measurements.

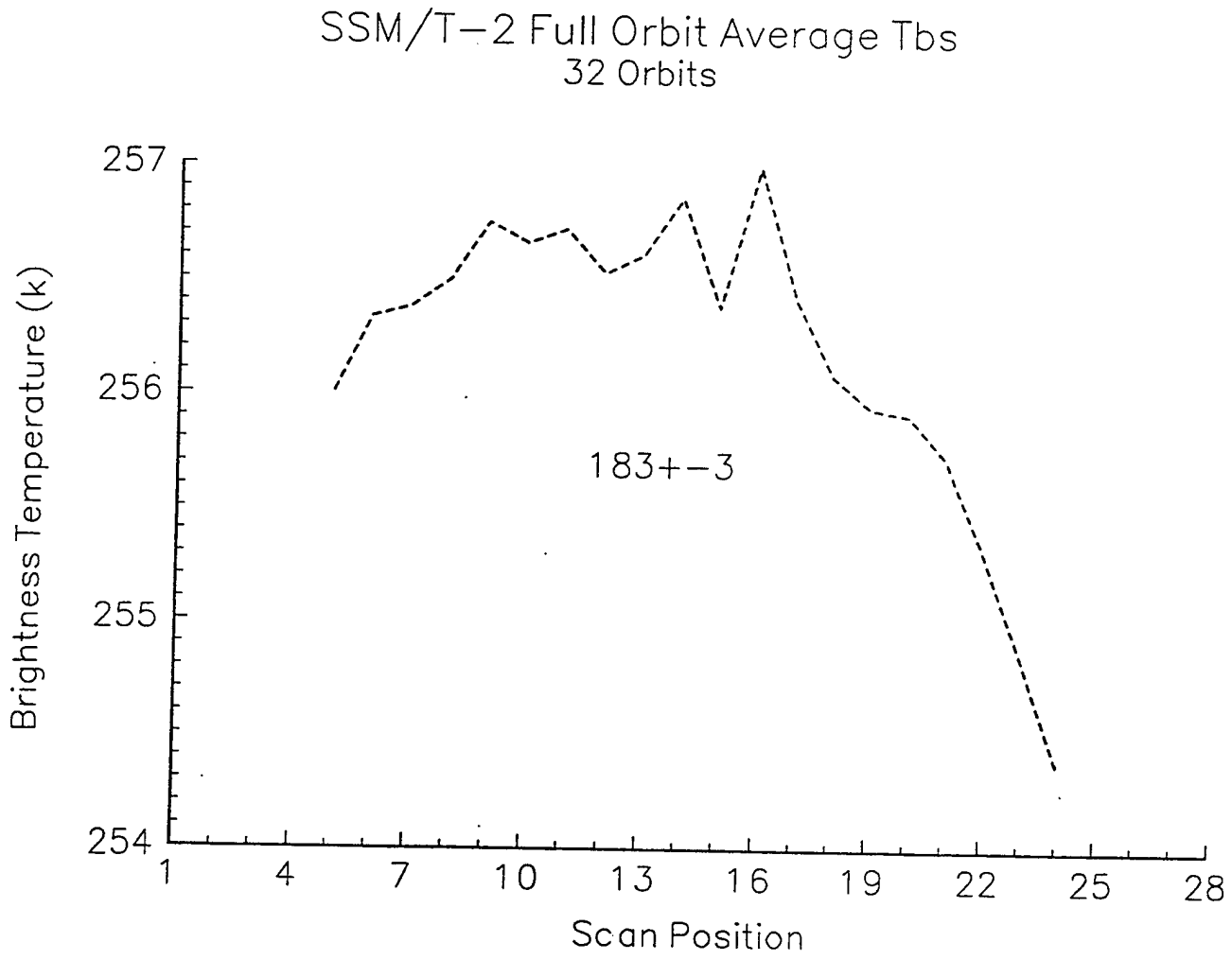

(a)

Figure 11. Graph of the average T_bs for the a) 183±7 GHz and b) 183±3 GHz channels as a function of scan position. Curves were taken from Figure 10 and expanded to display pertinent features.

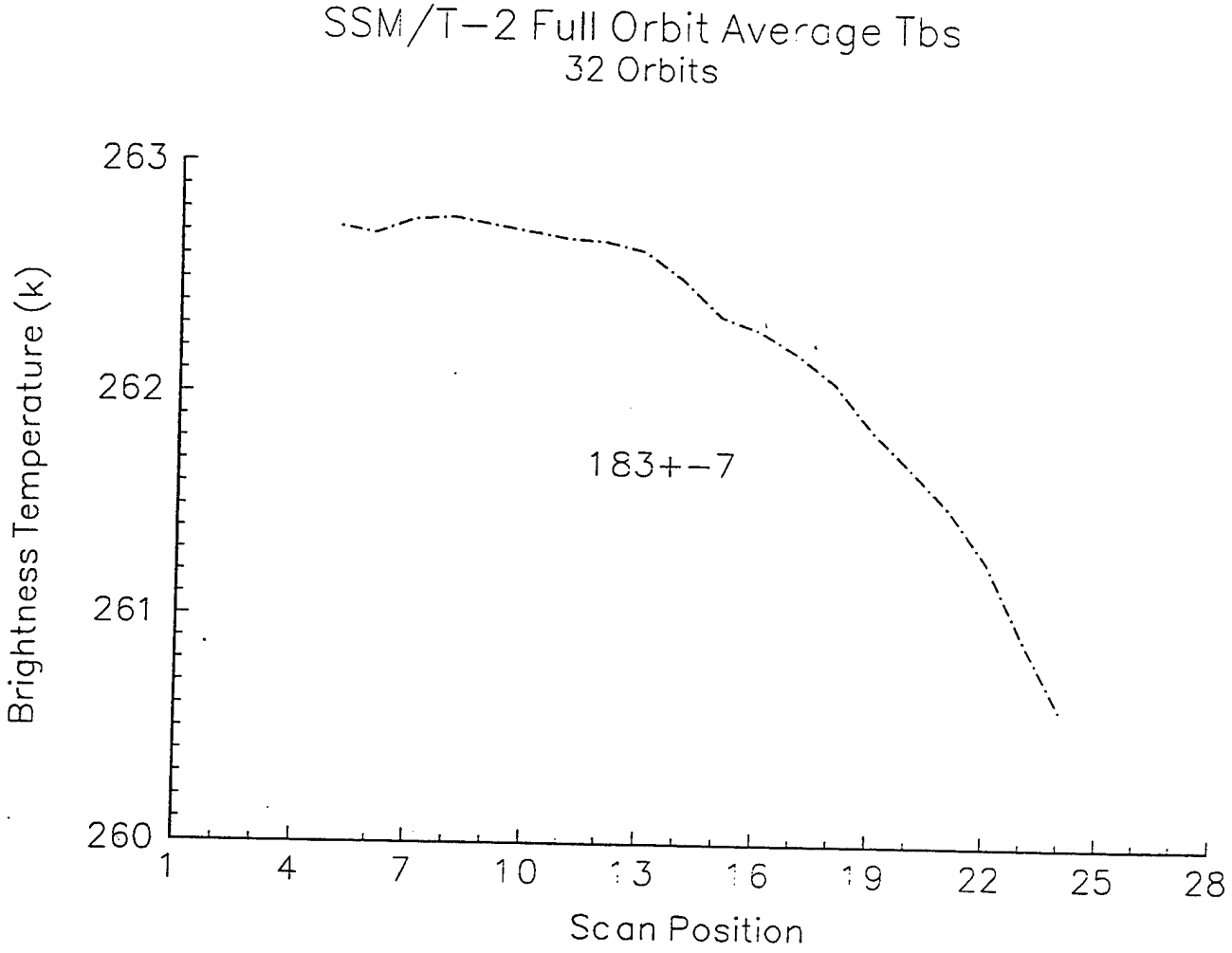

(b)

Figure 11. (continued) Graph of the average T_bs for the a) 183±7 GHz and b) 183±3 GHz channels as a function of scan position. Curves were taken from Figure 10 and expanded to display pertinent features.

The 183±7 GHz channel showed a marked decrease in T_b from right of subtrack (beam position 5) to left of subtrack (beam position 24, sunside). The likely source of this difference appeared to be the presence of Antarctica. The extremely dry atmospheric conditions and high mountainous terrain allowed all three 183 GHz channels to sense the surface. Since Antarctica is predominantly snow or ice covered, and snow has a significantly lower emissivity than land (soils and vegetation), the T_bs were significantly lower than those of the NH. Excluding this region from the computations provided a much closer comparison to the NH. The sharp decrease of T_bs across the swath noted in the above was due to the inclination of the F-11 orbit which resulted in one side of the swath (right-side/beam position 1) passing over higher latitudes and over Antarctica than the other side (left-side/beam position 28), which was over water. This marked and consistent bias occurred on each orbit.

2.8.2.2 PL/GPA Direct-Readout T_bs

The PL/GPA DMSP Direct-Readout Satellite Ingest System (referred to as the SeaSpace system) allowed the collection and analysis of real-time F-11 satellite data including both the OLS and the microwave sensor suite. An archive of 23 passes (11 ascending) over the Hanscom AFB, MA site was collected during late winter, early spring, 1994 (February through April). Since data were received only when the satellite was above the local horizon, the acquired passes were limited in latitude from 20 to 55°N. Also, no topographic information was included as was available for the AFGWC data. Figure 12 displays the average T_bs for four T-2 channels (150 GHz channel had ceased operating before these passes were archived) at each beam position. As with the AFGWC archived overpasses, only the 183±3 GHz channel displayed the beam position anomalies. Figure 13 divides the 23 orbits into ascending and descending passes. The same 183±3 GHz channel beam position anomalies as seen in the AFGWC data were present, essentially ruling out the data processing of the T-2 signal as a potential explanation for the effects.

The 183±7 and ±3 GHz ascending and descending passes had parallel relationships between average T_bs with respect to scan index. In both cases, the T_bs associated with the descending pass were cooler than those of the ascending passes. Since the F-11 is located on the terminator, and the sunside of both the ascending and descending passes are warmer than the terminator side. The F-11 descending passes over the east coast occurred during the morning and ascending passes during the evening. Complicating the problem, descending passes were parallel to the East Coast of the US while ascending passes cross from water to land. The window channel at 91 GHz should then display T_bs associated closely with the underlying surface type. Ascending nodes would have land surfaces to the left of track (higher beam positions) and water surfaces to the right (lower beam positions). Descending nodes had the opposite configuration. Since water surfaces have a much lower radiative temperature in the microwave than land surfaces this should be reflected in the ascending and descending curves for the 91 GHz channel. Figure 13 displays these characteristics quite clearly.

2.8.2.3 MIR T_bs

As part of the CALVAL experiment, the NASA ER-2 high altitude research aircraft underflew the track of the F-11 and F-12 spacecrafts. The ER-2 carried the MIR, which differed from the T-2 in several key ways: the beam widths were the same for all channels (1° averaged to 3°) and a scan width of ±48° resulted in a swath width of 50 km for an ER-2 flight altitude of 19 km. The same averaging technique utilized above was applied to the MIR channels in the chance that the same problem affecting the T-2 instrument would manifest itself in the MIR as well. Graphs of the matching channels on the MIR are plotted in Figure 14 for four CALVAL aircraft campaigns: West Coast of the US (May, 1992), East Coast of the US

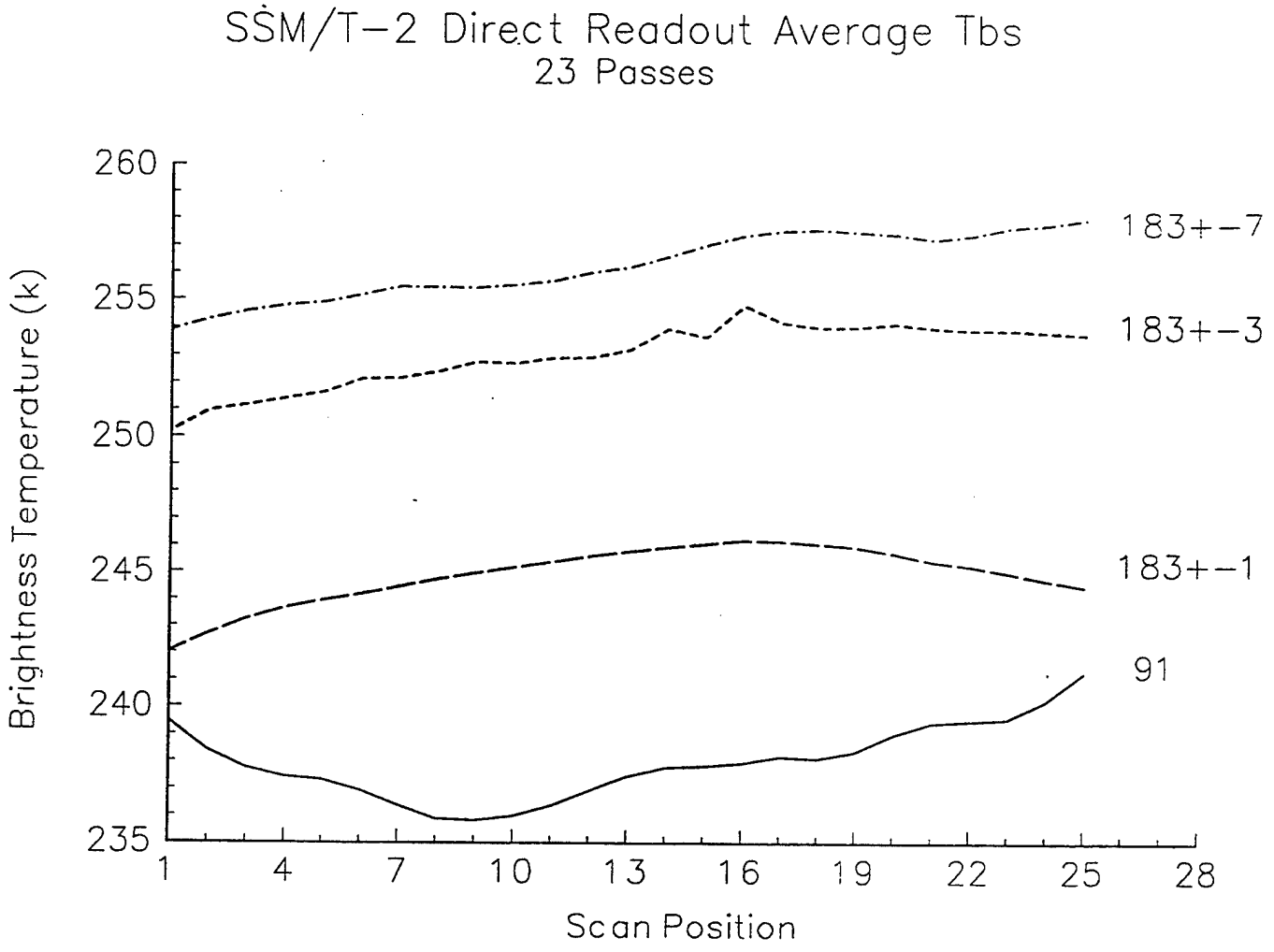

Figure 12. Plots of the average T_bs for four T-2 channels a function of scan position. Averages were taken over 23 passes collected by the PL/GPA DMSP direct readout satellite ingest station. Data was limited to a latitude range of 20 to 55°N and a longitude range of 55 to 95°W over the February-March, 1994, time period. Each average represented over 1,600 individual measurements.

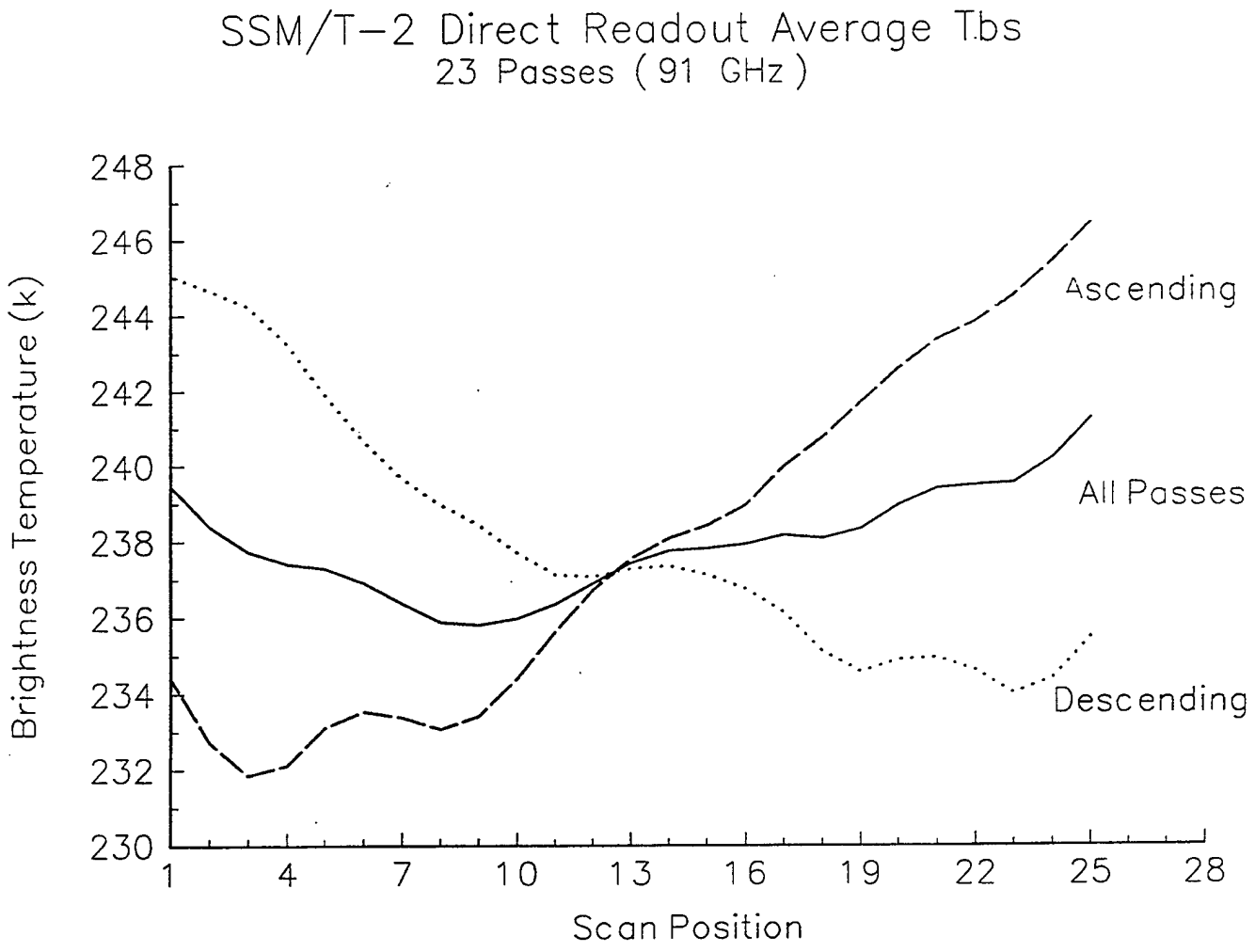

(a)

Figure 13. Graphs of the average T_bs for the a) 91 GHz b) 183±7 GHz and c) 183±3 GHz channels as a function of scan position. Curves are shown for both ascending (11 passes) and descending (12 passes).

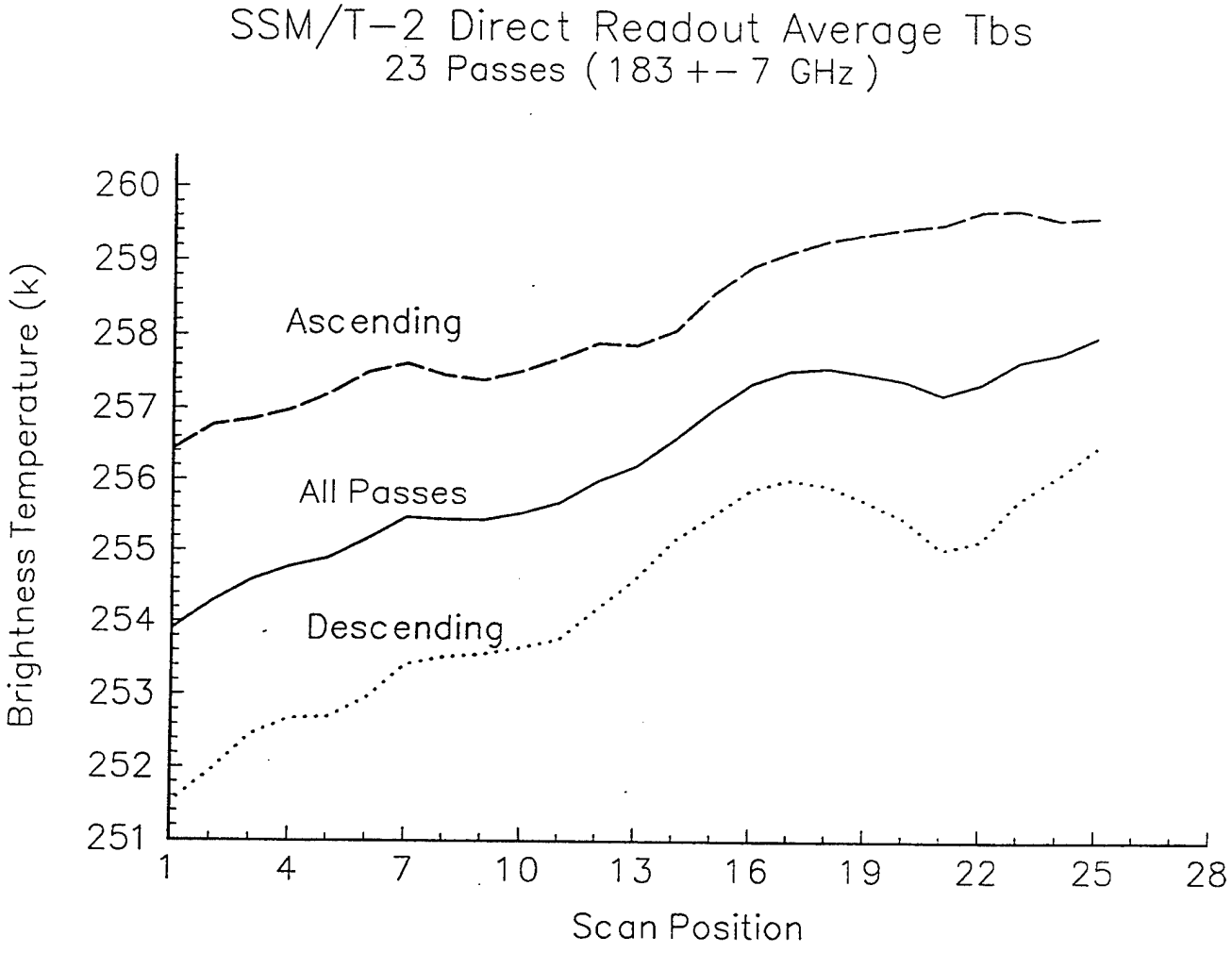

(b)

Figure 13. (continued) Graphs of the average T_bs for the a) 91 GHz b) 183±7 GHz and c) 183±3 GHz channels as a function of scan position. Curves are shown for both ascending (11 passes) and descending (12 passes).

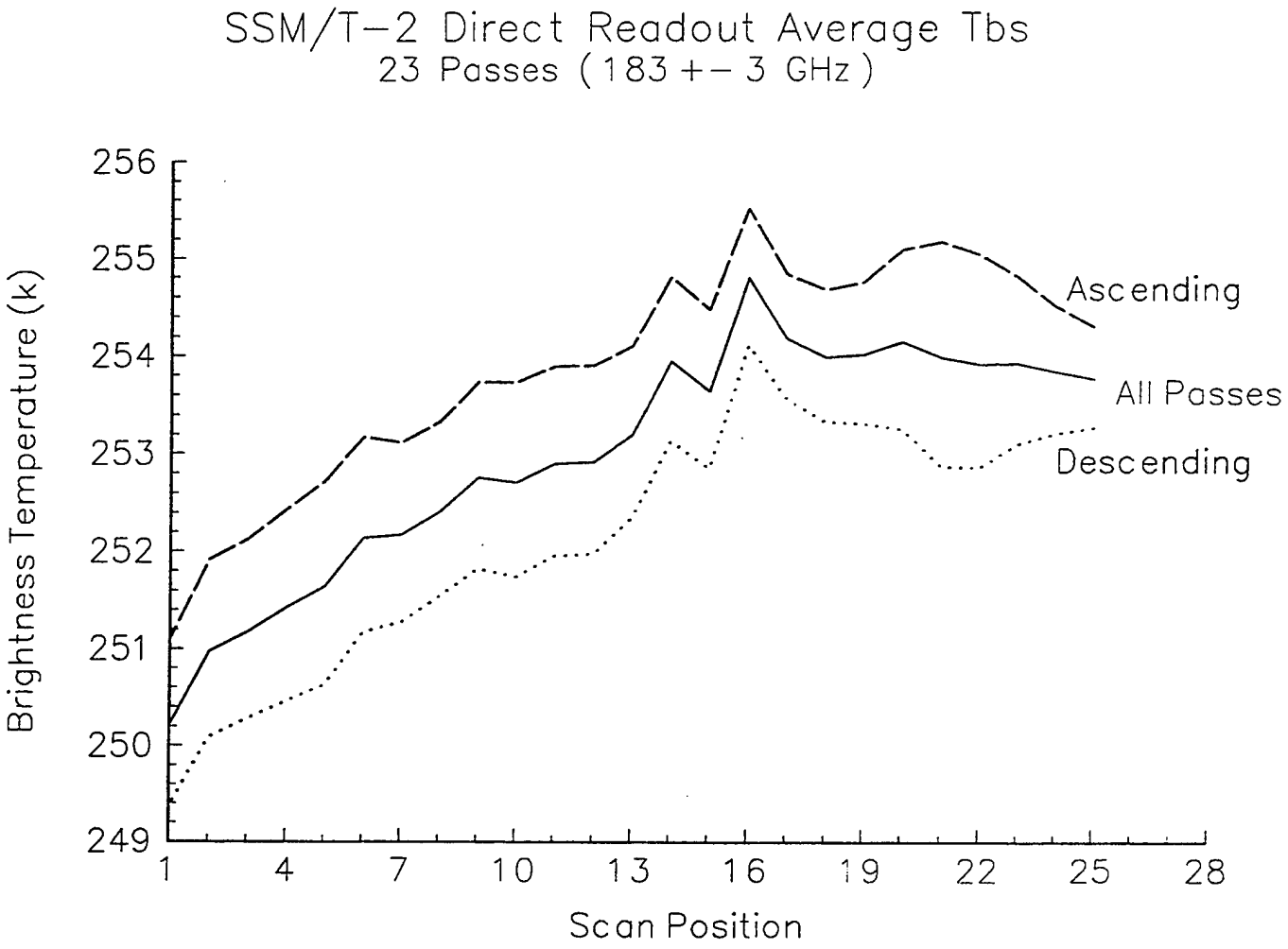

(c)

Figure 13. (continued) Graphs of the average T_bs for the a) 91 GHz b) 183±7 GHz and c) 183±3 GHz channels as a function of scan position. Curves are shown for both ascending (11 passes) and descending (12 passes).

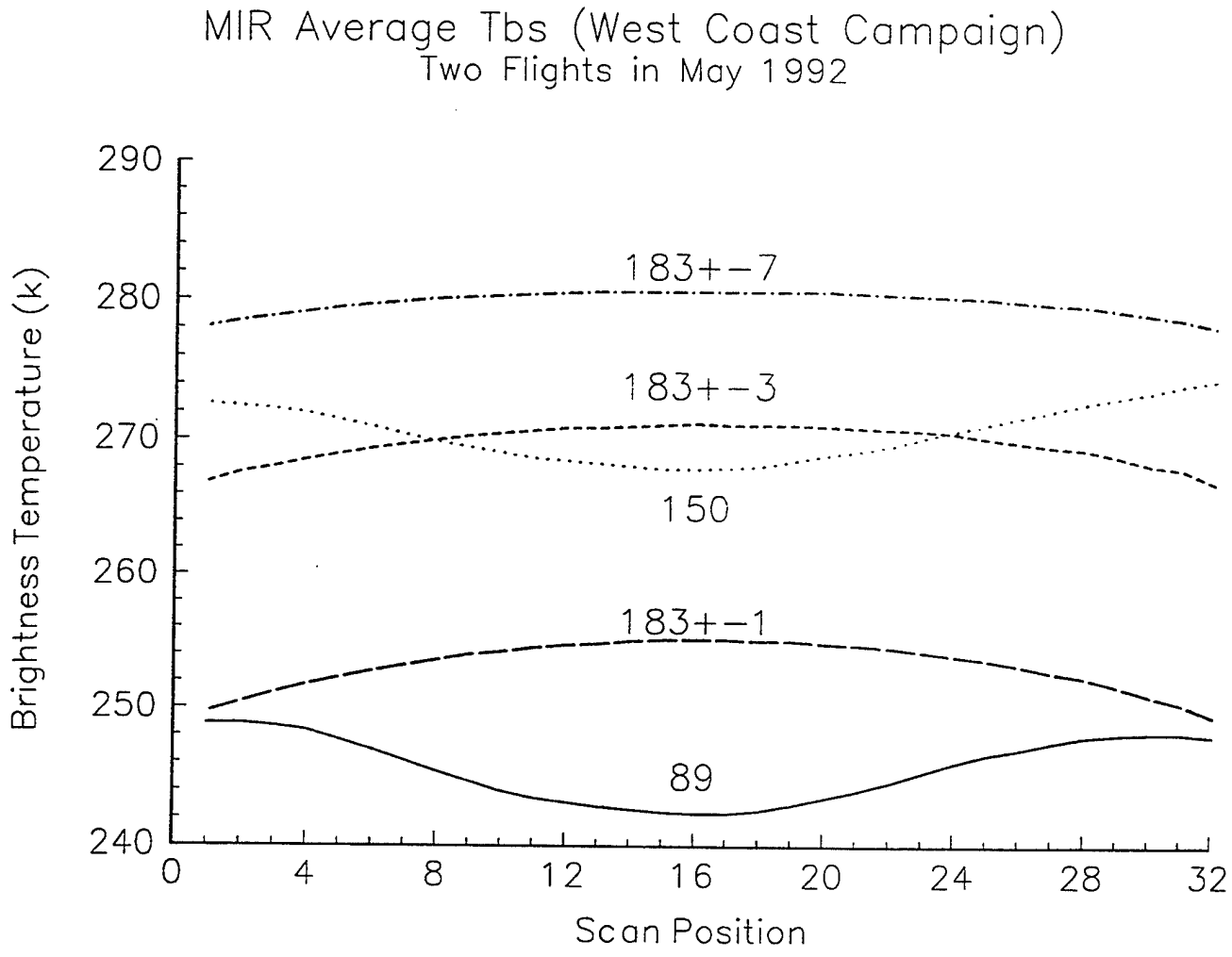

(a)

Figure 14. Plots of the average T_bs for MIR channels as a function of scan position for each CALVAL aircraft campaign. Averages are shown for the a) West Coast, b) East Coast, c) TOGA-COARE, and d) CAMEX aircraft flights.

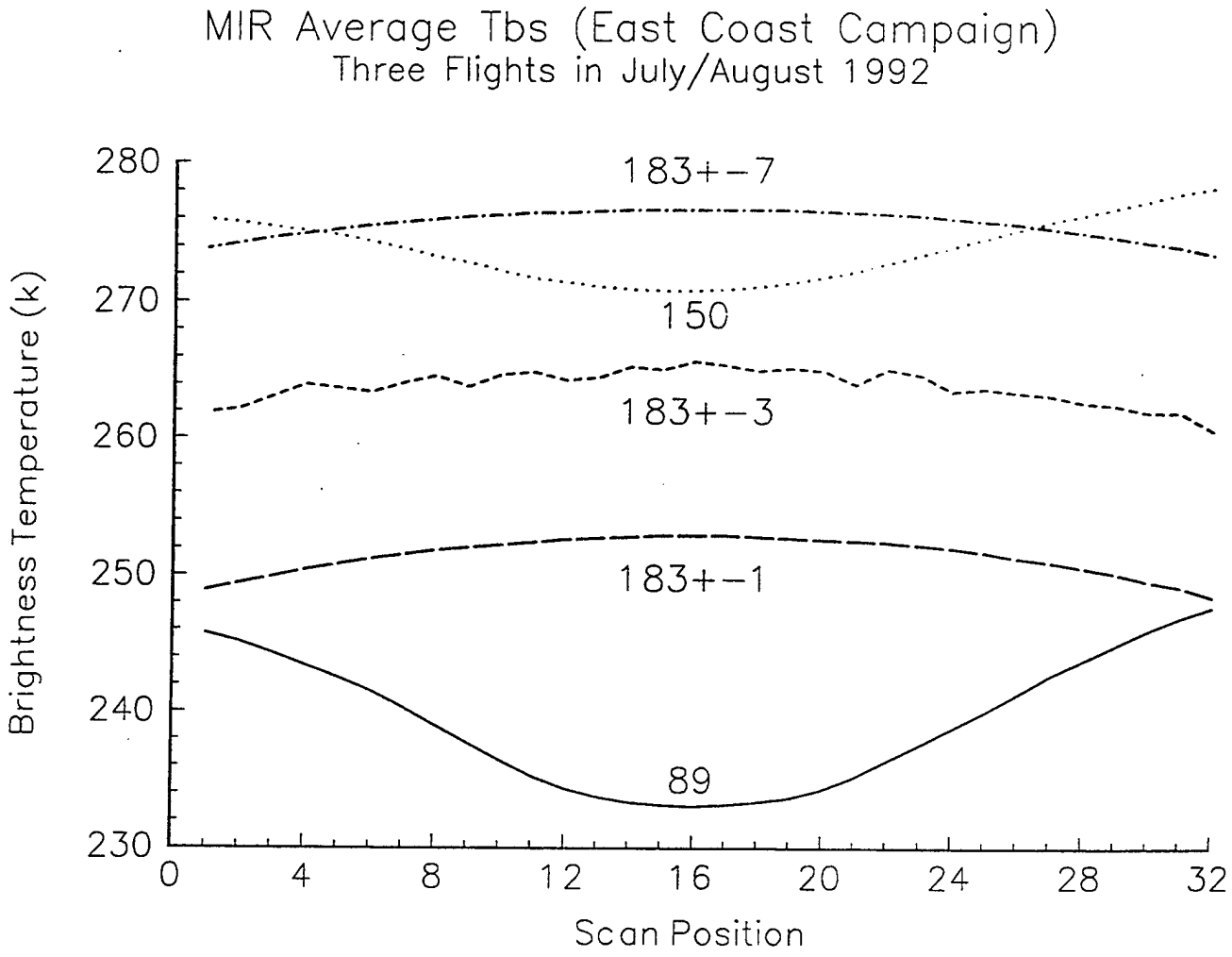

(b)

Figure 14. (continued) Plots of the average T_bs for MIR channels as a function of scan position for each CALVAL aircraft campaign. Averages are shown for the a) West Coast, b) East Coast, c) TOGA-COARE, and d) CAMEX aircraft flights.

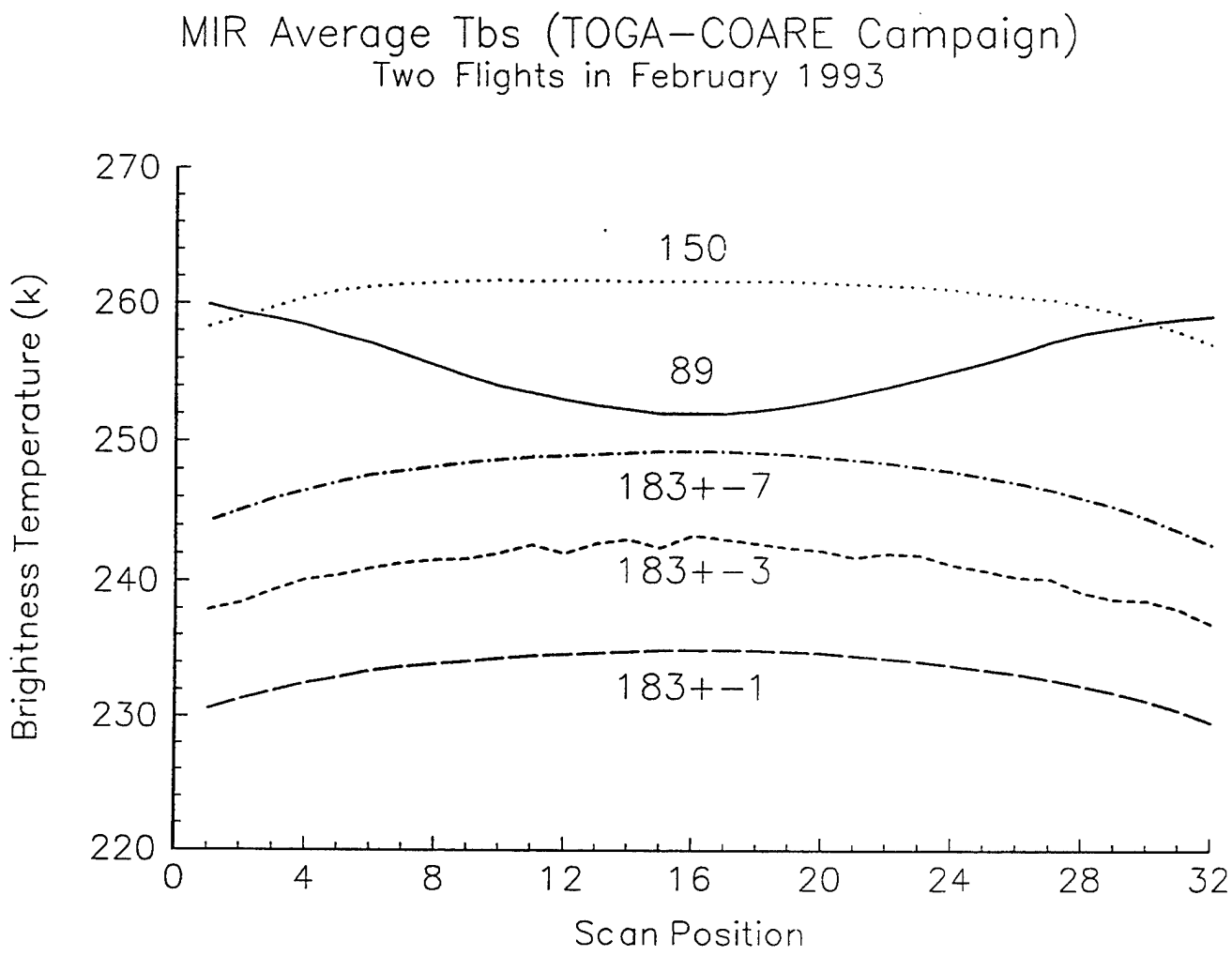

(c)

Figure 14. (continued) Plots of the average T_bs for MIR channels as a function of scan position for each CALVAL aircraft campaign. Averages are shown for the a) West Coast, b) East Coast, c) TOGA-COARE, and d) CAMEX aircraft flights.

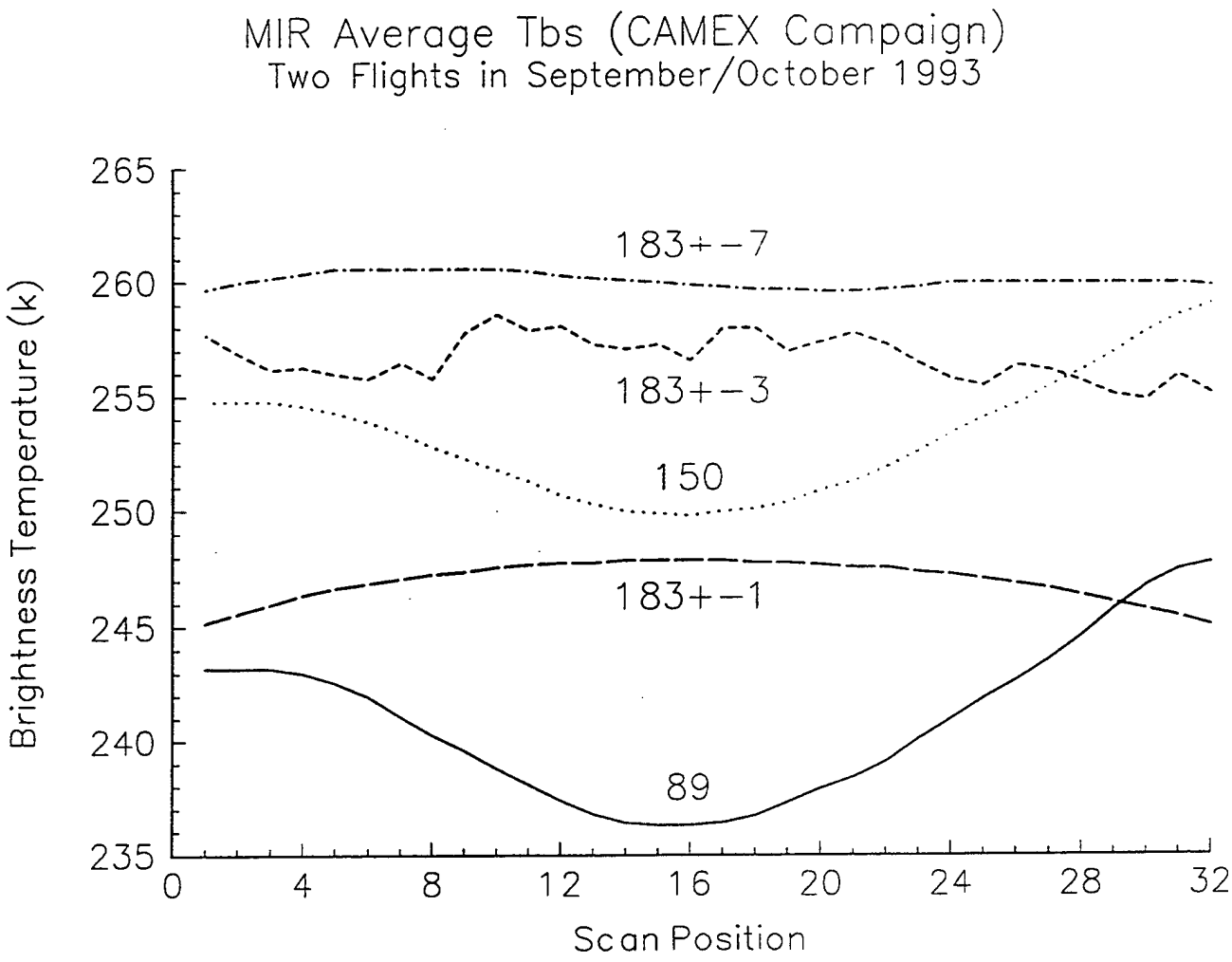

(d)

Figure 14. (continued) Plots of the average T_bs for MIR channels as a function of scan position for each CALVAL aircraft campaign. Averages are shown for the a) West Coast, b) East Coast, c) TOGA-COARE, and d) CAMEX aircraft flights.

(July/August, 1992), TOGA-COARE in the Western Equatorial Pacific (February, 1993), and CAMEX on the East Coast of the US (September/October, 1993). Overall, the only channel displaying any systematic anomalies was the 183±3 GHz channel. Figure 15 plots the 183±3 curves for all four campaigns on a single graph. Strangely, anomalies were not present for the West Coast data, but were apparent in the other campaigns that followed. Figure 16 displays curves for both the 183±7 and 183±3 GHz channels depicting the average T_bs at each beam position for three different atmospheric conditions: 1) clear skies, 2) cloudy/precipitating conditions, and 3) all cases combined. Cloud coverage was determined by performing a neph-analysis on colocated GOES visible imagery. Precipitation fields were computed from SSM/I imagery (Hollinger et al., 1991). The 183±3 GHz anomalies were present in both the clear and cloud/precipitating cases precluding the possibility that atmospheric effects alone accounted for these offsets.

The anomalies observed for the 183±3 GHz channel were not consistent from flight to flight. However, Wang (personal communication) detected repeatable anomalies in the cross-track data for a series of short-term (5 minute) averages. His finding suggested a problem in the MIR similar to the T-2 although he did not state if the beam positions were consistent with those exhibiting nonstandard behavior in the T-2. This is unlikely since the MIR employed a different scan mechanism than the T-2. In any case, the 183±3 GHz channel in a manner inconsistent with the other channels.

2.9 Climatology of Data Bases

The distribution statistics on the co-located T-2 brightness temperatures used in the global set of radiosondes and MIR data set were calculated to see if the data provided adequate variability for both the calibration and validation studies. Table 7 shows that both sets of T-2 values used to calibrate the T-2 instrument were not identical to those seen in a global distribution of T-2 values due to biasing of the co-located measurements over land and over more temperate latitudes. Table 8 shows the latitudinal distribution of moisture for the global set of co-located radiosondes used in this study. Although these values were biased toward land, they indicated that latitude significantly influenced the distribution of moisture, which in turn affected the level of the atmosphere being sensed by the T-2 channels (Table 9).

Table 7. Mean, standard deviation and range of T-2 T_bs sampled by the co-located MIR data set, the co-located radiosonde data set (2157 cases), and a set of 5 orbits of the satellite (> 80,000 T-2 FOVs).

T-2	MIR co-located pairs						5 satellite orbits		
Channel	Mean	St. Dev.	Range	Mean	St. Dev.	Range	Mean	St. Dev.	Range
[GHz]	[K]	[K]	[K]	[K]	[K]	[K]	[K]	[K]	[K]
91	239.5	28.3	88.2	257.9	26.0	133.0	236.1	29.9	159.3
150	268.2	13.4	50.7	264.7	25.8	139.2	254.6	30.0	169.2
183±7	278.4	3.9	18.3	265.3	15.7	107.9	262.2	22.6	159.4
183±3	267.7	5.3	21.4	258.4	9.6	83.8	256.6	16.0	135.0
183±1	253.1	6.1	21.4	247.6	7.6	65.4	246.8	11.0	106.2

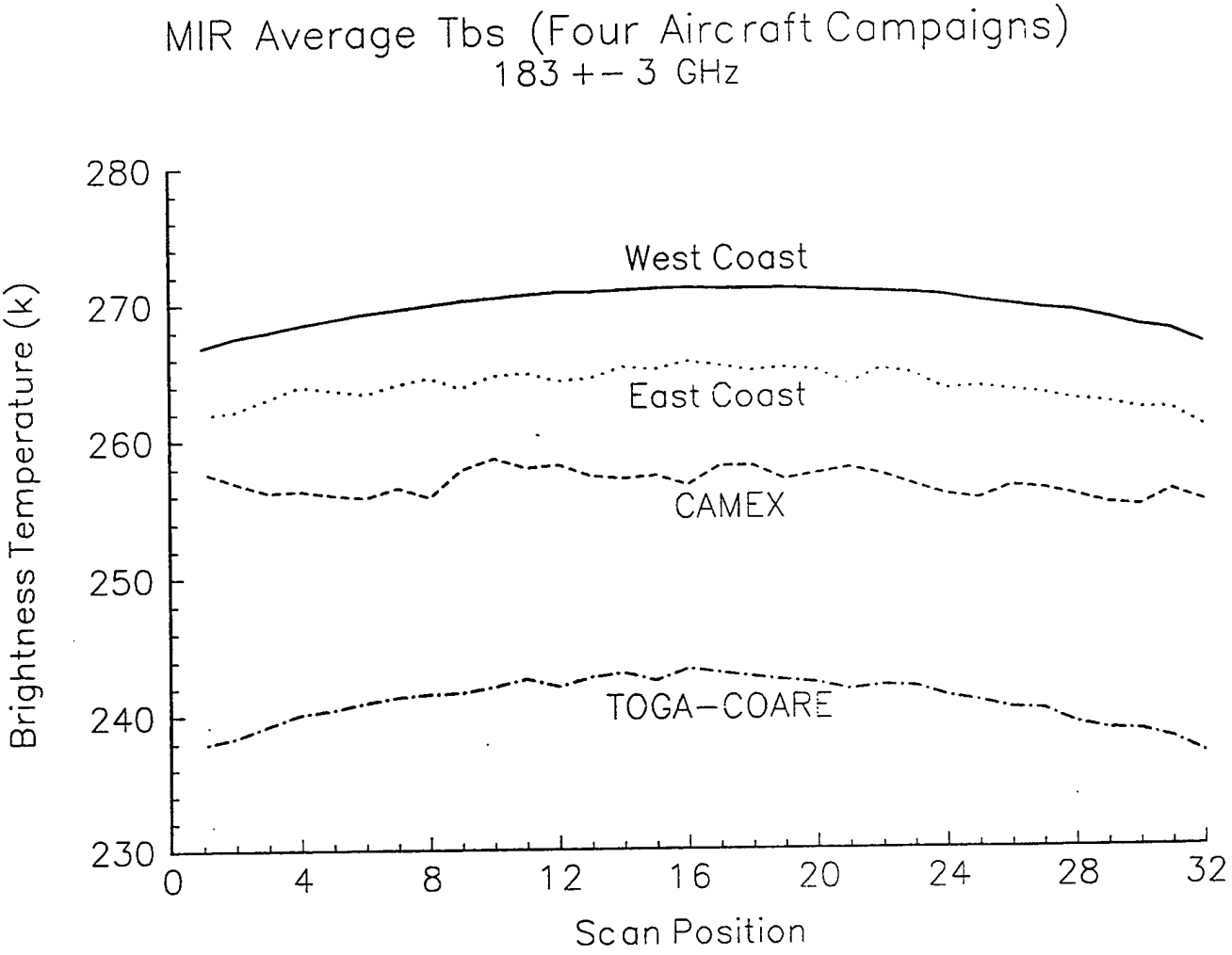

Figure 15. Graphs of the average T_bs for the 183±3 GHz channel on the MIR for all four CALVAL aircraft campaigns as a function of scan position.

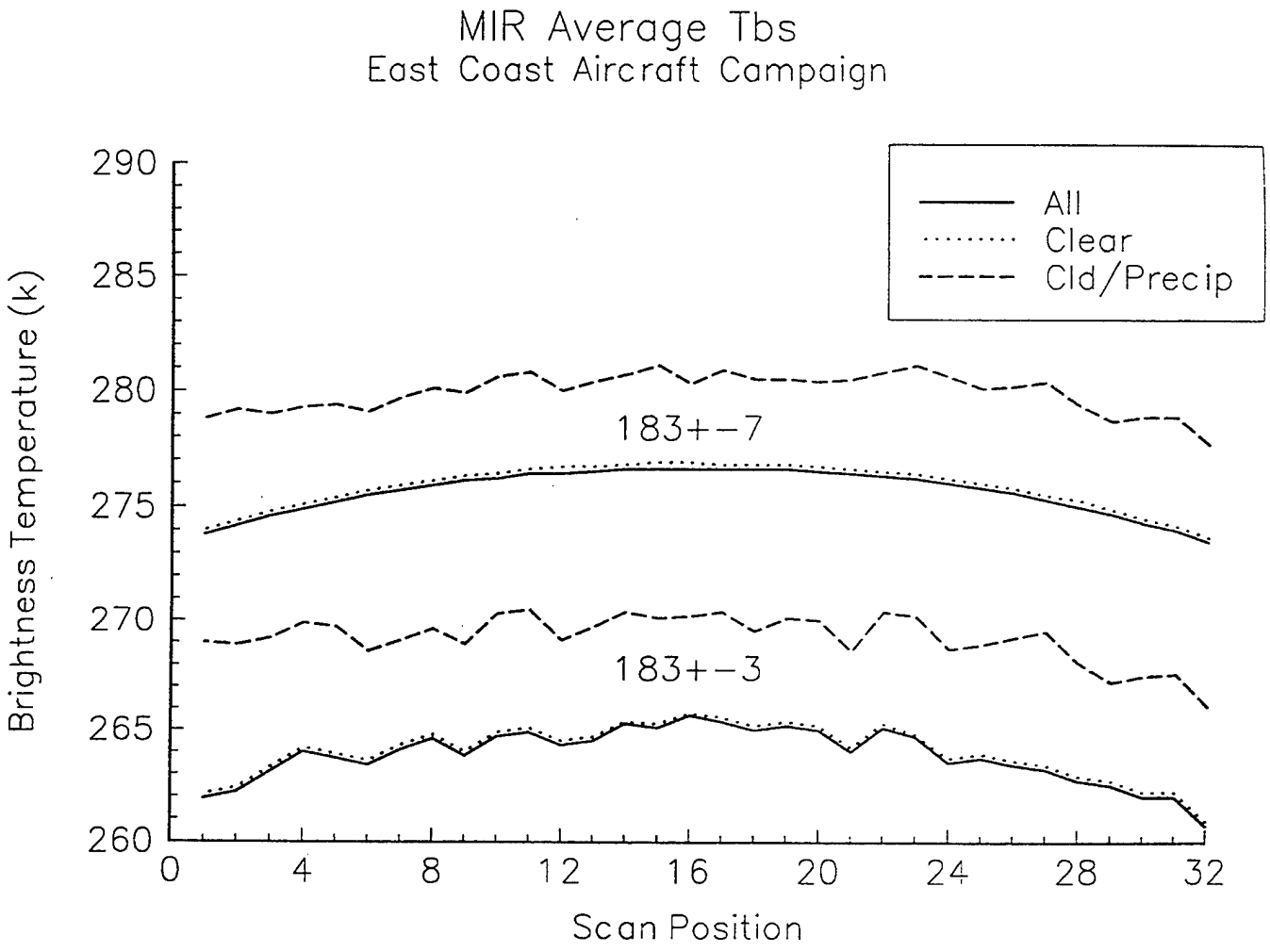

Figure 16. Plots of the average T_bs for the 183±3 GHz and the 183±7 GHz channels on the MIR for the East Coast CALVAL aircraft campaign as a function of scan position. Averages were computed for both clear and cloudy/ precipitating underlying conditions based upon colocated GOES visible imagery and SSM/I precipitation information.

Table 8. Latitudinal mean and standard deviation of the mixing ratio and relative humidity at 6 mandatory pressure levels based on the global set of co-located radiosondes used in the T-2 calibration study.

Latitude	1000 hPa	850 hPa	700 hPa	500 hPa	400 hPa	300 hPa
	Mean: Mixing Ratio [gm/kg] / Relative Humidity [%]					
70 - 90	2.3 / 78	1.7 / 69	1.1 / 58	0.4 / 52	0.17 / 49	0.05 / 44
60 - 70	3.3 / 62	2.5 / 65	1.4 / 54	0.5 / 48	0.25 / 46	0.08 / 42
50 - 60	4.7 / 66	3.8 / 61	2.2 / 57	0.7 / 48	0.33 / 45	0.10 / 44
40 - 50	5.7 / 66	4.6 / 56	2.9 / 56	1.0 / 49	0.41 / 45	0.11 / 40
30 - 40	10.4 / 75	7.0 / 65	4.2 / 62	1.6 / 54	0.69 / 50	0.22 / 48
20 - 30	15.9 / 79	10.2 / 67	6.2 / 62	2.5 / 51	1.20 / 45	0.42 / 42
10 - 20	17.5 / 77	11.1 / 67	6.6 / 58	2.7 / 51	1.34 / 47	0.44 / 46
0 - 10	17.4 / 83	11.5 / 74	7.1 / 69	3.1 / 60	1.47 / 49	0.41 / 39
TOTAL	9.4 / 72	6.0 / 63	3.6 / 59	1.3 / 51	0.60 / 47	0.19 / 43
	Standard Deviation: Mixing Ratio [gm/kg] / Relative Humidity [%]					
70 - 90	1.6 / 12	1.3 / 20	0.8 / 22	0.3 / 20	0.15 / 20	0.05 / 20
60 - 70	2.5 / 19	1.8 / 20	1.1 / 25	0.5 / 22	0.25 / 20	0.14 / 18
50 - 60	2.7 / 18	2.4 / 21	1.6 / 24	0.6 / 23	0.26 / 20	0.09 / 17
40 - 50	3.1 / 16	2.5 / 24	1.7 / 25	0.7 / 24	0.32 / 20	0.10 / 17
30 - 40	4.9 / 21	3.5 / 23	2.3 / 25	1.1 / 23	0.60 / 21	0.20 / 17
20 - 30	4.0 / 19	3.5 / 22	2.5 / 21	1.4 / 23	0.79 / 20	0.28 / 18
10 - 20	2.9 / 15	3.0 / 20	2.2 / 19	1.3 / 24	0.74 / 23	0.23 / 18
0 - 10	2.0 / 11	2.4 / 14	2.0 / 20	1.2 / 23	0.91 / 24	0.24 / 20
TOTAL	6.8 / 19	4.2 / 22	2.7 / 24	1.2 / 23	0.64 / 21	0.22 / 18

Table 9. Latitudinal average of the peak pressures (±1 standard deviation) of the weighting functions for the T-2 channels. Units are hPa.

T-2 Channel [GHz]	0 - 20°	20 - 40°	40 - 60°	60 - 90°	Total
91	942 ± 69	861 ± 100	924 ± 50	964 ± 22	913 ± 81
150	861 ± 83	830 ± 90	913 ± 55	952 ± 40	887 ± 86
183 ± 7	630 ± 92	661 ± 90	748 ± 73	825 ± 85	719 ± 110
183 ± 3	485 ± 54	541 ± 79	637 ± 99	678 ± 104	599 ± 113
183 ± 1	368 ± 50	409 ± 82	475 ± 131	522 ± 160	453 ± 134

2.10 Effects of Clouds and Precipitation on the Calibration

Since one flight during TOGA-COARE flew primarily over and around a tropical cyclone, the degree of inhomogeneity in the scattering of the microwave energy by clouds and convection became a concern for the calibration study since the MIR has a much finer resolution than the T-2. Clouds have been detected using various satellite sensors; however, the calibration effort forced limitations on the data available for these cloud identification schemes. Geostationary satellite imagery were not obtained to identify clouds during the TOGA-COARE flights; however, GOES imagery was obtained for the east and west coast CALVAL flights. It was felt that the smoothed and time-patched Satellite Global Data Base (SGDB) data generated at AFGWC could not provide accurate determination of real-time cloud cover due to the uncertainty of the time of the data.

Additional sensors on board the DMSP satellites can be used to identify clouds, but their utility for the calibration effort was limited. Co-located SSM/T-1 data could be used to identify the presence of clouds over water, but at a much coarser resolution than the T-2 data. A cloud amount algorithm using SSM/I data (Hollinger, 1991) was developed for the presence of clouds over land. However, the T-2 calibration concentrated most of the effort over ocean surfaces due to the enhanced contrast between the atmospheric emissions and the surface for the T-2 T_bs. The cloud liquid water (CLW) algorithm using SSM/I imagery over water surfaces (Hollinger, 1991) was evaluated to see if the presence of clouds could be determined. GOES cloud data coincident with the east and west coast CALVAL flights (May and July/August, 1992) indicated that the CLW value did not consistently go to zero when no clouds were observed within the T-2 FOV. Therefore, the effects of clouds on the calibration of the T-2 channels was only examined using the east and west coast CALVAL data co-located with GOES visible imagery.

The occurrence of rain within the T-2 FOVs was identified using co-located SSM/I sensor data. The rain rate algorithm developed by Hollinger (1991) was used to identify the occurrence of precipitation as well as the intensity of rain, both over land and ocean. The rain rate algorithm is not valid for coastal FOVs. Rain was not observed during the west coast CALVAL flights and was associated only with frontal activity on the east coast of August 6, 1992. Rain was observed during both CALVAL flights of TOGA-COARE.

Since the SSM/I FOVs were measured at a finer increment than the T-2 FOVs (Table 10), the SSM/I T_bs and rain rate values were averaged within each T-2 FOV. An SSM/I FOV was determined to be co-located with a T-2 FOV when the center of the SSM/I FOV was within the elliptical T-2 FOV. The limitations of co-locating SSM/I imagery with T-2 data included merging FOVs that were not identical in size and shape and that had different scan geometries (conical versus cross-track). However, the co-located data appeared to provide some valuable insight about the environment being probed. Two SSM/I data sets were generated for each F-11 pass: one for the low resolution data (19, 22 and 37 GHz) and one for the higher resolution data (85 GHz). If the co-located SSM/I T_bs were indicative of rain, then the retrieved rain rate was used to calculate the mean, standard deviation, maximum and minimum values for the T-2 FOV. Therefore, it was possible to quantify the percent of rain occurring within each T-2 FOV.

Table 10. Instrument beam characteristics for the microwave sensors on board the F-11 satellite.

Microwave Sensor	Channel Frequencies [GHz]	Subtrack FOV Diameter [km]		Subtrack FOV Spacing [km]
		Along Track	Cross Track	
SSM/I	19 V&H	69	43	25
SSM/I	22 V	50	40	25
SSM/I	37 V&H	37	29	25
SSM/I	85 V&H	15	13	12.5
SSM/T-1	50.5, 53.2, 54.35, 54.9, 58.4, 58.825 & 59.4	214		177
T-2	91	84		44
T-2	150	54		44
T-2	183±7, 3 & 1	48		44

The presence of rain (strictly convective in all cases observed by the MIR) often caused a significant amount of variance of the MIR measurements at all frequencies within the SSM/T-2 FOV (Figure 10), which suggested that the scale of the inhomogeneity of the rain's effect was quite fine. There were no consistent trends observed that indicated when and if large variances occurred within an T-2 FOV due to the influence of rain; although, the differences between the mean MIR T_bs and co-located T-2 T_bs were considerably larger than for non-precipitating conditions (Figure 18 and Table 11).

Table 11. RMS difference and bias between the mean of the co-located MIR T_bs and the observed T-2 T_bs from the TOGA-COARE flights. Rain rates were determined from algorithms using co-located SSM/I T_bs. Values are given in K, and number of cases enclosed in parentheses. There were no land topography cases.

T-2 FOV TOPOGRAPHY	91 GHz	150 GHz	183±7 GHz	183±3 GHz	183±1 GHz
WATER No Precip	1.7 / -1.2 (18)	1.2 / 0.5 (15)	0.8 / 0.3 (13)	0.9 / 0.3 (13)	1.3 / 0.8 (13)
WATER 0-1 mm/hr Precip	5.9 / -1.8 (32)	10.0 / 1.8 (21)	11.0 / -4.1 (18)	8.0 / -3.1 (18)	4.3 / -1.7 (18)
WATER 1-4 mm/hr Precip	13.4 / -10.0 (12)	36.7 / -25.4 (9)	36.0 / -30.6 (7)	29.5 / -25.4 (7)	19.5 / -15.0 (7)
WATER >4 mm/hr Precip	24.1 / -21.7 (5)	29.0 / -25.8 (4)	27.0 / -20.7 (4)	27.8 / -20.1 (4)	23.5 / -15.8 (4)
COAST	5.7 / -0.8 (22)	6.0 / 3.1 (13)	3.2 / 1.5 (11)	1.6 / 0.3 (11)	1.0 / 0.5 (11)

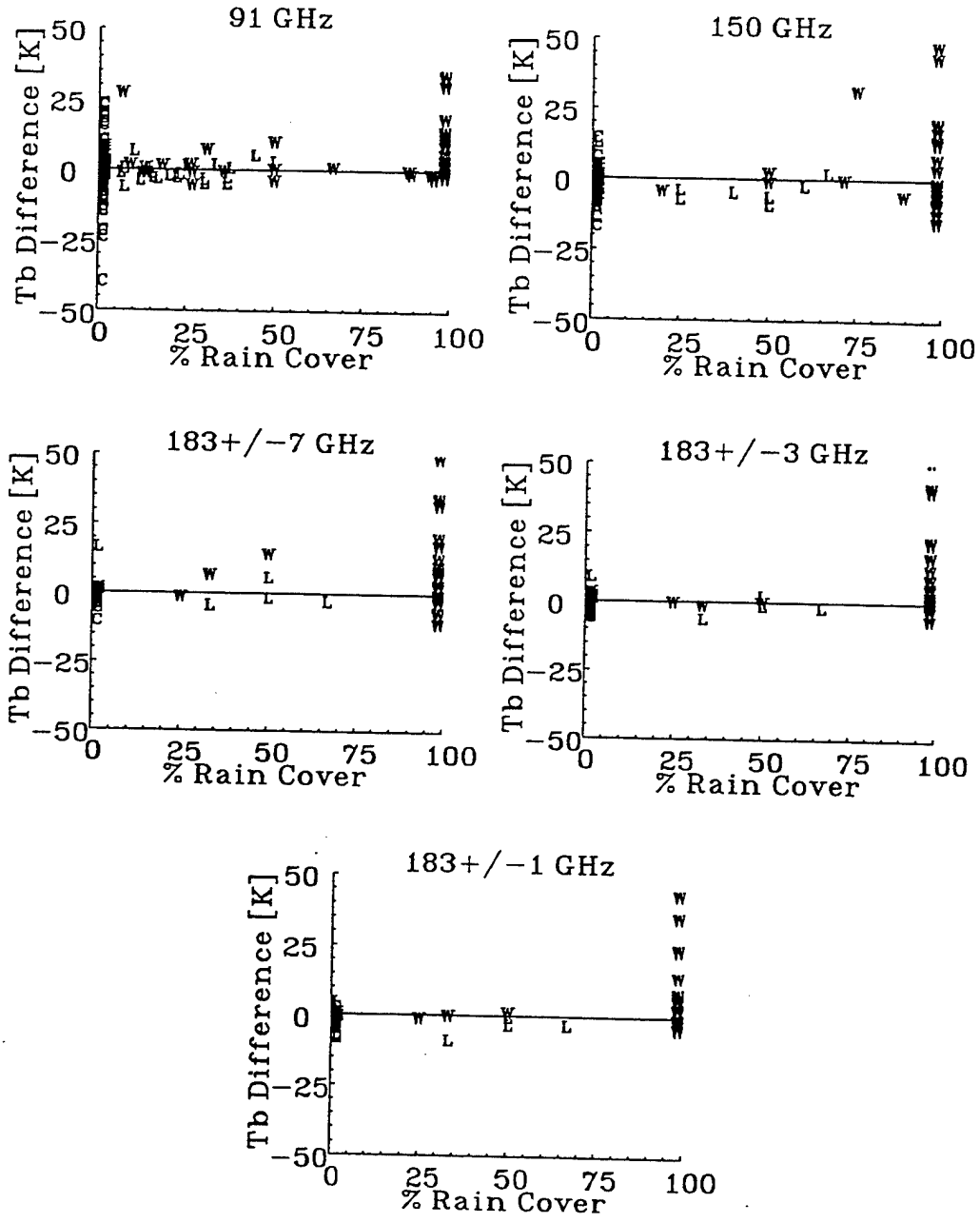

Figure 17. The effect of fractional precipitation on the range of the MIR T_bs for the T-2 channels. Data included TOGA-COARE and the east and west coast CALVAL flights. MIR data were limited to ±1 hour of the time of the SSM/T-2 observations and to only those which had the same scan angle as the co-located T-2 data. The topography of the T-2 FOVs is land = L, water = W, and coastal = C.

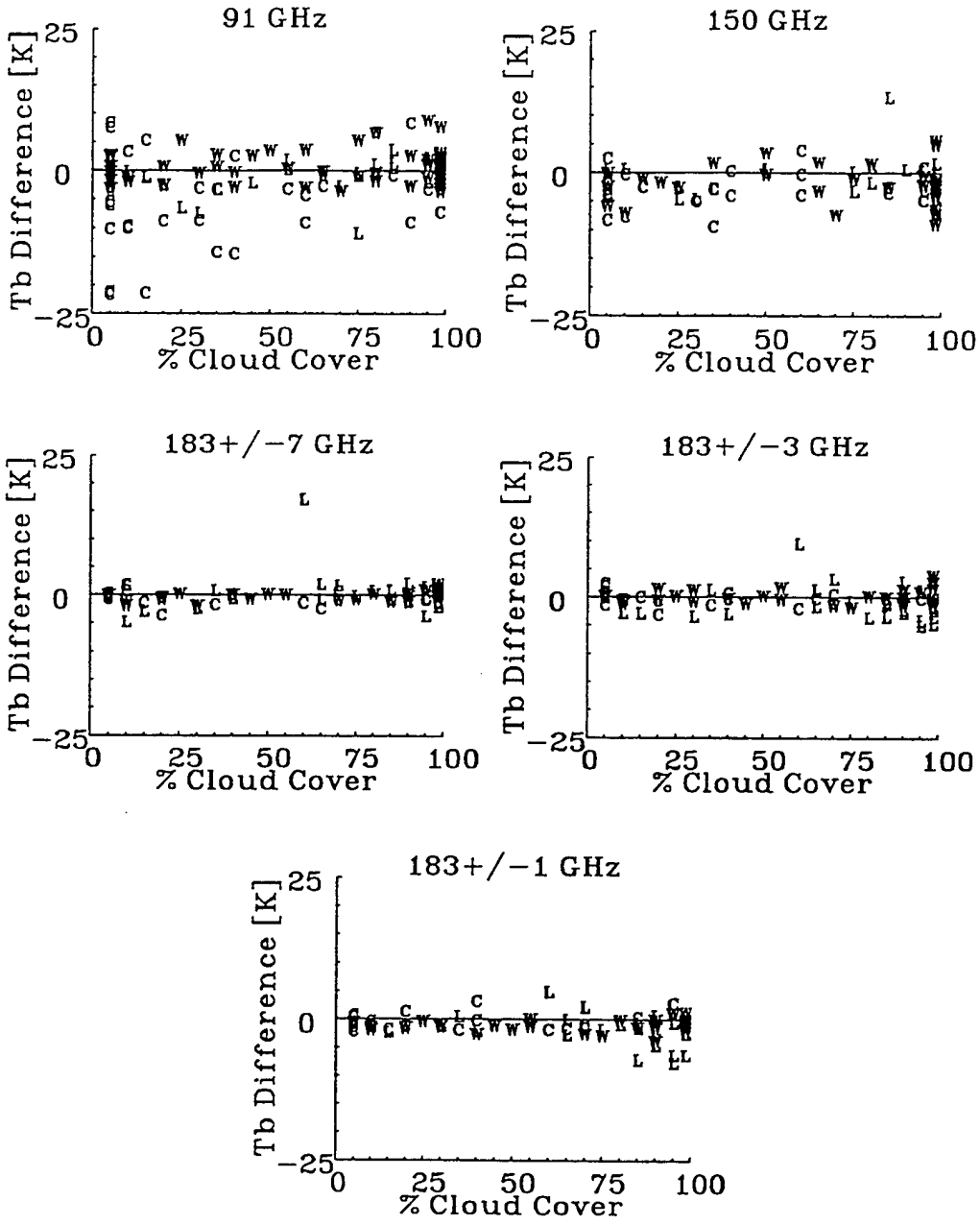

Min/Max Cloud Gray Shade = 0, 256

Figure 18. The effect of fractional precipitation on the difference between co-located mean MIR and T-2 T_bs for the T-2 channels. Same criteria and data base as Figure 17.

After precipitation was identified, the effects of non-precipitating clouds were studied. The variance of the MIR measurements within the T-2 FOV (Figure 19) appeared to be unrelated to the presence of non-precipitating clouds, nor did the difference between the mean MIR T_bs and co-located T-2 T_bs increase compared to clear cases (Figure 20 and Table 12).

Table 12. RMS differences for the co-located mean MIR and T-2 T_b measurements given for topographic type, T-2 channel and flight. Values are given in K. The "All" parameter indicates all 5 flights (2 along the west coast and 3 along the east coast) were used in the calculation.

Flights	Topo	91 GHz	150 GHz	183±7 GHz	183±3 GHz	183±1 GHz
West Coast	Water	3.4	2.4	0.7	0.8	1.3
East Coast	Water	3.7	3.6	1.2	2.1	1.2
All	Water	3.5	3.1	1.0	1.6	1.2
All *	Water	4.1	3.5	0.9	1.6	1.0
All	Coast	10.4	4.3	1.5	2.1	1.7
All	Land	3.9	3.9	3.4	2.8	2.8
All	All	3.8	3.8	2.0	2.1	1.9

* Only T-2 FOVs with 0 - 20% visible cloud coverage were used.

2.11 Representativeness of the Calibration Results

One concern of the calibration effort was whether the data were representative of the global conditions that will be measured by the sensor. Some basic statistics were calculated for various data bases of T-2 T_bs in order to compare the representative nature of each. The mean, standard deviation and range of T-2 channel T_bs sampled by the aircraft calibration study (7 total flights; two on the west coast, three on the east coast and two in the western Pacific), by the co-located radiosonde - T-2 pairs, and during 7 satellite orbits are listed in Table 13. The east and west coast calibration sites were biased toward mid-latitude climates collected during the spring and summer seasons over both land and ocean surfaces; the TOGA-COARE data represented tropical conditions predominantly over ocean. The radiosonde data was strongly weighted toward land sites. The means, standard deviations and ranges differed markedly between these two CALVAL data sets. Since the aircraft data contained a larger proportion of data collected over the ocean, the mean T_b for 91 GHz is much cooler than that observed for the land-biased radiosonde data set. The overall ranges for the orbital data set were quite large (>100 K). An effort was made to identify where many of the T_b anomalies occurred. One environment that produced many T_bs that fell outside of the CALVAL ranges was polar regions.

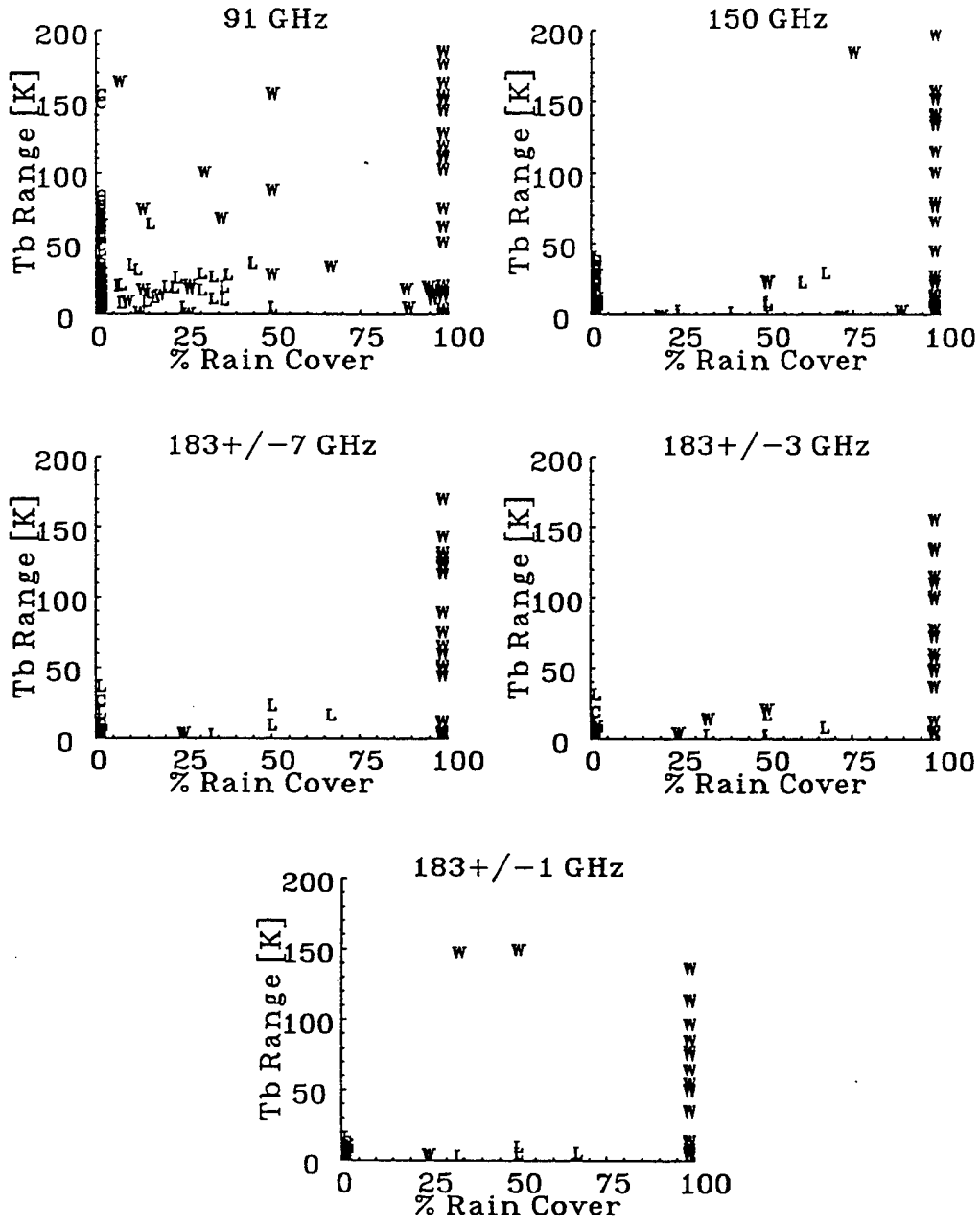

Figure 19. The effect of fractional non-precipitating cloud cover on the range of the MIR T_bs for the T-2 channels. Same criteria and data base as Figure 17.

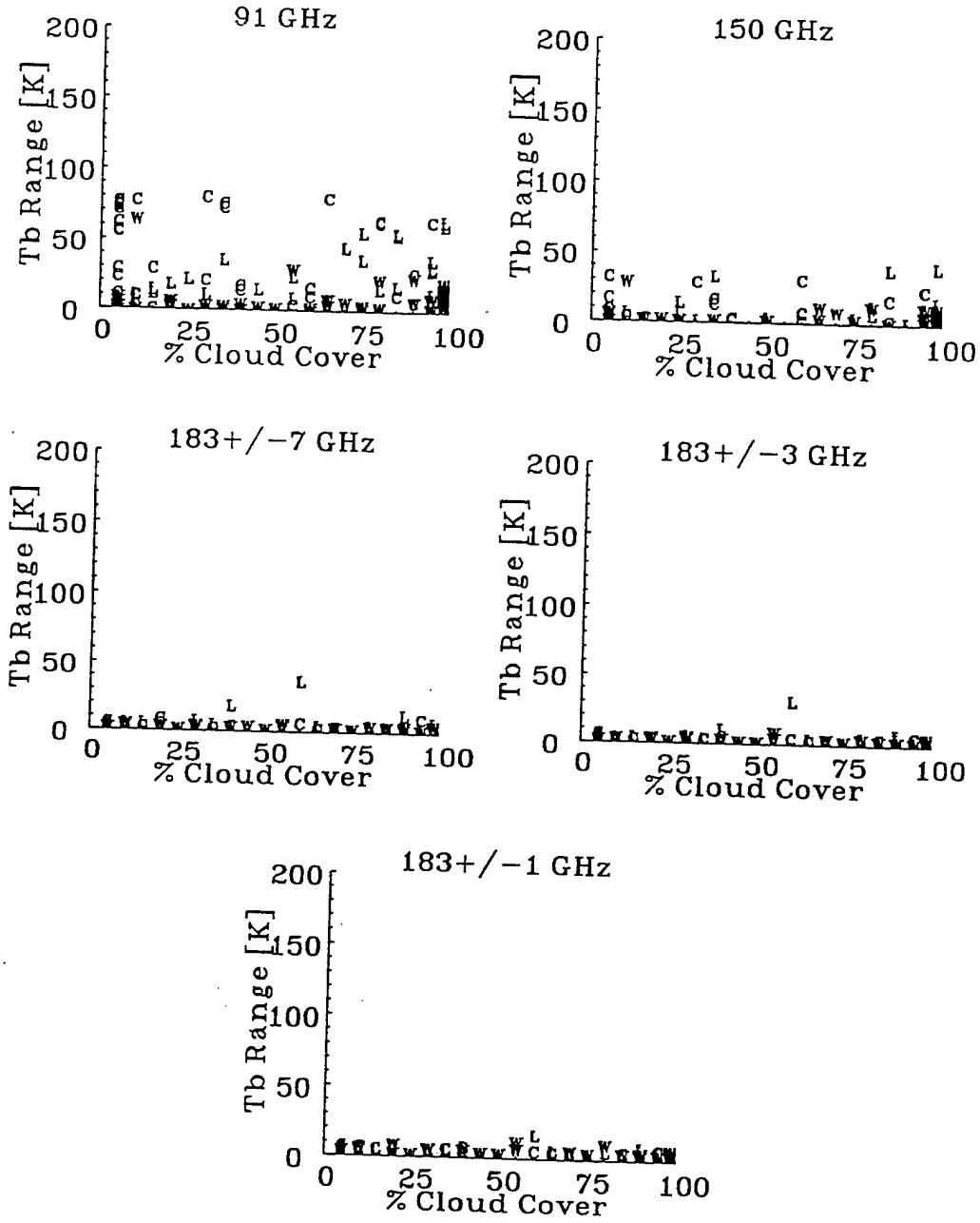

Figure 20. The effect of fractional non-precipitating cloud cover on the difference between co-located mean MIR and T-2 T_bs for the T-2 channels. Same criteria and data base as Figure 17.

Table 13. Mean, standard deviation and range of T-2 T_bs (K) sampled by the co-located MIR data set (319 cases), the co-located radiosonde data set (2157 cases), and a set of 7 orbits of the satellite (> 90,000 T-2 FOVs).

T-2 Channel [GHz]	MIR			Radiosonde			7 satellite orbits		
	Mean	St. Dev.	Range	Mean	St. Dev.	Range	Mean	St. Dev.	Range
91	244.4	27.7	88.2	257.9	26.0	133.0	233.4	29.7	140.7
150	265.3	21.2	123.7	264.7	25.8	139.2	252.1	32.0	132.8
183±7	270.2	21.5	130.6	265.3	15.7	107.9	260.2	24.8	135.9
183±3	260.7	18.1	113.4	258.4	9.6	83.8	255.6	16.6	149.4
183±1	247.7	13.6	83.9	247.6	7.6	65.4	246.4	10.7	170.6

2.12 Comparison of Co-located SSM/T-2 and SSM/I Results

An initial comparison of the total precipitable water (TPW) retrieved using the T-2 and the Special Sensor Microwave Imager (SSM/I) T_bs. The F-11 satellite carried both the T-2 and the SSM/I. The SSM/I, a seven channel passive radiometer, was first flown on the DMSP F-8 in June 1987. This instrument and algorithms which relate water-based meteorological parameters to the SSM/I frequencies, is completely described by Hollinger et al. (1987). The TPW algorithm, developed for this system by Alishouse et al. (1990) was based on a statistical comparison of T_b with integrated humidity from the radiosonde measurements and is only valid over water. This algorithm gave an RMS difference of 2.4 kg/m^2 when compared with radiosonde data. An initial method for estimating water vapor profiles based on the 183 GHz water vapor absorption line was proposed by Rosenkranz et al. (1982). Later, a D-matrix algorithm was developed by Aerojet Electronic Systems Division based on this method. The D-matrix produces specific humidity and water vapor mass estimates at the mandatory levels. Data from four separate days were used, two along the U.S. west coast (14 and 15 May 1992) and two along the east coast (29 July and 6 August 1992).

Since cloud conditions affected the response of both the T-2 and the SSM/I, the data were stratified according to cloud amount. The following procedure was used: (a) Visible images from the GOES satellite corresponding to the T-2 overpass of the regions studied were obtained. (b) A threshold gray shade (mask), subjectively selected, was used to define cloudy and clear portions of the GOES image. (c) FOVs for each of the 28 footprints in an T-2 scan were remapped on the GOES image. (d) The number of cloud pixels versus the clear pixels in each elliptical T-2 FOV were used to define the percent cloudiness for that footprint. This procedure was followed for each of the FOVs defined by the 183 GHz, 150 GHz, and 90 GHz channels. It was clear from the observations, that low stratus clouds were predominant on the west coast, while several types of clouds occurred along the east coast.

A set of TPW(SSM/I) values were calculated using SSM/I data located within the T-2 FOV. Since the spacing of SSM/I FOVs is considerably smaller than the T-2's, the mean and standard deviation of TPWs that fell within the ellipse of each T-2 FOV were determined. These mean values were compared with TPW(T-2) values. The data set was limited to ocean classified and nonprecipitating T-2 FOVs. The distribution of data as a function of estimated cloudiness are shown in Table 14.

Table 14. RMS difference, bias and standard deviation between TPW values determined using SSM/I and T-2 data. Units are kg/m^2.

Percent Visible Cloud	RMS	BIAS	Standard Deviation
0 - 10	2.7	2.3	1.4
10 - 20	3.2	2.3	2.2
20 - 30	2.8	2.1	1.9
30 - 40	3.4	2.1	2.7
40 - 50	3.2	2.1	2.4
50 - 60	4.0	1.9	3.5
60 - 70	4.1	2.9	2.9
70 - 80	3.1	0.8	3.0
80 - 90	1.7	0.3	1.7
90 - 100	3.9	1.3	3.7
TOTAL	3.4	1.7	2.9

Comparison of TPW's from satellite with values calculated from radiosondes required that the two data sources meet a co-location criteria defined by the close proximity of the radiosonde observation in time and space to a T-2 footprint. Eight stations located on islands or along coasts met the criteria of this study and a small sample of 31 cases were compared. The results of this analysis are shown Table 15. Although the sample size for this comparison was small, and included both low and high cloudiness cases, the RMS values compared well with both TPW algorithms.

Table 15. RMS difference, bias and standard deviation between TPW values calculated using co-located radiosonde profiles and SSM/I and T-2 T_bs. Units are kg/m^2.

	TPW (SSM/I - RAOB)	TPW (T-2 - RAOB)
RMS	4.2	3.9
BIAS	1.6	1.2
St. Dev	3.9	3.7

Results from both retrievals were generally within 20% of each other, regardless of air mass type and amount of cloudiness. Increased cloudiness introduced scatter in the comparisons; however, the overall trend was not affected. The SSM/I TPW algorithm included an adjustment for clouds but was not valid in rain conditions. The T-2 algorithm, despite not explicitly dealing with clouds, was not significantly influenced by cloud fraction for the CLW amounts in the sample set. The bias between the two retrievals indicate that either the TPW values based on SSM/I data overestimates the actual moisture content, or the T-2 retrievals underestimate the total water vapor mass. Comparison with the small amount of radiosonde data, while not resolving this question, tended to confirm the quality of both sets of satellite measurements.

3. RADIOSONDE CALIBRATION RESULTS

A global set of satellite data including T-2 T_bs and co-located radiosonde data were provided by Bruce Thomas of the Aerospace Corporation. Initial data were from 31 January to 7 March 1992. A second set of data represented 14 to 16 May 1992. Unfortunately, the data base was reduced due to a number of problems: (a) data were not saved if model input were missing - so roughly the first week and a half of data were eliminated, and (b) due to tape problems, the following two and a half weeks were not available. Therefore, only the data saved during the first week in March were consistent.

After the initial quality control of the data, programs were created to merge the data bases. Soundings were limited to those with moisture measurements extending up to at least 300 hPa and dewpoint depressions greater than 0 K and not equal to 30 K for the sounding between the surface and 300 hPa. Upper-air moisture climatology modeled after the work by Oltmans (1985) was supplied from the top of the radiosonde moisture profile to 0.1 hPa. An isothermal temperature profile was assumed from the top of the temperature sounding to 0.1 hPa. This upper-air climatology did not significantly affect the forward-calculated T_bs since the weighting functions for T-2 sensor channels peak at pressures greater than 300 hPa (Table 16). The resulting global set of 1601 radiosondes provided a wide range of realistic temperature and moisture profiles (see Table 17 for a statistical description of the data set), although this data was biased toward land cases. The radiosonde data were co-located with the T-2 data using the following criteria: ±1 hour between the release of the radiosonde and the time of the T-2 measurement and ±100 km between the radiosonde station location and the center of the T-2 FOV. The distribution of the co-located radiosonde/T-2 data was then examined. The data base processing procedure is summarized in Figure 21.

RT simulations of T-2 T_bs were performed using: (a) the RADTRAN computer code which was developed by the Air Force Phillips Laboratory, Geophysics Directorate (PL/GP) (Falcone et al., 1979, 1982), and (b) the Eyre microwave simulation model (Eyre and Woolf, 1988). The RADTRAN code has been utilized and tested against experimental data for frequencies up to 1000 GHz. RADTRAN provides atmospheric attenuation and brightness temperature calculations for typical atmospheric paths over the frequency range from 1 to 300 GHz. The version used in these simulations was the enhanced RADTRAN computer code which has been widely applied within the DoD and elsewhere to provide the capability to perform sensor simulation studies for satellite borne and ground based microwave and millimeter wave systems (Isaacs et al., 1989).

Table 16. Global average of the peak pressures (±1 standard deviation) of the weighting functions for the T-2 channels.

SSM/T-2 Channel [GHz]	Pressure [hPa]
91	913 ± 81
150	887 ± 86
183±7	719 ± 110
183±3	599 ± 113
183±1	453 ± 134

Table 17. The latitudinal mean ± standard deviation of the mixing ratio and relative humidity at 6 mandatory pressure levels based on the global set of radiosondes used in the T-2 calibration study.

	Mean ± 1 Standard Deviation of Relative Humidity [%]					
Latitude	1000 hPa	850 hPa	700 hPa	500 hPa	400 hPa	300 hPa
70 - 90	78 ± 12	69 ± 20	58 ± 22	52 ± 20	49 ± 20	44 ± 20
60 - 70	62 ± 19	65 ± 20	54 ± 25	48 ± 22	46 ± 20	42 ± 18
50 - 60	66 ± 18	61 ± 21	57 ± 24	48 ± 23	45 ± 20	44 ± 17
40 - 50	66 ± 16	56 ± 24	56 ± 25	49 ± 24	45 ± 20	40 ± 17
30 - 40	75 ± 21	65 ± 23	62 ± 25	54 ± 23	50 ± 21	48 ± 17
20 - 30	79 ± 19	67 ± 22	62 ± 21	51 ± 23	45 ± 20	42 ± 18
10 - 20	77 ± 15	67 ± 20	58 ± 19	51 ± 24	47 ± 23	46 ± 18
0 - 10	83 ± 11	74 ± 14	69 ± 20	60 ± 23	49 ± 24	39 ± 20
TOTAL	72 ± 19	63 ± 22	59 ± 24	51 ± 23	47 ± 21	43 ± 18
	Mean ± 1 Standard Deviation of Mixing Ratio [gm/kg]					
Latitude	1000 hPa	850 hPa	700 hPa	500 hPa	400 hPa	300 hPa
70 - 90	2.3 ± 1.6	1.7 ± 1.3	1.1 ± 0.8	0.4 ± 0.3	0.17 ± .15	0.05 ± .05
60 - 70	3.3 ± 2.5	2.5 ± 1.8	1.4 ± 1.1	0.5 ± 0.5	0.25 ± .25	0.08 ± .14
50 - 60	4.7 ± 2.7	3.8 ± 2.4	2.2 ± 1.6	0.7 ± 0.6	0.33 ± .26	0.10 ± .09
40 - 50	5.7 ± 3.1	4.6 ± 2.5	2.9 ± 1.7	1.0 ± 0.7	0.41 ± .32	0.11 ± .10
30 - 40	10.4 ± 4.9	7.0 ± 3.5	4.2 ± 2.3	1.6 ± 1.1	0.69 ± .60	0.22 ± .20
20 - 30	15.9 ± 4.0	10.2 ± 3.5	6.2 ± 2.5	2.5 ± 1.4	1.20 ± .79	0.42 ± .28
10 - 20	17.5 ± 2.9	11.1 ± 3.0	6.6 ± 2.2	2.7 ± 1.3	1.34 ± .74	0.44 ± .23
0 - 10	17.4 ± 2.0	11.5 ± 2.4	7.1 ± 2.0	3.1 ± 1.2	1.47 ± .91	0.41 ± .24
TOTAL	9.4 ± 6.8	6.0 ± 4.2	3.6 ± 2.7	1.3 ± 1.2	0.60 ±. 64	0.19 ± .22

The Eyre simulation model is an accurate "rapid algorithm" model for the desired spectral region required using an exact line-by-line RT simulation model as a driver. The approach is described by Eyre and Woolf (1988) and is similar to that employed by NOAA / NESDIS to model passive infrared temperature channel transmittances (Fleming and McMillin, 1977). In the microwave spectral region, the rapid algorithm results in a computational savings of at least 50 times over the line-by-line method using a preselected set of microwave lines only. Accuracy of the desired band model is variable by a certainty of 1% or less. Using the global set of radiosondes, the enhanced RADTRAN and the Eyre model produced an RMS T_b difference of 1 K at 183±3 GHz for 1169 radiosondes with TPWs ranging from 10 to 90 kg/m^2; therefore, the computationally faster band model was used in the following analyses.

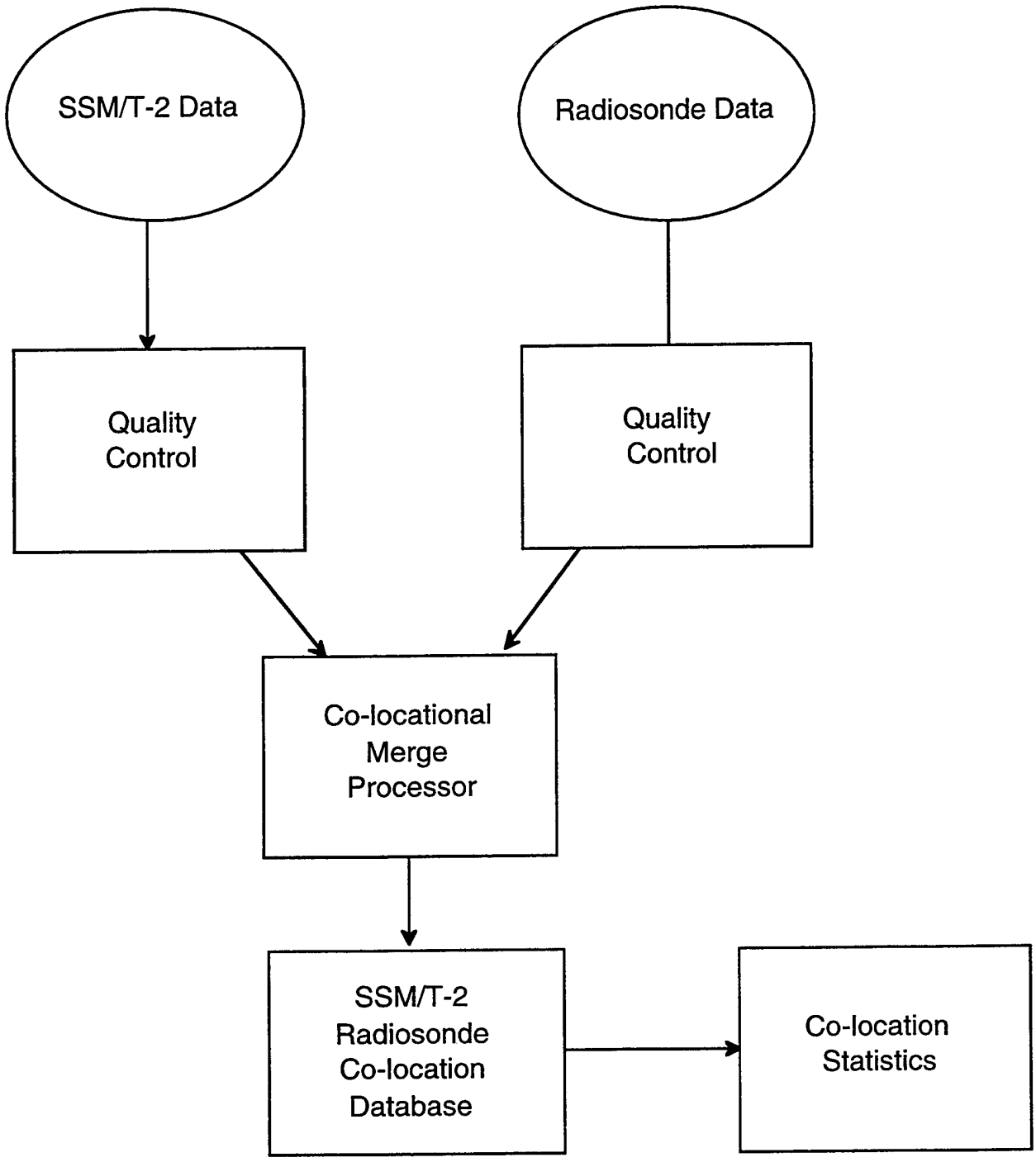

Figure 21. T-2 - radiosonde co-location processing flowchart.

The results of the intercomparison for an ensemble of 1601 T-2 T_bs and co-located radiosonde profiles is shown in Table 18. There was fair agreement of RT calculated T_bs and observed satellite data. To define an appropriate surface emissivity for these observations, the Eyre RT model was modified to iteratively retrieve the best surface emissivities for 1601 stations using the co-located upper air data to supply information on atmospheric profiles. The distributions of the surface emissivities for the 91 and 150 GHz channels were quite reasonable compared to surface emissivity models over land and water at these frequencies. For each T-2 channel, the mean surface emissivities for land-, coast- and water-classified terrains were then used in the Eyre model calculations. Discrepancies remained for the window channels which see the surface due to the degree of variability of surface emissivities. Other sources of discrepancies between the forward calculated and the satellite-measured T_bs were the lack of consideration of clouds and/or precipitation within the RT model, uncertainties of low RH radiosonde measurements, varying abilities of the different types of radiosonde instruments to measure temperature and moisture, different reporting procedures of radiosonde data used by different countries (Garand et al., 1992), and the addition of estimated high altitude (> 300 hPa) moisture data for input into the RT models. Interestingly, the differences between the forward-calculated and observed 183 GHz T_bs were similar to the average variation of co-located MIR T_bs within elliptical T-2 FOVs. This suggests that using point sources for calibration cannot be used to calibrate a satellite sensor with a relatively large footprint.

The sounding data came from many different types of radiosonde instruments. These sonde instruments have been shown to have both random and bias differences when flown on the same balloon (Nash and Schmidlin, 1987; and Schmidlin, 1988). Radiosonde system differences did indeed contribute to the overall scatter of the data between the observed and calculated T_bs. In the global data for 183±7 GHz, there was a significant group of relatively moist data around the computed 270 K which bulges out to the left of the calculated/observed line. Combined data from the United States and India contributed over 60% of the points to this feature. Whereas combined data from Scandinavia, England, Germany and Russia contributed only one point to this anomaly. This was one example demonstrating the differences due to various types of radiosondes. The problems associated with using a worldwide radiosonde data base to either calibrate a satellite system or to act as the basis of an empirical fit are complex due to the many sources of error which corrupt such a data base.

Table 18. RMS difference and bias between the calculated T_bs generated by the Eyre RT simulation model using a global set of radiosondes and co-located T-2 T_bs at the T-2 channels. Bias was based on T-2 T_bs - co-located Eyre-calculated T_bs. Co-location criteria were ±1 hour and ±100 km.

Precipitable Water [kg/m^2]	91 GHz	150 GHz	183±7GHz	183±3GHz	183±1GHz
0 - 10	18.5 / 6.4	16.4 / 6.5	10.3 / 4.4	5.9 / 0.0	5.3 / -1.4
10 - 20	22.6 / 15.4	13.5 / 9.1	4.5 / -0.4	4.0 / -0.7	5.6 / -0.8
20 - 30	20.9 / 13.8	9.1 / 3.8	5.9 / -1.7	4.9 / -0.6	6.6 / 0.9
30 - 40	17.2 / 5.8	9.0 / -0.8	8.8 / -2.1	7.4 / -0.7	8.8 / 1.3
40 - 50	13.6 / -4.0	10.3 / -3.3	8.3 / -3.3	6.0 / -2.2	6.6 / -0.2
50 - 60	12.3 / -7.0	6.9 / -3.2	6.5 / -2.4	5.7 / -1.2	6.6 / 1.1
60 - 70	10.8 / -4.8	22.2 / -13.6	17.0 / -10.2	12.5 / -4.1	12.5 / 1.7
TOTAL	19.2 / 8.1	12.7 / 4.0	7.8 / -0.2	5.7 / -0.7	6.5 / -0.1

A second technique for examining the possible impact of radiosonde errors on the calculated T_bs was tried. Using the summed errors caused by insolation and thermal lag (Brousaides and Morrissey, 1974) on the ability of radiosondes to measure water vapor at various levels of the atmosphere, maximum correction factors were determined for the pressure levels used in the Eyre RT program up to 300 hPa. These correction factors were used to estimate the moistest profile that the radiosonde could have passed through and still report the observed measurements. Keeping the temperature profile and surface emissivity constant, these moister profiles were used to calculate the changes in T_bs relative to the change in TPW for the T-2 channels. The global set of 1601 radiosondes represented land and coastal stations ranging from tropical to polar climates. These calculations did not take into account weather conditions (rain, clouds, etc.) or the type of radiosonde instrument (AIR, Vaisala, VIZ, etc.). The moister profiles produced up to a 3 K increase in 91 GHz T_bs, a 1 K decrease in 150 GHz T_bs, and generally a 2-3 K decrease in the 183 GHz T_bs. The drier subset of profiles tended to generate smaller positive changes in the 91 GHz T_bs, and larger positive changes in the 150 and 183±7 and ±3 GHz T_bs compared to the moister profiles.

4. RADIATIVE TRANSFER MODELING OF T_b SENSITIVITY

The Eyre model was used with the global set of radiosondes to examine the sensitivity of the T-2 channels to atmospheric moisture and temperature, surface emissivity and temperature, and satellite viewing angle. The general premise was to hold all but one of the variables constant (Table 19 shows the constant and variable values of each parameter) and examine the change in the RT-model-generated T_bs with respect to the TPWs of the original sounding profiles. Note that during parameter modification, if saturation occurred, the moisture at that level was not modified further. Also, the formation of clouds was not considered as saturation was approached. Conversely, the minimum moisture limit was set to 0.003 gm/kg. These restrictions may have produced anomalous moisture modification factors whenever very dry or very moist layers occurred in a region being sensed by a T-2 channel.

Table 19. Values used to examine the sensitivities of the parameters. When a parameter was varied, the other parameters were kept at these constant values.

Parameter	Constant Value	Variable Values
RH Profile	0% Change	±10% Change
Temperature Profile	0 K Change	±1 K Change
Ground Temperature	285 K	290 & 280 K
Surface Emissivity	0.90	0.95 & 0.85
Viewing Angle	0°	0 & 40.5°

4.1 T_b Sensitivity to Atmospheric Water Vapor

Figures 22 and 24 illustrate the varied sensitivities of the T-2 channels to moisture profile modification. These examples were generated from profiles with TPWs of 7.8 and 56.3 kg/m^2, respectively. The relative humidity was modified by a constant percent at all levels resulting in a change in T_b for each channel with respect to the nominal (0% RH change) T_b. In general, when a channel sensed predominantly surface radiation, as with the window channels (91 and 150 GHz), there was a positive relationship between moisture and T_b changes. When a channel sensed predominantly atmospheric moisture contributions (the 183 GHz channels), there

Figure 22. The change in T_b for the T-2 channels as the moisture profile was modified in the RT band model. The original sounding profile had a TPW of 7.8 kg/m^2.

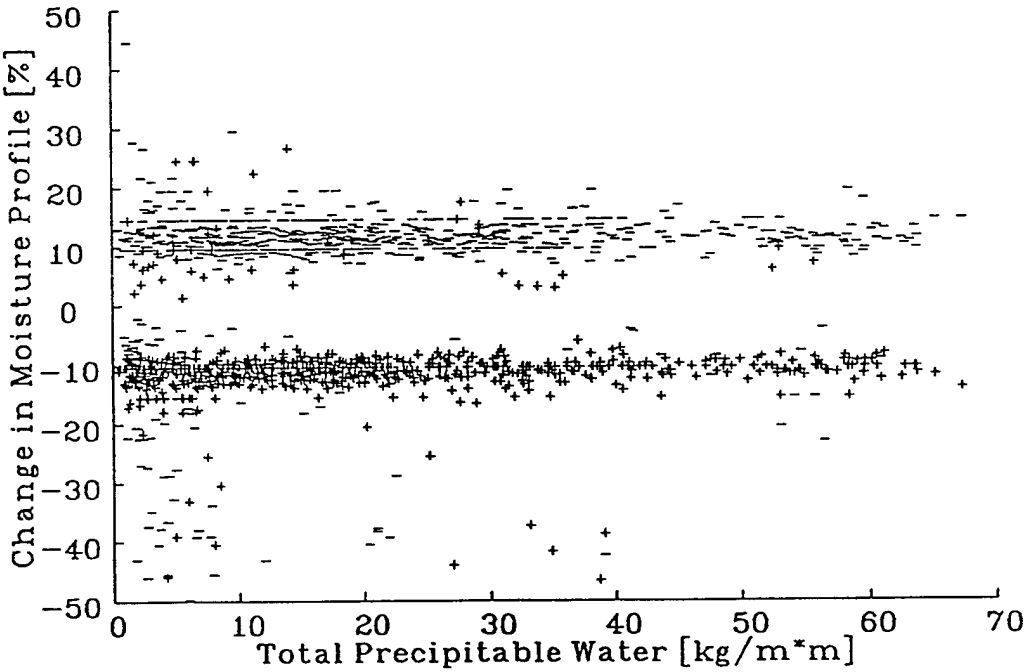

Figure 23. The amount of moisture profile modification required to change the forward-calculated 183±3 GHz T_b by -1 K (- symbols) and by +1 K (+ symbols). The RT bandwidth model used a global distribution of radiosonde temperature and moisture profiles.

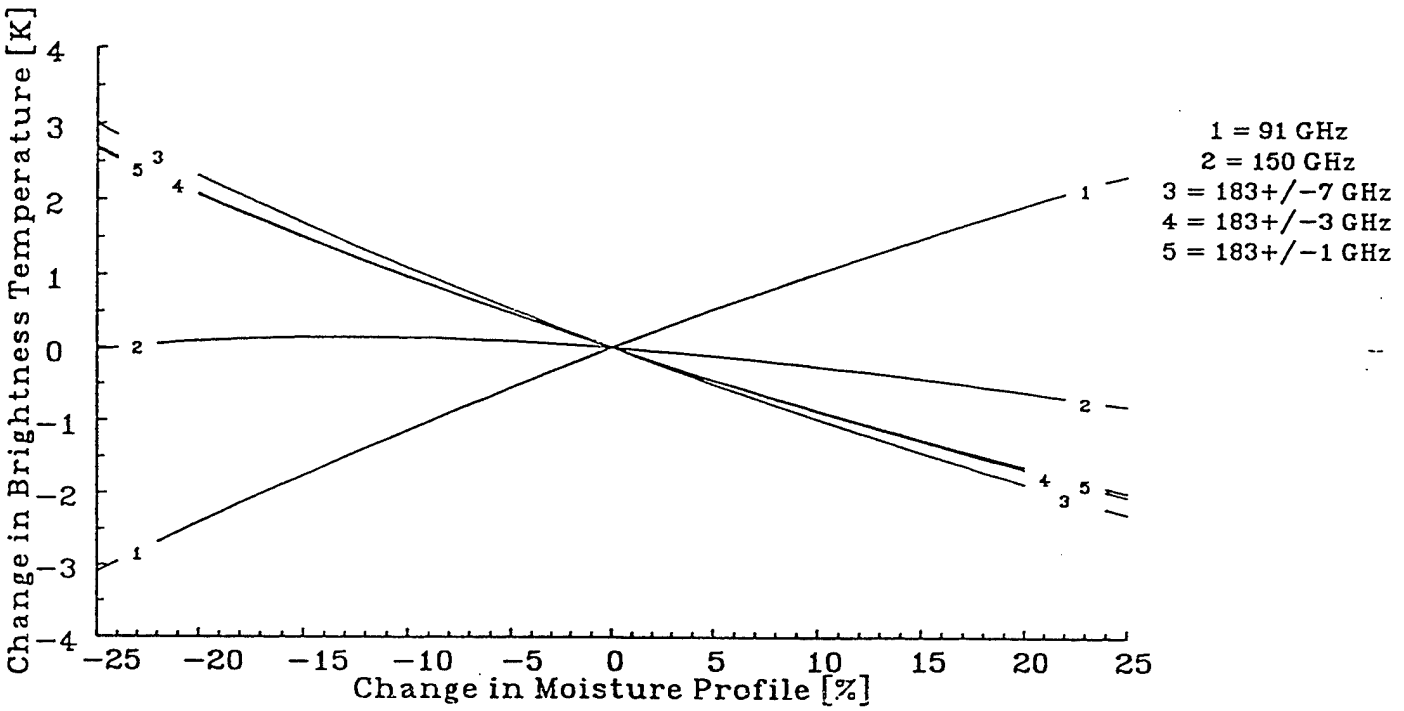

Figure 24. The change in T_b for the T-2 channels as the moisture profile was modified in the RT band model. The original sounding profile had a TPW of 56.3 kg/m^2.

was a negative relationship. A non-monotonic relationship (see 183±7 GHz in Figure 22 and 150 GHz in Figure 24) occurred when the channel sensed significant contributions from both the surface and the atmosphere; as the moisture content decreased, the channel behaved as a window channel, and when the moisture increased, it responded like an atmospheric channel. Even the 183±1 GHz channel sensed the surface in mountainous terrain or extremely dry atmospheres, and, conversely, window channels can had significant atmospheric contributions when the profile was very moist, i.e. in the tropics or at large viewing angles.

With all other parameters held constant, the sensitivities of the overall T_b and its three main components (atmospheric emission, surface emission and surface reflectivity) to varying atmospheric moisture profiles (±10%) were plotted against TPW (Figure 25). The atmospheric and surface emission contributions were quite sensitive to changes in the moisture profiles. The atmospheric channels were more sensitive when the moisture profile was dry, and the window channels were more sensitive when the TPW was large. These components tended to counter one another, producing nominal sensitivity of the overall T_b. For all T-2 channels, there was a distinct limit of T_b sensitivity with a tight grouping of the population along this boundary. However, there was a significant population that did not show any variation with respect to TPW. For the 183±3 and 1 GHz channels, the "noisy" data were a result of the atmospheric emission component, not the surface emission or surface reflectivity terms; however, for the 91, 150 and 183±7 GHz channels, the large scatter was a result of both the atmospheric and surface emission components. This large degree of scattering was not observed in the sensitivity studies to other parameters that follow.

4.1.1 Relating SSM/T-2 T_b Limits to Moisture Retrieval Accuracy

Using the techniques and results of the modeled T_b sensitivity to atmospheric moisture, an attempt was made to quantify the limits of moisture retrievals due to calibration accuracy limits of the T-2 measurements. The moisture profiles were modified by a constant percent change until the forward-calculated T_b changed by the limits of accuracy determined by the calibration study. This accuracy limit was selected to be 1 K (actual values between 0.9 and 1.6 K were observed for the 183±3 GHz channel). The 183±3 GHz channel was used because it was least likely to be influenced by surface radiation and by possible influences of upper-air climatology data and uncertainties in upper-air radiosonde moisture measurements.

Figure 23 shows a scatter diagram of the percent change in moisture profile required to change T_b by ±1 K at 183±3 GHz with respect to TPW in the unmodified radiosonde sounding. Table 20 summarizes the mean, median and standard deviation of the absolute values shown in the figure. A 12% change in the moisture profile was equivalent to a 1 K change in T_b regardless of atmospheric temperature and moisture profiles. This could be said to be the limit of accuracy of the retrieved water vapor profiles since any RMS RH error values below that value would be equivalent to a T_b error value less than 1 K (in the noise of the sensor). Any RMS value greater than 12% would indicate inefficiencies in the retrieval algorithm.

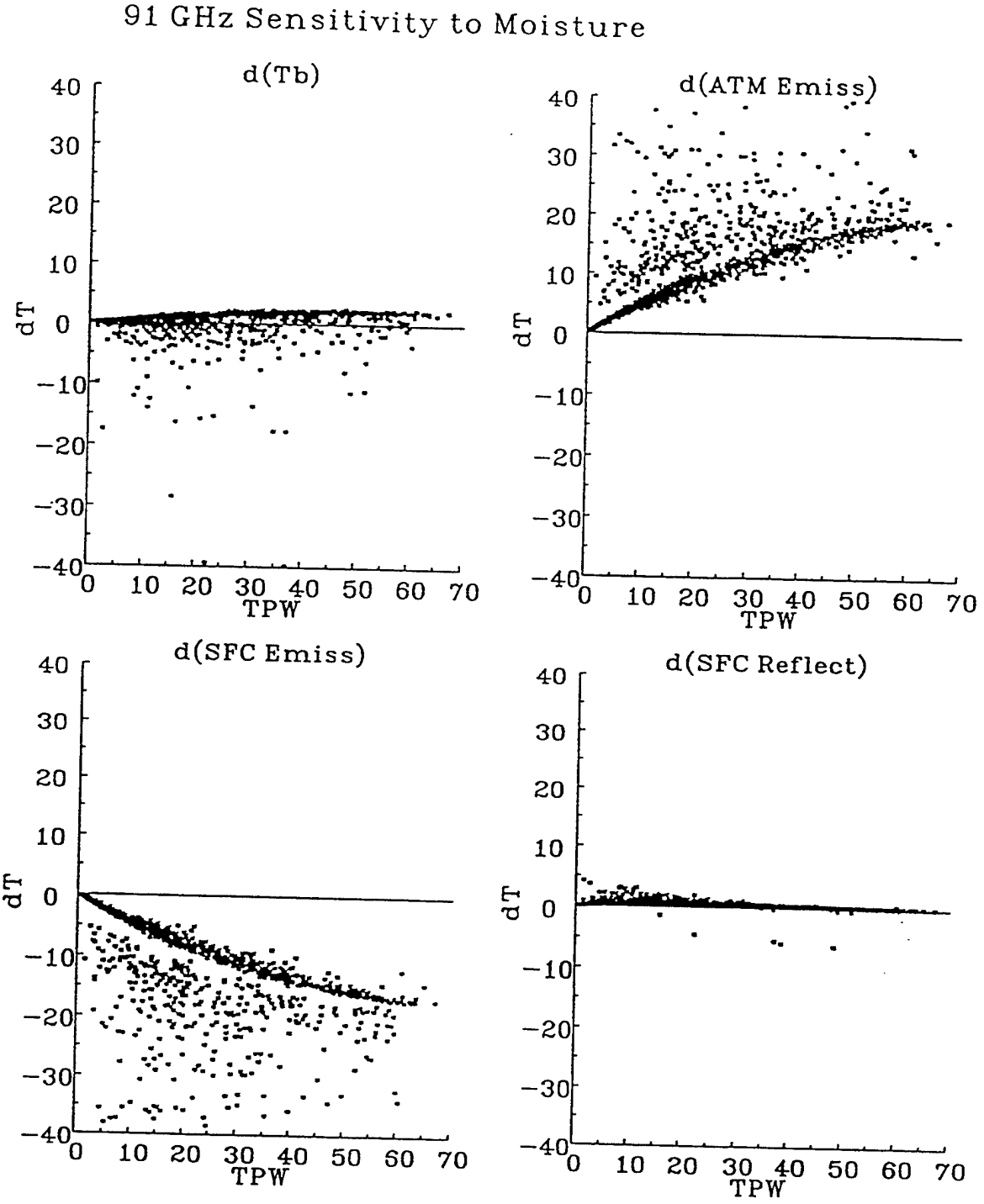

Figure 25. The change in T_b and its three dominant components (atmospheric and surface emissions and surface reflectance) for the T-2 channels as the moisture profile was modified by ±10%. All other parameters were set to constant values.

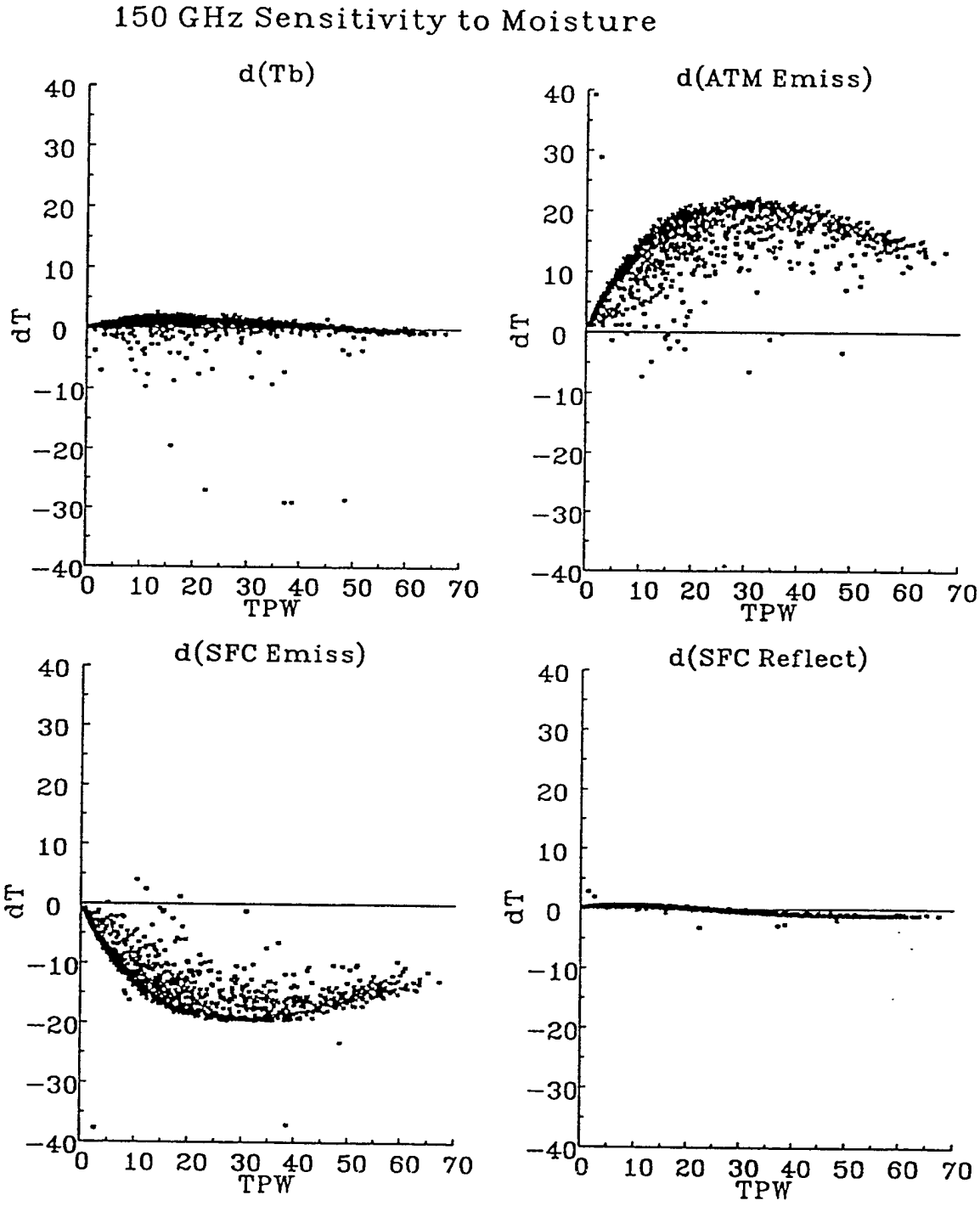

Figure 25. (continued) The change in T_b and its three dominant components (atmospheric and surface emissions and surface reflectance) for the T-2 channels as the moisture profile was modified by ±10%. All other parameters were set to constant values.

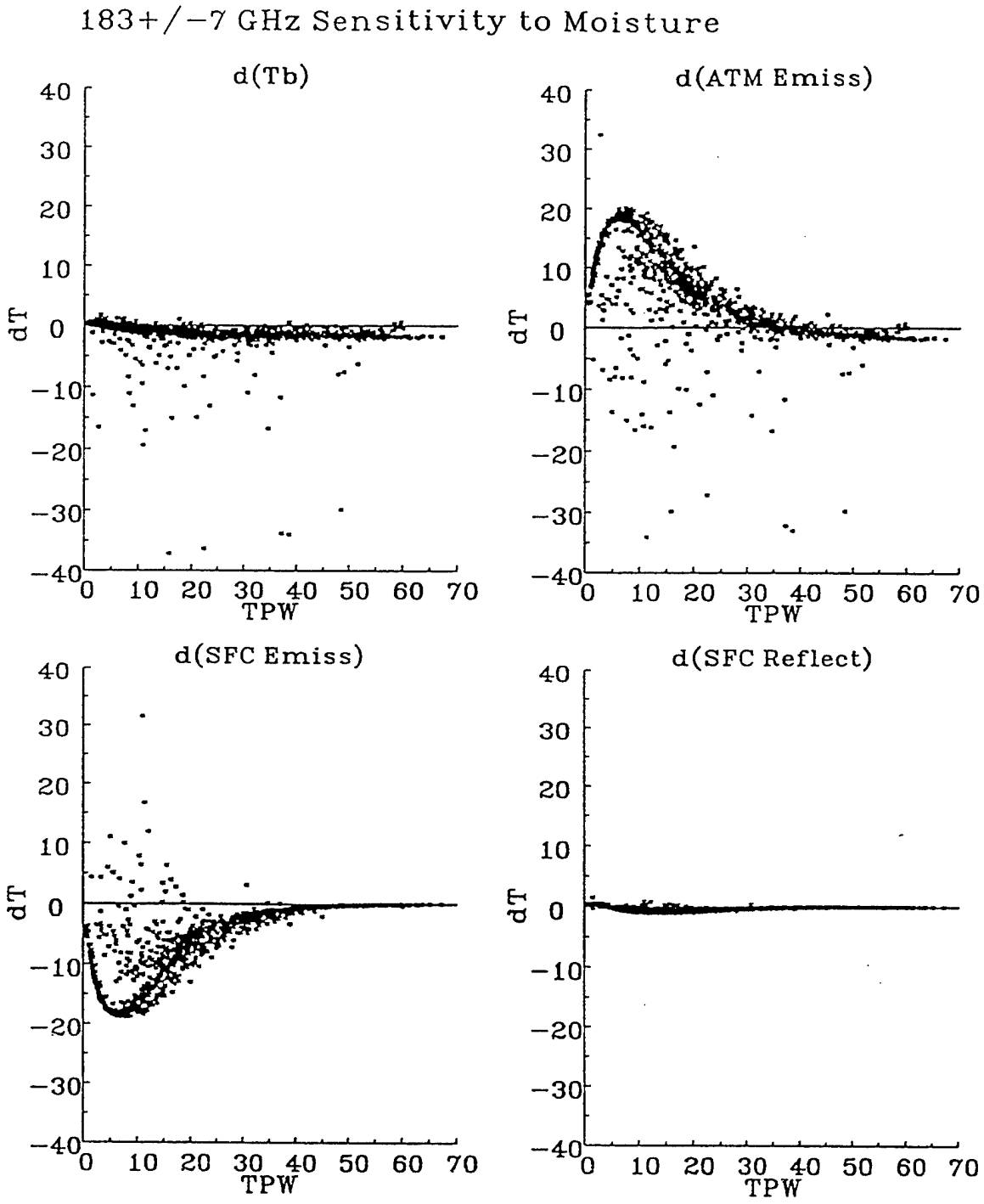

Figure 25. (continued) The change in T_b and its three dominant components (atmospheric and surface emissions and surface reflectance) for the T-2 channels as the moisture profile was modified by ±10%. All other parameters were set to constant values.

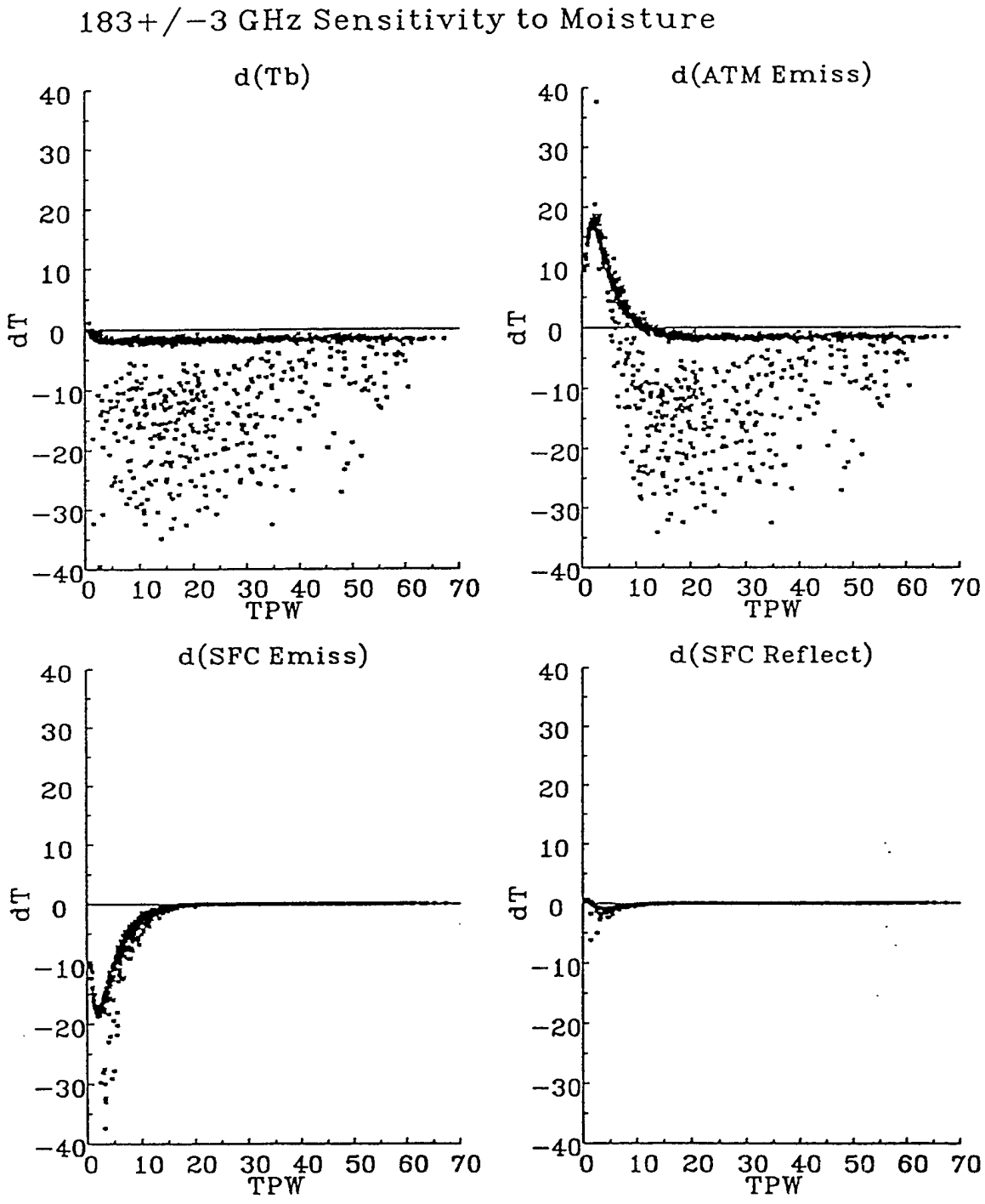

Figure 25. (continued) The change in T_b and its three dominant components (atmospheric and surface emissions and surface reflectance) for the T-2 channels as the moisture profile was modified by ±10%. All other parameters were set to constant values.

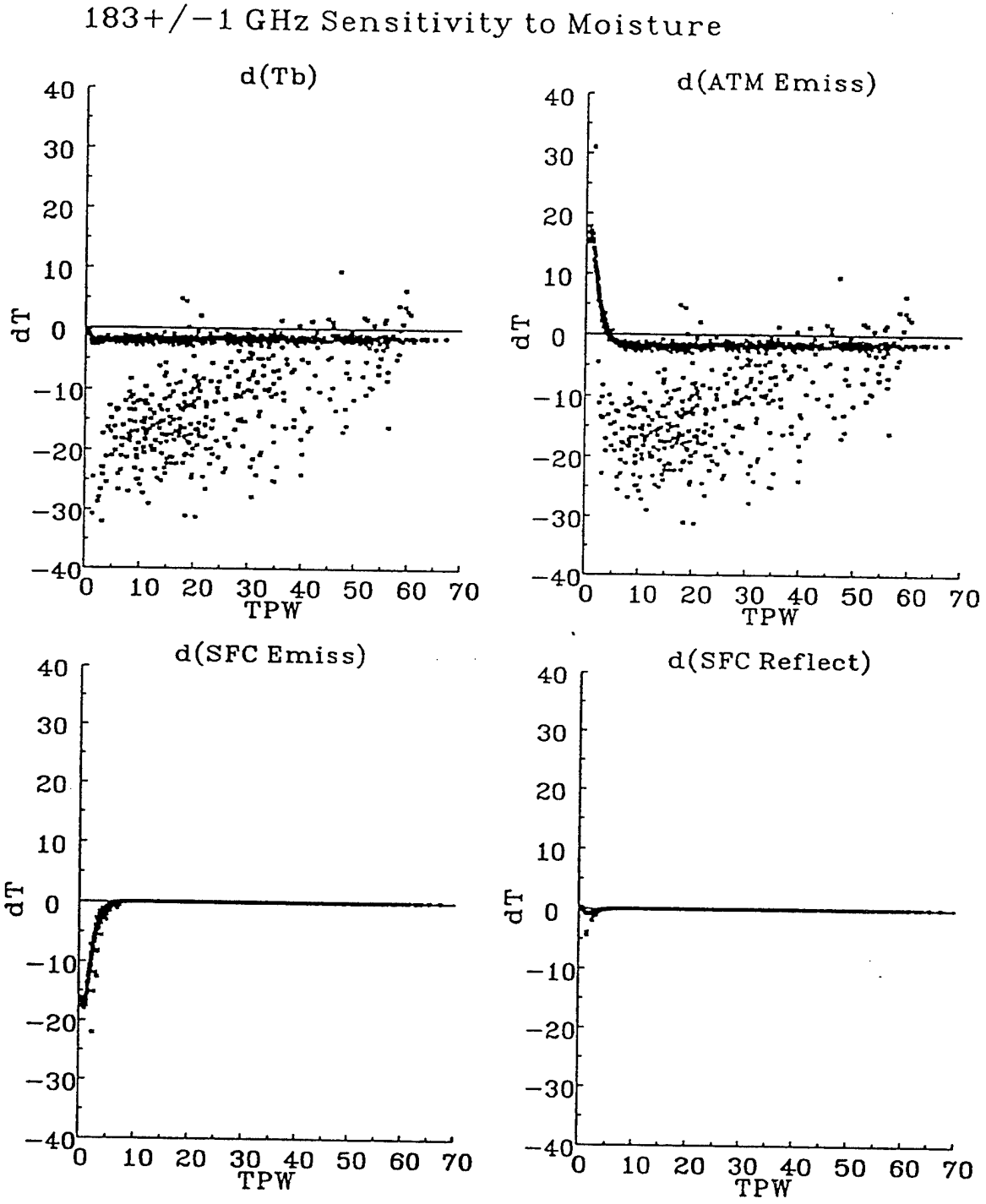

Figure 25. (continued) The change in T_b and its three dominant components (atmospheric and surface emissions and surface reflectance) for the T-2 channels as the moisture profile was modified by ±10%. All other parameters were set to constant values.

Table 20. Mean, median and standard deviation of the absolute values of moisture modification required to change the 183±3 GHz T_b by ±1 K.

Precipitable Water [kg/m^2]	Number of Cases	Mean [%]	Median [%]	Standard Deviation [%]
0 - 20	823	12.5	10.4	6.9
20 - 40	444	11.4	10.7	2.0
40 - 60	205	12.1	11.3	2.0
60 - 99	38	12.4	11.8	2.3
TOTAL	1510	12.1	10.7	5.3

4.2 T_b Sensitivity to Atmospheric Temperature

Figures 26 and 27 illustrate the sensitivities of the T-2 channels to temperature profile modification. These were generated from profiles with TPWs of 7.8 and 56.3 kg/m^2, respectively. When a channel sensed predominantly surface radiation, there was a decreased sensitivity between temperature and T_b changes. As the channel sensed greater atmospheric moisture contributions, there was a greater sensitivity to the atmospheric temperature change. Notice that for the dry profile, only the 183±3 and 1 GHz channels produced a greater amount of change in T_b compared to the change in temperature profile, as evident by a slope greater than 45°. For the moister environment, all the atmospheric channels produced a larger change in T_b than was used in the temperature profile modification.

With all other parameters set to constant values, the sensitivities of T_b and its three main components (atmospheric emission, surface emission and surface reflectivity) to varying atmospheric temperature profiles (±1 K) are plotted against TPW in Figure 28. The sensitivities for the 91 and 150 GHz displayed a gradual increase with increasing TPW while the 183 GHz channels tended to become constant by roughly 10 kg/m^2, showing no appreciable increase for moister environments. The responses of the atmospheric channels were bounded.

4.3 T_b Sensitivity to Satellite Viewing Angle

Increasing the satellite viewing angle increased the atmospheric path contributing to the T-2 T_bs (Figure 29). Using the T-2 range in satellite viewing angle from 0° to 40.5°, examples of the effect of increasing viewing angle to forward-calculated T_bs are presented in Figures 30 and 31. The first example was produced from a radiosonde profile with 7.8 kg/m^2, the second with 56.3 kg/m^2.

For relatively dry atmospheric profiles, limb-cooling occurred for the 183 GHz channels as a result of the increasing atmospheric path length increased the amount of water being sensed, causing the weighting function to shift to higher, cooler altitudes. Limb-warming was noted for the two window channels, 91 and 150 GHz since the majority of the weighting functions were beneath the earth's surface; therefore, the additional atmospheric contribution, which was warmer than the surface contribution, increased the forward-calculated T_bs. For moister atmospheric profiles, limb-warming only occurred for the 91 GHz channel.

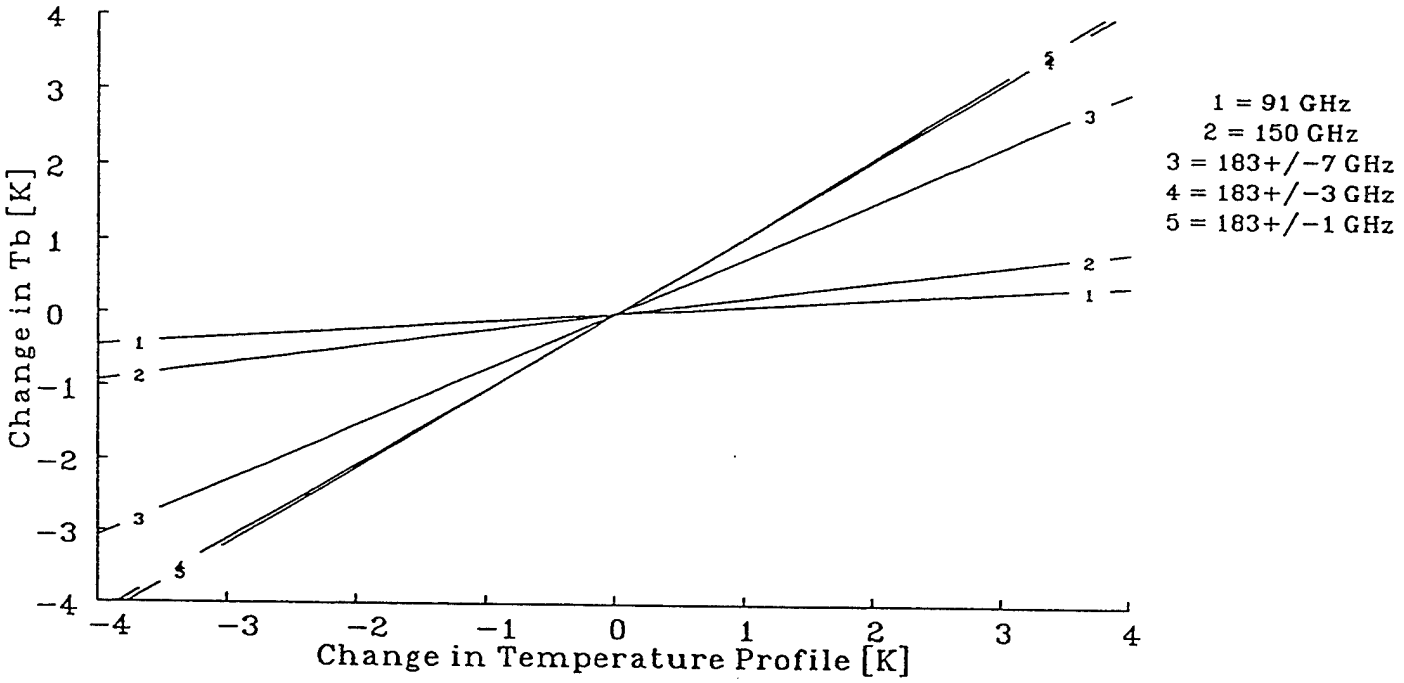

Figure 26. The change in T_b for the T-2 channels as the temperature profile was modified in the RT band model. The sounding profile had a TPW of 7.8 kg/m^2.

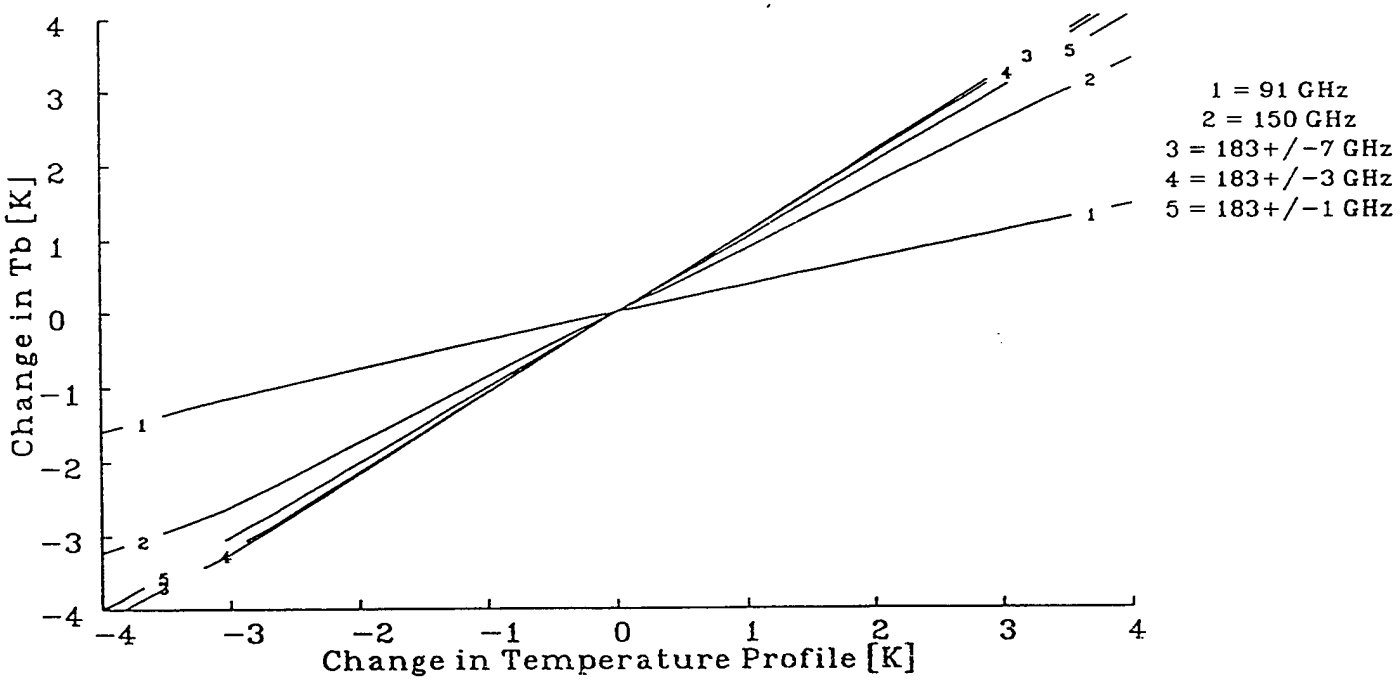

Figure 27. The change in T_b for the T-2 channels as the temperature profile was modified in the RT band model. The sounding profile had a TPW of 56.3 kg/m^2.

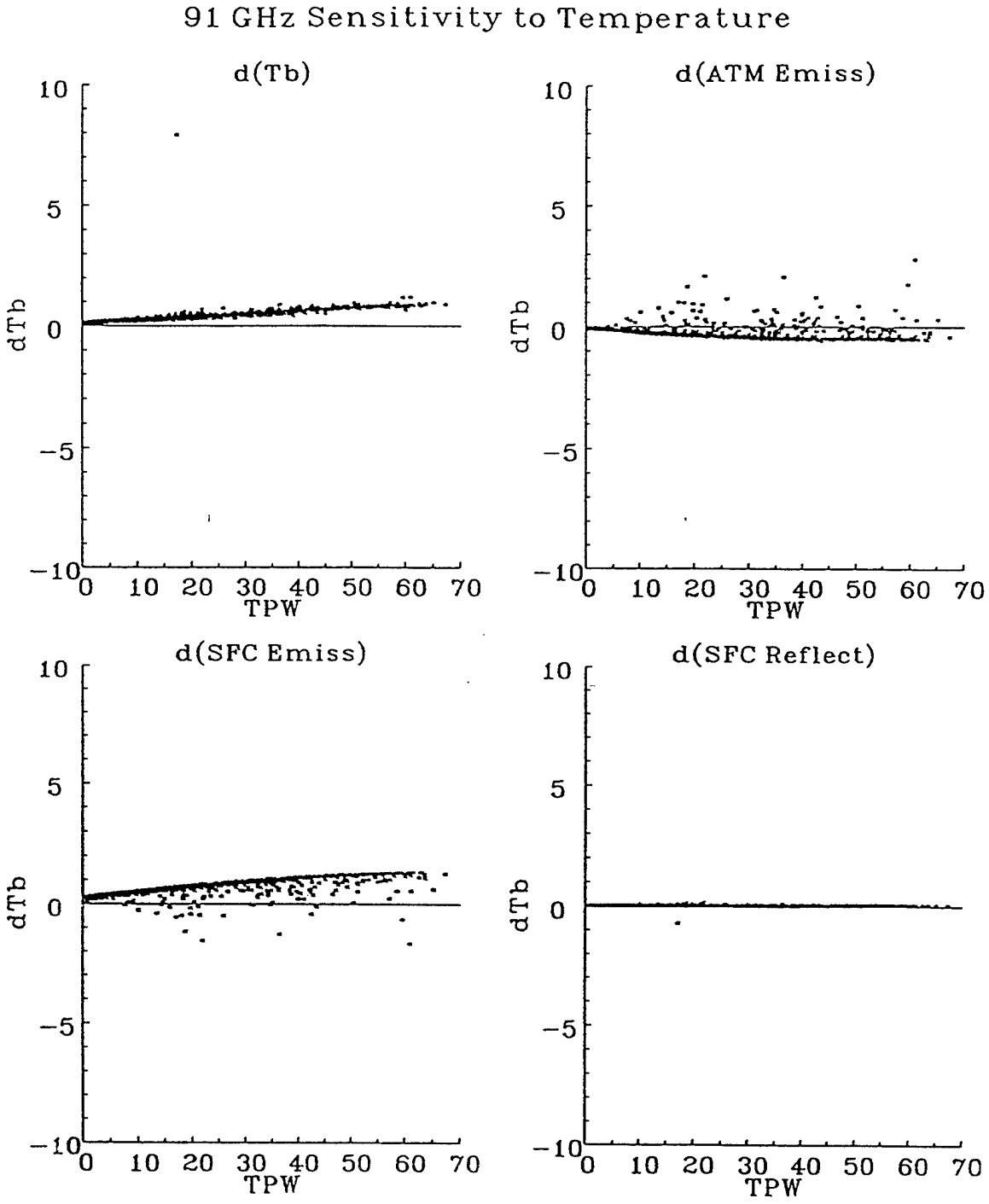

Figure 28. The change in T_b and its three dominant components (atmospheric and surface emissions and surface reflectance) for the T-2 channels as the temperature profile was modified by ±1 K. All other parameters were set to constant values.

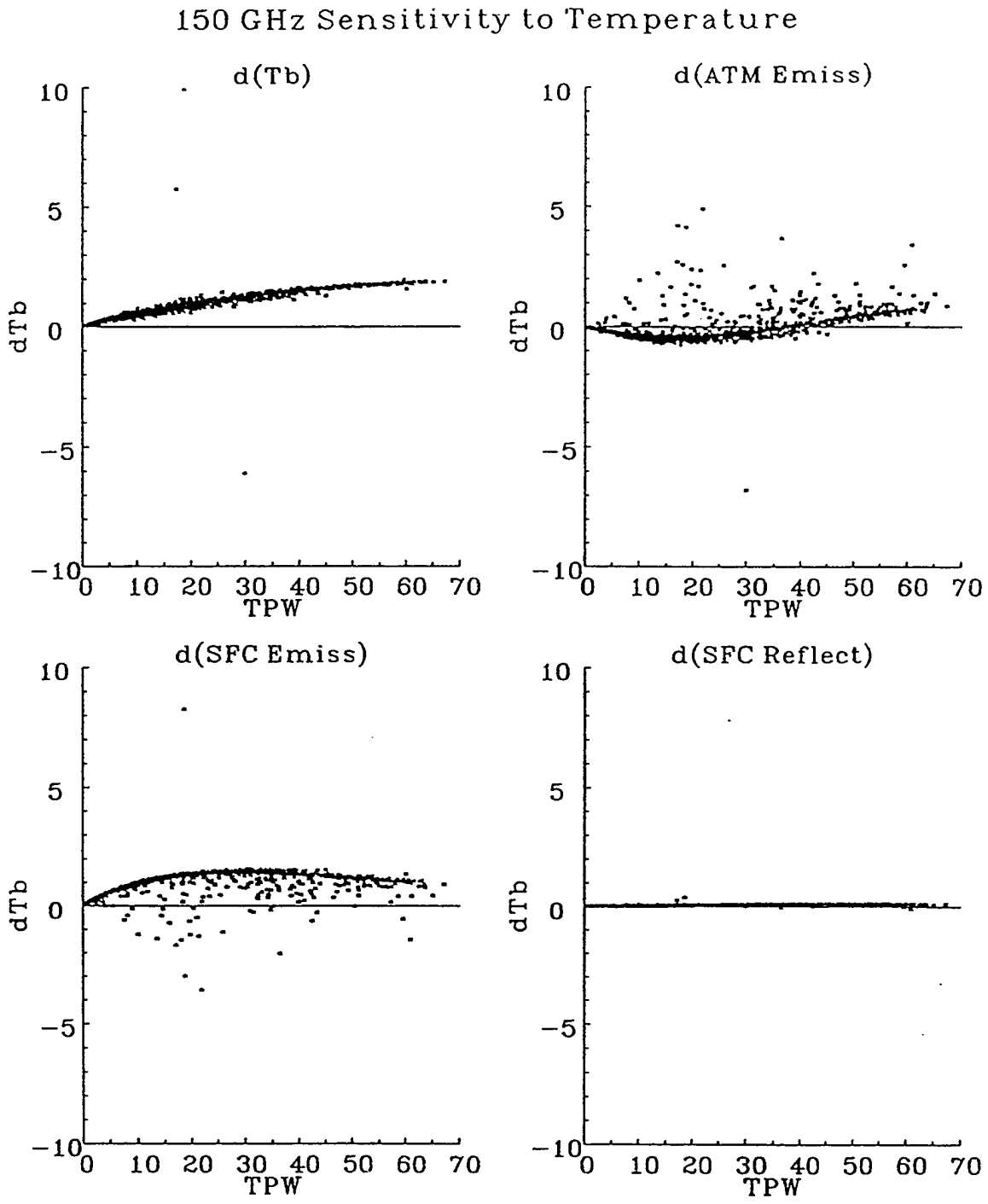

Figure 28. (continued) The change in T_b and its three dominant components (atmospheric and surface emissions and surface reflectance) for the T-2 channels as the temperature profile was modified by ±1 K. All other parameters are set to constant values.

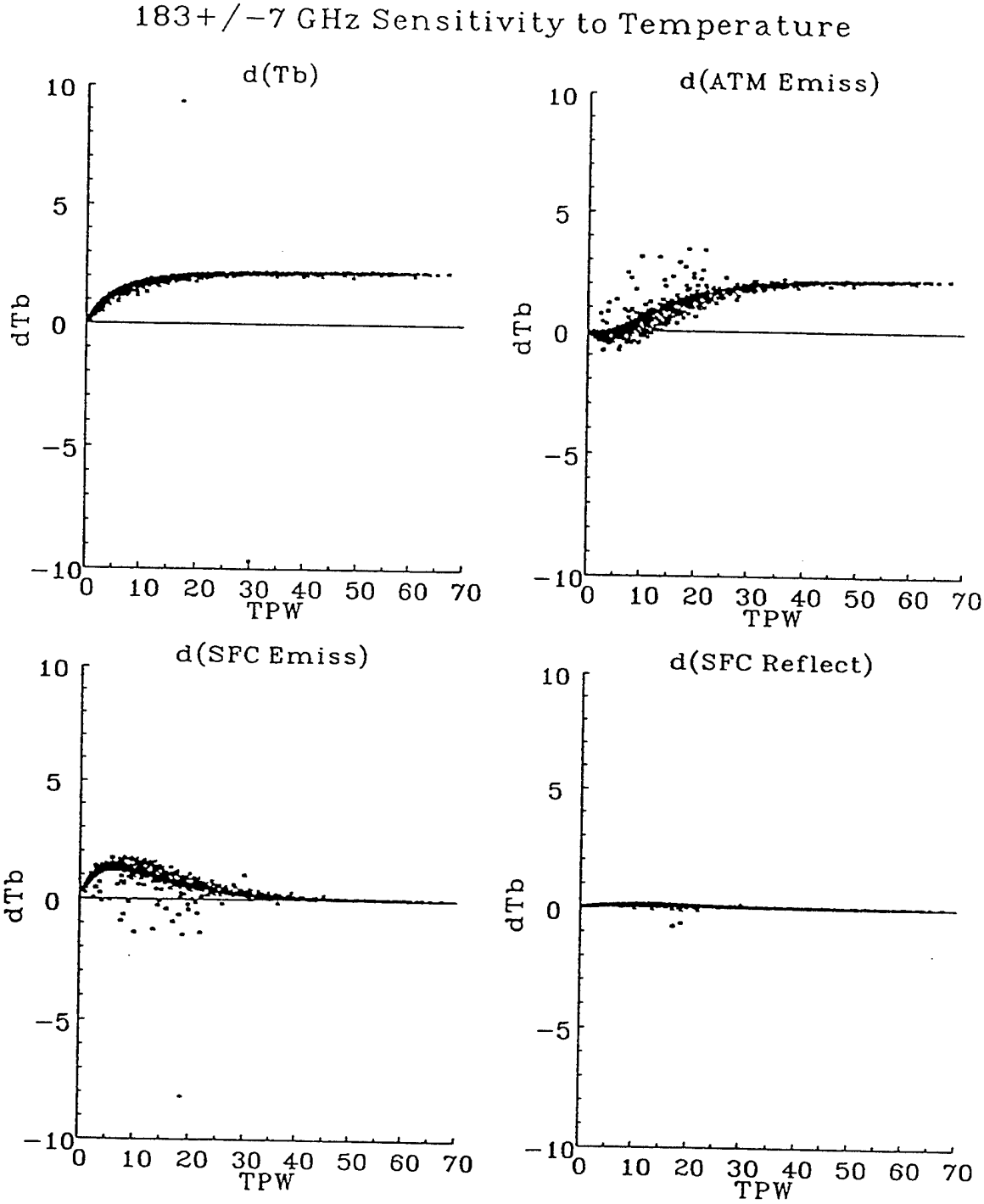

Figure 28. (continued) The change in T_b and its three dominant components (atmospheric and surface emissions and surface reflectance) for the T-2 channels as the temperature profile was modified by ±1 K. All other parameters are set to constant values.

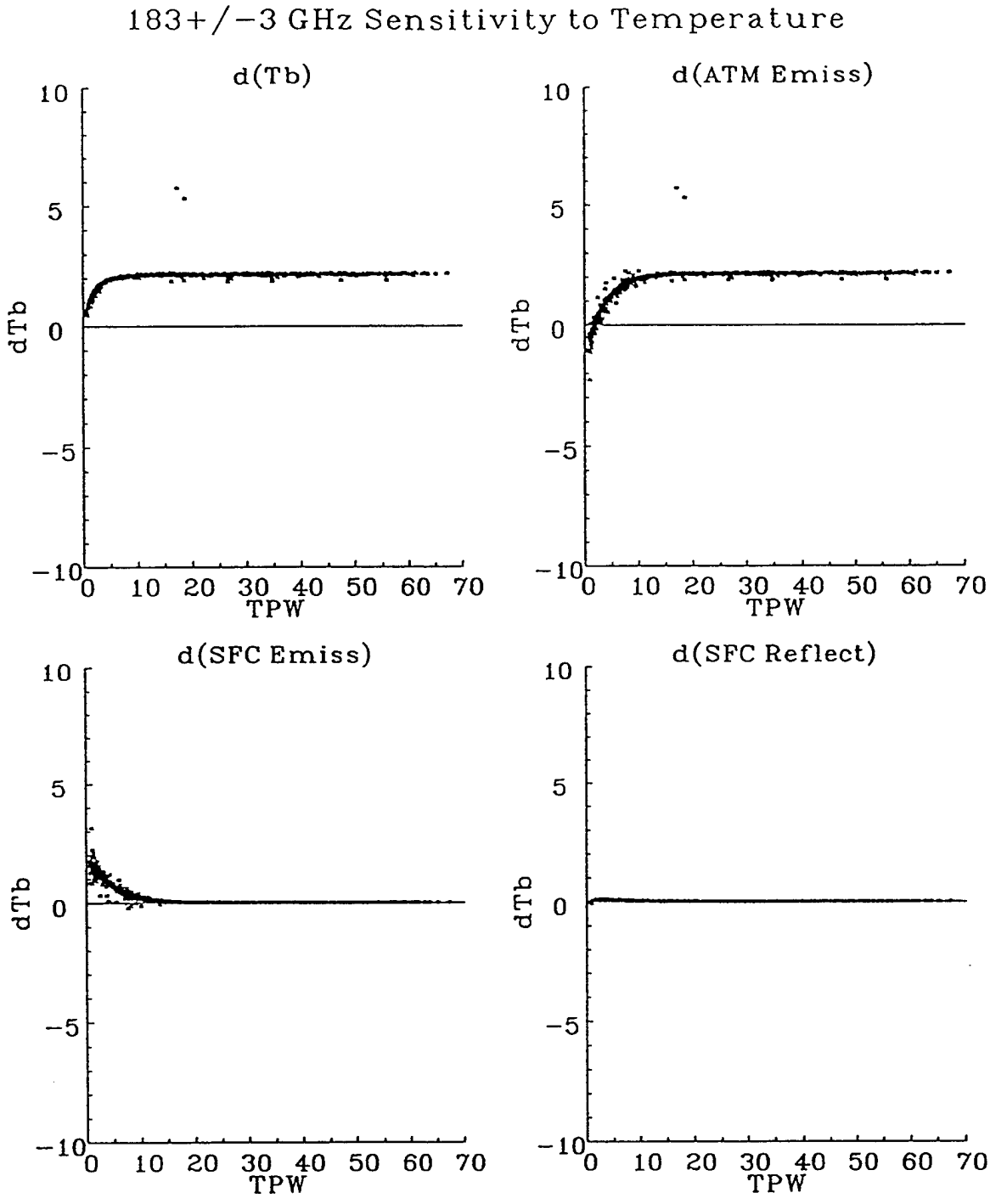

Figure 28. (continued) The change in T_b and its three dominant components (atmospheric and surface emissions and surface reflectance) for the T-2 channels as the temperature profile was modified by ±1 K. All other parameters are set to constant values.

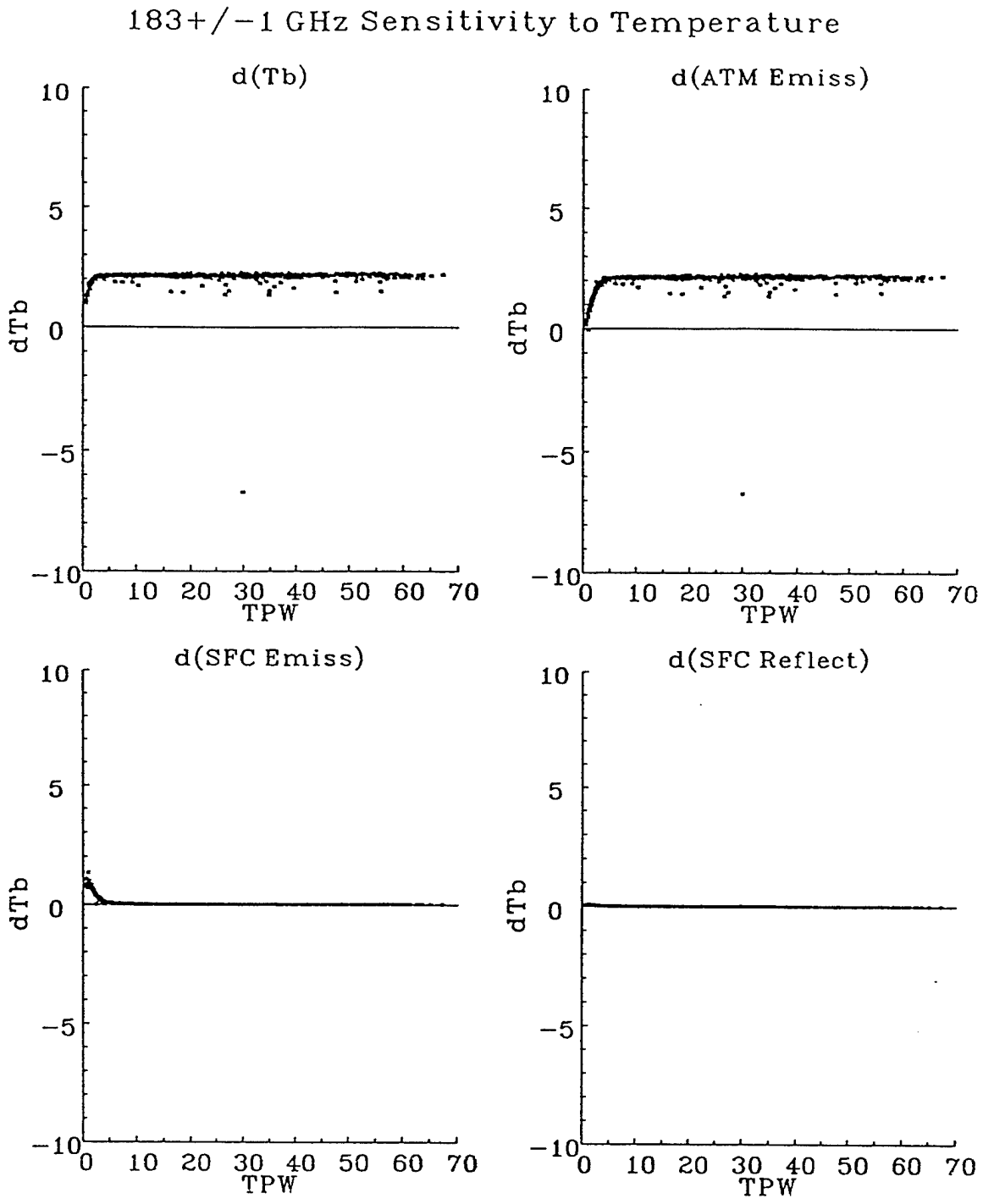

Figure 28. (continued) The change in T_b and its three dominant components (atmospheric and surface emissions and surface reflectance) for the T-2 channels as the temperature profile was modified by ±1 K. All other parameters are set to constant values.

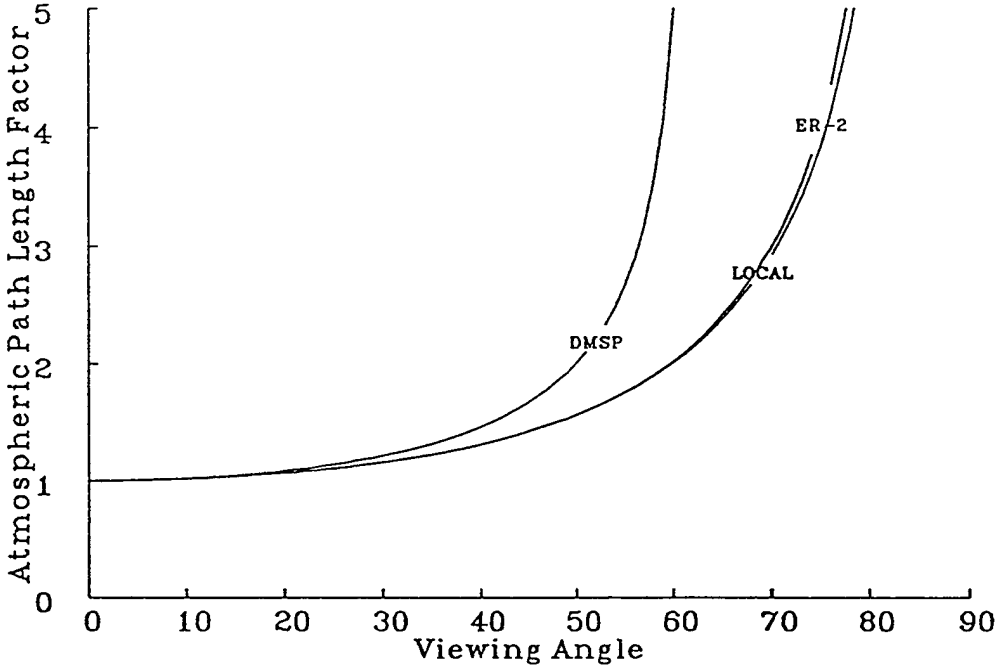

Figure 29. Relationship between atmospheric path length (normalized to one atmosphere thickness) and satellite viewing angle and local incidence (or look) angle.

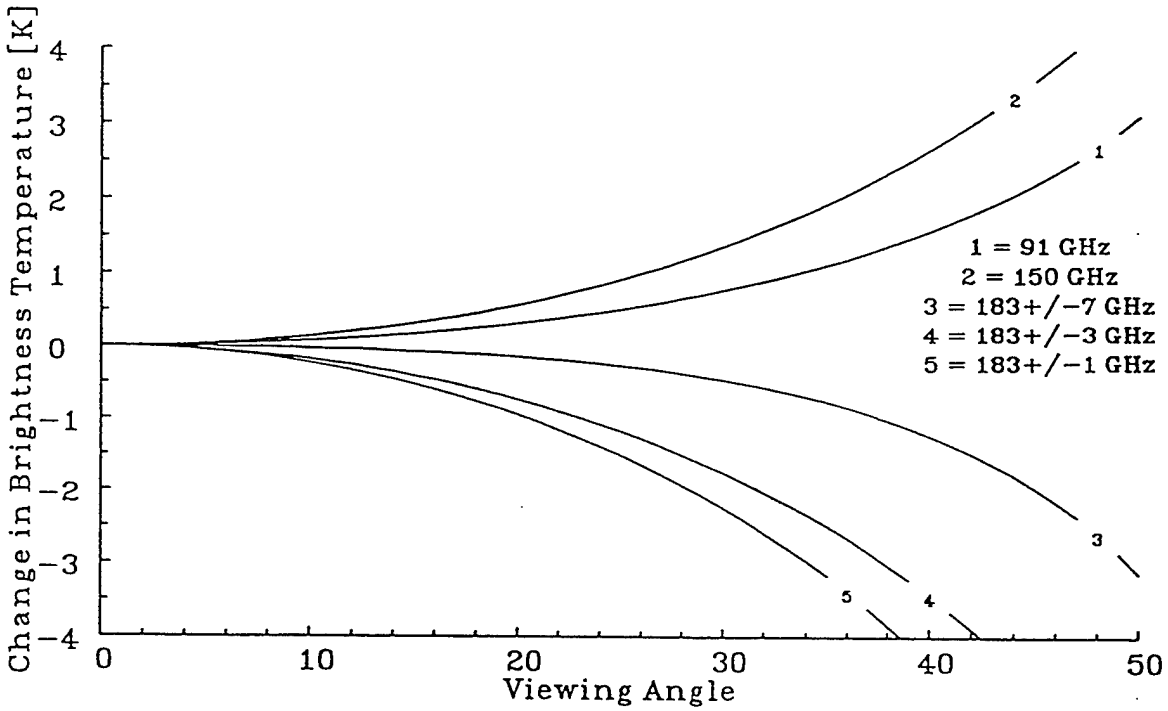

Figure 30. Change in T_b for the T-2 channels as the satellite viewing angle was modified from 0° to 40.5° in the RT band model. The sounding profile had a TPW of 7.8 kg/m^2.

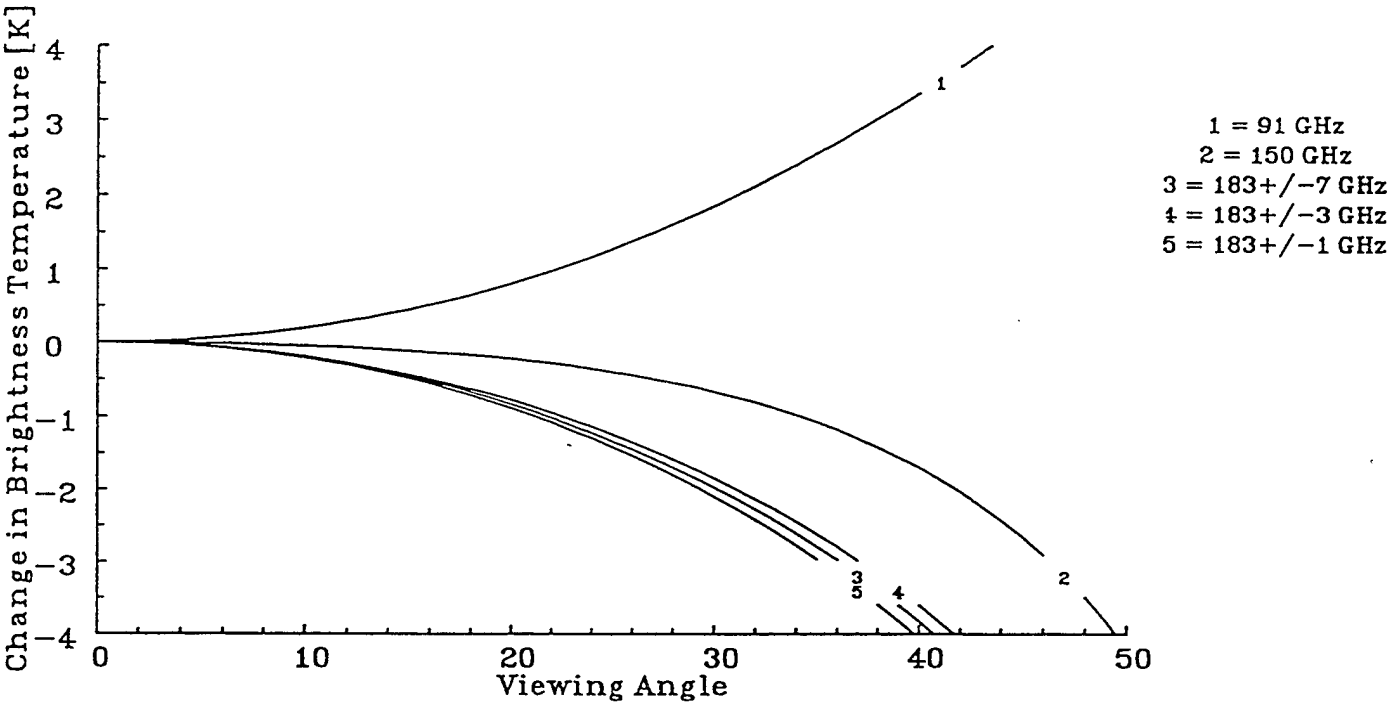

Figure 31. Change in T_b for the T-2 channels as the satellite viewing angle was modified from 0° to 40.5° in the RT band model. The sounding profile had a TPW of 56.3 kg/m^2.

In an attempt to study how the satellite viewing angle changed the levels of the atmosphere being sensed, the characteristics of the weighting functions were examined. Due to the fine vertical structure of moisture and temperature distributions and having a limited vertical resolution in the Eyre model, the peak of the weighting functions did not consistently shift to higher altitudes (lower pressure levels) as the viewing angle increased (Figure 32). However, the median of the weighting function increased consistently in altitude (Figure 33). The median of the weighting function is sometimes referred to as the energy balanced peak of the weighting function.

Table 21 demonstrates the complex nature of the contributions of the three major radiative components as satellite viewing angle is changed. For the two window channels, the increase in the atmospheric emission contribution was greater than the decrease in surface emission term, thereby causing limb-warming. This was similar for the 183±7 GHz channel, but the large decrease in the surface reflectance contribution created a drop in the forward-calculated T_b. The change in the 183±3 GHz T_b was dominated by a decrease in surface emission; whereas, the change in atmospheric emission created the entire change in the 183±1 GHz T_b.

Table 21. Change in total T-2 T_b and the atmospheric emission, surface emission and surface reflectance contributions as the viewing angle increased from 0° to 40.5°.

	TPW = 7.8 kg/m^2			
Frequency	d(T_b)	d(Atm Em)	d(Sfc Em)	d(Sfc Ref)
91 GHz	2.0	18.2	-17.4	1.1
150 GHz	2.5	33.6	-31.6	0.5
183±7 GHz	-2.2	21.1	-21.5	-1.9
183±3 GHz	-2.4	-1.2	-1.0	-0.1
183±1 GHz	-2.7	-2.7	0.0	0.0
	TPW = 56.3 kg/m^2			
Frequency	d(T_b)	d(Atm Em)	d(Sfc Em)	d(Sfc Ref)
91 GHz	1.9	38.4	-36.3	-0.1
150 GHz	-2.9	22.3	-23.2	-2.0
183±7 GHz	-4.0	-3.9	-0.1	0.0
183±3 GHz	-3.7	-3.7	0.0	0.0
183±1 GHz	-4.2	-4.2	0.0	0.0

For moist atmospheric profiles (for example, the 56.3 kg/m^2 case in Figure 31), only the 91 GHz channel experienced limb-warming and at a much lower rate than that observed in the drier case. The 150 and 183 GHz channels displayed limb-cooling in moist atmospheres. The responses of the three radiative components as the viewing angle increased differed from that observed in the drier atmosphere. The magnitude of the 91 GHz atmospheric and surface emission changes were much larger for the moist environment, despite producing a smaller overall warming response, which may be partially a result of warmer and increased amounts of near-surface moisture in this profile compared to the previous one. All three 183 GHz channels behaved as the 183±1 GHz channel in the drier environment.

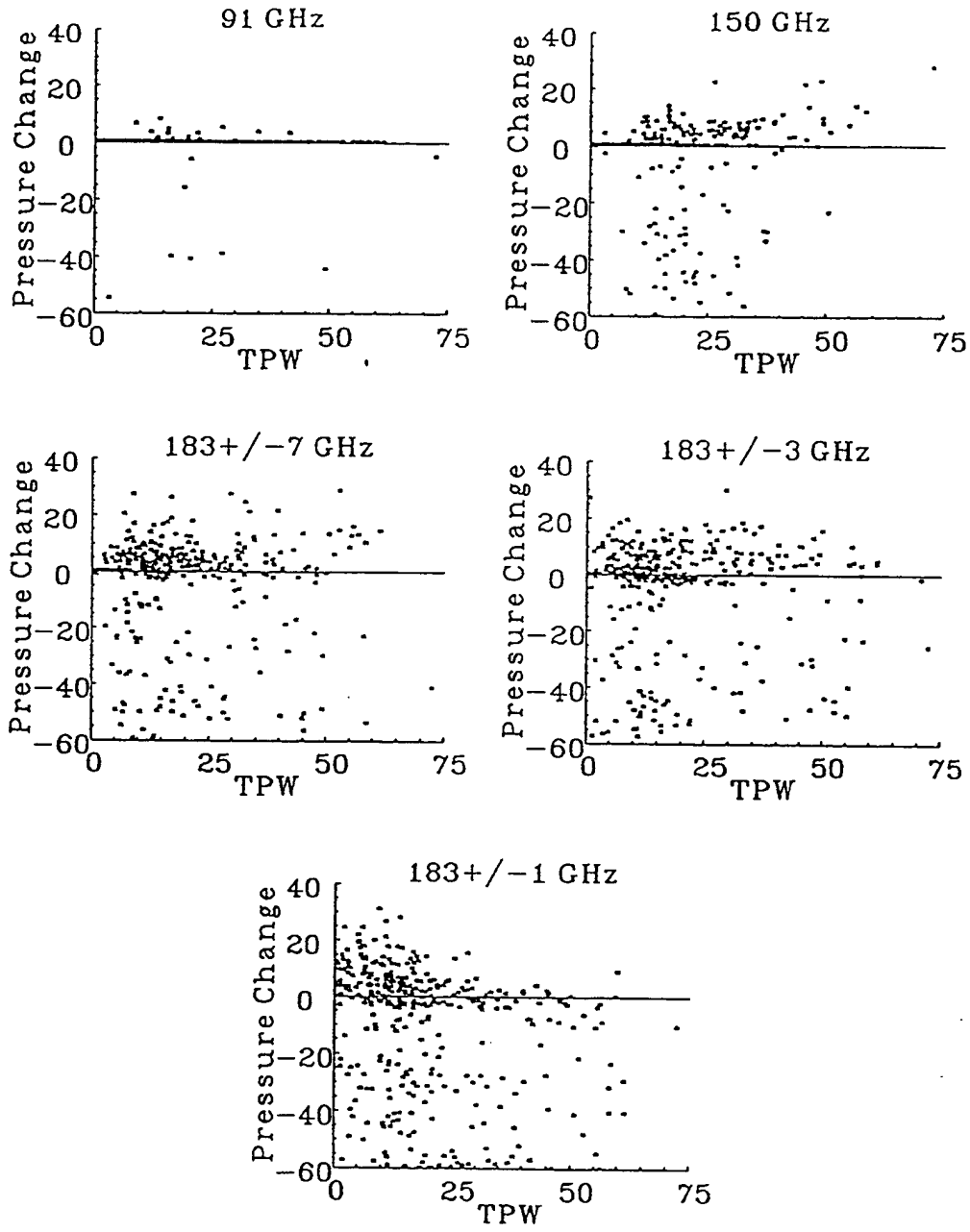

Figure 32. Change in the pressure levels of the peak of the weighting functions for the T-2 channel frequencies as the satellite viewing angle increased from 0° to 40.5°.

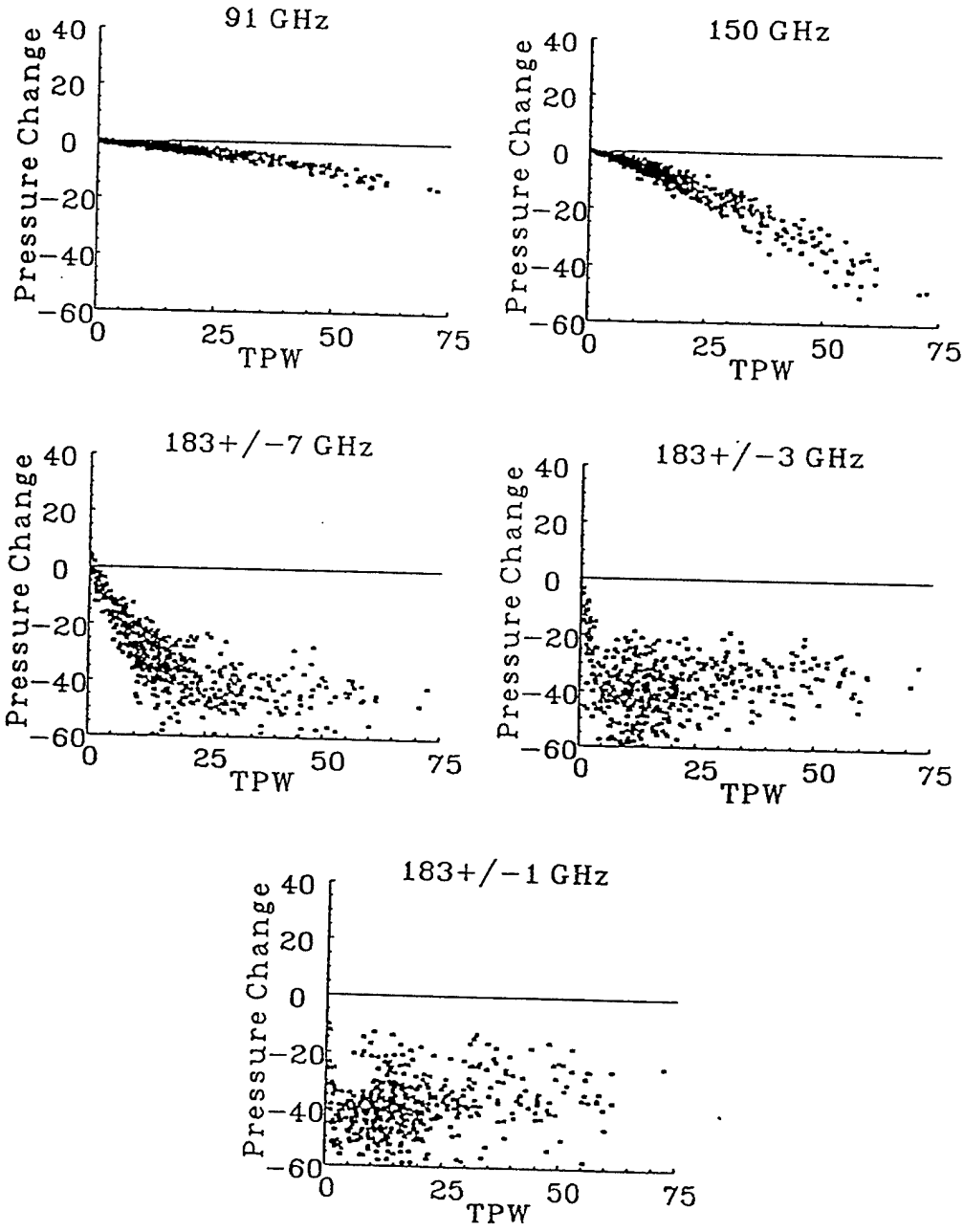

Figure 33. Change in the pressure levels of the median of the weighting functions for the T-2 channel frequencies as the satellite viewing angle increased from 0° to 40.5°.

Using the set of 1601 global radiosonde observations as input to the Eyre model, the differences between forward-calculated T_bs, atmospheric emission, surface emission and surface reflectance terms generated with a viewing angle of 0° and that with a viewing angle of 40.5° are displayed in Figure 34. Limb-warming for the 91 GHz channel occurred for all 1601 atmospheres, regardless of TPW; however, the amount of limb-warming peaked near a TPW of 23 kg/m^2 and decreased for larger TPWs. For the 150 GHz channel, limb-warming occurred in the drier atmospheres (almost always when the TPW was less than 19 kg/m^2 and possibly when TPW was between 19 and 38 kg/m^2). Limb-cooling occurred almost exclusively when the TPW was greater than 38 kg/m^2. Limb-warming occurred for the 183 GHz channels only for very dry atmospheres; limb-cooling was the predominant response for the atmospheric channels. The mean (and minimum) amount of limb-cooling for the 183±7, 3, and 1 was -3 (-5), -4 (-6), and -5 (-10) K, respectively.

4.3.1 High Incidence Angle Results

The MIR data provided a chance to examine the effects of viewing angle along a swath width of roughly 50 km, versus over 1700 km of the T-2. Variability along the MIR's swath occurred due to inhomogeneity of atmospheric temperature and moisture as well as the presence of clouds and precipitation. However, when examined in bulk, average trends were observed. Note that since the ER-2 aircraft flew at a much lower elevation than the F-11 satellite (20 km versus 874 km), the atmospheric path length factors change markedly at viewing angles greater than 30° (Figure 29). For example, when the viewing angles for the ER-2's MIR were 60, 70 and 80°, the equivalent atmospheric path lengths were observed when the T-2 viewing angles are 50, 56 and 61°, respectively.

Whenever the aircraft banked, the MIR sensor scanned beyond the normal limits (±48°). MIR data taken during banked turns were gathered from seven of the T-2 CALVAL flights; 2 from the west coast of the United States, 3 from the east coast of the United States and 2 from the TOGA-COARE experiment. Each group of flight data was examined separately due to the drastically different total precipitable water characteristics of all three regions. The swath data of the 91 GHz T_bs from the TOGA-COARE flights (Figures 35 through 37) shows limb warming, agreeing with the model results described above.

Note that these data were filtered since there was a large population showing considerable deviation from observed trends. Examining the 220 GHz data, an additional MIR channel not part of the T-2 sensor that is more sensitive to scattering from large particles or precipitation, showed two relatively distinct populations. One population displayed consistent limb-cooling at temperatures above roughly 255 K and another showed rather dramatic temperature deviations across its swath at temperatures consistently below 255 K. A simple filter was developed to eliminate the swaths with average 220 GHz T_bs below 255 K.

The drier west coast atmosphere showed both limb-warming and limb-cooling for both the 91 and 150 GHz channels (Figure 38). Figure 39, which are based on measurements taken while the aircraft was banking and while flying level, show that limb-cooling was confined almost exclusively to land surfaces (most within the San Joaquin and Salina Valleys and a few in the Mojave Desert) and limb-warming to water surfaces. Limb-cooling for 91 GHz can be modeled if the ground temperature is very warm and/or surface emissivities are near unity. There were few limb-cooling instances observed during the east coast flights.

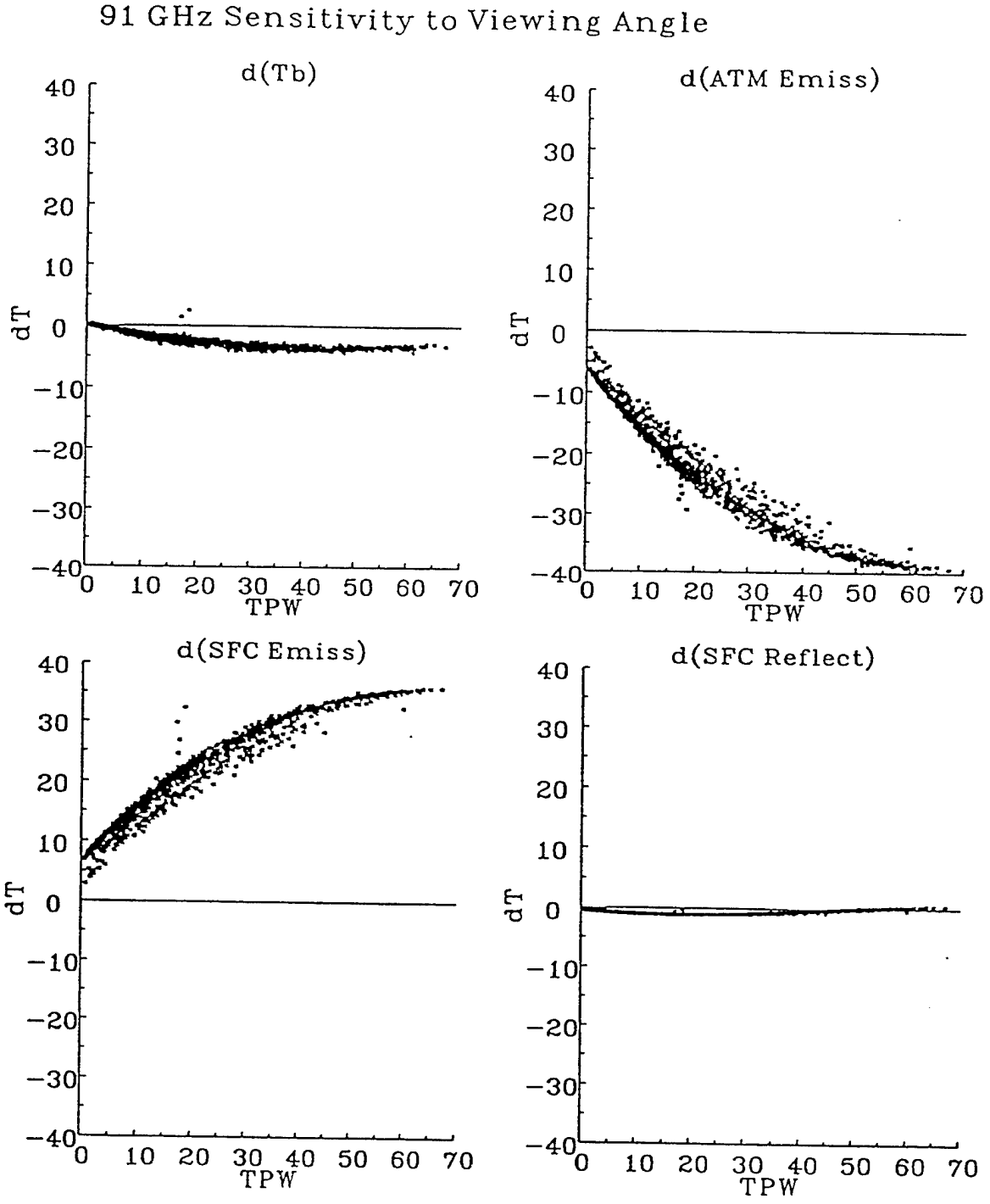

Figure 34. Changes in T_b and its three dominant components (atmospheric and surface emissions and surface reflectance) for the T-2 channels as the scan angle was modified from 0° to 40.5°. All other parameters were set to constant values.

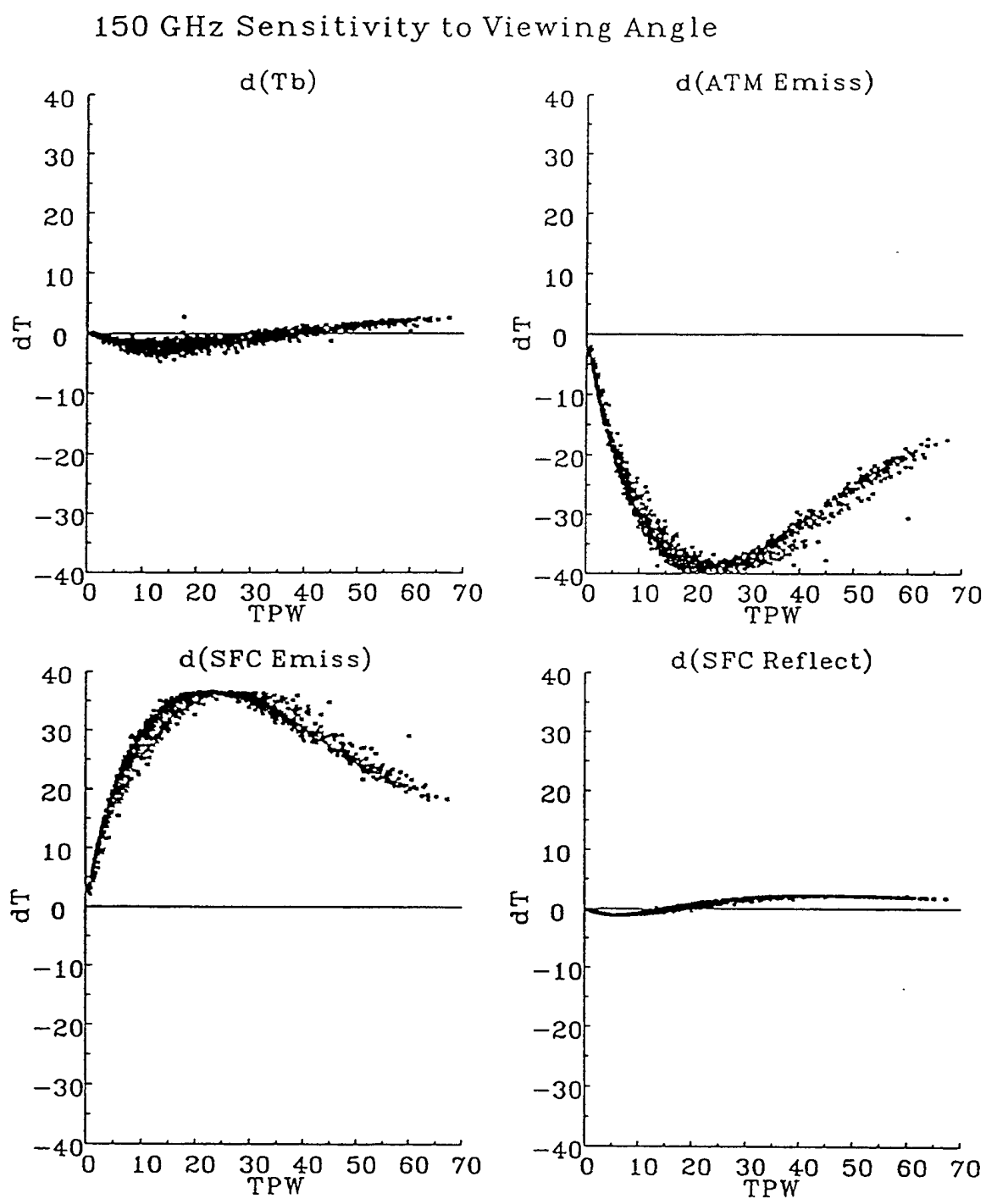

Figure 34. (continued) Changes in T_b and its three dominant components (atmospheric and surface emissions and surface reflectance) for the T-2 channels as the scan angle was modified from 0° to 40.5°. All other parameters were set to constant values.

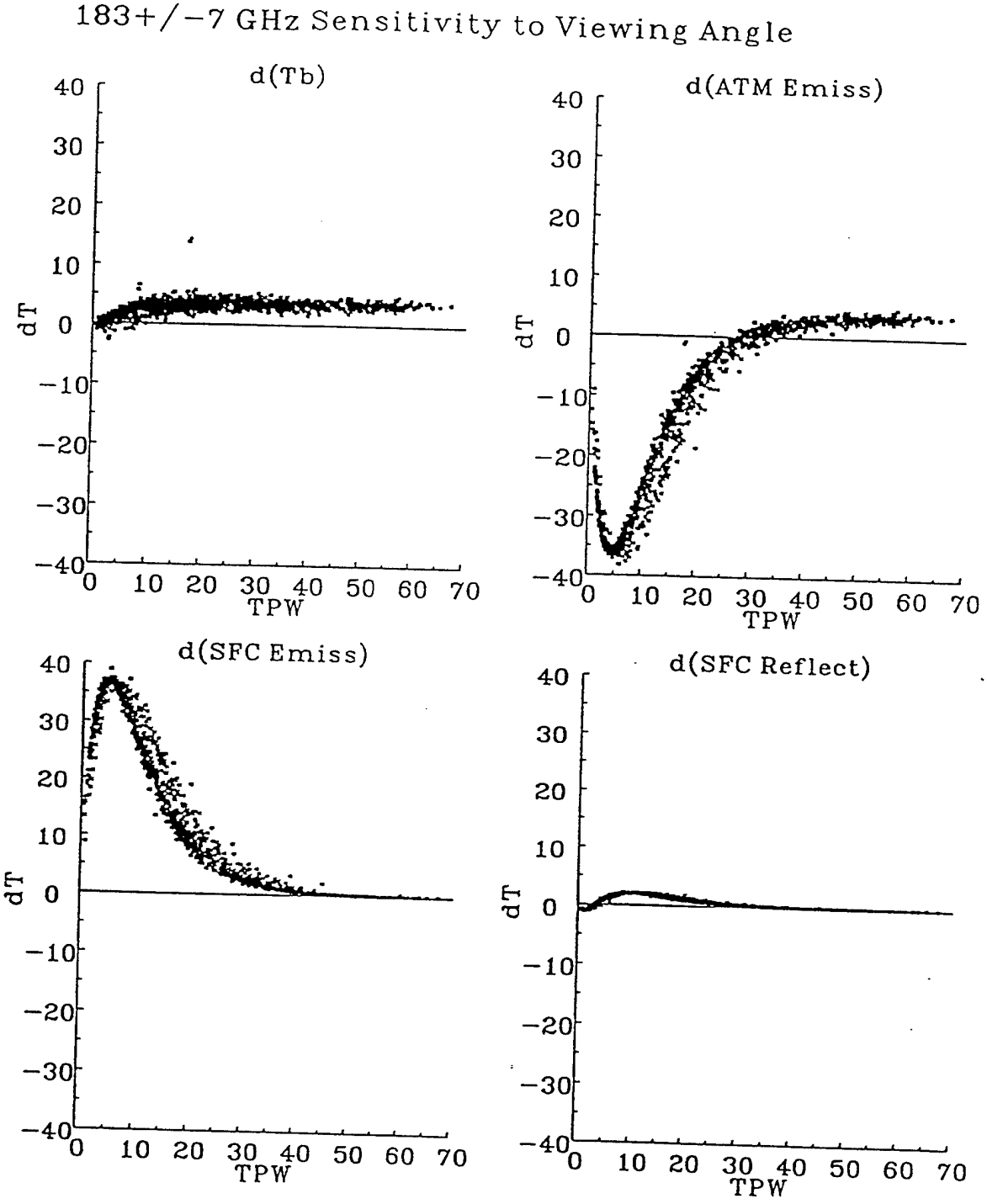

Figure 34. (continued) Changes in T_b and its three dominant components (atmospheric and surface emissions and surface reflectance) for the T-2 channels as the scan angle was modified from 0° to 40.5°. All other parameters were set to constant values.

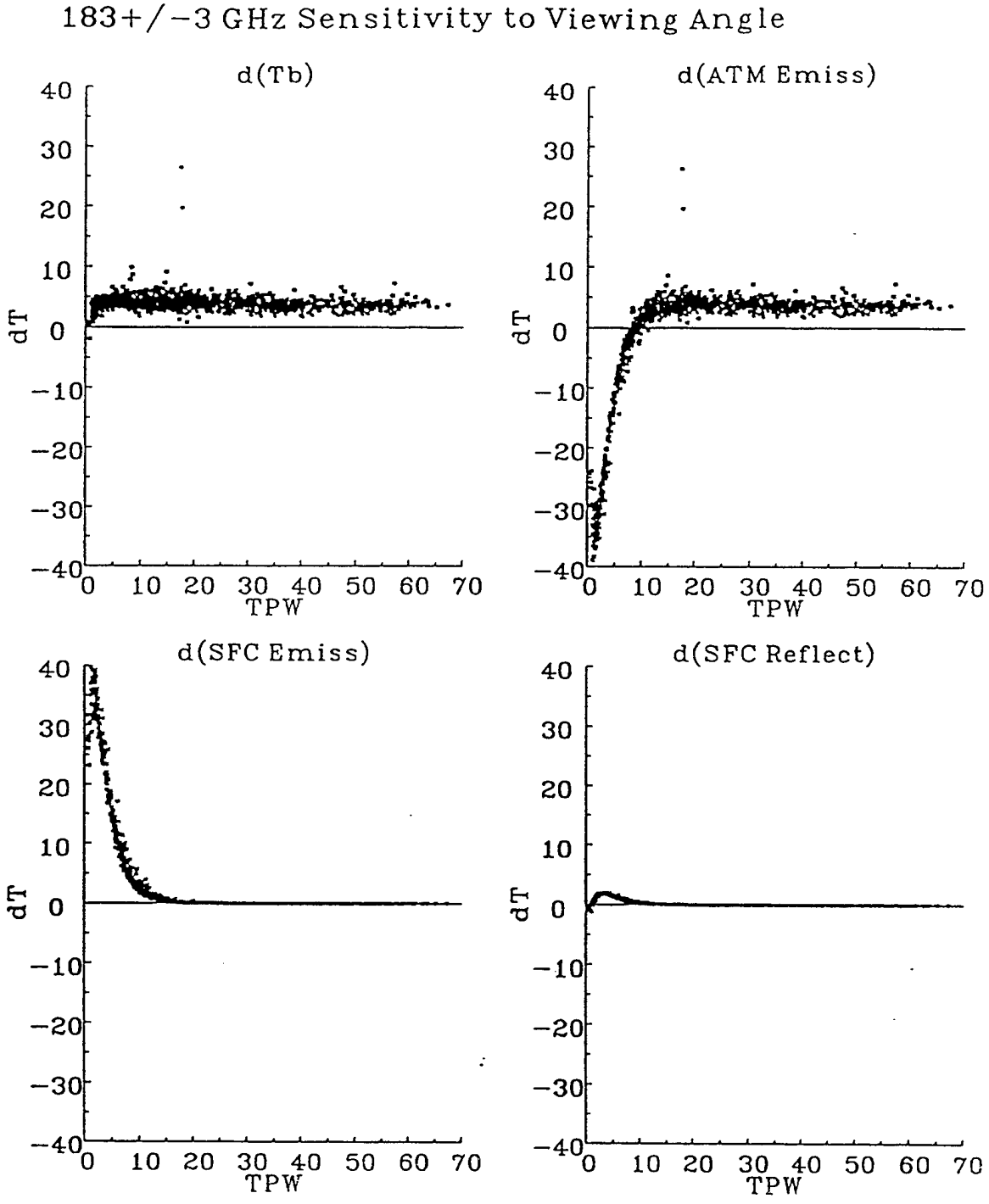

Figure 34. (continued) Changes in T_b and its three dominant components (atmospheric and surface emissions and surface reflectance) for the T-2 channels as the scan angle was modified from 0° to 40.5°. All other parameters were set to constant values.

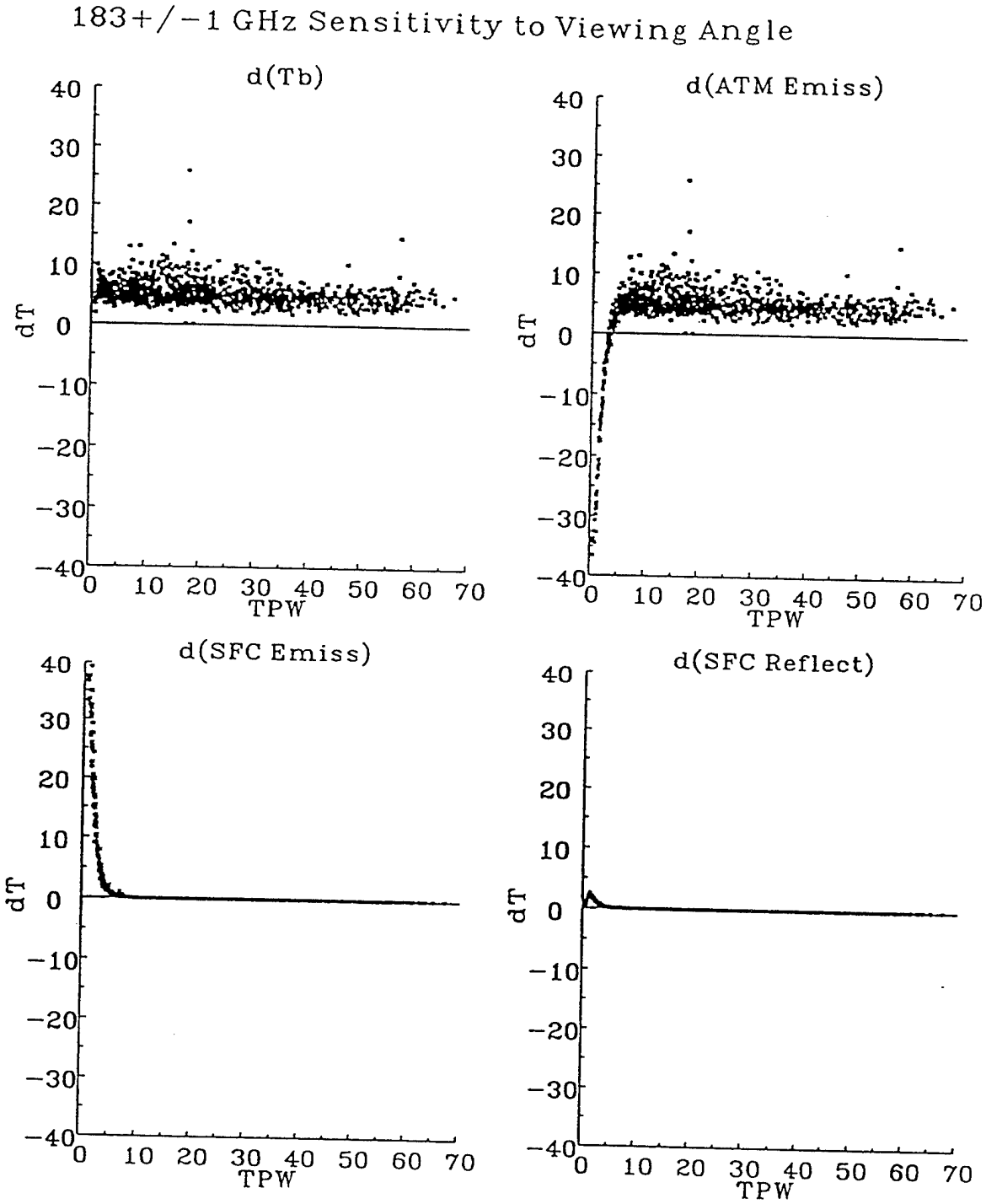

Figure 34. (continued) Changes in T_b and its three dominant components (atmospheric and surface emissions and surface reflectance) for the T-2 channels as the scan angle was modified from 0° to 40.5°. All other parameters were set to constant values.

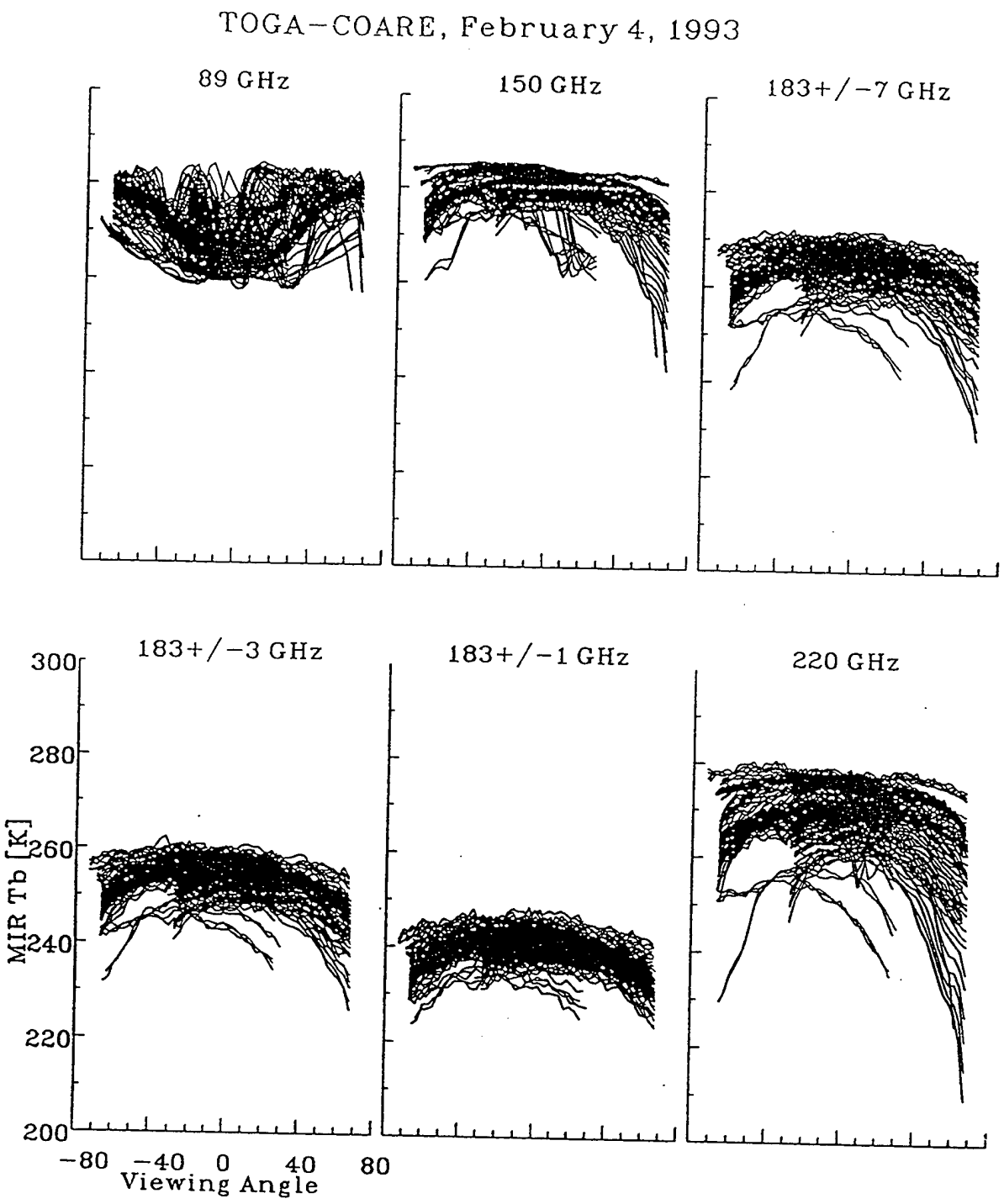

Figure 35. MIR T_bs plotted versus scan angles across the 50 km swath during the TOGA-COARE flight of February 4, 1993. Only data were used when the aircraft banked at least 20° and when the average T_b across the swath was greater than 255 K.

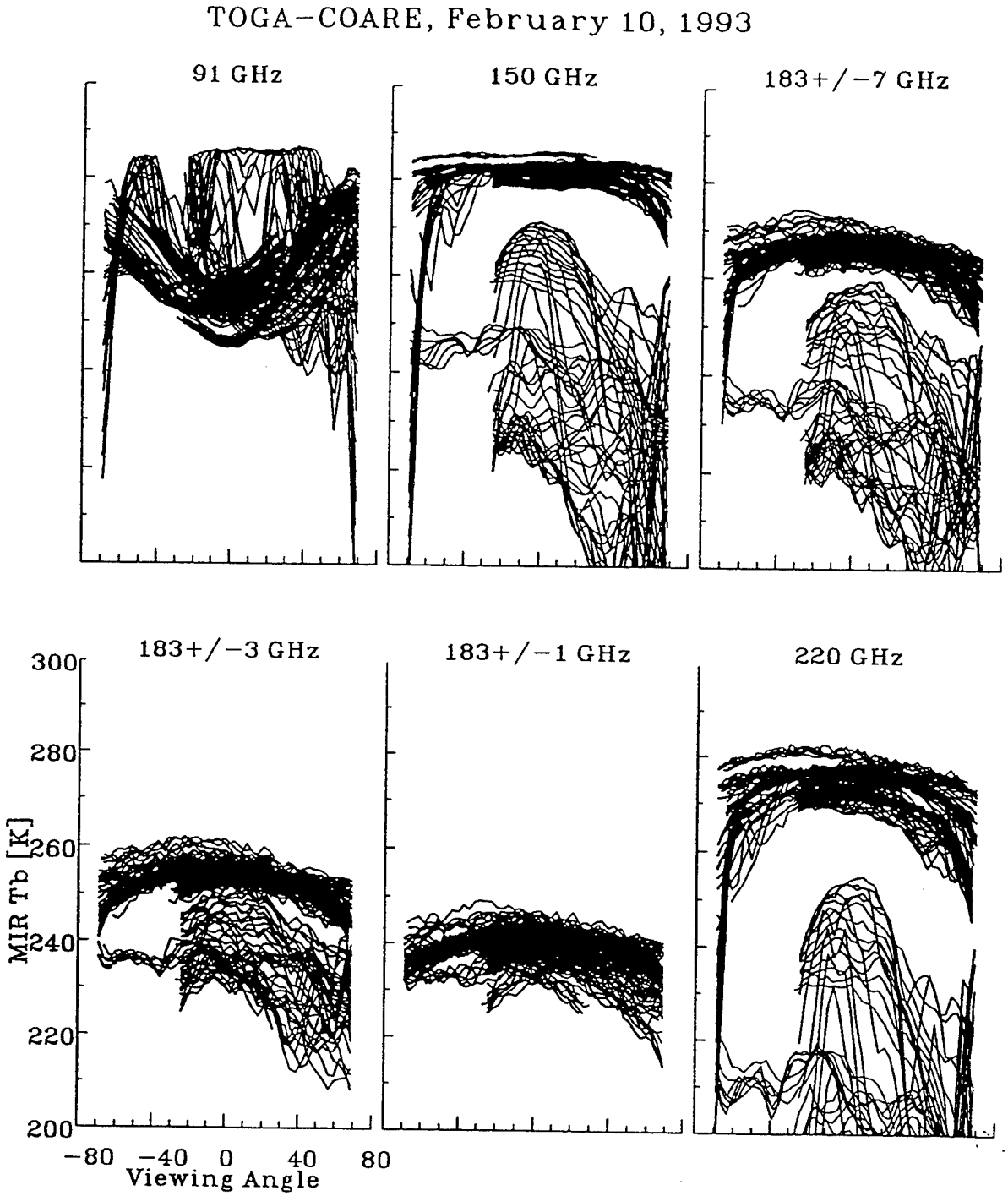

Figure 36. MIR T_bs plotted versus scan angles across the 50 km swath during the TOGA-COARE flight of February 10, 1993. Only data were used when the aircraft banked at least 20° and when the average T_b across the swath was greater than 255 K.

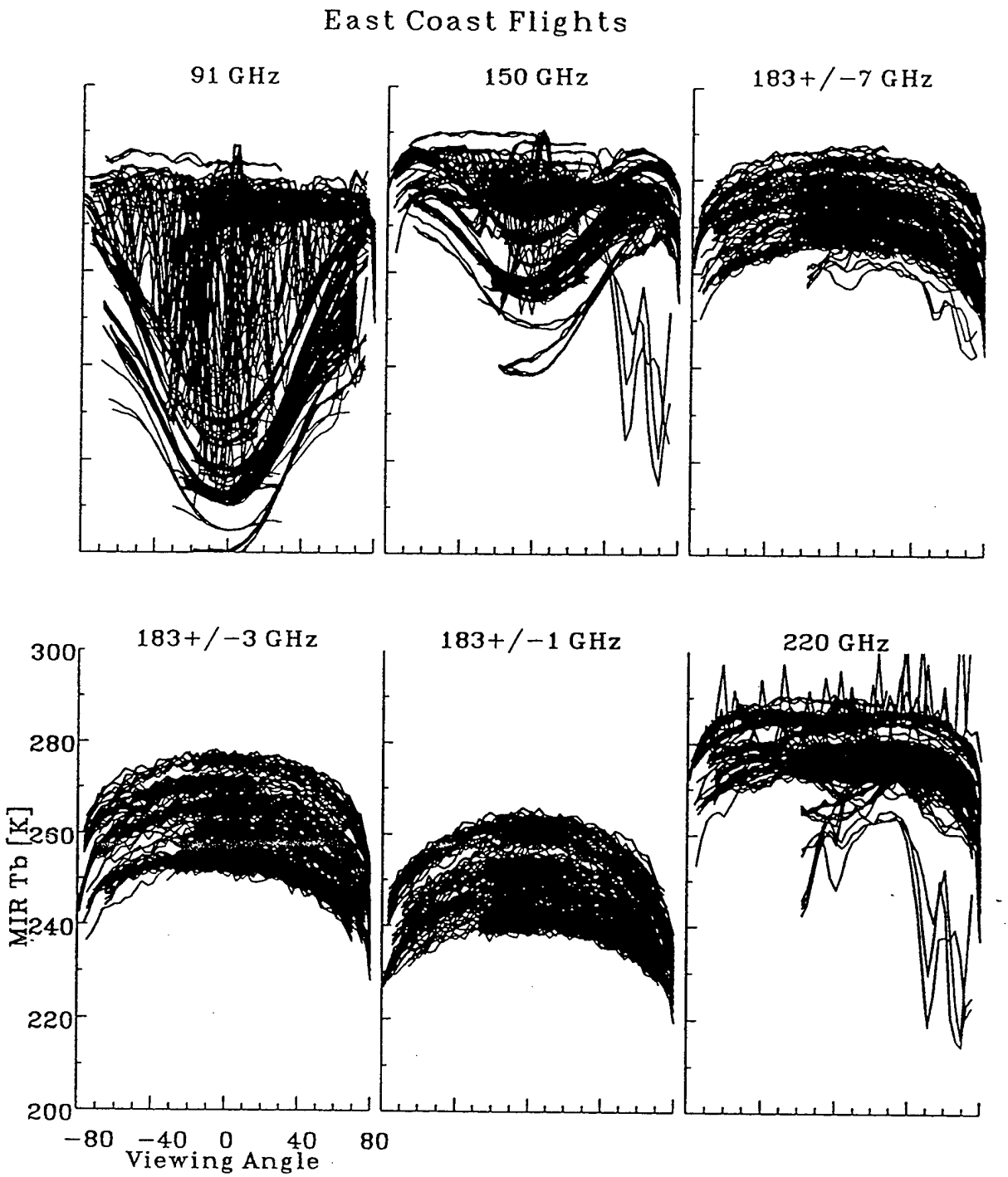

Figure 37. MIR T_bs plotted versus scan angles across the 50 km swath during the three east coast MIR flights of the summer, 1992. Only data were used when the aircraft banked at least 20° and when the average T_b across the swath was greater than 255 K.

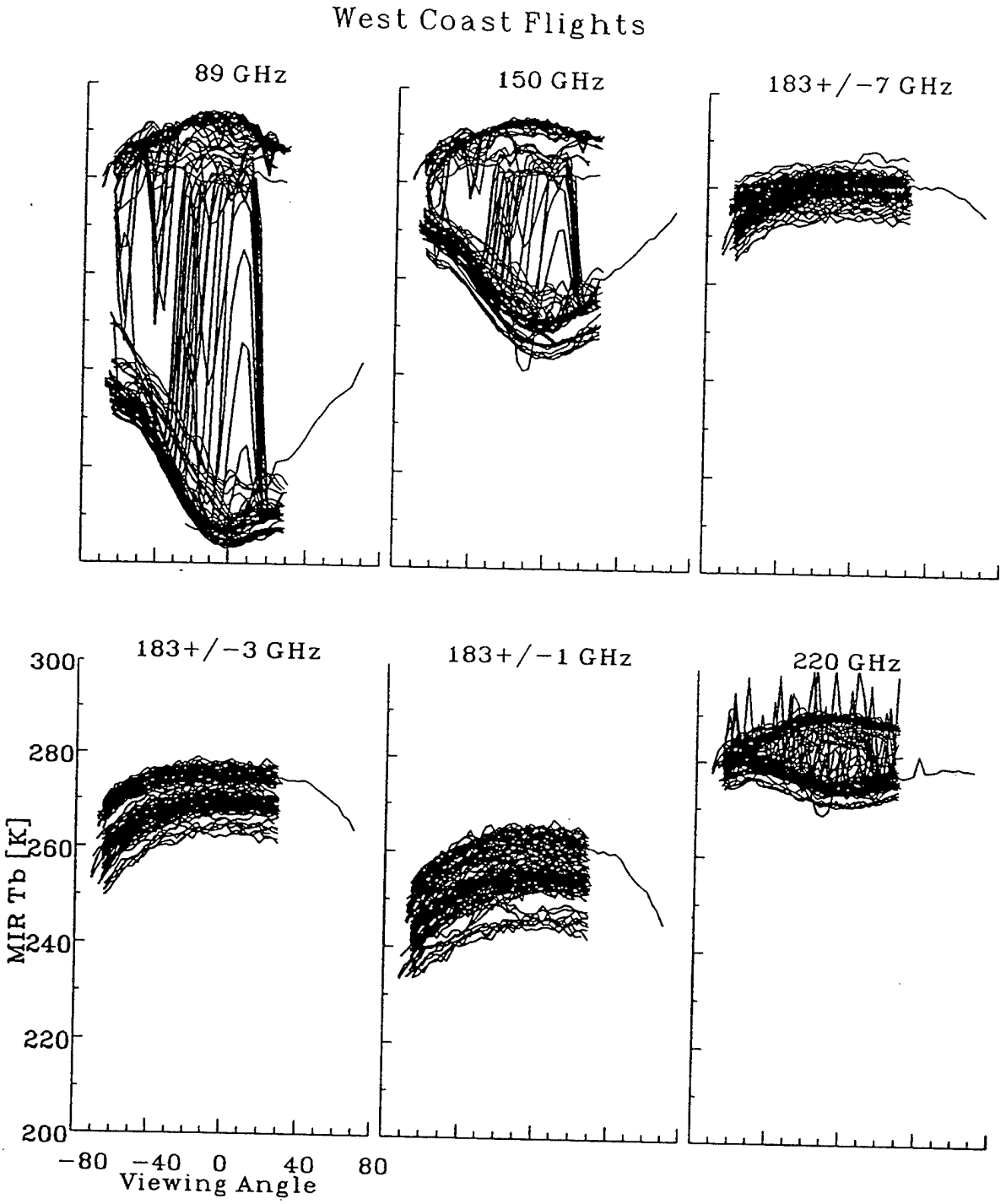

Figure 38. MIR T_bs plotted versus scan angles across the 50 km swath during the two west coast MIR flights of the summer, 1992. Only data were used when the aircraft banked at least 20° and when the average T_b across the swath was greater than 255 K.

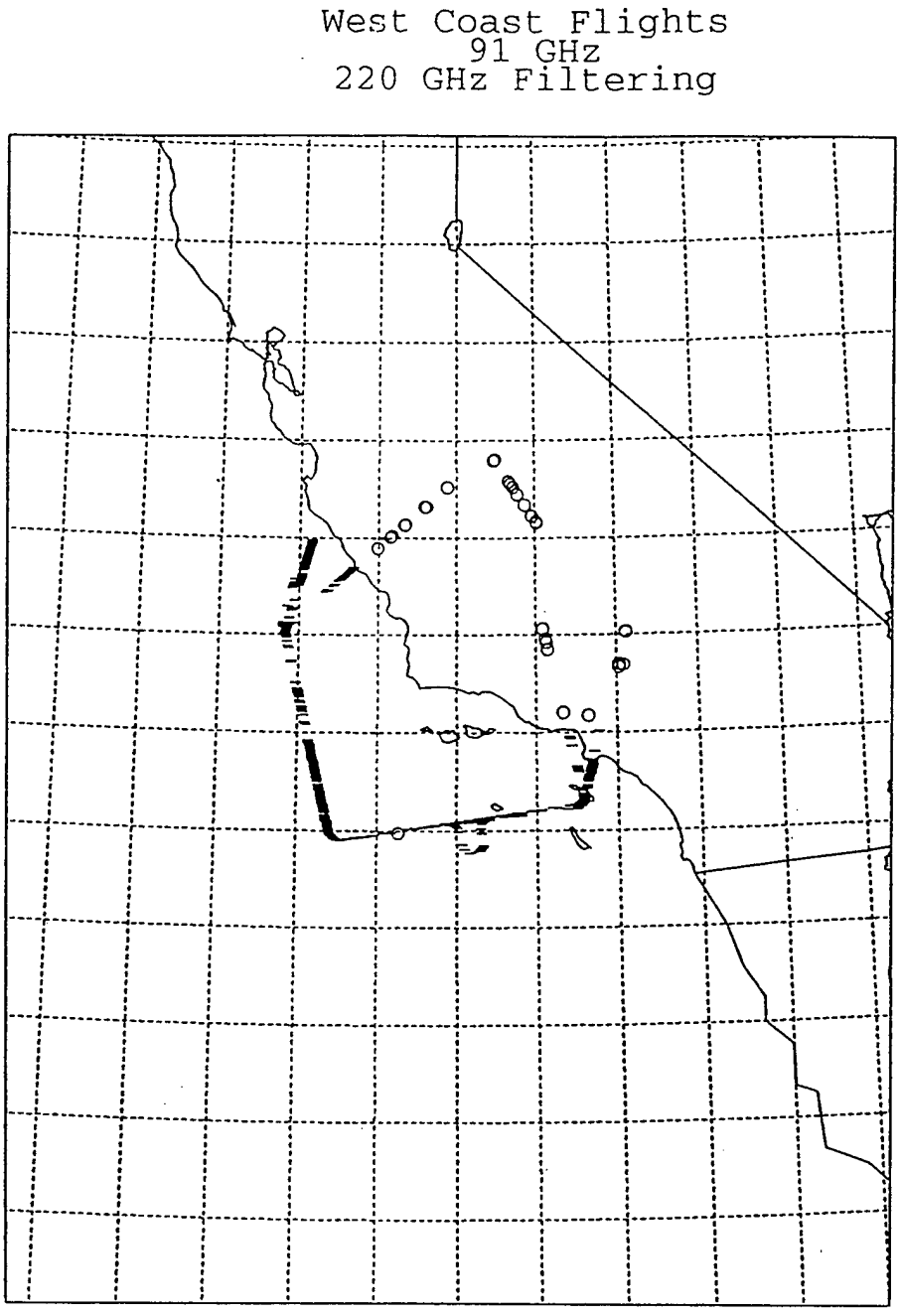

Figure 39. Locations of limb-warming (-) and limb-cooling (+) during level flight along the west coast during the two CALVAL flights of 1992.

4.4 T_b Sensitivity to Ground Temperature

Figures 40 and 41, illustrate the varied sensitivities of the T-2 channels to ground temperature. These were generated from profiles with TPWs of 7.8 and 56.3 kg/m^2, respectively. In general, as a channel sensed greater surface radiation, the sensitivity between ground temperature and T_b increased. With all other parameters set to constant values, the sensitivities of the T_b, atmospheric emission, surface emission and surface reflectivity terms to varying ground temperatures (295 to 285 K) are plotted against TPW in Figure 42. All T-2 channels became less sensitive to ground temperature as TPW increased.

4.5 T_b Sensitivity to Surface Emissivity

Figures 43 and 44 illustrate the varied sensitivities of the T-2 channels to surface emissivity. These were generated from profiles with TPWs of 7.8 and 56.3 kg/m^2, respectively. Similar to the sensitivity to ground temperature, as a channel sensed increased amounts of surface radiation, there was an increased sensitivity between surface emissivity and T_b changes. The sensitivities of T_b and its main components atmospheric emission, surface emission and surface reflectivity to varying surface emissivity (0.95 to 0.85) are plotted against TPW in Figure 45. The T_b sensitivities of all T-2 channels to surface emissivity decrease as TPW increases. Even the 183±1 GHz channel sensed the surface radiation when moisture profile was dry. Notice that surface emission was the dominant factor in determining T_b sensitivity; overriding the decrease in the surface reflectance.

4.6 Surface Emissivity Retrievals

Frequency dependent surface emissivity is a useful quantity to characterize surface parameters such as topography type, soil moisture, snow cover, sea ice, etc. Fundamental surface characteristics such as moisture volume and depth can be related to surface emissivity through deterministic models (Isaacs, 1987). RT models require a surface emissivity value along with ground temperature and profiles of temperature, moisture and pressure to calculate a brightness temperature for a particular frequency. The T-2 calibration study (Falcone et al., 1992) required, as a minimum, mean surface emissivities for land, ocean and coastal regions for the surface and near-surface channel frequencies of 91, 150 and 183±7 GHz. To produce these values, a global set of co-located radiosonde profiles and T-2 measurements were used with the Eyre model to iteratively retrieve surface emissivity (Pickle and Isaacs, 1994). Co-location criteria for this effort are the same as outlined in the calibration report: the center of the closest T-2 FOV be within 100 km of the radiosonde release station and the time of the overpass must be within 1 hour of the release of the radiosonde. Note that only one T-2 measurement, the one spatially closest to the radiosonde launch site, was used in the RT model iterative scheme.

4.6.1 General Procedure for Calculating Surface Emissivity

Radiosonde profiles of temperature and dew point were used in the Eyre model to estimate T_bs for the surface and near surface T-2 channels, 91 and 150 GHz, respectively. The RT model was initially executed with the surface emissivity of 0 and then with an emissivity of 1. If the satellite-measured T_b was between the two model results, then an iterative scheme was used to determine the surface emissivity that forced the model-calculated T_b to match the satellite measurement. If the satellite-measured T_b was outside the bounds produced by the model, then no surface emissivity was retrieved.

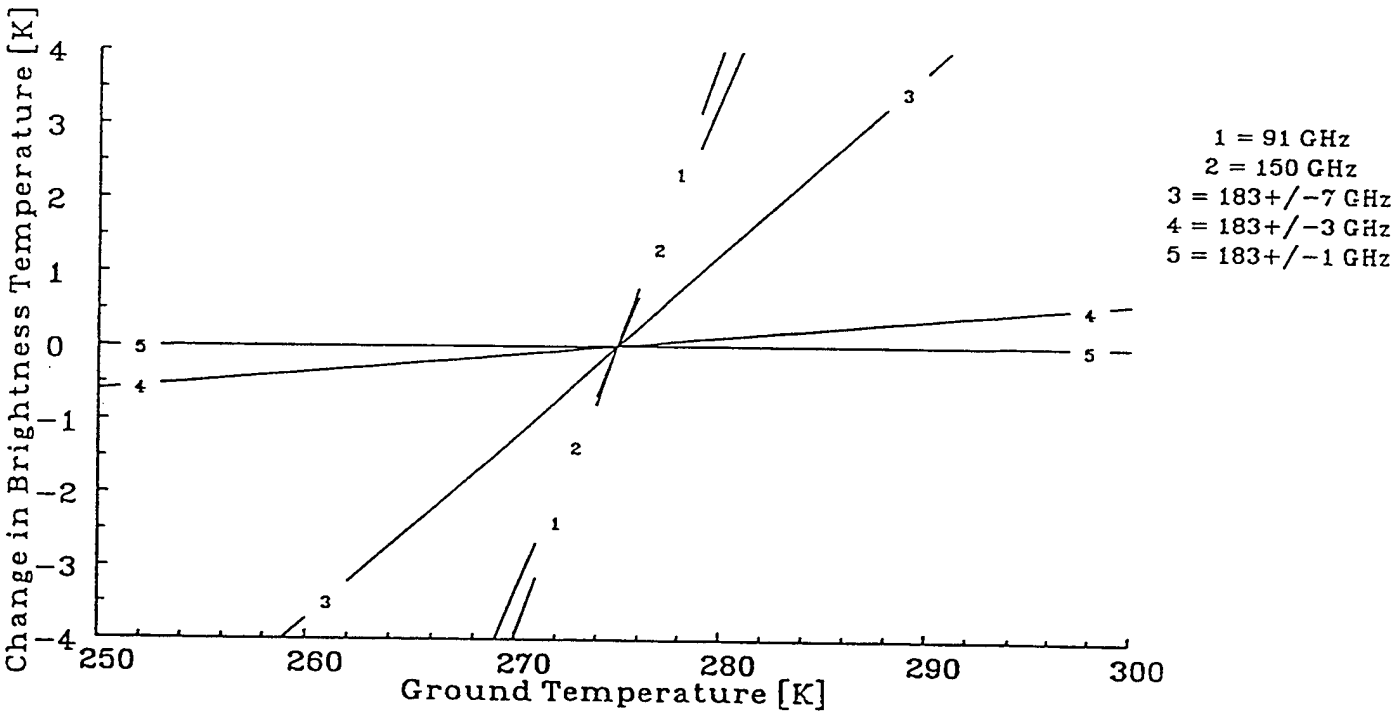

Figure 40. The change in T_b for the T-2 channels as the ground temperature was modified from 295 to 285 K in the RT band model. The sounding profile had a TPW of 7.8 kg/m^2.

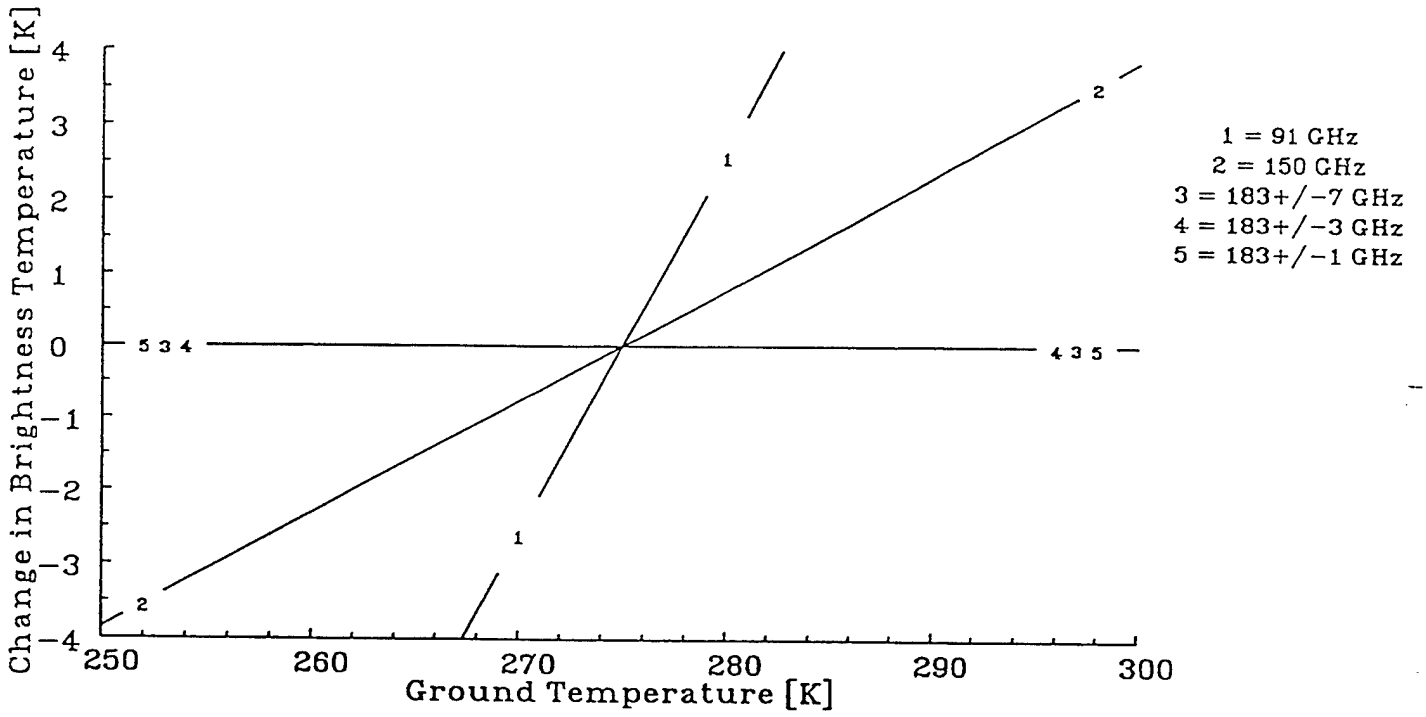

Figure 41. The change in T_b for the T-2 channels as the ground temperature was modified from 295 to 285 K in the RT band model. The sounding profile had a TPW of 56.3 kg/m^2.

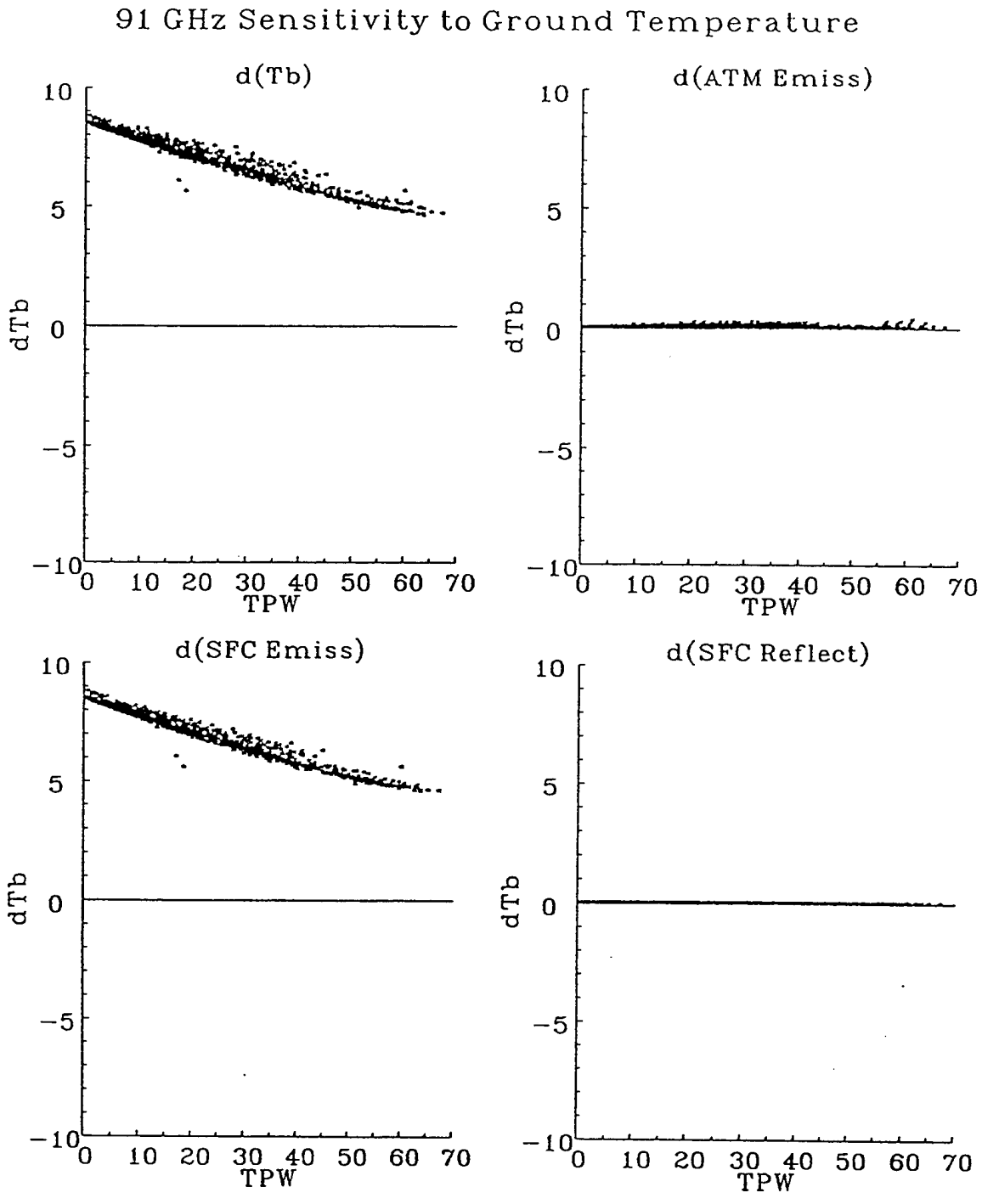

Figure 42. The change in T_b and its three dominant components (atmospheric and surface emissions and surface reflectance) for the T-2 channels as the ground temperature was modified from 295 to 285 K. All other parameters were set to constant values.

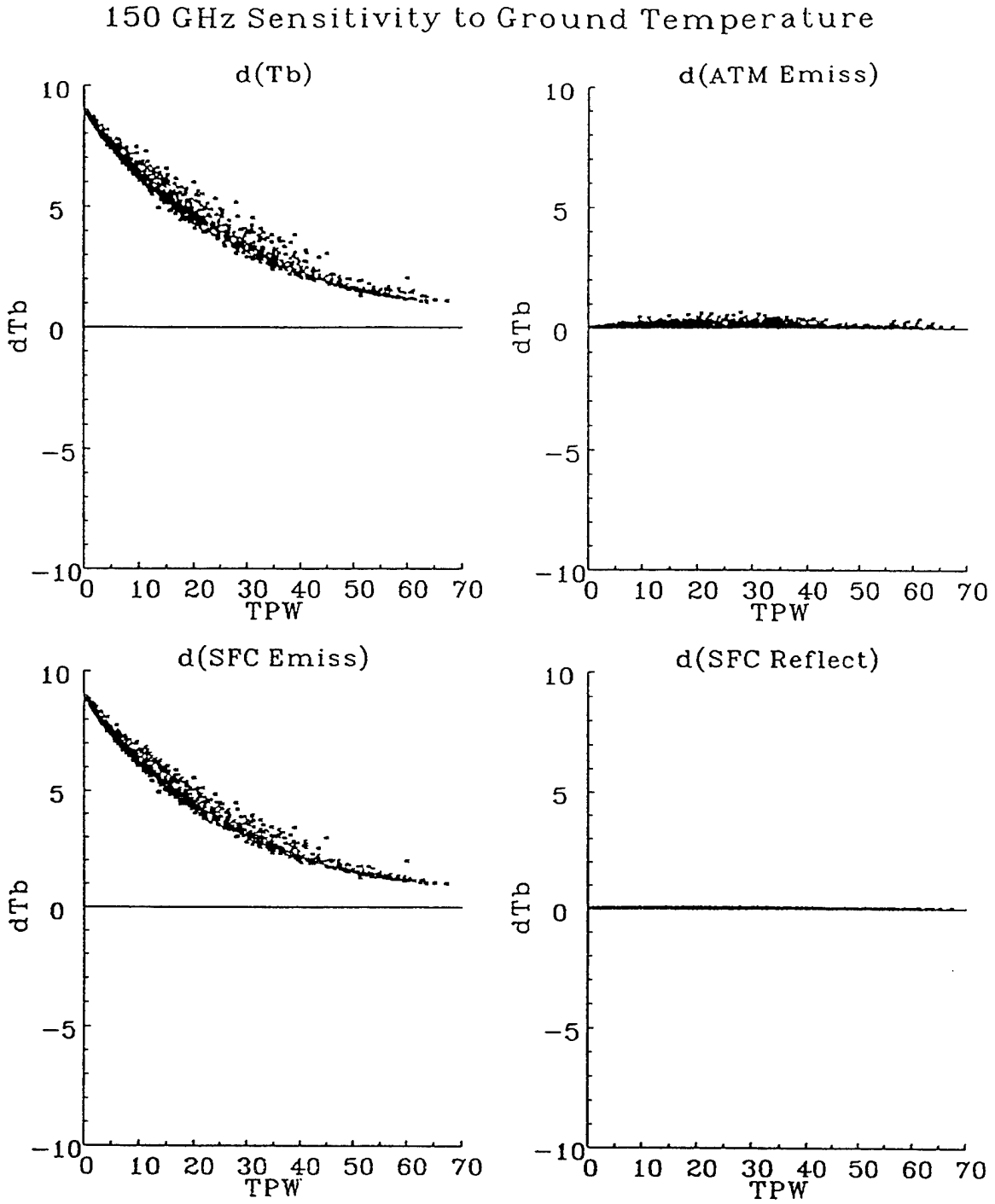

Figure 42. (continued) The change in T_b and its three dominant components (atmospheric and surface emissions and surface reflectance) for the T-2 channels as the ground temperature was modified from 295 to 285 K. All other parameters were set to constant values.

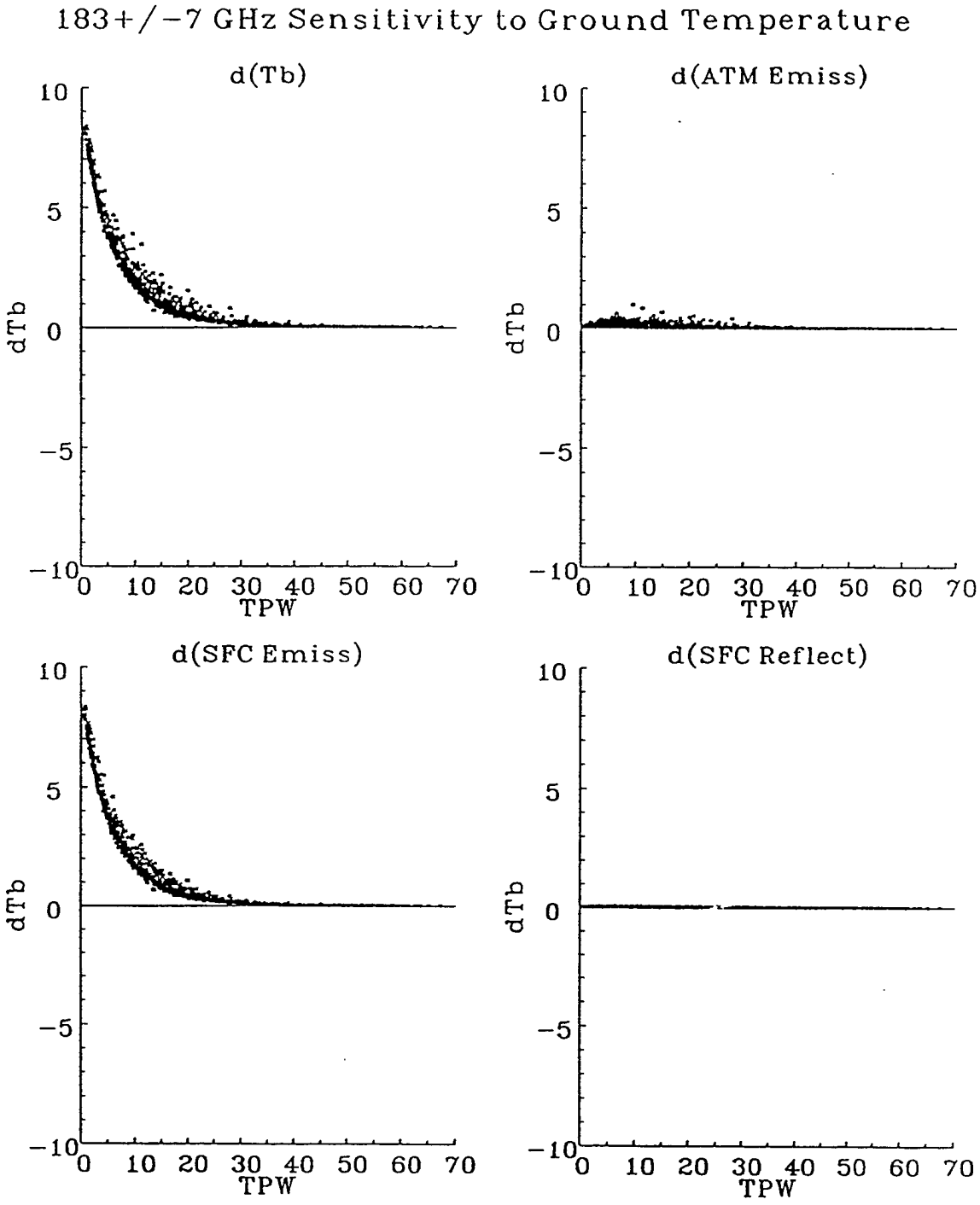

Figure 42. (continued) The change in T_b and its three dominant components (atmospheric and surface emissions and surface reflectance) for the T-2 channels as the ground temperature was modified from 295 to 285 K. All other parameters were set to constant values.

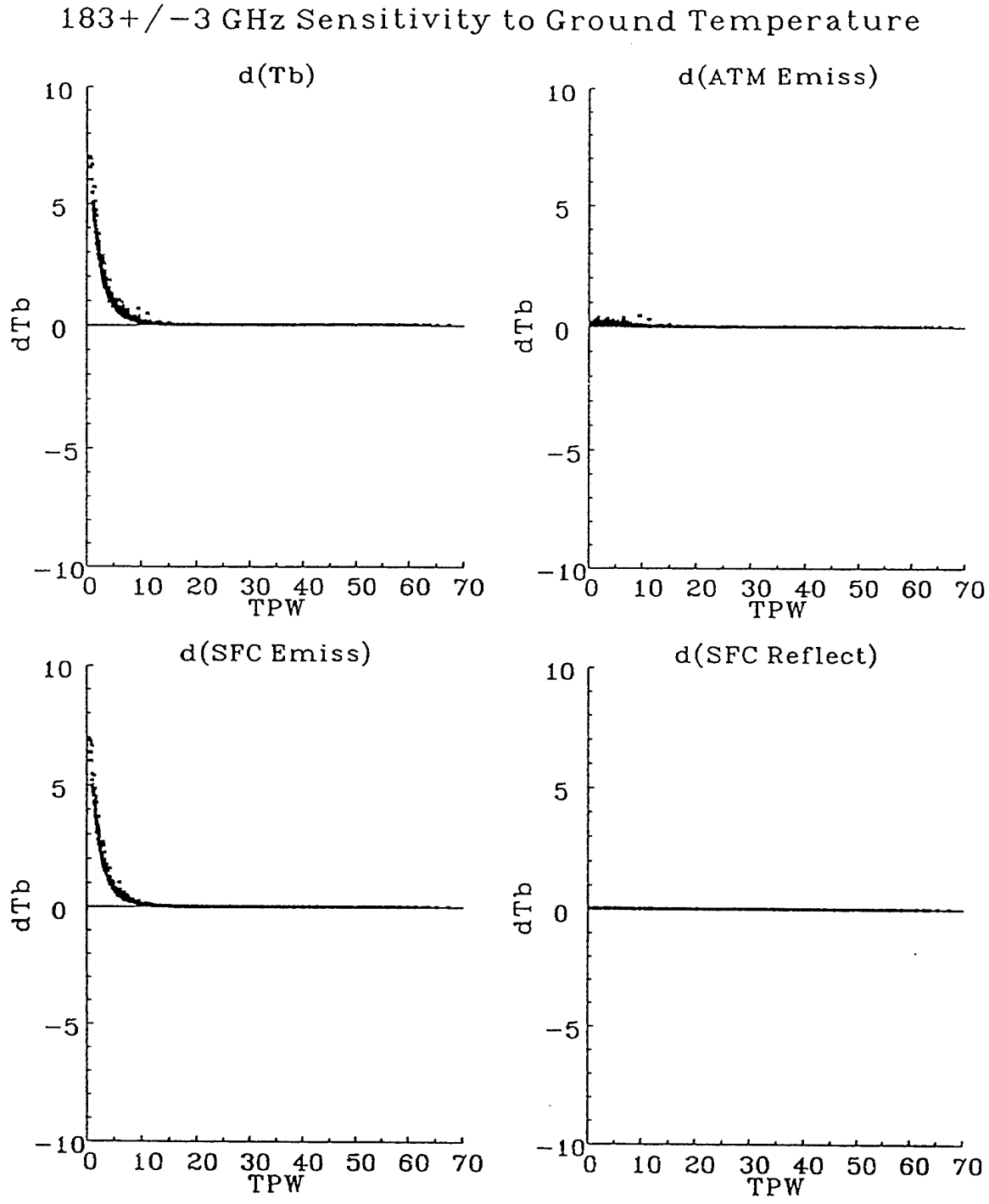

Figure 42. (continued) The change in T_b and its three dominant components (atmospheric and surface emissions and surface reflectance) for the T-2 channels as the ground temperature was modified from 295 to 285 K. All other parameters were set to constant values.

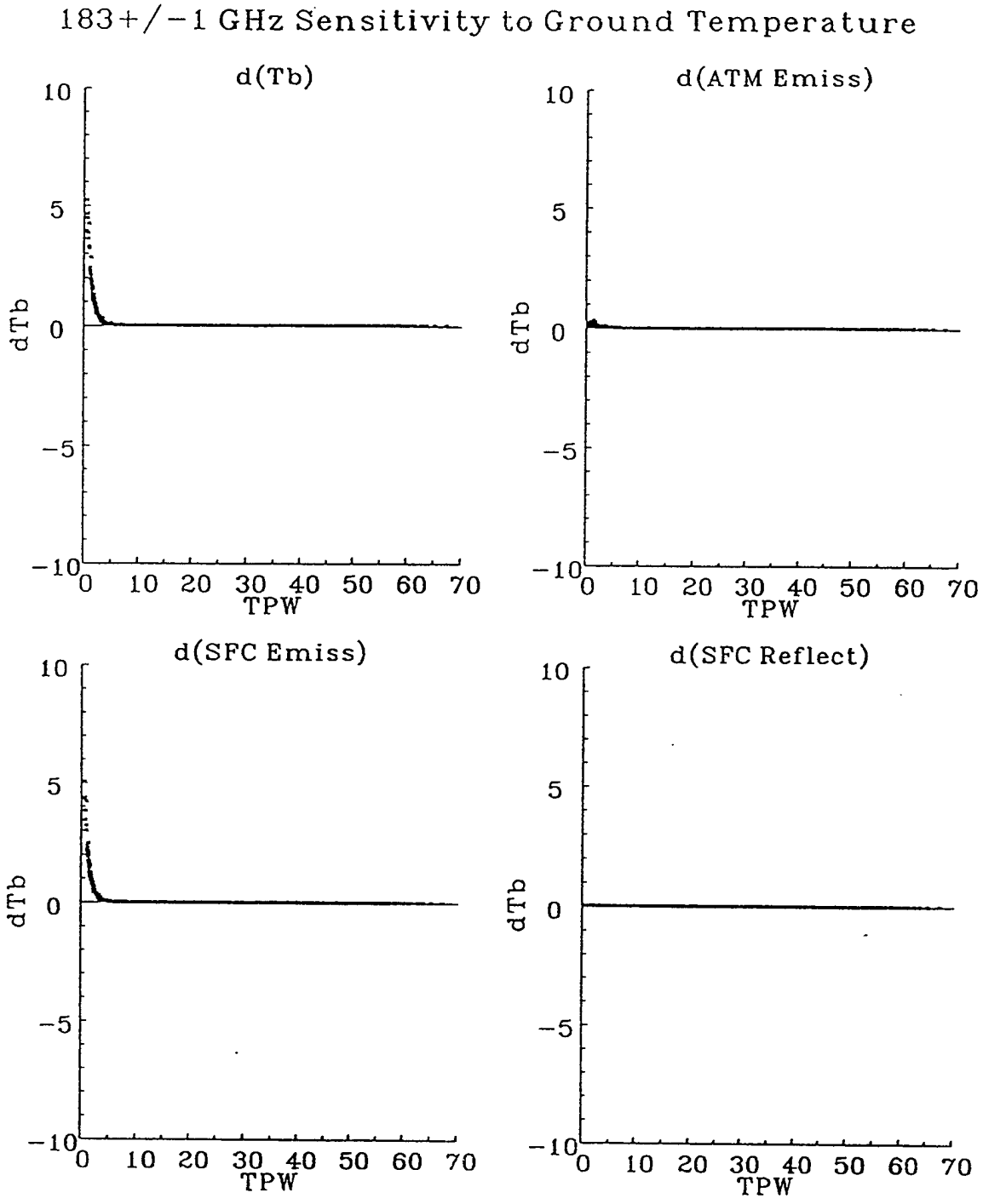

Figure 42. (continued) The change in T_b and its three dominant components (atmospheric and surface emissions and surface reflectance) for the T-2 channels as the ground temperature was modified from 295 to 285 K. All other parameters were set to constant values.

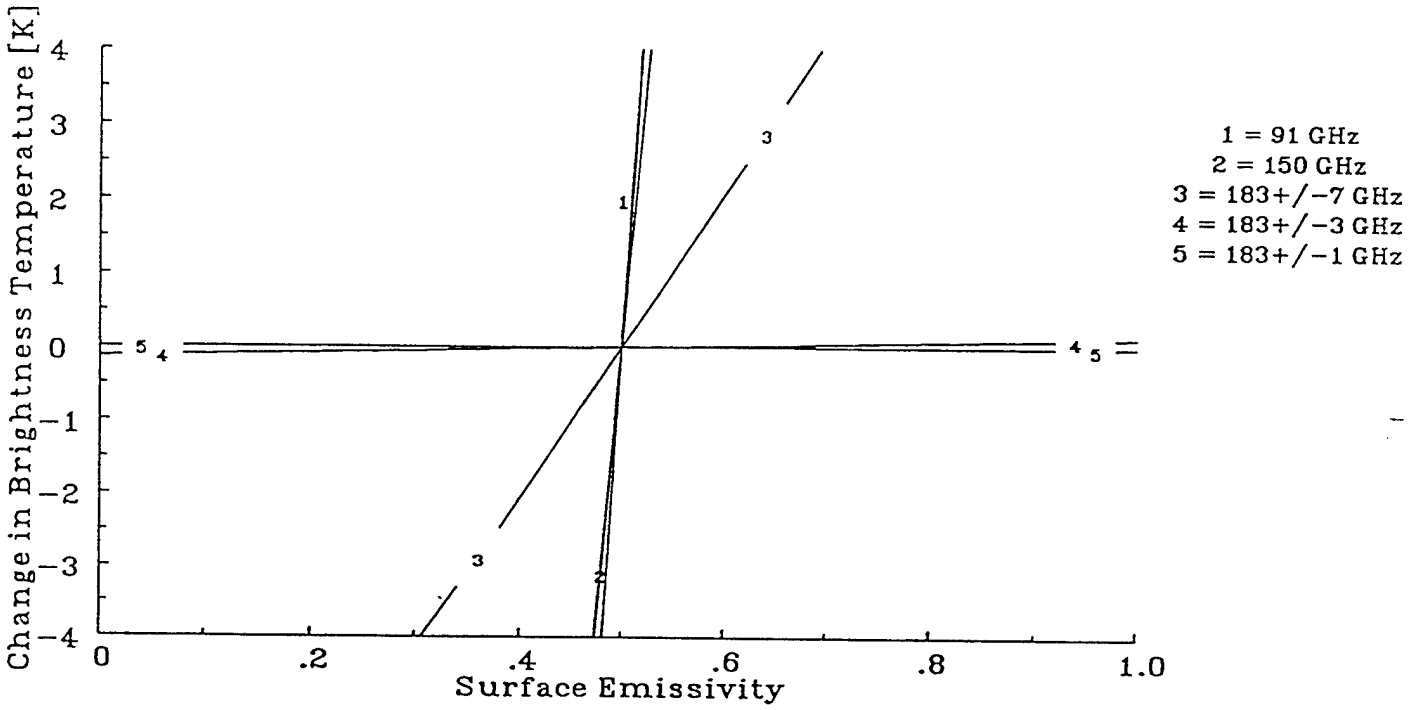

Figure 43. The change in T_b for the T-2 channels as the surface emissivity was modified from 0.95 to 0.85 in the RT band model. The sounding profile had a TPW of 7.8 kg/m^2.

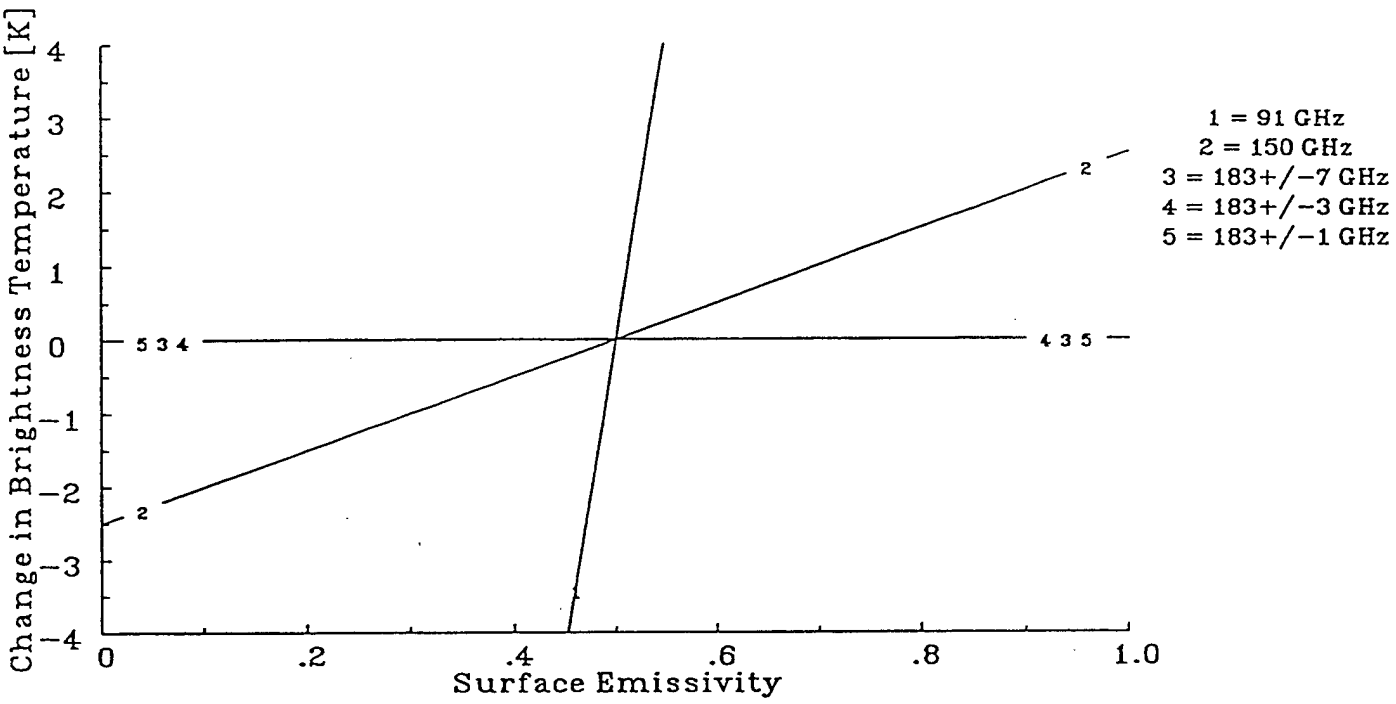

Figure 44. The change in T_b for the T-2 channels as the surface emissivity was modified from 0.95 to 0.85 in the RT band model. The sounding profile had a TPW of 56.3 kg/m^2.

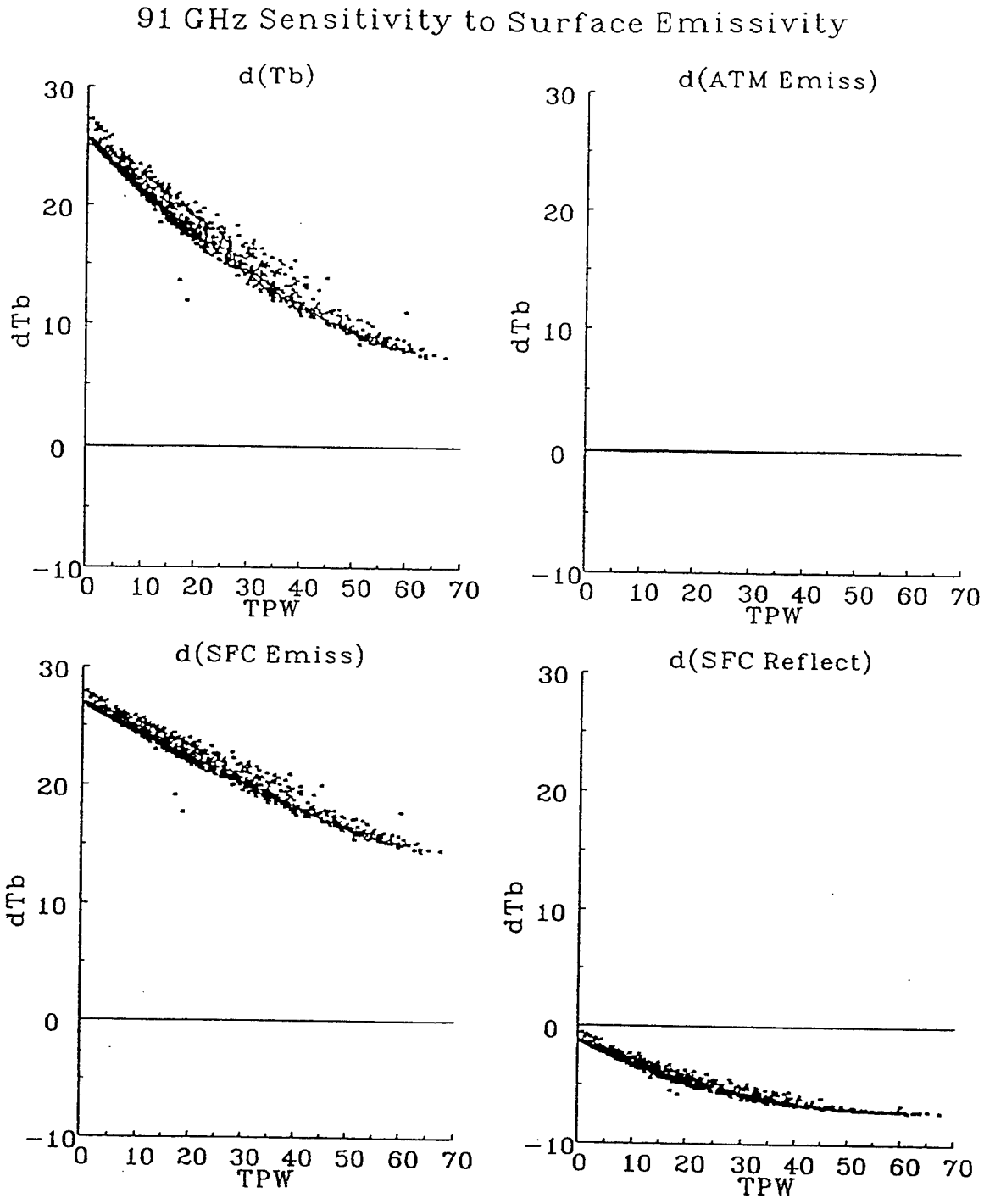

Figure 45. The change in T_b and its three dominant components (atmospheric and surface emissions and surface reflectance) for the T-2 channels as the surface emissivity was modified from 0.95 to 0.85. All other parameters were set to constant values.

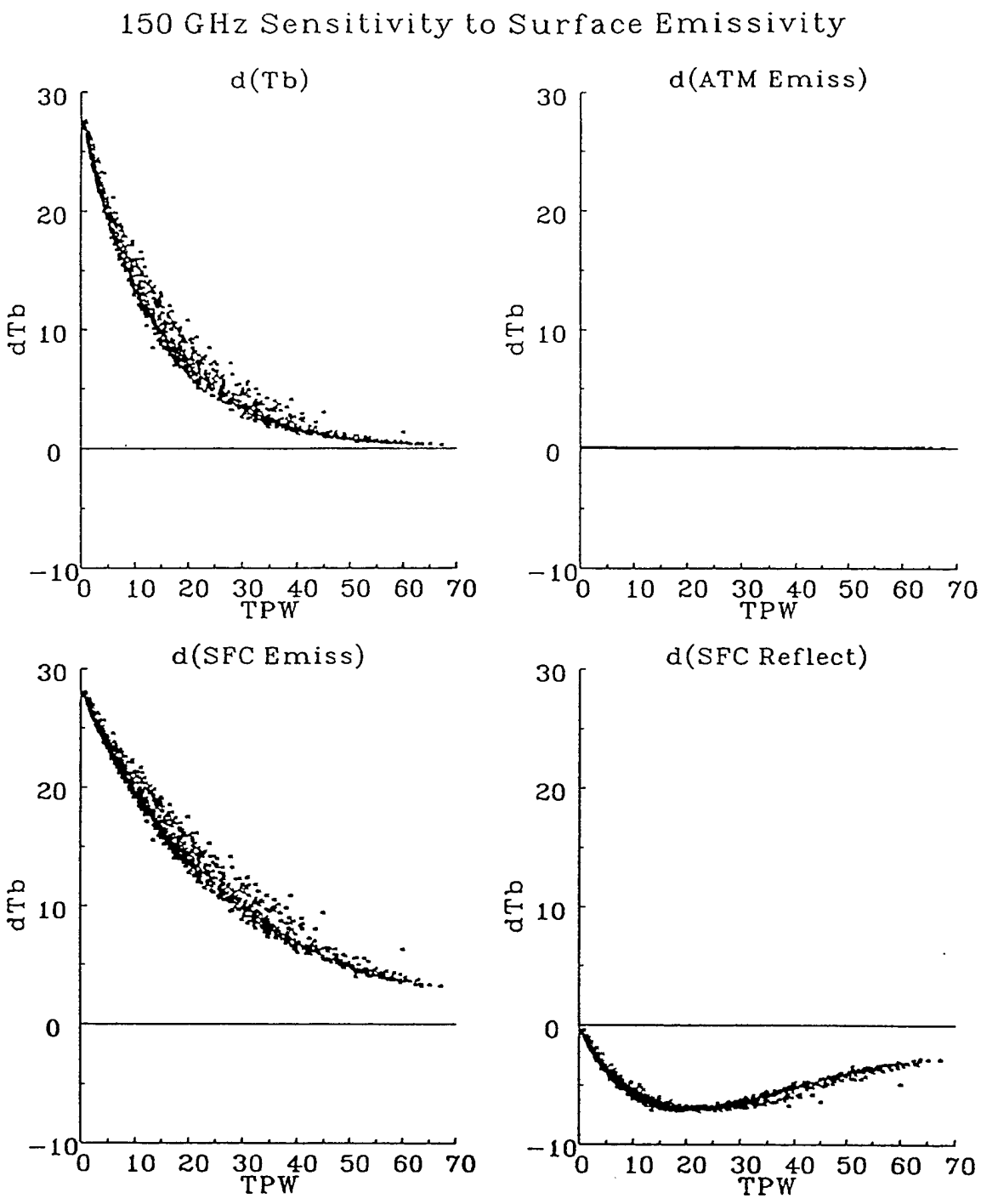

Figure 45. (continued) The change in T_b and its three dominant components (atmospheric and surface emissions and surface reflectance) for the T-2 channels as the surface emissivity was modified from 0.95 to 0.85. All other parameters were set to constant values.

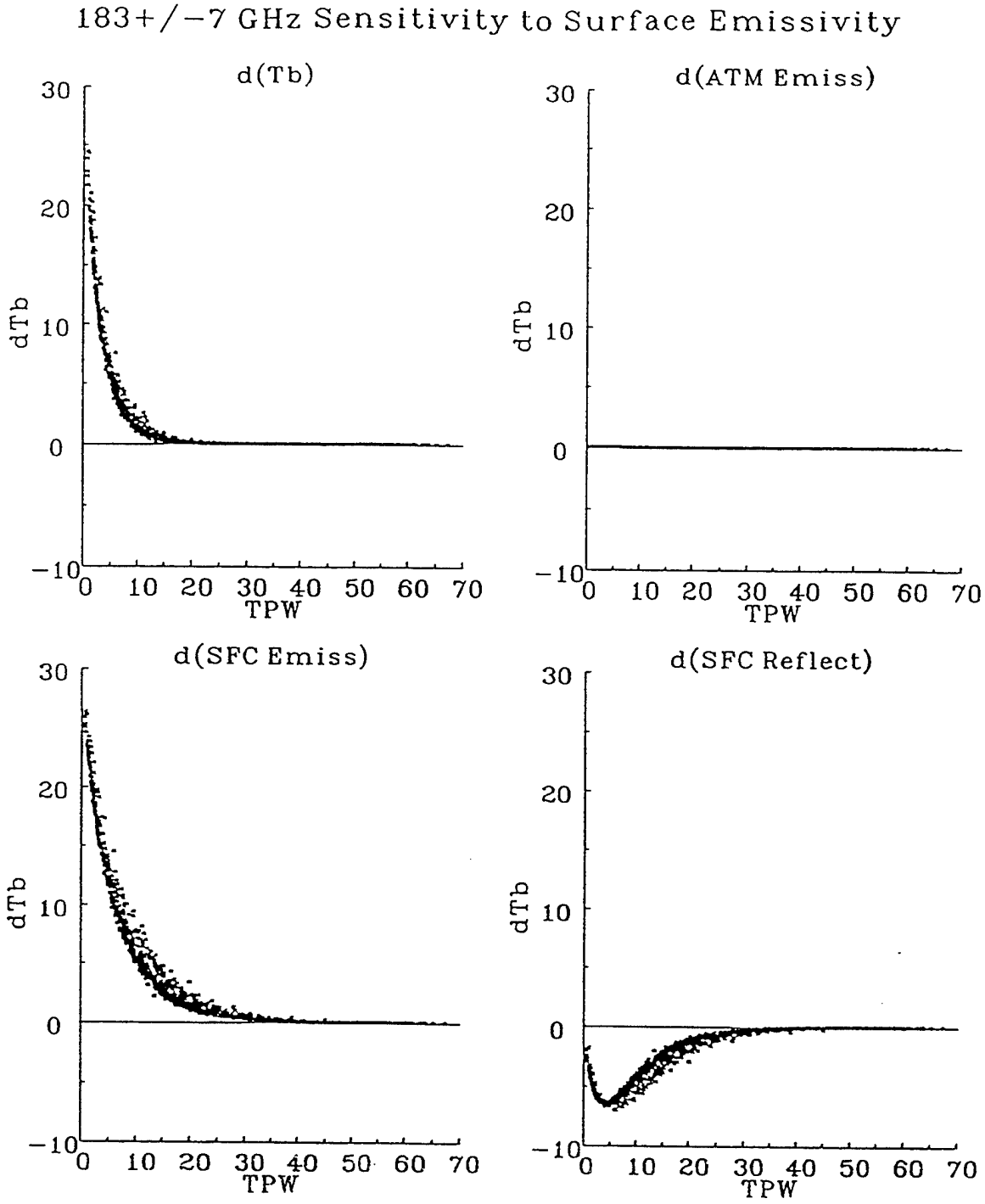

Figure 45. (continued) The change in T_b and its three dominant components (atmospheric and surface emissions and surface reflectance) for the T-2 channels as the surface emissivity was modified from 0.95 to 0.85. All other parameters were set to constant values.

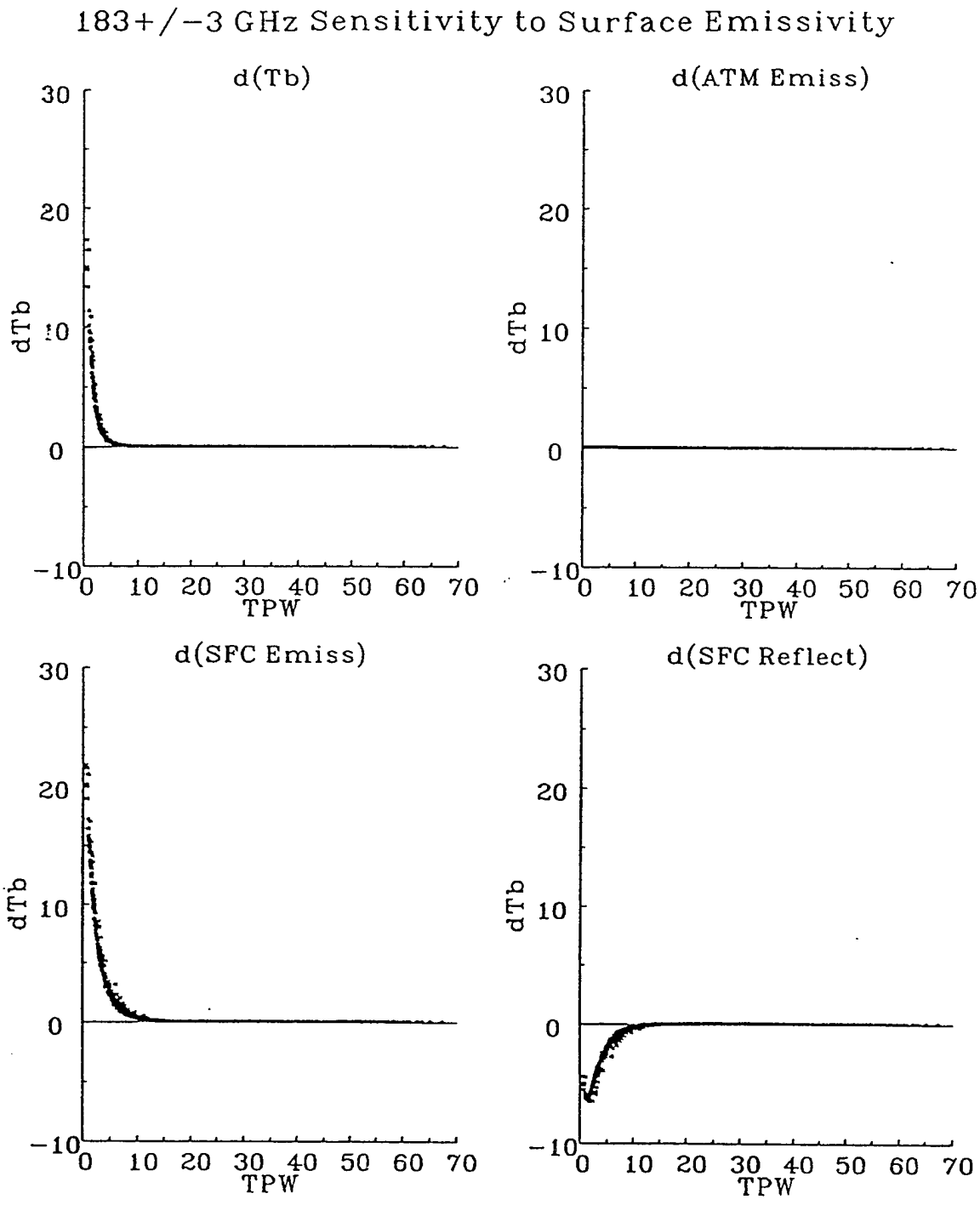

Figure 45. (continued) The change in T_b and its three dominant components (atmospheric and surface emissions and surface reflectance) for the T-2 channels as the surface emissivity was modified from 0.95 to 0.85. All other parameters were set to constant values.

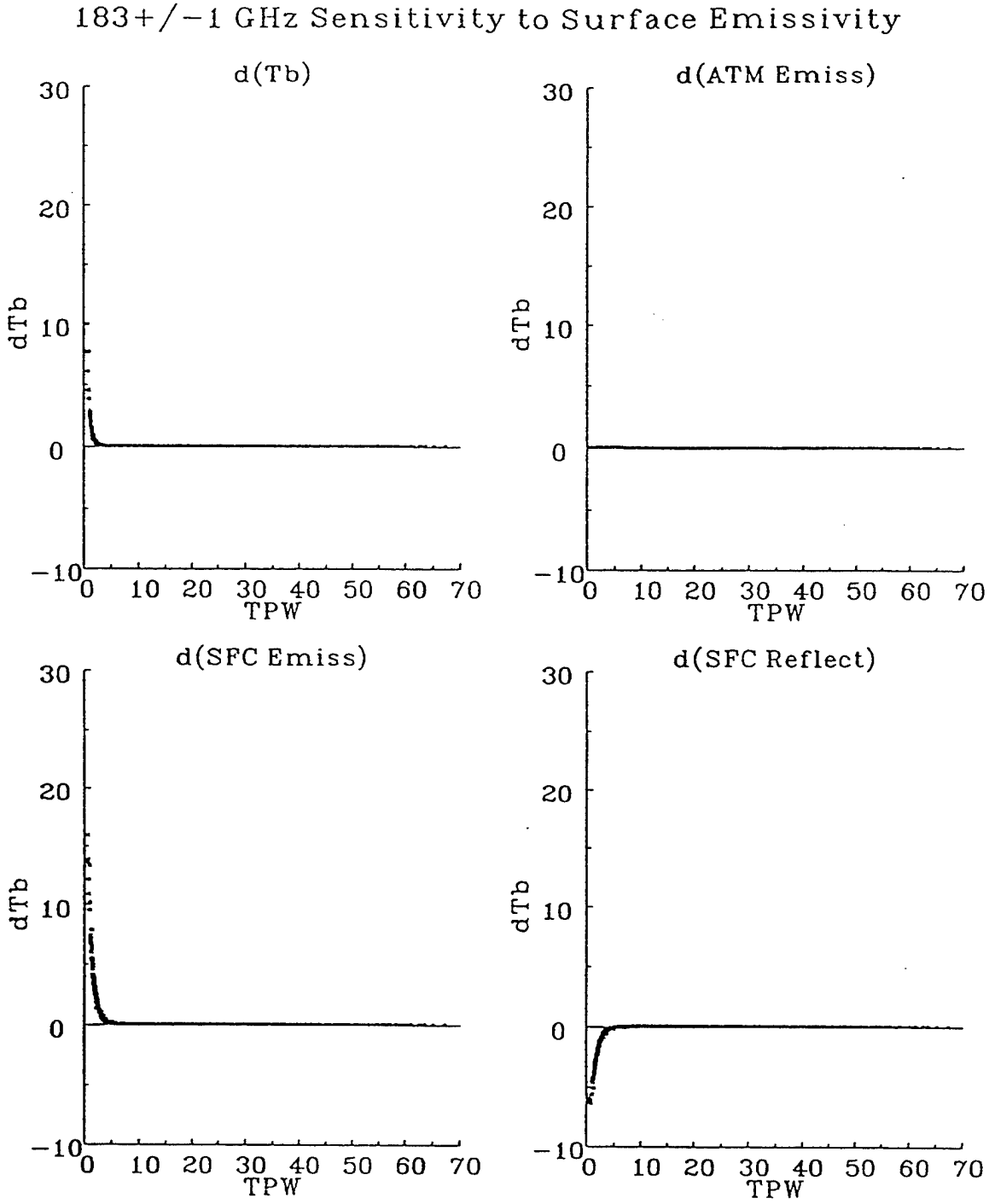

Figure 45. (continued) The change in T_b and its three dominant components (atmospheric and surface emissions and surface reflectance) for the T-2 channels as the surface emissivity was modified from 0.95 to 0.85. All other parameters were set to constant values.

4.6.2 General Distribution of Retrieved Surface Emissivities

There is a considerable range in retrieved surface emissivities using the global set of 1601 co-located T-2 SDRs and radiosondes (Figure 46) due in part to the wide range in TPW of the dataset. Surface emissivities for 91 GHz ranged from roughly 0.5 to 0.98 with no relationship between the surface emissivity and TPW in the radiosonde profile. There was a noticeable increase in range of retrieved surface emissivity for 150 GHz with increasing TPW. Surface emissivities at 183±7 GHz could not be retrieved when the TPW was greater than 30 kg/m^2 because the contribution from the surface was negligible.

The global set of co-located radiosondes and T-2 T_bs were divided into three terrain categories: water, land and coast. The data base was biased toward land and coastal terrains since most radiosondes were released from land stations. As expected, the land category consistently had the highest surface emissivity values, followed by coastal terrain and then water surfaces (Table 22).

Table 22. Distribution of retrieved surface emissivities for the 91 and 150 GHz channels. Unsaturated profiles are soundings with RH < 90% throughout the entire profile; saturated profiles are soundings with at least one layer having RH > 90%.

Topography	Mean	Mode	Standard Deviation	Frequency of Occurrence
	91 GHz Surface Emissivities: **Unsaturated** Profiles			
Water	0.61	0.56	0.07	21
Coast	0.78	0.82	0.10	241
Land	0.92	0.95	0.05	488
Total	0.86	0.95	0.11	750
	91 GHz Surface Emissivities: **Saturated** Profiles			
Water	0.59	0.54	0.06	19
Coast	0.79	0.79	0.10	350
Land	0.89	0.95	0.08	481
Total	0.84	0.93	0.11	850
	150 GHz Surface Emissivities: **Unsaturated** Profiles			
Water	0.61	0.56	0.17	20
Coast	0.73	0.79	0.21	232
Land	0.88	0.93	0.15	456
Total	0.82	0.93	0.19	708
	150 GHz Surface Emissivities: **Saturated** Profiles			
Water	0.45	0.31	0.25	16
Coast	0.71	0.87	0.25	331
Land	0.81	0.95	0.20	469
Total	0.76	0.87	0.23	816

4.6.3 Reproducibility of Retrieved Surface Emissivities

In order to study the reproducibility of retrieved surface emissivities, data was collected under clear conditions over a period of time (late spring to summer, 1992) for several land stations. The clear sky criteria required each profile to be unsaturated to thinly saturated (saturation thickness < 50 hPa). Sets of at least 5 retrieved surface emissivities for each station

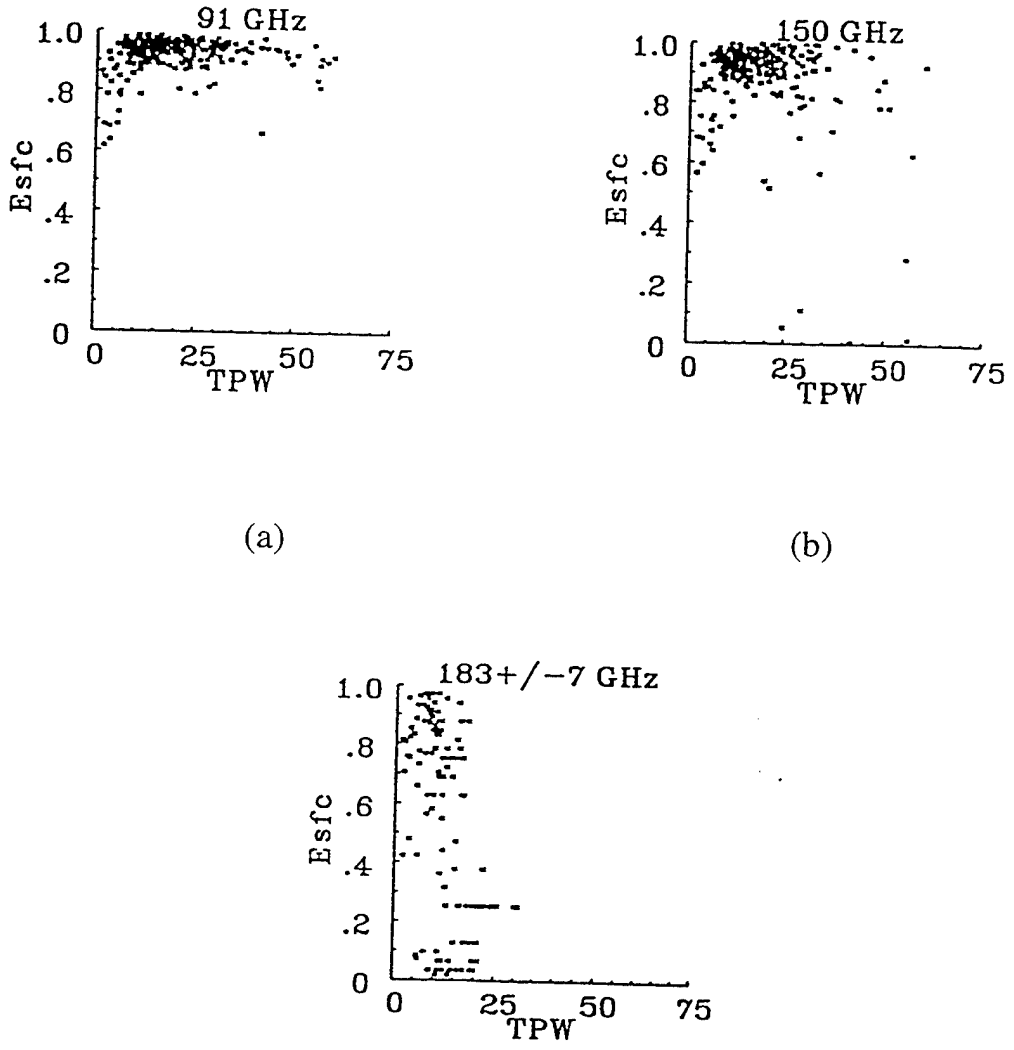

Figure 46. Distribution of retrieved surface emissivities for the (a) 91, (b) 150 and (c) 183±7 GHz channels. Only unsaturated soundings over land were used.

were used to examine the variation of surface emissivity for a particular location. The surface emissivities for 91 GHz appear to vary the least (be the most reproducible). The average standard deviation of retrieved 91 GHz surface emissivities was 0.022 for 15 stations. This value increased significantly for the 150 and 183±7 GHz channels (Table 23).

Table 23. Statistical distribution of the standard deviation for series of retrieved surface emissivities for individual land locations. Each series was required to have at least 5 unsaturated to thinly saturated (saturation thickness less than 50 hPa) radiosonde profiles. Data was collected during the late spring and summer months of 1992.

T-2 Channel	Mean of Standard Deviations	Standard Deviation of Standard Deviations	Frequency of Occurrence
91 GHz	0.022	0.014	15
150 GHz	0.050	0.041	15
183±7 GHz	0.270	0.124	9

4.6.4 Effect of Clouds and Precipitation

As shown in Table 24, the co-located radiosonde and T-2 SDR data were divided into two additional categories, unsaturated and saturated radiosonde profiles, in order to grossly identify the effects of clouds and/or precipitation on sensing the ground. Saturation was defined to occur when the relative humidity at any level within the sounding was greater than or equal to 90%. When the temperature at a given level was less than 0 C, then the relative humidity with respect to ice was used to identify saturation; and when the temperature was greater than or equal to 0 C, the relative humidity with respect to liquid water was used. Roughly half the radiosonde profiles were identified as saturated. The actual occurrence of clouds and/or precipitation in the T-2 FOV when there were saturated layers in the radiosonde profile was not verified. In addition, the amount of clouds and/or precipitation within each FOV could not be determined. Despite these limitations, the mean and modal surface emissivities for unsaturated atmospheres were generally larger than for saturated atmospheres for the 91 and 150 GHz channels (see Table 22). On average, as saturation thickness increased, regardless whether saturation occurred at temperatures above or below freezing, the retrieved surface emissivity decreased (Table 24).

Using data from varied weather conditions over the same location showed less conclusive relationships between retrieved surface emissivity and saturation thickness. Table 25 shows retrieved surface emissivities for a location with a sequence of 10 soundings which indicate that saturation thicknesses on the order of 200 - 300 hPa were needed to significantly decrease the retrieved surface emissivity lower than those retrieved for unsaturated cases on June 28 and 29. However, not all locations with co-located data measured with unsaturated and saturated conditions (at least 3 unsaturated cases) displayed these trends (Figure 47). Retrieved surface emissivities for both 91 and 150 GHz had anomalously large departures at all saturation thicknesses.

For the more poleward locations, unsaturated profiles during late winter through spring produced retrieved surface emissivities consistently and significantly lower than those retrieved during the summer months (Table 26). This would suggest the presence of snow during the cooler months.

Table 24. Distribution of retrieved surface emissivities for the 91 and 150 GHz channels for saturated profiles over low-lying land (0-200 m) only. Saturation thickness is examined for three conditions of saturation: 1) whenever the temperature (T) < 0 C (may have additional saturation with T > 0 C, 2) only when T > 0 C (no saturation with T < 0 C) and 3) any saturation, regardless of temperature.

Saturation Thickness [hPa]	Temp < 0 C			Temp > 0 C			Any Temp		
	Mean	St. Dev	# Cases	Mean	St. Dev	# Cases	Mean	St. Dev	# Cases
91 GHz									
0	.928	.044	193	.928	.044	193	.928	.044	193
1 - 49	.915.	.054	95	.927	.034	31	.915	.054	97
50 - 99	.910	.064	66	.931	.043	14	.916	.060	69
100 - 149	.902	.075	34	.907	.064	16	.907	.066	62
150 - 199	.897	.085	30	-	-	-	.898	.085	30
200 - 249	.880	.072	27	-	-	-	.874	.075	30
250 - 299	.906	.070	27	-	-	-	.913	.068	30
300 - 349	.819	.128	15	-	-	-	.862	.085	19
350 - 399	.814	.110	8	-	-	-	.874	.107	14
400 - 999	.835	.094	43	-	-	-	.845	.102	57
150 GHz									
0	.898	.137	178	.898	.137	178	.898	.137	178
1 - 49	.849	.203	91	.884	.161	31	.862	.188	95
50 - 99	.853	.184	65	.831	.257	13	.885	.133	67
100 - 149	.842	.187	34	.712	.337	15	.790	.274	60
150 - 199	.822	.205	29	-	-	-	.837	.192	29
200 - 249	.778	.218	27	-	-	-	.755	.261	30
250 - 299	.818	.195	26	-	-	-	.869	.119	29
300 - 349	.702	.300	14	-	-	-	.764	.202	19
350 - 399	.757	.186	8	-	-	-	.804	.173	13
400 - 999	.782	.114	43	-	-	-	.734	.208	56

Table 25. Distribution of retrieved surface emissivities for one location under various thicknesses of saturation. "Elev" is the average surface elevation of the sensed FOV. "Thick" represents the thickness [hPa] of saturated conditions (RH > 90%) within the profile presented for two temperature regimes.

Station	23472	Turuhansk	Russia	65.78° N		87.95° E		32 m	
	Surface Emissivity			TPW	Scan	Elev	P(sfc)	Thick	Thick
Date	91	150	183±7	kg/m^2	Angle	m	hPa	T<0C	T>0C
2/5/92	.887	.882	.867	6.0	25.5°	113	1016	345	0
3/1/92	.810	.758	.760	1.1	16.5°	126	1030	577	0
3/6/92	.807	.804	.844	2.4	37.5°	126	1012	791	0
6/11/92	.927	.932	.938	8.1	22.5°	126	1005	137	0
6/12/92	.897	.877	.688	11.1	13.5°	113	1005	646	0
6/12/92	.894	.723	.063	14.6	22.5°	126	988	574	59
6/28/92	.933	.945	-	13.9	22.5°	113	1014	0	0
6/29/92	.937	.949	-	12.7	13.5°	126	1016	0	0
6/29/92	.935	.916	-	9.8	22.5°	126	1017	0	0
8/6/92	.922	.934	-	17.8	13.5°	113	1007	12	0
Mean	.895	.872	-						
StDev	.049	.082	-						

Table 26. Distribution of retrieved surface emissivities for one location at various times of the year and saturation conditions. "Elev" is the average surface elevation of the sensed FOV. "Thick" represents the thickness [hPa] of saturated conditions (RH > 90%) within the profile presented for two temperature regimes.

Station	51644	Kuqu	China	41.71° N		82.95° E		1100 m	
	Surface Emissivity			TPW	Scan	Elev	P(sfc)	Thick	Thick
Date	91	150	183/7	kg/m^2	Angle	m	hPa	T<0C	T>0C
2/5/92	.807	.809	.680	5.2	40.5°	1275	901	0	0
3/2/92	.890	.902	.500	8.7	40.5°	921	898	167	0
3/3/92	.877	.882	.781	8.3	28.5°	1275	897	0	0
3/6/92	.886	.852	.750	9.4	16.5°	1381	900	42	0
5/14/92	.918	.924	.563	17.4	16.5°	1275	889	123	0
5/15/92	.920	.924	.813	14.9	1.5°	1275	888	0	0
5/21/92	.900	.900	.938	10.9	28.5°	1186	886	0	0
6/13/92	.908	.891	.313	19.1	1.5°	1952	886	55	0
6/29/92	.894	.727	.125	24.2	4.5°	1275	881	153	0
6/30/92	.922	.930	-	29.0	37.5v	1275	881	308	0
Mean	.892	.874	-						
StDev	.034	.064	-						

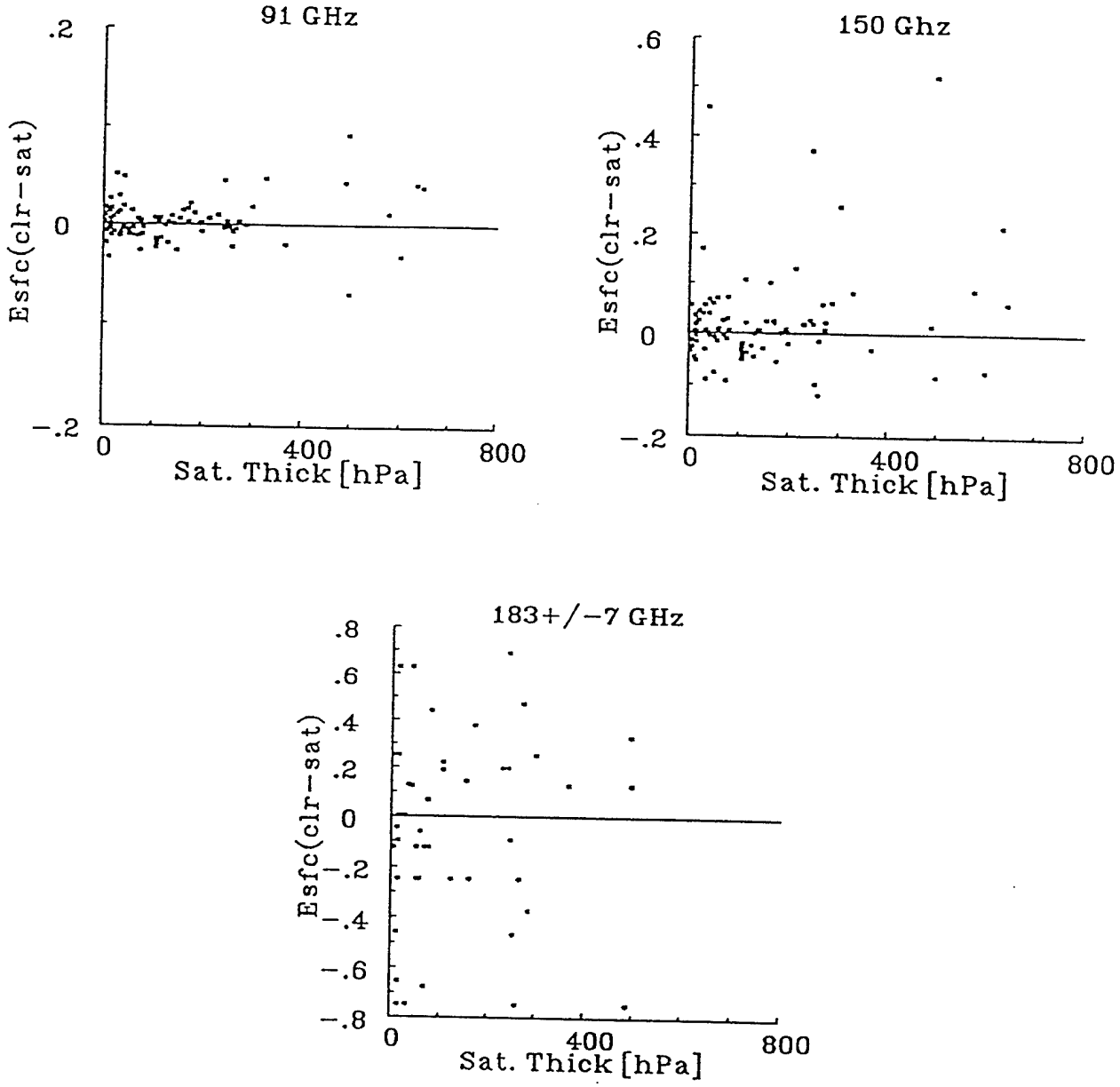

Figure 47. Differences between the mean surface emissivity retrieved from a radiosonde station with at least 3 cases of unsaturated profiles and surface emissivities retrieved soundings with varying thickness of saturation present. Only profiles measured at low-lying (0-200 m elevation) land stations during late spring and summer, 1992 were used.

4.6.5 Effect of Satellite Viewing Angle

As the apparent moisture in the atmosphere increased, either due to increasing water vapor amount or lengthening the atmospheric path by increased satellite viewing angle, the T-2 channels sensed less of the surface. Table 27 shows the retrieved surface emissivities over land for 91 and 150 GHz using unsaturated profiles with a TPW of less than 30 kg/m^2. Despite including the wide variety of surface types (snow, varying elevation, dry/wet conditions and varied vegetation), retrieved surface emissivities decreased with increasing satellite viewing angle for both frequencies. Note that these retrieved surface emissivities required using the satellite viewing angle associated with each SDR.

Table 27. Distribution of retrieved surface emissivities for the 91 and 150 GHz channels with respect to satellite viewing angle. Only unsaturated profiles with TPW less than 30 kg/m^2 were used. Only land cases provided an adequate number of cases per viewing angle.

Viewing Angle Index	Mean	Mode	Standard Deviation	Number of Cases
		91 GHz Surface Emissivity for Land		
1 - 28 (40.5°)	0.876	0.875	0.055	20
2 - 27 (37.5°)	0.875	0.925	0.070	14
3 - 26 (34.5°)	0.886	0.925	0.099	9
4 - 25 (31.5°)	0.900	0.925	0.076	12
5 - 24 (28.5°)	0.922	0.925	0.038	45
6 - 23 (25.5°)	0.915	0.925	0.063	30
7 - 22 (22.5°)	0.919	0.925	0.048	31
8 - 21 (19.5°)	0.924	0.925	0.036	21
9 - 20 (16.5°)	0.928	0.925	0.050	23
10 - 19 (13.5°)	0.929	0.925	0.039	24
11 - 18 (10.5°)	0.911	0.925	0.069	28
12 - 17 (7.5°)	0.923	0.925	0.041	24
13 - 16 (4.5°)	0.944	0.975	0.025	12
14 - 15 (1.5°)	0.916	0.925	0.052	24
		150 GHz Surface Emissivity for Land		
1 - 28 (40.5°)	0.804	0.875	0.191	20
2 - 27 (37.5°)	0.858	0.925	0.076	14
3 - 26 (34.5°)	0.856	0.925	0.125	8
4 - 25 (31.5°)	0.891	0.925	0.077	12
5 - 24 (28.5°)	0.887	0.925	0.140	43
6 - 23 (25.5°)	0.906	0.925	0.078	29
7 - 22 (22.5°)	0.891	0.925	0.098	30
8 - 21 (19.5°)	0.916	0.925	0.058	21
9 - 20 (16.5°)	0.926	0.925	0.065	21
10 - 19 (13.5°)	0.911	0.925	0.070	24
11 - 18 (10.5°)	0.895	0.925	0.081	26
12 - 17 (7.5°)	0.920	0.925	0.055	24
13 - 16 (4.5°)	0.944	0.925	0.027	12
14 - 15 (1.5°)	0.909	0.925	0.071	24

4.6.6 Effect of Total Precipitable Water

Examining the distribution of retrieved surface emissivities with respect to TPW (Figure 46) indicated little relationship between the two variables. Only the range in the retrieved 150 GHz surface emissivity increase with increasing TPW. This was due in part to the inclusive nature of the data set: all surface types and terrains (land, ocean, coast, snow and ice) and elevations, all seasons, all viewing angles, and all cloud and precipitation conditions.

4.6.7 Effect of Moisture Profile Uncertainty

The surface emissivities retrieved when the radiosonde RH amounts at each significant level were increased and decreased by 10% are presented in Figure 48. For both the 91 and 150 GHz frequencies, the range of surface emissivity changes increased when the TPW of the original sounding was increased. The enhanced moisture almost always lowered the 91 GHz retrieved surface emissivity; whereas, for 150 GHz, surface emissivity generally decreased with increasing moisture but with a significant number of exceptions. The range of differences increased from 91 GHz to 150 GHz. Classifications of saturated and unsaturated were based on the unmodified moisture profile; changes in saturation classification were not tested after the moisture profile was modified.

4.6.8 Effect of Temperature Profile Uncertainty

The surface emissivities retrieved when the air temperature profiles were increased and decreased by 1 K at all levels are presented in Figure 49. For both the 91 and 150 GHz frequencies, the range in difference between the surface emissivities increased with increasing TPW of the original sounding. The increased temperature lowered the 91 and 150 GHz retrieved surface emissivities. The range of differences increased from 91 GHz to 150 GHz. The effect of increasing air temperature on the 91 GHz was confined to a surface emissivity change of less than 0.02 for the entire range of TPW cases; whereas the difference for the 150 GHz emissivities ranged up to 0.7. Again, classifications of saturated and unsaturated were based on the unmodified moisture profile; changes in saturation classification were not tested after the moisture profile was modified.

4.6.9 Effect of Ground Temperature Uncertainty

The surface emissivities retrieved when the ground temperatures (set to the atmospheric temperature closest to the ground for this case) were increased and decreased by 5 K are presented in Figures 50. For both the 91 and 150 GHz frequencies, the range in difference between the surface emissivities increased with increasing TPW of the original sounding. The increased ground temperature lowered the 91 and 150 GHz retrieved surface emissivities. The effect of increasing ground temperature on the 91 GHz was confined to a surface emissivity difference between 0.02 and 0.06 for the entire range of TPW cases; whereas the difference for the 150 GHz emissivities ranged up to 0.26.

4.6.10 Effect of SDR T_b Uncertainty

The surface emissivities retrieved when the satellite brightness temperatures were increased and decreased by 1 K are presented in Figure 51. This range in SDR T_bs defines the limit of accuracy for the atmospheric channels determined during the T-2 CALVAL study (Falcone et al., 1992; Griffin et al., 1993; and Pickle et al., 1993). Increased SDR T_bs required increased retrieved surface emissivities since the ground temperature remained constant.

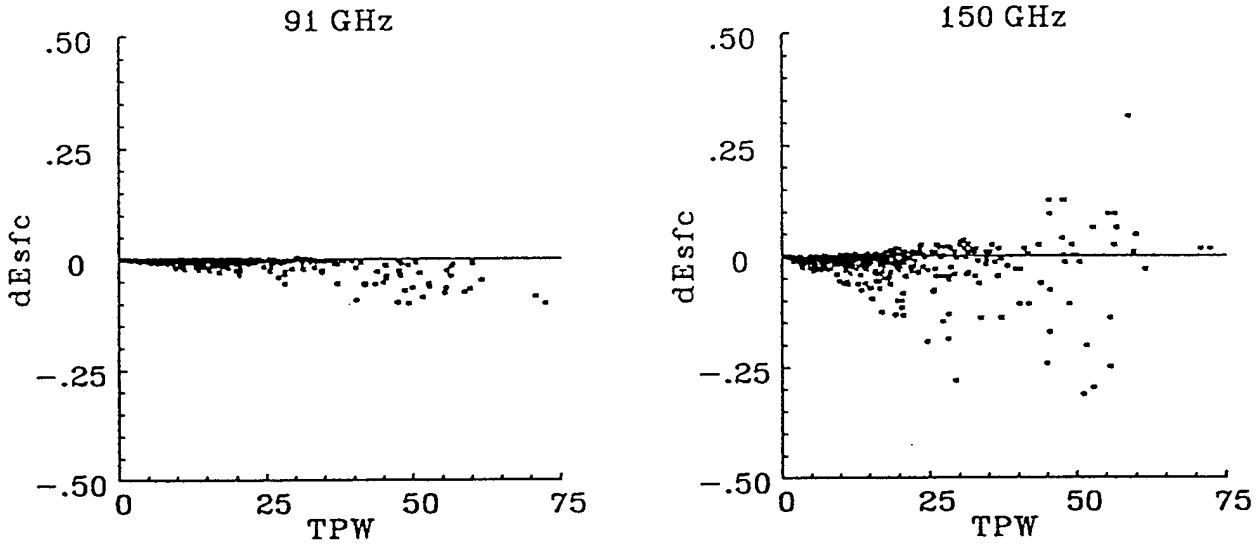

Figure 48. Change in retrieved surface emissivities for the 91 and 150 GHz channel as the RH was varied from 90% to 110% of the original profile values.

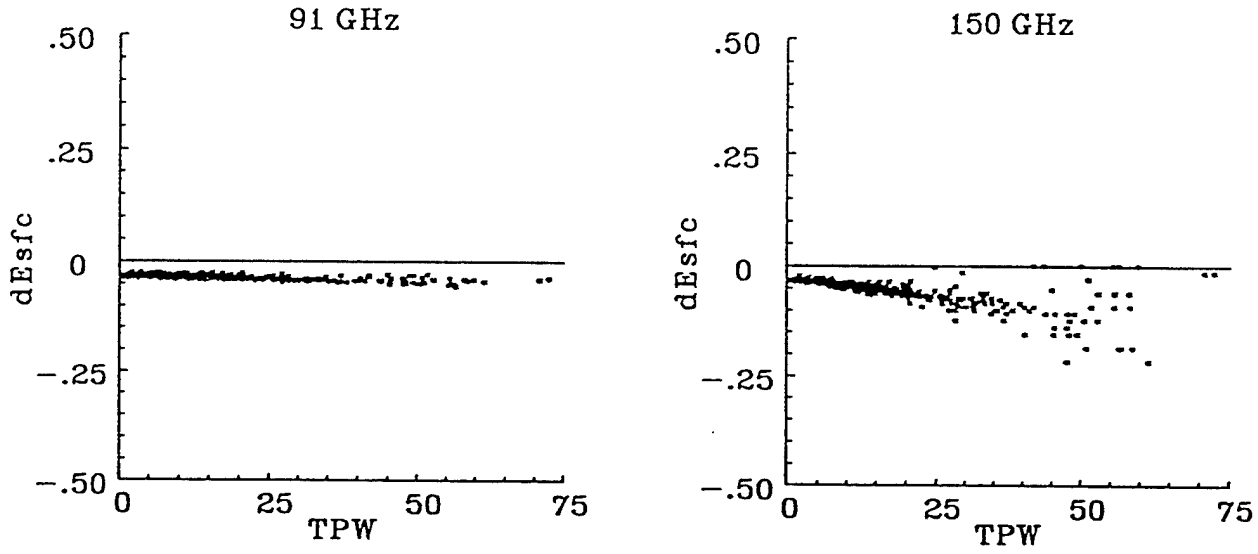

Figure 49. Change in retrieved surface emissivities for the 91 and 150 GHz channels as the temperature profile was increased from -1 K of the original values to +1 K.

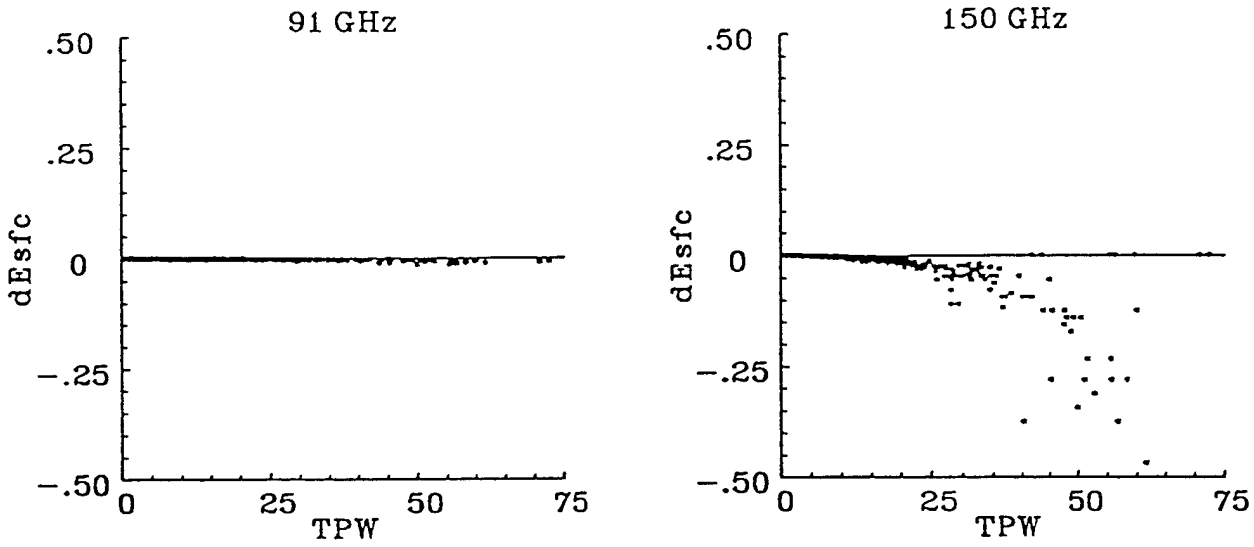

Figure 50. Change in retrieved surface emissivities for the 91 and 150 GHz channels as the ground temperature was increased from -5 K of the closest near-surface atmospheric temperature to +5 K.

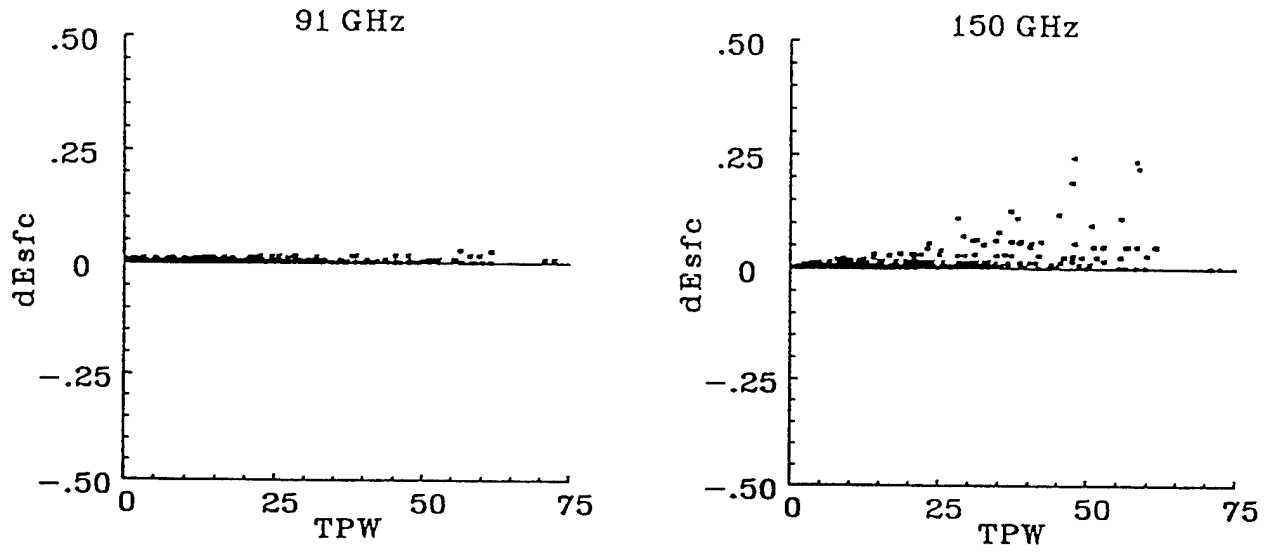

Figure 51. Change in retrieved surface emissivities for the 91 and 150 GHz channel as the satellite T_b was increased from -1 K of the original value to +1 K.

For both the 91 and 150 GHz frequencies, the range in modification of retrieved surface emissivities increased with increasing TPW since the proportion of surface contribution to the satellite T_b decreased as the atmospheric moisture increased. The range of surface emissivity change increased from 91 GHz to 150 GHz. The maximum change of the retrieved surface emissivity at 91 GHz was less than 0.03 for the entire range of TPW cases; whereas, the change for the 150 GHz emissivities reached 0.26.

4.6.11 Surface Emissivity Retrieval Conclusions

Surface emissivity is a critical component in RT model calculations and physical retrievals of meteorological parameters. A technique was developed to iteratively retrieve surface emissivity using temperature and moisture profiles and co-located T-2 T_bs. Overall, uncertainty in retrieving the surface emissivity was dependent upon whether obstructions (clouds and precipitation which may mitigate sensing of the surface) are in the SDR FOV, the unknown radiative ground temperature, the possible errors in the radiosonde moisture and temperature profiles, errors in the SDR T_b, the satellite viewing angle and the amount of atmospheric water vapor in the profile. Although the influence of precipitation and clouds were not quantified, the influence of many parameters on retrieving surface emissivity over a reasonable range of values is presented in Table 28. Parameters that significantly influenced the retrieved 91 GHz surface emissivity did not necessarily produce similar effects on the 150 GHz surface emissivity.

Table 28. Sensitivity of the retrieved surface emissivity for 91 and 150 GHz to various atmospheric and surface parameters. Realistic ranges of each parameter were selected.

	Parameter	91 GHz							
Parameter	Range	Mean	Mode	Med.	StDev	Min	Max	Range	Cases
Scan Angle	0-40.5°	-	-	-	-	-	.040	-	-
TPW	0-70 kg/m^2	-	-	-	-	-	.100	-	-
RH Profile	± 10%	-.009	-.002	-.003	.017	-.119	.004	.123	519
T Profile	± 1 K	-.002	-.001	-.002	.002	-.016	.0	.016	519
$T_{(Ground)}$	± 5 K	-.039	-.040	-.038	.005	-.059	-.025	.033	512
SDR T_b	± 1 K	.002	.001	.001	.004	.0	.027	.027	519
Clouds	0-300 hPa	-	-	-	-	-	.060	-	-
		150 GHz							
Scan Angle	0-40.5°	-	-	-	-	-	.100	-	-
TPW	0-70 kg/m^2	-	-	-	-	-	.150	-	-
RH Profile	± 10%	-.017	-.031	-.008	.047	-.313	.313	.625	477
T Profile	± 1 K	-.025	-.030	-.006	.065	-.594	.0	.594	475
$T_{(Ground)}$	± 5 K	-.057	-.055	-.050	.028	-.219	.0	.219	452
SDR T_b	± 1 K	.010	.012	.003	.025	.0	.242	.242	509
Clouds	0-300 hPa	-	-	-	-	-	.100	-	-

Surface and near-surface channel T_bs were highly influenced by surface emissivity on the order of 1 K per 0.01 change in surface emissivity. Iteratively retrieving the surface emissivity using RT models with co-located T-2 T_bs and radiosonde profiles yielded general trends that agreed with observations (i.e. surface emissivity over land was generally greater than over water). The retrieved surface emissivities appeared to be quite reproducible for the same location; on the order of 0.02 for 91 GHz for 15 different locations.

4.7 Climatology of Atmospheric and Surface Contributions and Weighting Functions

Since the RT model results were non-linear, the climatologies of the weighting functions and the contributions from the atmosphere and surface were calculated to provide a reference for users of T-2 data. The climatologies are with respect to TPW, which are similar to that with respect to latitude. The Eyre RT model using the global set of radiosonde profiles were used to generate the statistics.

Only 10% of the weighting functions for 91 GHz peaked above the earth's surface. This result led to the near constant pressure levels of the peak of the weighting function despite increasing TPW and the pressure levels of the 25th, 50th, and 75th percentiles of the weighting functions being at consistently lower values compared to the weighting functions for 150 GHz (Table 29). However, the percent contributions from the surface emissions to the 91 GHz T_b decreased steadily as TPW increased (Table 30). The trends observed for the other 4 T-2 channels were similar: weighting functions shifted to lower pressures and less of the surface and more of the atmosphere was sensed as TPW increased. Notice that as TPW increased, the weighting functions of the 183 GHz channels sensed a smaller band of the atmosphere (see the difference between the pressure levels of the 75th and 25th percentiles of the weighting functions in Table 29) and the overlap of the weighting functions decreased (see the difference between the pressure levels of the peaks of the weighting functions).

5. SYNTHESIS OF 150 GHZ BRIGHTNESS TEMPERATURES

Since the failure of the 150 GHz sensor of the T-2 instrument on board the F-11 satellite in June 1993, techniques were needed to simulate T_bs for the channel in order to continue statistical retrievals of water vapor profiles. Since the T-2 channels sense overlapping vertical segments of the atmosphere, relationships between the T_bs for various atmospheric and topographic conditions (clouds, rain, ice, ocean, land, etc.) were examined using CALVAL data gathered before the failure of the 150 GHz sensor. It was observed that a majority of observed T_b sets had similar relationships between channels and that individual T_bs were bounded by ranges of temperature, especially for clear sky conditions.

Those findings led to the selection of a multiple regression method to synthesize the 150 GHz T_bs since all channels contributed some information about the atmosphere which affected the 150 GHz T_bs (Table 31). The upper atmospheric channels (183±3 and 1 GHz) indicated if thick clouds or precipitation were present. The near-surface 183±7 GHz T_b provided information on the amount of lower atmospheric moisture and to a lesser extent the surface contributions. The 91 GHz T_bs provided information about the surface contributions. The 150 GHz channel sensed a combination of low-level atmospheric moisture and surface emission, which was dependent on the TPW.

As an initial test of the multiple regression technique, terrain categories (water, ice and land with elevation categories of 0-500 m, 500 - 1000 m, and > 1000 m) and four latitude categories (90 - 65, 65 - 40, 40 - 20, and 20 - 0) were selected. Note that no coastal categories were used, and each latitude category included both northern and southern hemisphere points.

Table 29. Mean pressure levels of statistical features of the weighting functions with respect to TPW for each of the T-2 channels.

Average Pressure Level of the Peak of the Weighting Functions [hPa]						
TPW [kg/m^2]	TPW [kg/m^2]	91 GHz	150 GHz	183±7 GHz	183±3 GHz	183±1 GHz
0	5	979	954	877	799	676
5	10	982	974	872	721	562
10	20	980	960	799	659	507
20	30	969	939	722	594	476
30	40	980	924	691	553	445
40	50	996	909	657	524	422
50	90	992	876	594	471	370
Average Pressure Level of the Median of the Weighting Functions [hPa]						
TPW [kg/m^2]	TPW [kg/m^2]	91 GHz	150 GHz	183±7 GHz	183±3 GHz	183±1 GHz
0	5	812	847	830	773	671
5	10	846	862	822	712	561
10	20	854	856	783	650	506
20	30	848	836	726	588	462
30	40	855	830	693	557	427
40	50	859	820	660	530	407
50	60	845	788	600	468	357
Average Pressure Level of the 25th Percentile of the Weighting Functions [hPa]						
TPW [kg/m^2]	TPW [kg/m^2]	91 GHz	150 GHz	183±7 GHz	183±3 GHz	183±1 GHz
0	5	665	738	717	657	553
5	10	719	759	711	603	464
10	20	742	756	680	554	421
20	30	739	733	629	507	388
30	40	748	726	599	478	358
40	50	747	711	568	456	344
50	90	725	671	510	403	301
Average Pressure Level of the 75th Percentile of the Weighting Functions [hPa]						
TPW [kg/m^2]	TPW [kg/m^2]	91 GHz	150 GHz	183±7 GHz	183±3 GHz	183±1 GHz
0	5	916	929	918	877	787
5	10	933	940	911	817	661
10	20	933	931	876	740	590
20	30	926	917	822	668	534
30	40	932	914	787	632	494
40	50	940	912	752	598	468
50	90	932	892	692	534	410

Table 30. Mean percent contributions of the three dominant components of the brightness temperature with respect to TPW.

Average Percent Contribution of T_b from Atmospheric Emission						
TPW [kg/m^2]	TPW [kg/m^2]	91 GHz	150 GHz	183±7 GHz	183±3 GHz	183±1 GHz
0	5	9	12	41	76	92
5	10	13	26	72	97	100
10	20	19	43	90	100	100
20	30	26	58	98	100	100
30	40	34	71	99	100	100
40	50	40	79	100	100	100
50	90	46	85	100	100	100
Average Percent Contribution of T_b from Surface Emission						
TPW [kg/m^2]	TPW [kg/m^2]	91 GHz	150 GHz	183±7 GHz	183±3 GHz	183±1 GHz
0	5	91	87	57	22	8
5	10	86	72	26	30	0
10	20	80	55	10	0	0
20	30	72	39	3	0	0
30	40	64	27	1	0	0
40	50	58	19	0	0	0
50	90	52	13	0	0	0
Average Percent Contribution of T_b from Surface Reflectance						
TPW [kg/m^2]	TPW [kg/m^2]	91 GHz	150 GHz	183±7 GHz	183±3 GHz	183±1 GHz
0	5	1	1	2	2	1
5	10	1	2	2	0	0
10	20	2	3	1	0	0
20	30	2	3	0	0	0
30	40	2	2	0	0	0
40	50	2	2	0	0	0
50	90	3	1	0	0	0

Table 31. Mean T_bs [K] for the T-2 channels using seven revolutions of data from late winter and mid-summer, 1992 and winter, 1993. This data were used as the training data in the multiple regression technique.

			Land		
Latitude	Water	Ice	0 - 500 m	500 - 1000 m	> 1000 m
			91 GHz		
90 - 65	219.9	215.4	250.5	221.1	188.8
65 - 40	214.3	217.2	275.3	267.7	263.4
40 - 20	226.8	-	284.2	277.5	270.0
20 - 0	247.9	-	287.5	284.2	276.4
			150 GHz		
90 - 65	242.7	219.8	256.0	224.1	185.7
65 - 40	241.8	231.4	277.6	269.7	263.8
40 - 20	263.2	-	284.2	280.2	272.0
20 - 0	278.8	-	286.0	283.1	278.9
			183±7 GHz		
90 - 65	261.2	243.1	261.8	239.5	198.6
65 - 40	262.2	253.0	271.1	266.5	265.1
40 - 20	274.6	-	272.9	274.7	270.7
20 - 0	274.4	-	271.3	270.4	271.6
			183±3 GHz		
90 - 65	255.2	247.3	255.8	245.6	217.0
65 - 40	256.3	251.7	260.2	257.3	257.9
40 - 20	265.8	-	262.6	264.2	262.4
20 - 0	264.4	-	260.1	260.1	263.1
			183±1 GHz		
90 - 65	245.0	241.5	245.7	241.4	226.7
65 - 40	246.1	244.0	247.7	246.2	248.1
40 - 20	253.4	-	250.1	252.7	252.4
20 - 0	251.4	-	246.8	247.1	252.0

Based on the observation that the majority of T_bs were within a 20 K range and that the multiple regressions perform better on distinct populations, three T_b categories were created for the four functioning T-2 channels (91 and 183±7, 3, and 1 GHz) based on mean climatological T_bs (T_c) for each terrain and latitude category: $T_b - T_c \leq -10$ K, $-10 < T_b - T_c > 10$, and $T_b - T_c \geq 10$ K. Mean values for each of the 20 possible terrain/latitude categories were developed using over 90,000 cases (Table 31) from seven complete revolutions of T-2 data which occurred during mid-May 1992, late July - early August 1992, and early February, 1993. These cases constituted the training data set. The independent data were from 7 revolutions recorded in mid-July, 1992.

For each of the 20 terrain/latitude categories there are 81 possible combinations of the 4 T-2 channel T_bs and 3 T_b bins, resulting in a total of 1620 possible combinations. One additional category was created to include those categories with fewer than 10 training cases. These were usually cases that were quite anomalous in all four channels. All points were used in development and testing of the regression procedure. Multiple regression coefficients were developed on the same 7 revolutions used for the mean climatology.

5.1 Synthesis of 150 GHz T_bs Results

Testing of the multiple regression technique on the training data set resulted in the following results:

Mean difference = -0.0001 K,
Standard Deviation = 2.5 K,
Minimum difference = -21.0 K,
Maximum difference = 20.4 K,
Number of Cases = 96,142.

The difference was defined as the actual 150 GHz T_b minus the synthesized 150 GHz T_b. There were 572 cases that were placed in the catch-all bin described previously and only 271 of the 1620 possible categories produced regression coefficients.

Testing of the multiple regression technique on the independent data resulted in the following results:

Mean difference = 0.23 K,
Standard Deviation = 2.94 K,
Minimum difference = -29.0 K,
Maximum difference = 18.9K,
Number of Cases = 91,186.

Table 32 lists the mean, standard deviation, maximum, and minimum differences and the frequency of occurrence based on the 5 terrain classifications and 4 latitude categories.

6. T-2 T_b SIGNATURES

One observation of the T-2 T_b climatology was that the range in T_bs increased as the domain being sensed increased. There were three basic data sets created during this CALVAL study: 1) T-2 T_bs and co-located radiosonde profiles (1601 cases), 2) T-2 and co-located SSM/I and SSM/T-1 data for the seven CALVAL flights and 3) complete revolutions of T-2 T_bs. The second data set can be further divided into days with co-located GOES imagery and those that do not have geostationary satellite imagery. The first data set, the co-located T-2 T_bs and radiosondes, included information about the moisture content of the atmosphere from the sounding. If saturation was present in the profile, then clouds may have been present within the FOV. The pressure level and thickness and average temperature of the saturated layer(s) provided some insight into the possible cloud characteristics. Unfortunately, the fractional cloud cover in the T-2 FOV was not determined, nor was the presence of clouds be verified. The data set was mostly restricted to land and coastal environments; however, the stations were distributed between 75° N and S. The second data set included information on the presence and fractional coverage of cloud and precipitation in the T-2 FOV. However, the cloud type, thickness and structure was not determined. Using the SSM/I CALVAL TPW algorithm (Hollinger, 1991), the TPW in non-precipitating ocean environments was determined. The data represented land and ocean environments in the mid-latitudes and ocean environments in the tropics. The third data set provided continuous global coverage of the earth. However, there was no independent data indicating the presence/type of clouds and precipitation.

Table 32. Mean, standard deviation, maximum and minimum differences between the actual 150 GHz T_b minus the synthesized 150 GHz T_b [K] for the 5 terrain classifications and 4 latitude categories. Results were based on the independent data set.

Latitude	Water FOVs	Ice FOVs	Land FOVs by Elevation [m]		
			0 - 500	500 - 1000	> 1000
			Mean Difference		
90 - 65	1.6	0.8	0.2	1.5	0.5
65 - 40	0.1	0.4	-0.2	-0.2	0.2
40 - 20	0.7	-	-1.4	-1.1	0.0
20 - 0	0.0	-	0.1	0.2	-0.3
			Standard Deviation		
90 - 65	4.1	4.5	2.3	3.4	3.3
65 - 40	2.8	4.1	1.8	2.4	2.4
40 - 20	2.9	-	2.7	2.7	2.7
20 - 0	2.2	-	2.6	2.2	2.6
			Maximum Difference		
90 - 65	13.4	15.9	12.1	16.9	14.3
65 - 40	16.1	18.9	7.9	16.2	7.7
40 - 20	15.7	-	6.4	9.7	14.4
20 - 0	15.2	-	13.6	7.2	6.9
			Minimum Difference		
90 - 65	-15.8	-15.0	-10.5	-18.5	-17.8
65 - 40	-17.2	-12.4	-12.3	-19.9	-15.4
40 - 20	-29.0	-	-11.2	-10.4	-13.1
20 - 0	-15.5	-	-10.1	-13.0	-14.9
			Number of Cases		
90 - 65	2327	6856	2026	1082	7217
65 - 40	17657	1096	5397	1906	1835
40 - 20	15155	-	2671	1027	3157
20 - 0	18320	-	2487	694	276

6.1 SSM/T-2 T_b Signatures: Effects of Clouds over Water

Using the co-located SSM/I and GOES data, the effects of clouds over water on the T-2 T_bs were examined. Only data with relatively dry moisture profiles (10-20 kg/m^2) were used. The relatively cloud-free FOVs (0 to 20% cloud-filled) showed uniform T_b signatures: the warmest T_b occurred at 183±7 GHz and the coolest T_bs at 91 GHz. The data for all channels displayed ranged of 10 - 30 K (Figure 52). As the fractional cloud amount in the FOV increased, the ranges of 91 and 150 GHz T_bs increased; however the warmest T_bs were still observed at 183±7 GHz. When the limits on TPW were eliminated, the ranges of T_bs increased; however, the warmest T_b still occurred at 183±7 GHz (Figure 53).

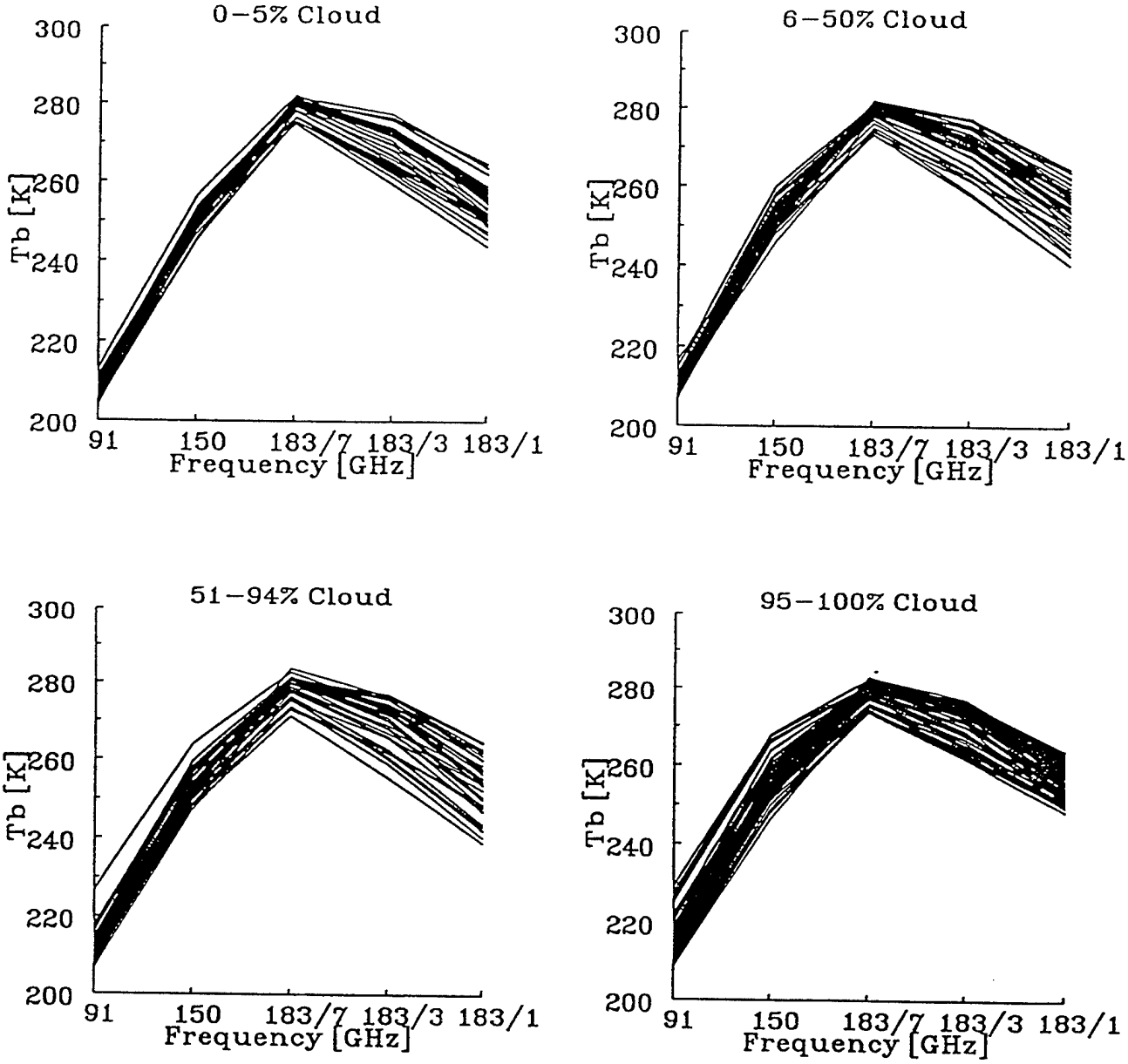

Figure 52. T-2 T_b cloud signatures over water surfaces. Data were limited to TPW ranging from 10 to 20 kg/m^2 with varying amounts of non-precipitating clouds in the FOV: 0-5%, 6-50%, 51-94%, and 95-100%.

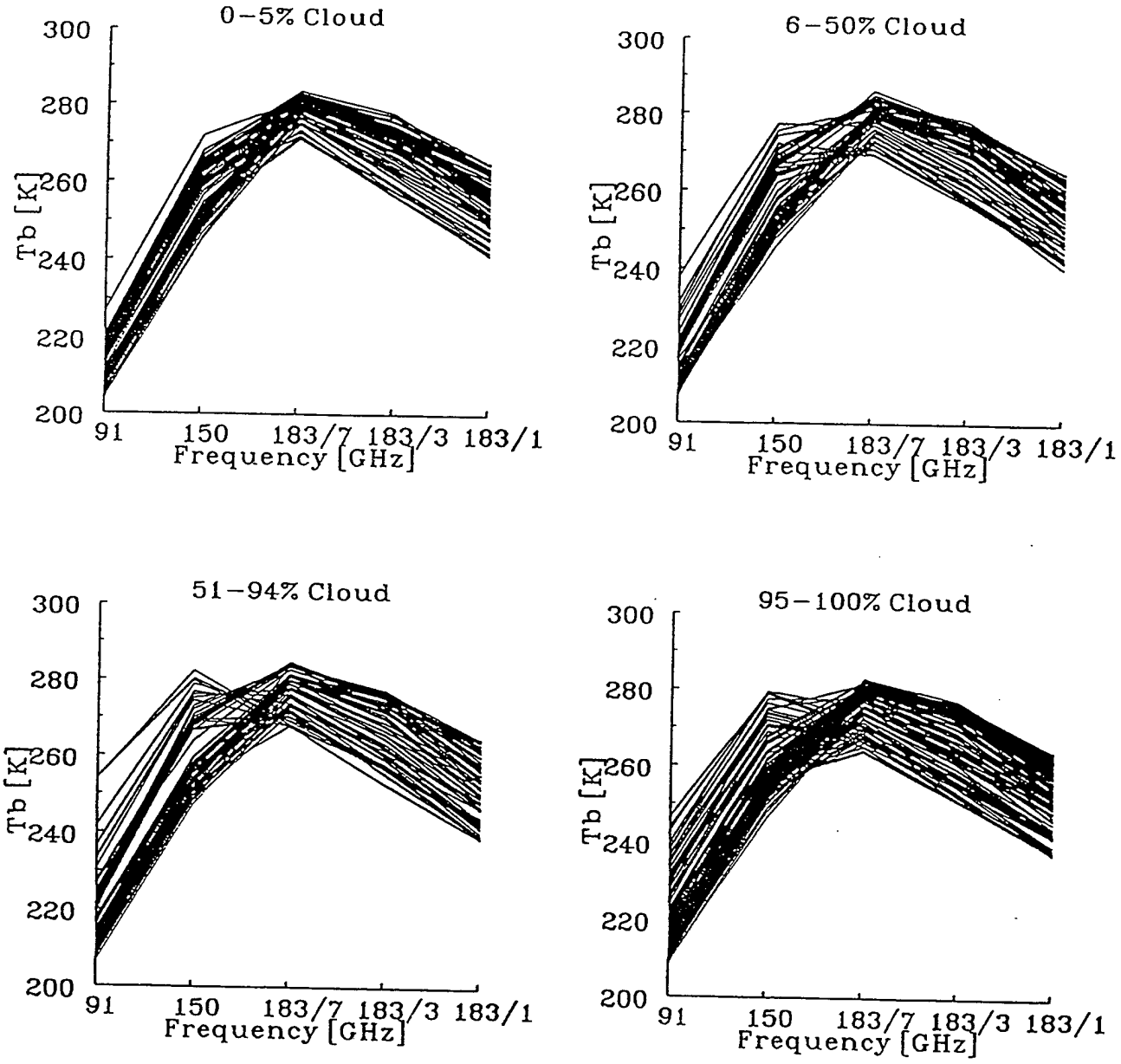

Figure 53. T-2 T_b cloud signatures over water surfaces. Data were not limited by TPW and were categorized by the amount of non-precipitating clouds in the FOV: 0-5%, 6-50%, 51-94%, and 95-100%.

6.2 SSM/T-2 T_b Signatures: Effects of Rain over Water

Using the co-located SSM/I and GOES data, the effects of rain are immediately noticeable compared to the effects of clouds over water (Figure 55). Light rain cases with rain filling less than 80% of the T-2 FOV produced the warmest T_bs at 150 GHz rather than 183±7 GHz. At 100% light precipitation within the FOV, two populations are present: one with peak T_bs at 150 GHz and one with peak T_bs at 91 GHz. As the rain rate increased, the first population decreased so that only those cases with peak T_bs at 91 GHz were observed (Figure 56). For this population, the minimum T_bs were typically at 183±7 GHz.

6.3 SSM/T-2 T_b Signatures: Effects of Clouds over Land

As expected, the T_b signature over relatively cloud-free FOVs over land were markedly different compared to over water (Figure 57). The surface and near surface channel T_bs were much warmer over land with the warmest T_bs occurring at 150 GHz. The ranges of 183±3 and 1 GHz T_bs were similar for land and water FOVs. There were too few cloud-filled land FOVs to determine if distinct trends or differences occurred as the amount of clouds increased in the FOV. However, there were no noticeable changes in T_b signatures as the amount of cloud increased in the FOV over land.

6.4 SSM/T-2 T_b Signatures: Effects of Rain over Land

There were too few rain-filled land FOVs to determine if trends occurred as the amount and intensity of rain increased in the FOV. The few case points that were available indicated different trends than those observed over water. Although the warmest T_bs occurred at 91 GHz, the coolest T_bs occurred at 183±1 GHz (Figure 54).

6.5 SSM/T-2 T_b Signatures: Effects of Surface Ice

Using the global revolutions of T-2 T_bs, an interesting observation was noted: the cases with the warmest T_b at 183±1 GHz were confined to the poles and Greenland (Figure 3). Also, when the effects of TPW over land were examined using the co-located radiosonde database, the very dry profiles (TPWs ranging from 0 to 5 kg/m^2) had similar polar signatures (Figure 58). These radiosonde profiles were from northerly stations.

7. Effects of Clouds and Precipitation

Griffin et al. (1994) showed a clear difference between T-2 T_b signatures for clear and cloud-filled FOVs over ocean; however, there was not an apparent signal over land. In order to continue examining the effects of clouds on T-2 channels, microwave and OLS data were collected on the SeaSpace system. The OLS data were used to generate cloud fields using the SERCAA algorithms. Data coverage included OLS swaths along the eastern to central North American continent. SERCAA algorithms needed to be rewritten to handle the condensed data set (about 60% of the swath was saved since the T-2 swath is much narrower than the OLS swath), the varying boundaries and incorporation of large-scale surface temperature climatology. Data were manually quality controlled and then colocated with T-2 FOVs (the 91, 150 and 183 GHz). These data were used to identify cloud signatures in the T-2 T_bs.

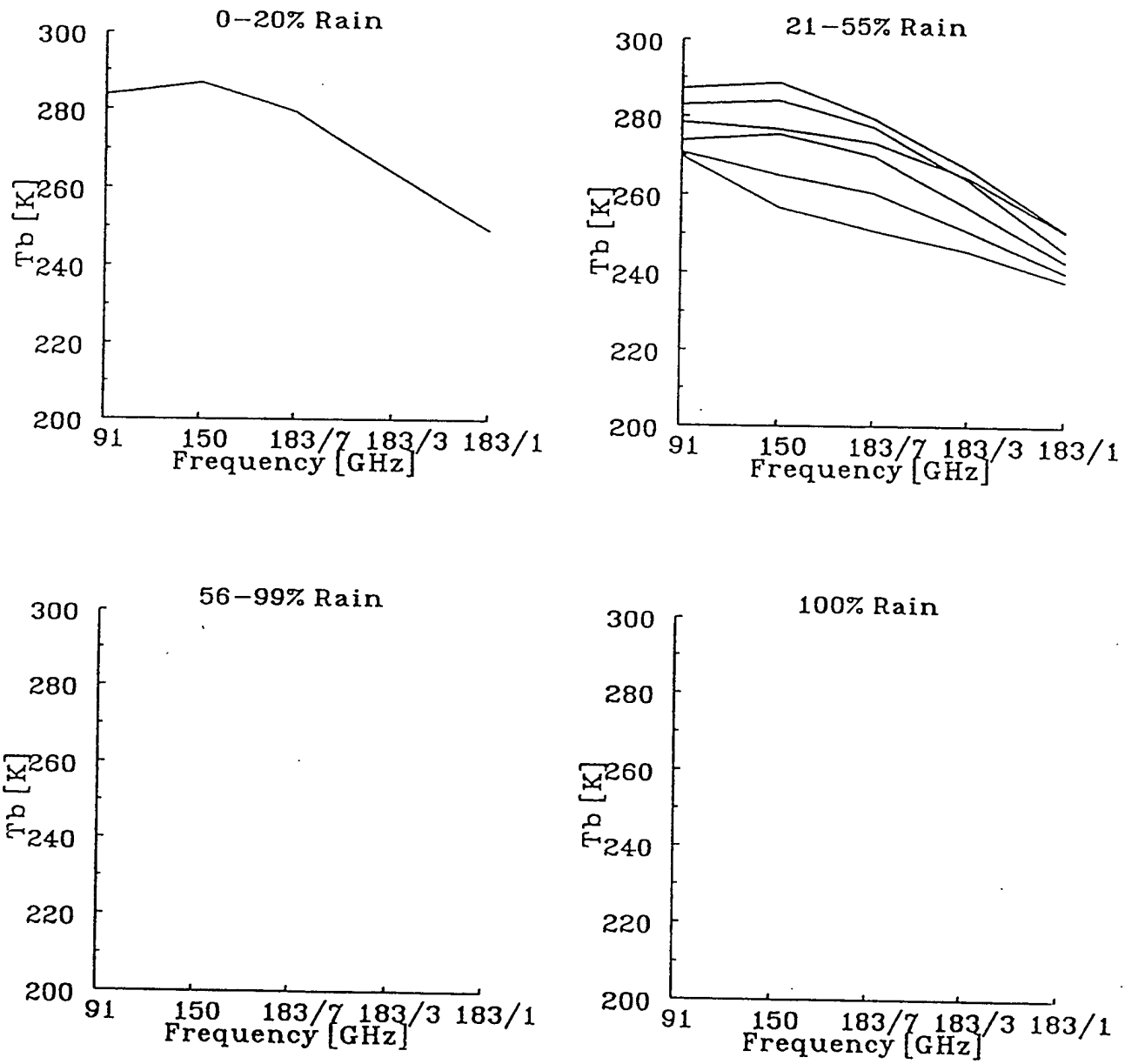

Figure 54. T-2 T_b rain signatures over land surfaces. Data included all rain intensity levels.

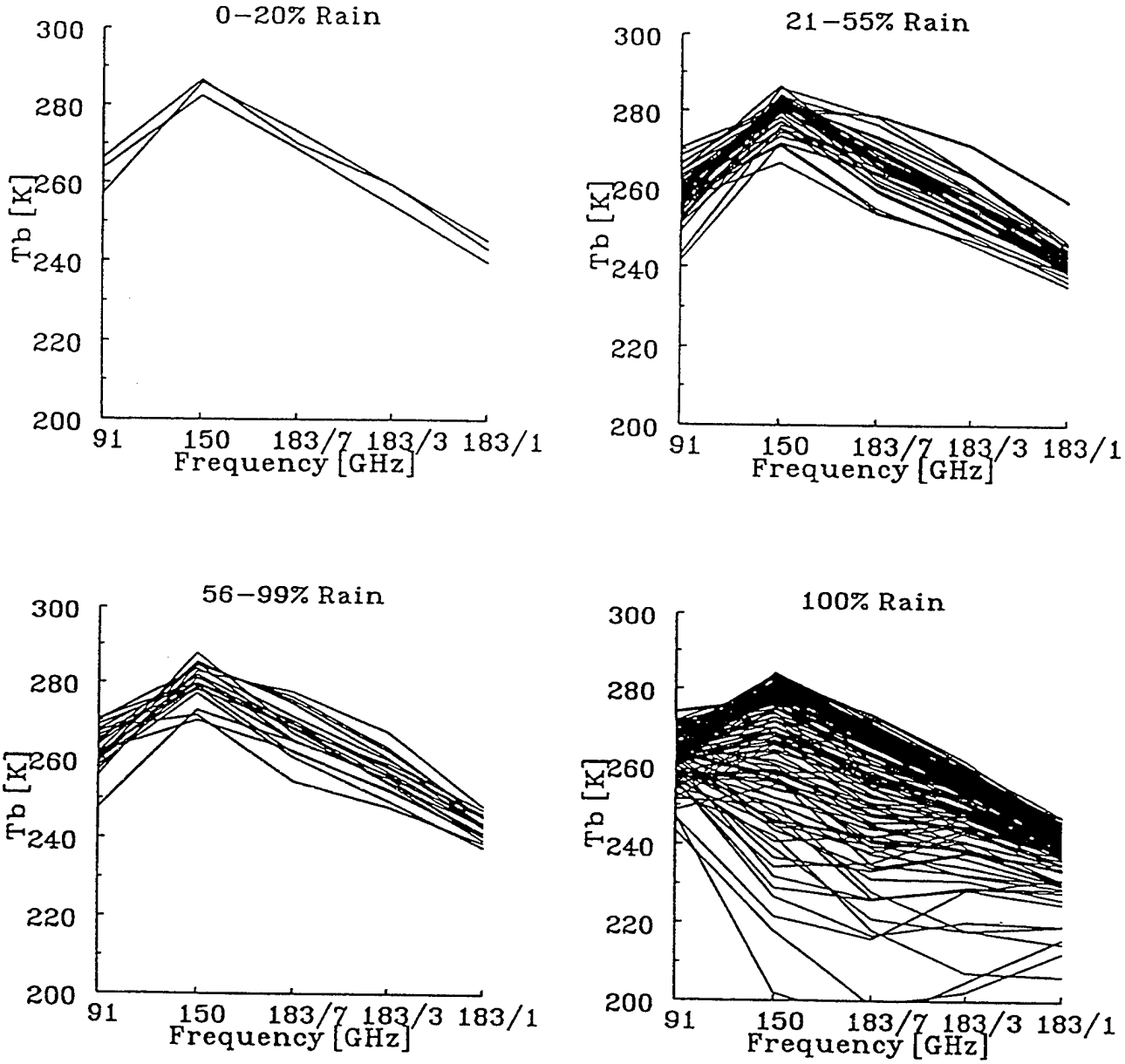

Figure 55. T-2 T_b rain signatures over water surfaces. Data were limited to light rain rates (0 to 2 mm/hr) with varying amounts of precipitation in the FOV: 0-20%, 21-55%, 56-99%, and 100%.

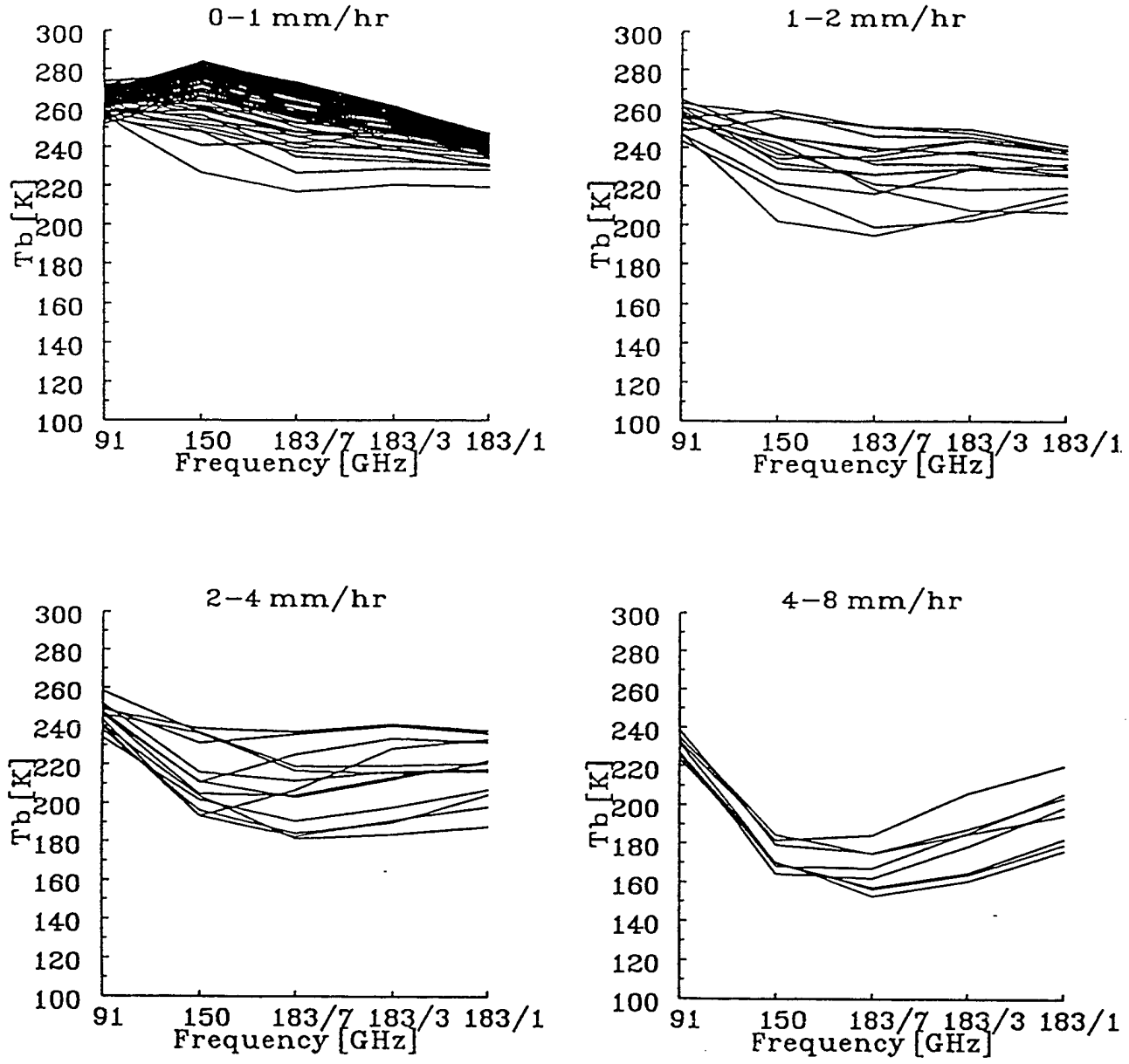

Figure 56. T-2 T_b rain signatures over water surfaces. Data were limited to FOVs that are 100% precipitation and were categorized by the average rain intensity within the FOV: 0-1 mm/hr, 1-2 mm/hr, 2-4 mm/hr, and 4-8 mm/hr.

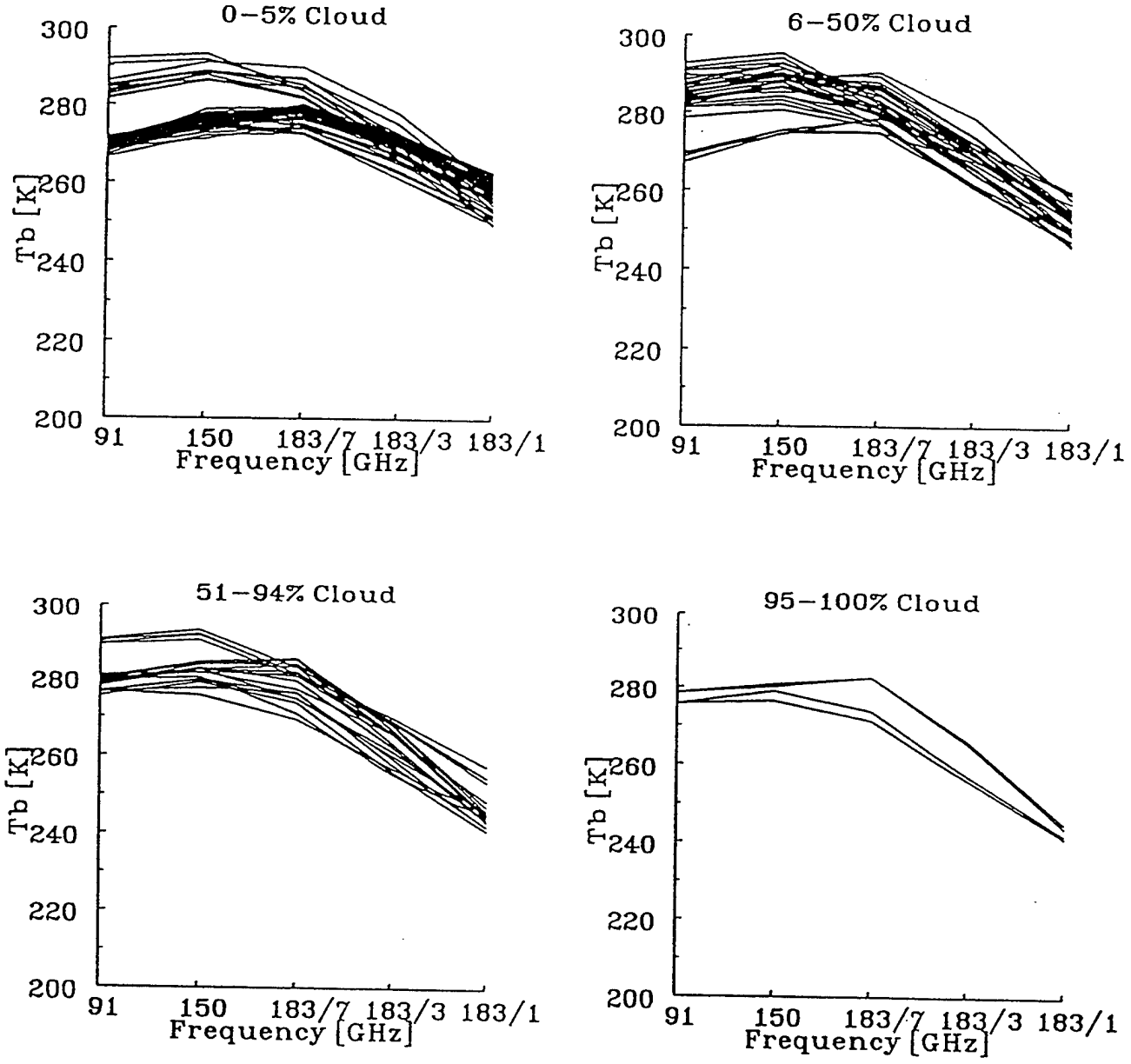

Figure 57. T-2 T_b cloud signatures over land. Data were limited to TPW ranging from 10 to 20 kg/m^2 with varying amounts of non-precipitating clouds in the FOV: 0-5%, 6-50%, 51-94%, and 95-100%. Data were not screened for satellite viewing angle.

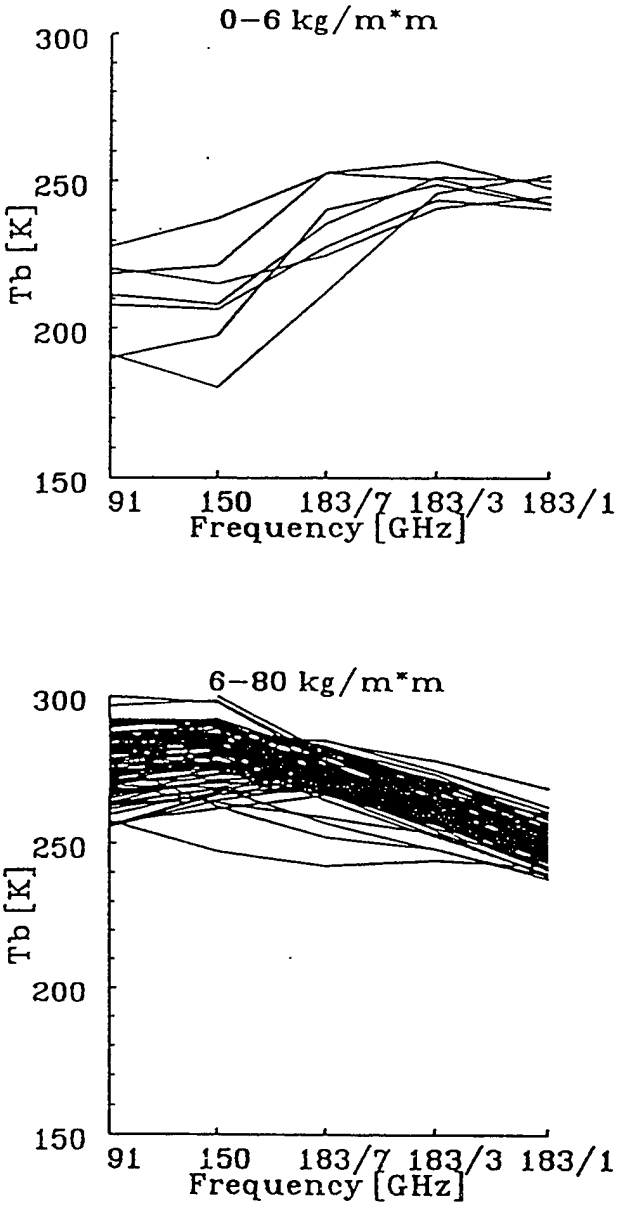

Figure 58. T-2 T_b signatures for FOV over land. Data did not have saturated layers in the radiosonde profiles and were categorized by TPW: (a) 0-10 kg/m^2 and (b) >20 kg/m^2. Data were not screened for satellite viewing angle.

Griffin et al. (1994) also showed a distinct T_b signature of heavy precipitation (data set used was that from a developing typhoon in the western South Pacific Ocean). In order to expand the precipitation cases, data were collected from AIMS (Air Force Interactive Meteorological System), the Geophysics Directorate's meteorological computer system. Data collected were the MDR data (manually digitized radar data) which included VIP intensities for a national grid system and the height of specific echoes; Service_A observations which included surface temperature, dewpoint, pressure, visibility, current weather, snow depth, precipitation during the past 3 and 24 hours, and cloud amount and height for four levels in the atmosphere; radiosonde profiles which included temperature, dewpoints, pressure and height for mandatory and significant levels of the atmosphere, and sea surface temperatures which included ship and buoy reports of air and water temperatures and wave height. These data were combined with the satellite data collected from SeaSpace computer and antenna system: the microwave data from F-11 satellite (SSM/I, SSM/T-1, and T-2) and OLS visible and infrared data.

One of the most difficult challenges was definitively identifying of the phenomena being examined, either clouds or precipitation in this case. Varying spatial and temporal resolutions of the phenomena and the sensors contribute to the challenge, as well as the transient nature of clouds and rain and possible time offsets with the data sources being colocated. For example, MDR data was collected and transmitted hourly, but the satellite may have passed over 30 minutes between the two data sets. Considering a typical thunderstorm's life is 45 minutes long, this contributed to considerable uncertainty as to what was really there at the time of the T-2 measurement. And finally, each technique identifying cloud or rain had uncertainties and known weaknesses. MDR data may have been incomplete in given areas due to poor coverage (over the Rocky Mountains) or due to radar equipment problems. SSM/I rain algorithms are known not to work well over land and coastal regions.

Two approaches were undertaken to identify precipitation: case studies and "bulk" data analysis. It was noticed from case studies that the majority of precipitation cases were quite identifiable with T-2 data; however, there were certain types of precipitation, possibly when ice was not associated with the rain, that had very little if any signature in the T-2 T_b fields (a good example is presented in Figure 59). The bulk data analysis was used to test the robustness of trends identified using case studies. Rain and clear data sets were developed. In order to maximize the certainty that the desired phenomenon was really there, strict limits were imposed. Rain cases required that rain was identified within the T-2 FOV by the SSM/I rain algorithm and both sets of MDR data (the sets previous and following the T-2 observations). Clear cases were identified if there was no rain identified within 100 km of the T-2 FOV using all three data sets.

Based on the results of the case studies where sharp T_b boundaries corresponded to precipitation boundaries, the nearest neighbor or "buddy" analysis was developed to quantify the average difference of values from that point to the eight surrounding FOVs. This technique was useful for identifying gradients in the data fields of T-2 T_bs and differences between several T_bs. One technique was developed based on the T-2 T_bs and buddy differences. Depth of convection was estimated based on whether anomalous values were present in the channels sensing higher in the atmosphere. For example, precipitation would be considered shallow if anomalies were observed in the 183±7 GHz T_bs and not the 183±3 and 1 GHz T_bs. Also, the confidence in the precipitation identification was determined by checking to see if the anomalies were present in the channels that sense lower in the atmosphere than the channel that first identified precipitation.

Another precipitation identification technique was based on a stepwise logistic regression scheme using the bulk analysis data sets. Nearest neighbor differences and T-2 T_bs served as independent variables to predict the probability of precipitation. As above, clear cases were identified if there was no rain identified within 100 km of the T-2 FOV, and rain cases required

that rain was identified within 25 km of the center of the T-2 FOV by both the SSM/I rain algorithm and MDR data. The resulting equation was:

$$PoP = (1 + \exp(-28.285 - 0.0816*T_b(91\ GHz) + 0.2167*T_b(183\pm7\ GHz) - 1.3318*Bsdv(91\ GHz) + 0.3877*Bsdv(150\ GHz) - 1.6368*[Bsdv(183\pm7\ GHz) + 0.8252*Bsdv(183\pm1\ GHz) + 1.2825*Bsdv(183\pm7\ GHz\text{-}91\ GHz) - 0.8008*Brms(91\ GHz\text{-}150\ GHz) - 1.084*Brms(183\pm3\ GHz\ -183\pm1\ GHz)))^{(-1)}$$

where PoP = probability of precipitation [0->1]
Bsdv = standard deviation of buddy differences
Brms = RMS of buddy differences

Figures 59 and 60 show how these techniques applied for several case studies. Included in the comparisons are the SSM/I rain rate algorithm, MDR data and Norm Grody's (NOAA/NESDIS) algorithm (personal communication, 1994). As with most techniques, there are strengths and weaknesses. One of the strengths in the regression scheme is its performance in the subtropical convection over Florida and out over the Gulf Stream.

8. UPPER TROPOSPHERIC HUMIDITY FIELDS

A technique was developed to generate fields of upper-tropospheric humidity (UTH) using 183±1 GHz T_bs recorded from the SeaSpace system and temperature profiles from radiosonde data collected on the Air Force Interactive Meteorological System (AIMS) at the Phillips Directorate, Hanscom AFB. This technique was patterned after Fred Wu's work that was discussed at the AGU Chapman conference held in Jekyll Island, Georgia during October, 1994 (Wu and Hayden, 1994). The basic idea was to iteratively calculate the constant relative humidity profile necessary to produce the colocated T_b using a known temperature profile in a RT model (the modified Eyre code) (Figure 61). Because radiosondes were used as the source of the temperature profiles, the T-2 data were limited to be near 00 and 12 UTC (the time of radiosonde data).

Previous modifications to this RT code were very helpful for the development and validation of this technique. The calculation of the atmospheric emission, surface emission and surface reflection contributions quantified the uncertainty in the UTH calculation. If there were a large surface component, there was less certainty in the UTH value since two additional unknowns were estimated - surface emissivity and ground temperature in order to calculate a T_b. Also, since characteristics of the weighting functions were calculated (e.g. the pressure levels of the various percentiles of the weighting function), comparison of the average relative humidity from the radiosonde profile could be calculated for the same layer of the temperature profile used to generate the UTH value. Testing of this technique with the 1601 colocated radiosonde/T_b data set indicated that the RMS difference between the constant relative humidity profiles and the averaged relative humidity between the 75th and 25th percentiles of the 183±1 GHz weighting function was 18%. If only unsaturated profiles were used (minimized the chance of clouds within the T-2 FOV), then the RMS was reduced to 14%.

In order to expand this technique to generate fields of UTH, an interpolation/ extrapolation technique was developed to extend the radiosonde temperature profiles to the positions of the T-2 FOVs. Generated UTH fields were coherent in gradients (Figures 62 and 63), roughly paralleling the 183±1 GHz T_b field, and may be useful in identifying upper-tropospheric clouds, especially deep convective systems. Even in very dry conditions, when

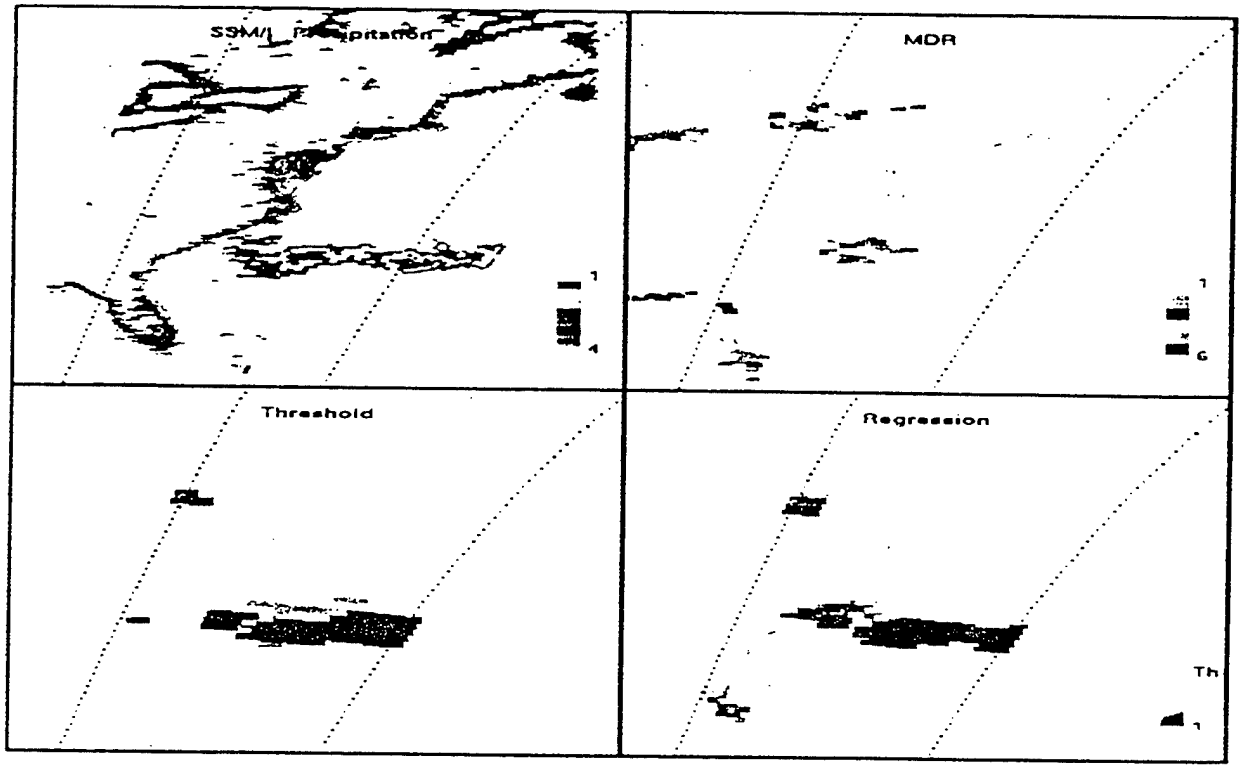

Figure 59. Plots of precipitation identification technique based on thresholds of T-2 T_bs and gradients of T_bs (Threshold), stepwise logistic regression scheme (Regression), SSM/I rain algorithm, MDR data and combined coverage of SSM/I-identified rain and MDR data for 1037 UTC on July 29, 1992.

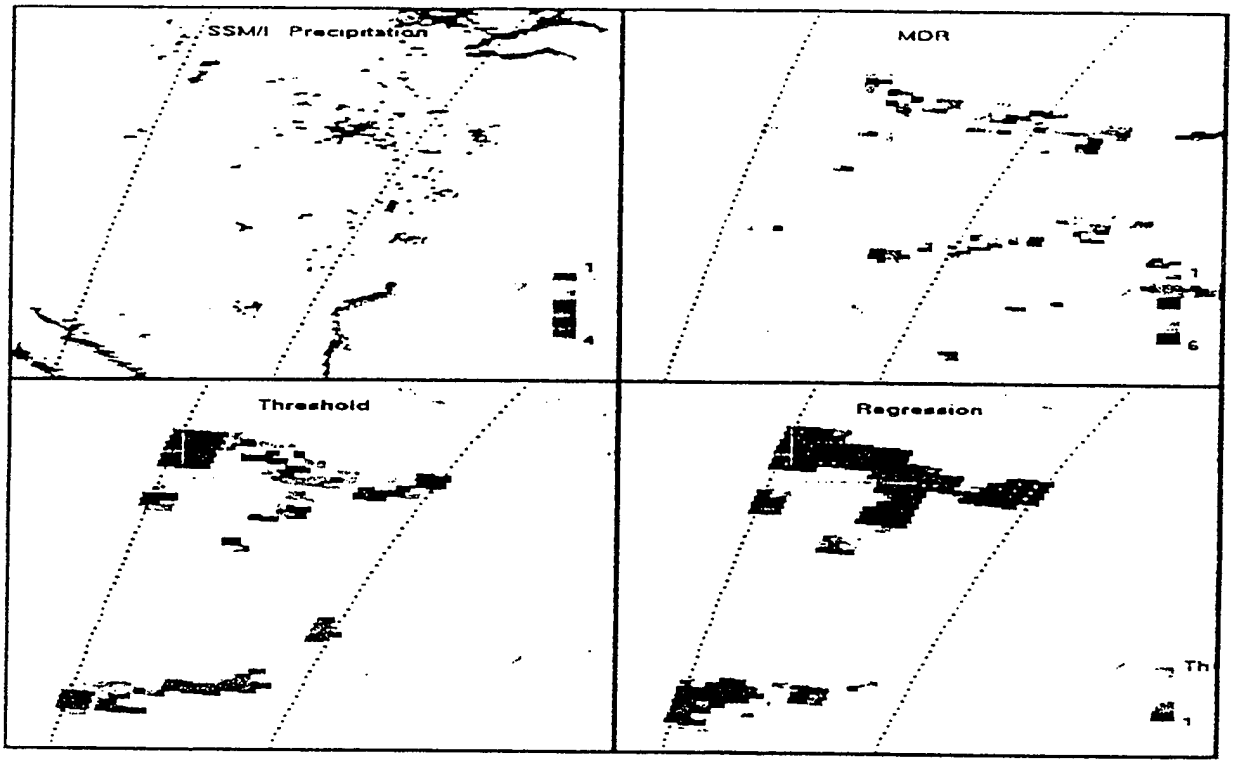

Figure 60. Plots of precipitation identification technique based on thresholds of T-2 T_bs and gradients of T_bs (Threshold), stepwise logistic regression scheme (Regression), SSM/I rain algorithm, MDR data and combined coverage of SSM/I-identified rain and MDR data for 1219 UTC on July 29, 1992.

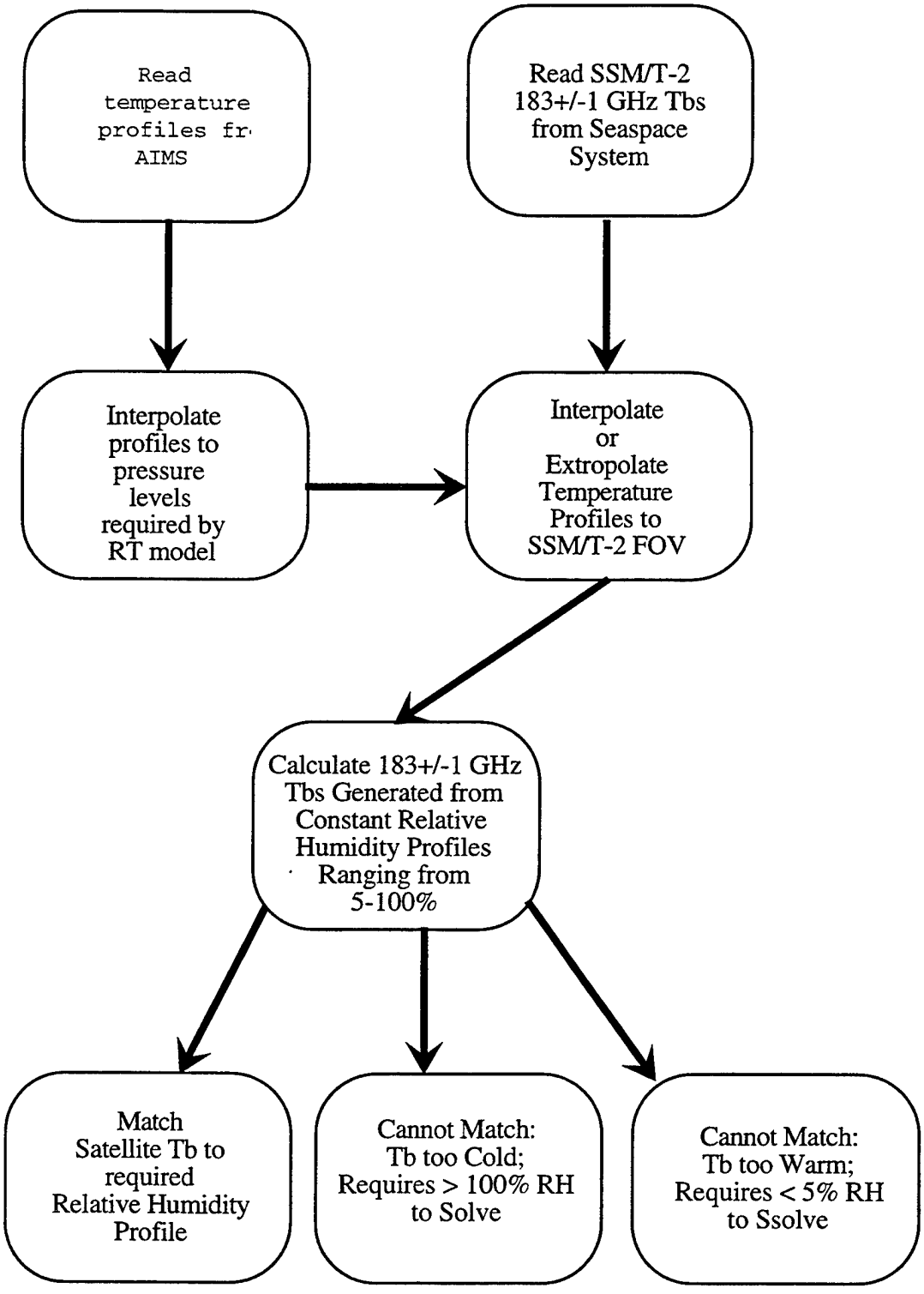

Figure 61. Flow diagram of the technique to calculate UTH from the 183±1 GHz T_b.

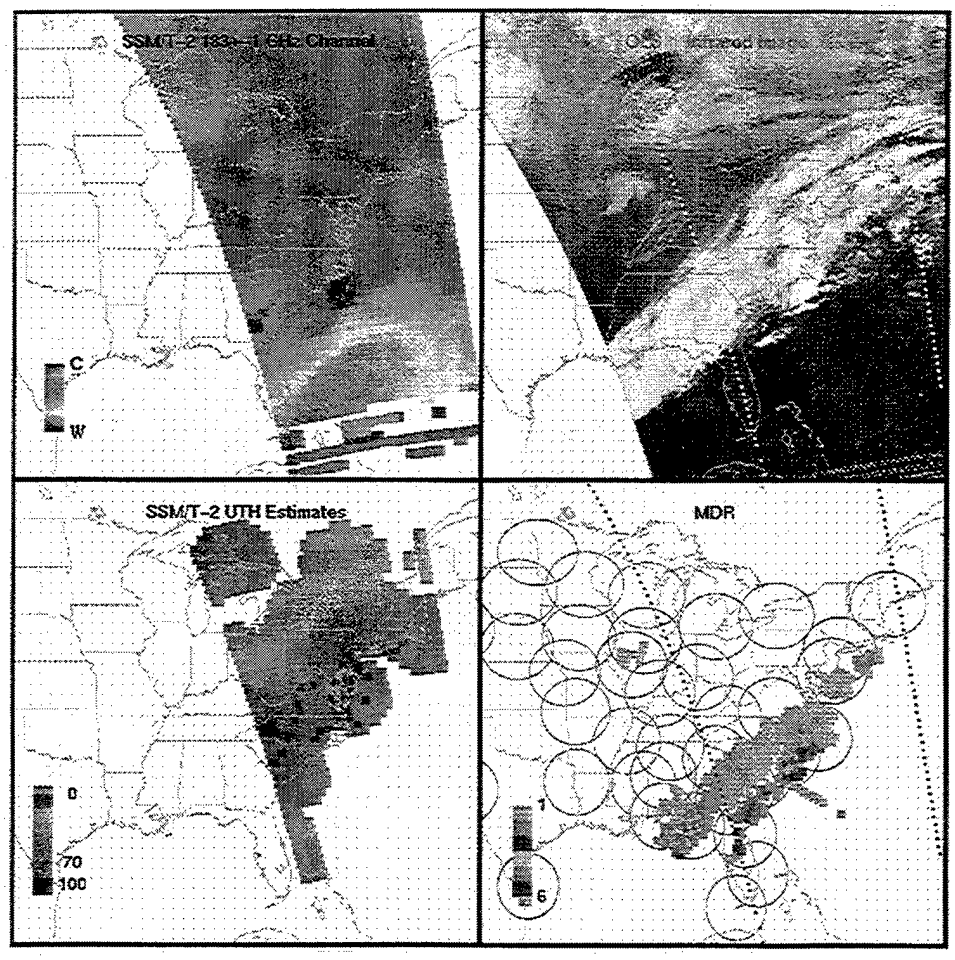

Figure 62. Plots of T-2 183±1 GHz T_b, OLS visible imagery, MDR data and UTH values for 2240 UTC on November 29, 1994. UTH calculations required that at least one radiosonde be within 250 km, thereby limiting the coverage of the fields. Circles in MDR panel represent estimated coverage of reporting radar stations.

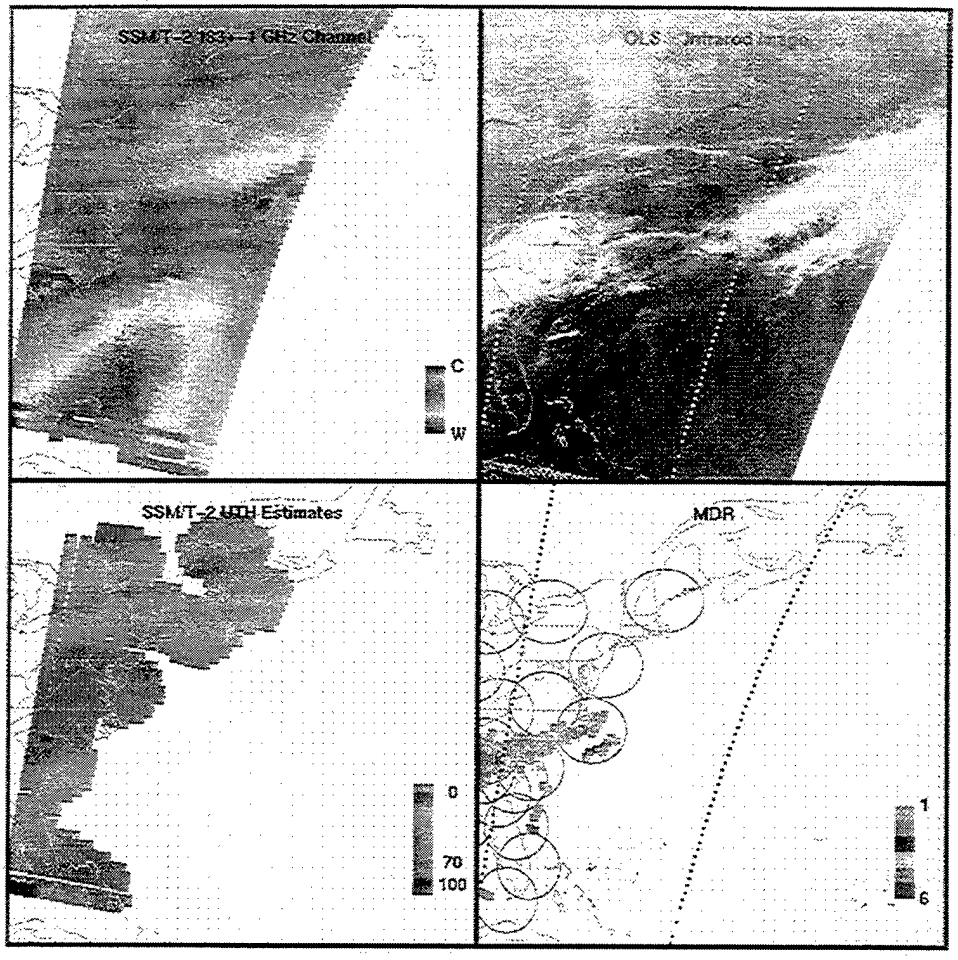

Figure 63. Plots of T-2 183±1 GHz T_b, OLS visible imagery, MDR data and UTH values for 0156 UTC on November 30, 1994. UTH calculations required that at least one radiosonde be within 250 km, thereby limiting the coverage of the fields. Circles in MDR panel represent estimated coverage of reporting radar stations.

relatively large contributions of the T_b came from the surface, the UTH values appeared coherent in distribution. This technique could be easily adapted to run in an operational sense any time T-2 data and temperature profiles are available, such as temperature analysis and/or forecast fields.

9. AMPR DATA ANALYSIS

The Advanced Microwave Precipitation Radiometer (AMPR) (Spencer et al., 1993) sensed at several frequencies similar to the SSM/I (Table 33) and was flown on board NASA's ER-2 aircraft during the TOGA-COARE and CAMEX flights. Significant differences between the two sensors were that the SSM/I is a conical scanning sensor, AMPR a cross-track scanning sensor; only the 19, 37 and 85 GHz channel were similar on both sensors; and while the SSM/I measured both the vertical and horizontal polarizations at each FOV, the AMPR only measured the vertical (horizontal) at the 45° left (right) of nadir (all other measurements across the scan are a combination of both polarizations). Two of the Stokes parameters ([V+H]/2 and [V-H]/2) for both sensors were examined (Figure 64 for AMPR data and Figure 65 for SSM/I data). The two data sets appeared drastically different with the AMPR data creating trapezoidal shapes and the SSM/I creating linear shapes, except for the 85 GHz channel. Land and ocean masks were created (there was no topographic classification of the SSM/I FOVs by AFGWC as there was with the T-2 data) and the relationships between the Stokes parameters were reexamined (Figure 66 for AMPR data observed over water, Figure 67 for AMPR data over land, Figure 68 for SSM/I data over water and Figure 69 for SSM/I data over land). The trapezoidal shapes observed previously for the AMPR data nearly disappeared, suggesting that the coastal scenes were the source of the large scatter, e.g. one side of the swath (say the vertically polarized T_b) was seeing land and the other (horizontally polarized T_b) was viewing water. Another source of scatter would have been the presence of cloud boundaries across the scan. As expected, the two sensors produced similar T_bs for the land FOVs since polarization was minimal (i.e. [V-H]/2 ~ 0). Over water, [V+H]/2 were comparable for both sensors; however, the SSM/I's [V-H]/2 was greater by 10-15 K. One source for this difference was that the local viewing angles for AMPR and SSM/I were 45° and 53.1°, respectively.

Table 33. Characteristics of the AMPR sensor that was flown on board NASA's ER-2 (from Spencer et al., 1993).

Frequency	Antenna Size	3 dB Beamwidth	Ground Resolution	Over-Sampling
10.7 GHz	24.6 cm	8.0°	2.8 km	4.4 x
19.35 GHz	13.5 cm	8.0°	2.8 km	4.4 x
37.1 GHz	13.5 cm	4.2°	1.5 km	2.3 x
85.5 GHz	13.5 cm	1.8°	0.6 km	1.0 x

Since a significant amount of noise was in the AMPR data because the horizontally and vertically polarized FOVs were separated by 50 km and since the AMPR and the SSM/I viewing angles differed by 8.1°, the AMPR data were not used for more detailed CALVAL work.

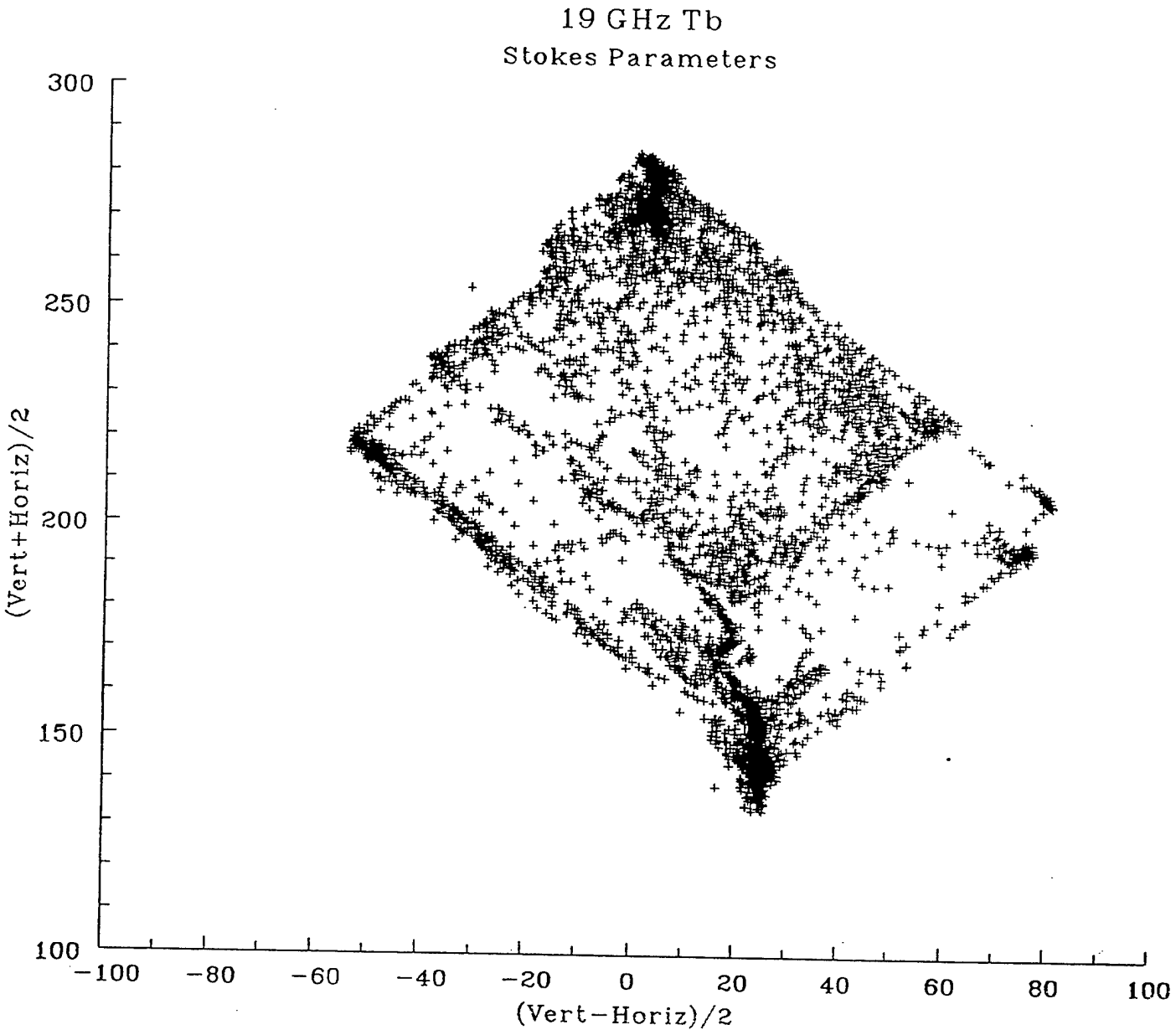

(a)

Figure 64. Two of the Stokes parameters ([V+H]/2 and [V-H]/2) for the AMPR data taken during the CAMEX and TOGA-COARE flights. Three of the AMPR channels are displayed: a) 19 GHz, b) 37 GHz and c) 85 GHz. V represents the vertically polarized T_bs (measure at 45° left of nadir) and H represents the horizontally polarized T_bs (measured at 45° right of nadir). Only data measured when the aircraft was at an altitude of at least 19 km and in level flight were used.

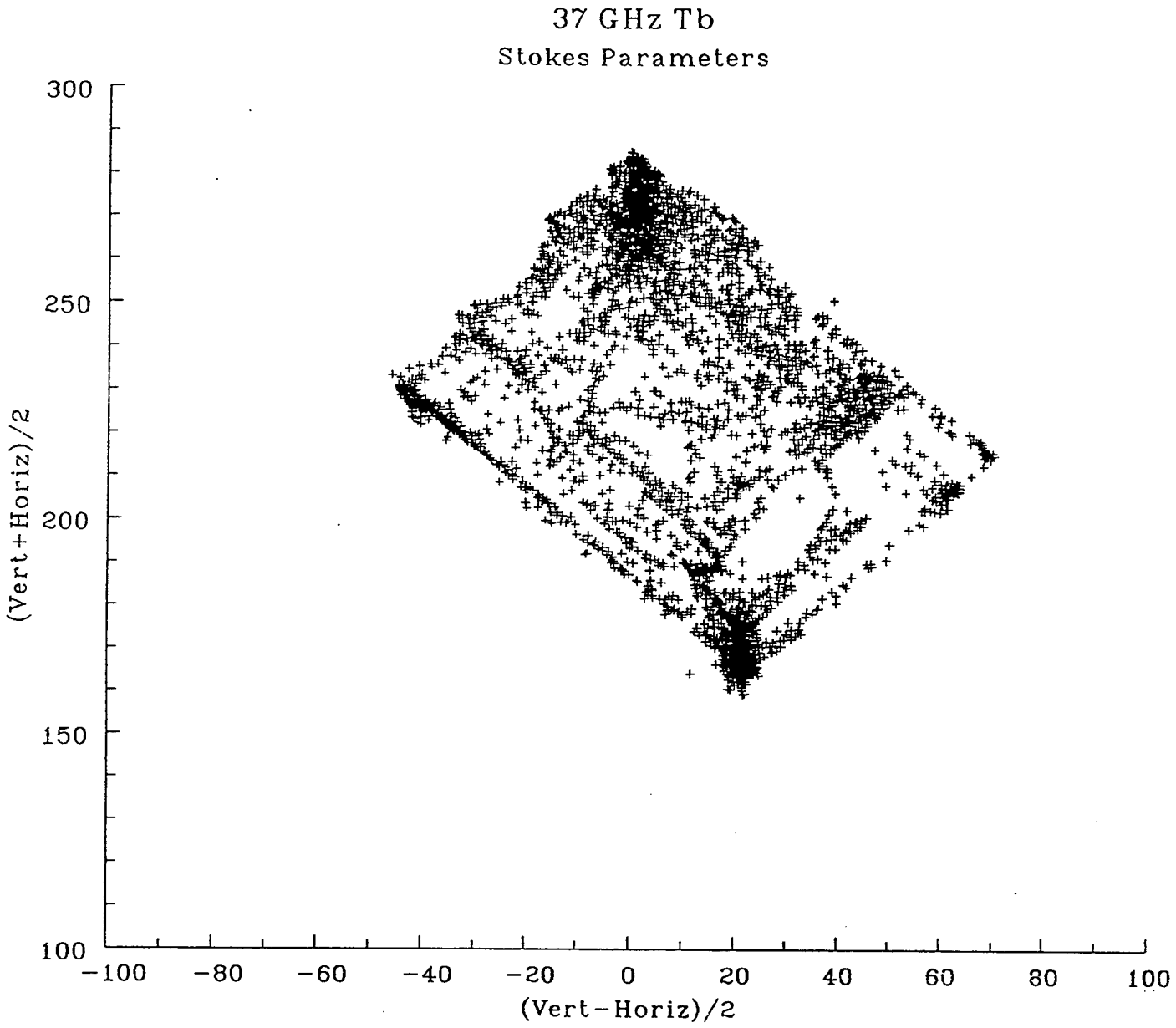

(b)

Figure 64. (continued) Two of the Stokes parameters ([V+H]/2 and [V-H]/2) for the AMPR data taken during the CAMEX and TOGA-COARE flights. Three of the AMPR channels are displayed: a) 19 GHz, b) 37 GHz and c) 85 GHz. V represents the vertically polarized T_bs (measure at 45° left of nadir) and H represents the horizontally polarized T_bs (measured at 45° right of nadir). Only data measured when the aircraft was at an altitude of at least 19 km and in level flight were used.

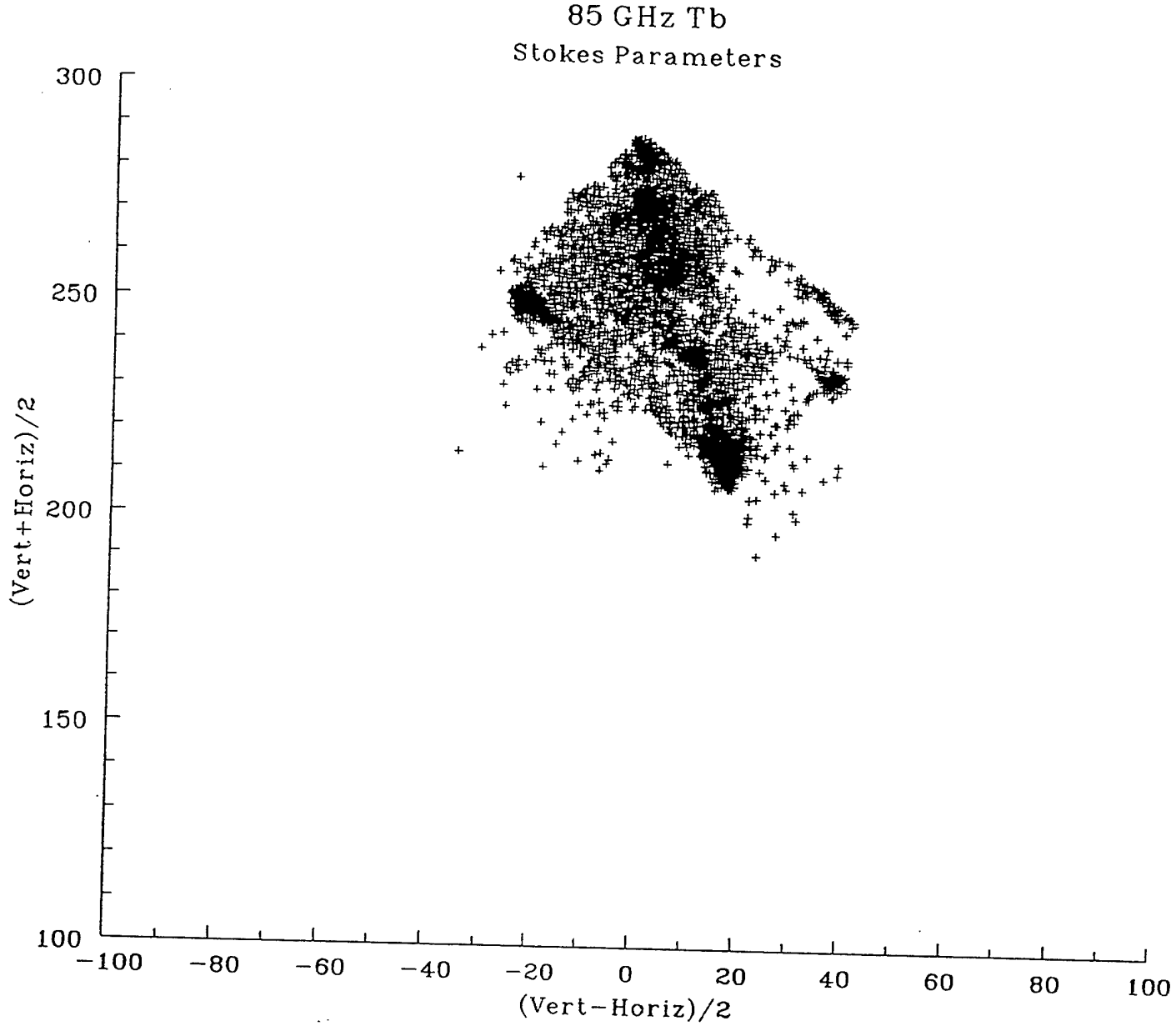

(c)

Figure 64. (continued) Two of the Stokes parameters ([V+H]/2 and [V-H]/2) for the AMPR data taken during the CAMEX and TOGA-COARE flights. Three of the AMPR channels are displayed: a) 19 GHz, b) 37 GHz and c) 85 GHz. V represents the vertically polarized T_bs (measure at 45° left of nadir) and H represents the horizontally polarized T_bs (measured at 45° right of nadir). Only data measured when the aircraft was at an altitude of at least 19 km and in level flight were used.

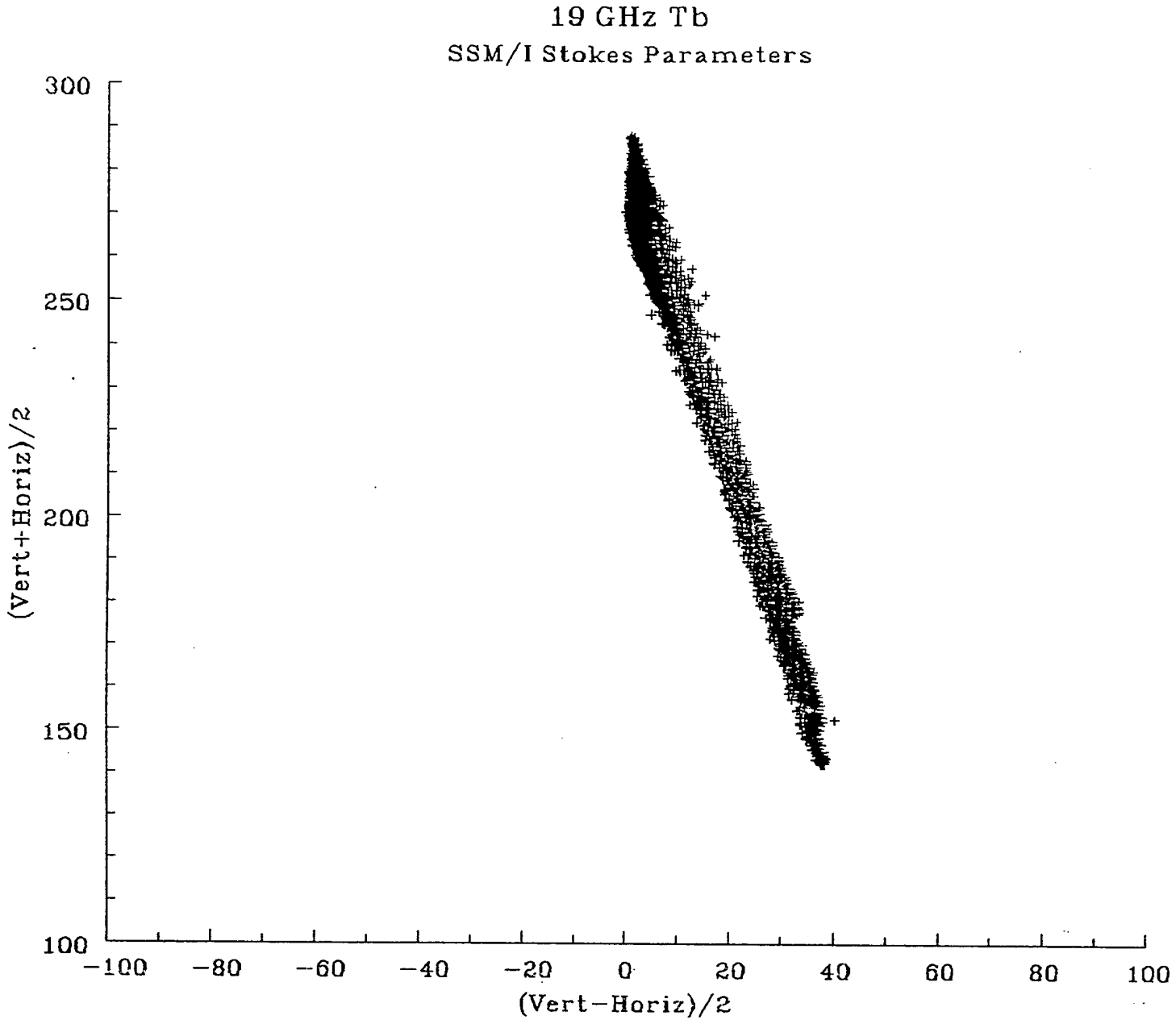

(a)

Figure 65. Two of the Stokes parameters ([V+H]/2 and [V-H]/2) for the SSM/I data observed within the region of the aircraft flights during the CAMEX and TOGA-COARE experiments. Three pairs of the SSM/I channels are displayed: a) 19 GHz, b) 37 GHz and c) 85 GHz. V represents the vertically polarized T_bs and H represents the horizontally polarized T_bs.

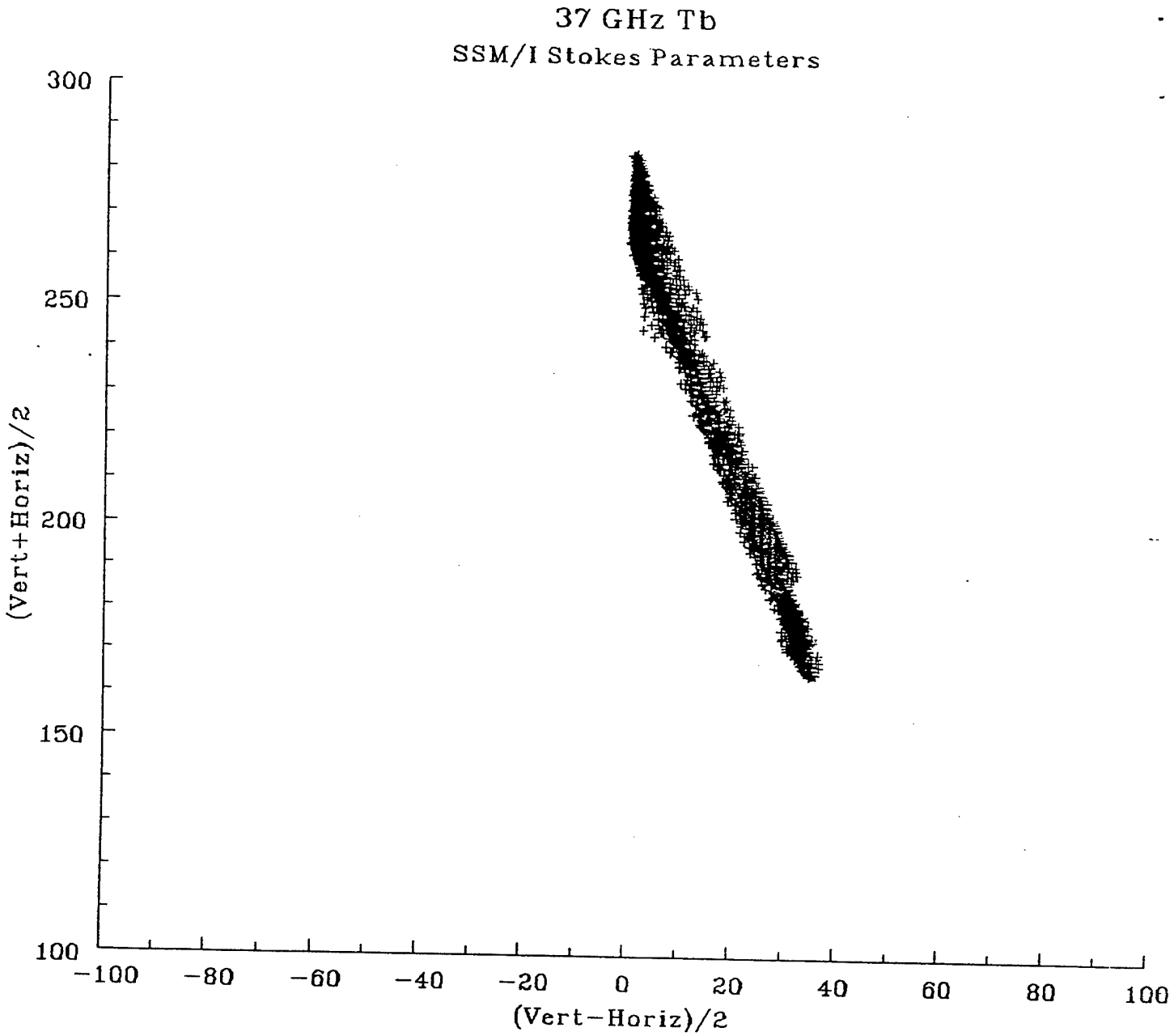

(b)

Figure 65. (continued) Two of the Stokes parameters ([V+H]/2 and [V-H]/2) for the SSM/I data observed within the region of the aircraft flights during the CAMEX and TOGA-COARE experiments. Three pairs of the SSM/I channels are displayed: a) 19 GHz, b) 37 GHz and c) 85 GHz. V represents the vertically polarized T_bs and H represents the horizontally polarized T_bs.

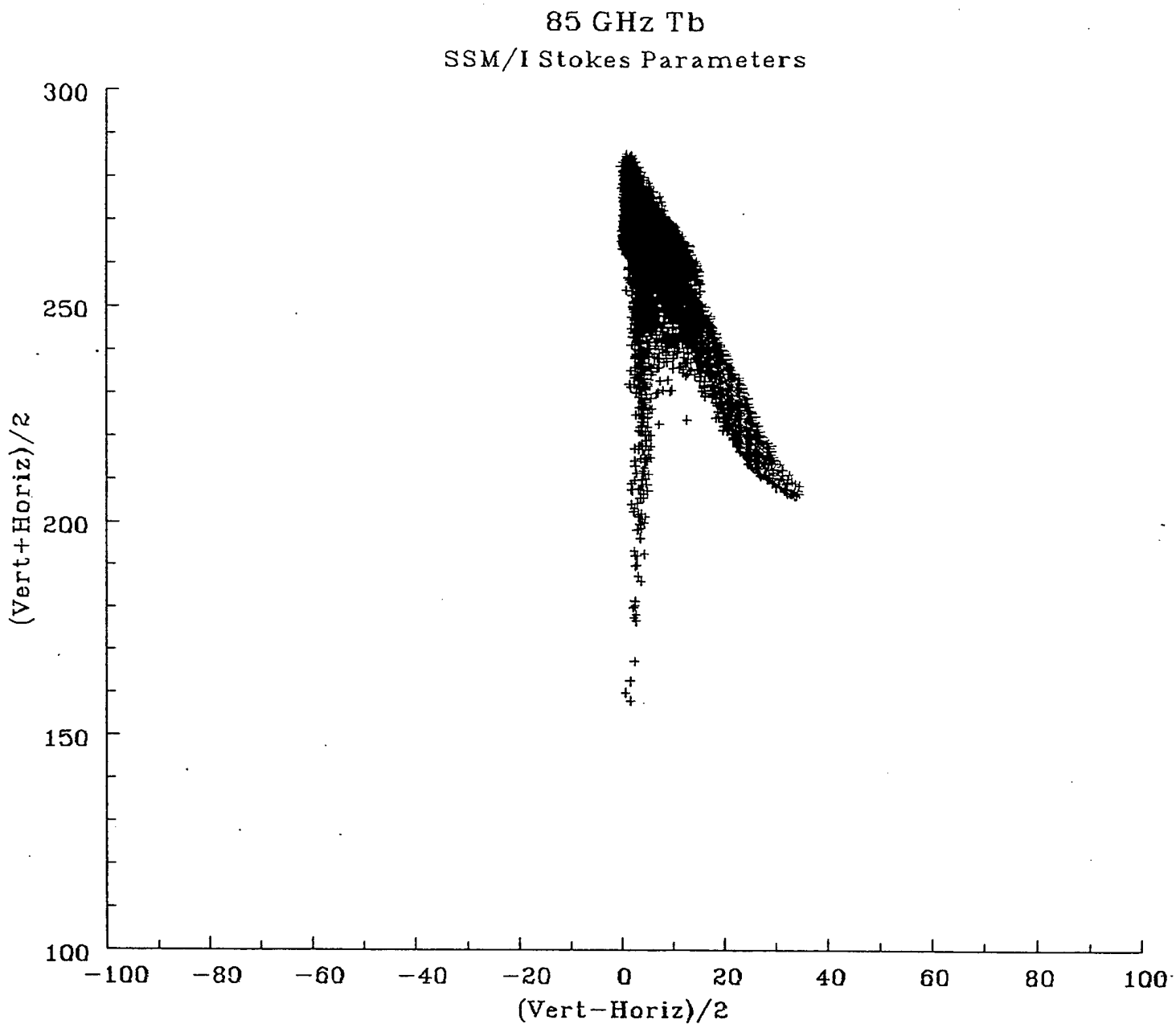

(c)

Figure 65. (continued) Two of the Stokes parameters ([V+H]/2 and [V-H]/2) for the SSM/I data observed within the region of the aircraft flights during the CAMEX and TOGA-COARE experiments. Three pairs of the SSM/I channels are displayed: a) 19 GHz, b) 37 GHz and c) 85 GHz. V represents the vertically polarized T_bs and H represents the horizontally polarized T_bs.

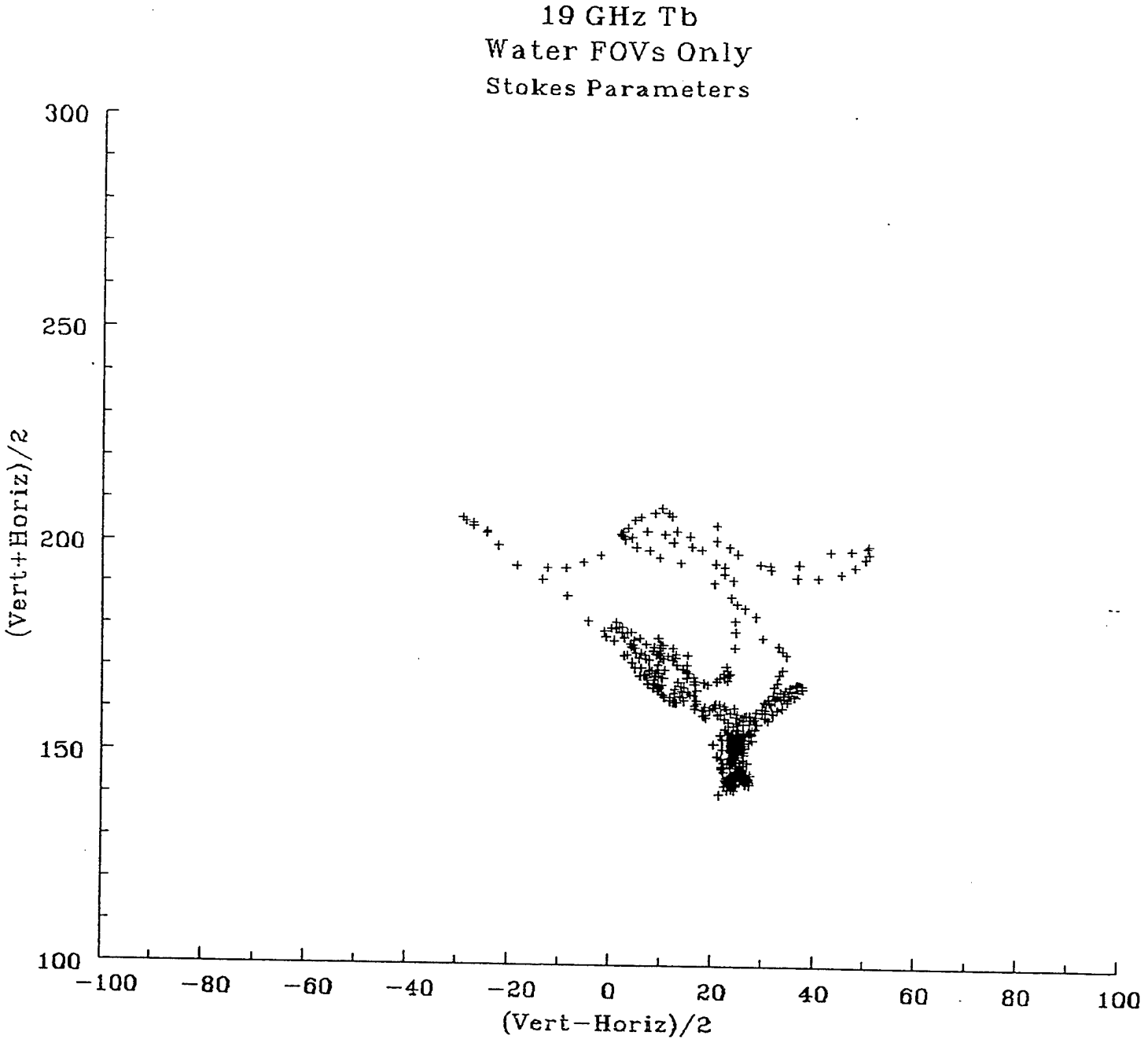

(a)

Figure 66. Two of the Stokes parameters ([V+H]/2 and [V-H]/2) for the AMPR data measured over water taken during the CAMEX and TOGA-COARE flights. Three of the AMPR channels are displayed: a) 19 GHz, b) 37 GHz and c) 85 GHz. V represents the vertically polarized T_bs (measured at 45° left of nadir) and H represents the horizontally polarized T_bs (measured at 45° right of nadir). Only data measured when the aircraft was at an altitude of at least 19 km and in level flight were used.

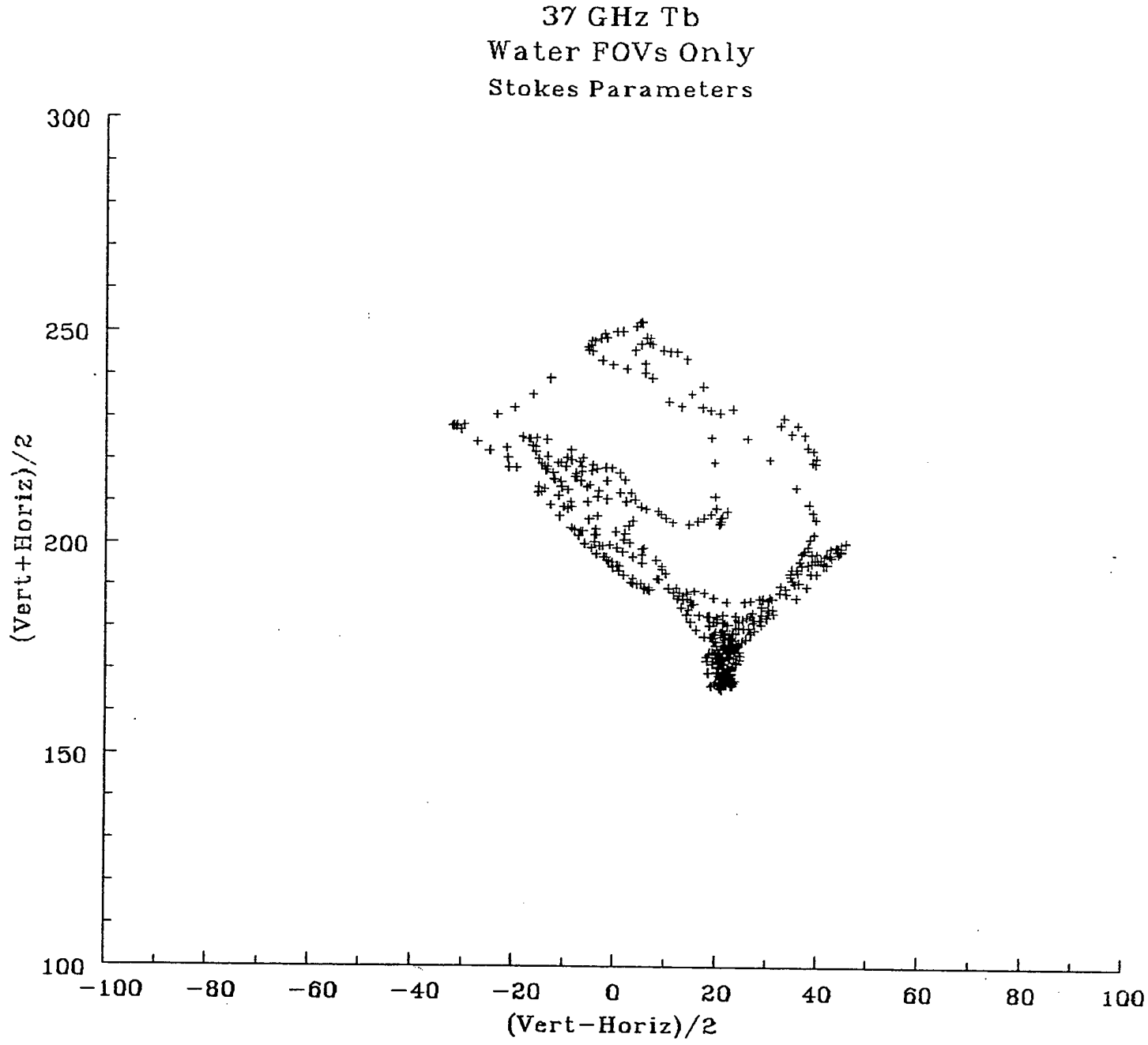

(b)

Figure 66. (continued) Two of the Stokes parameters ([V+H]/2 and [V-H]/2) for the AMPR data measured over water taken during the CAMEX and TOGA-COARE flights. Three of the AMPR channels are displayed: a) 19 GHz, b) 37 GHz and c) 85 GHz. V represents the vertically polarized T_bs (measured at 45° left of nadir) and H represents the horizontally polarized T_bs (measured at 45° right of nadir). Only data measured when the aircraft was at an altitude of at least 19 km and in level flight were used.

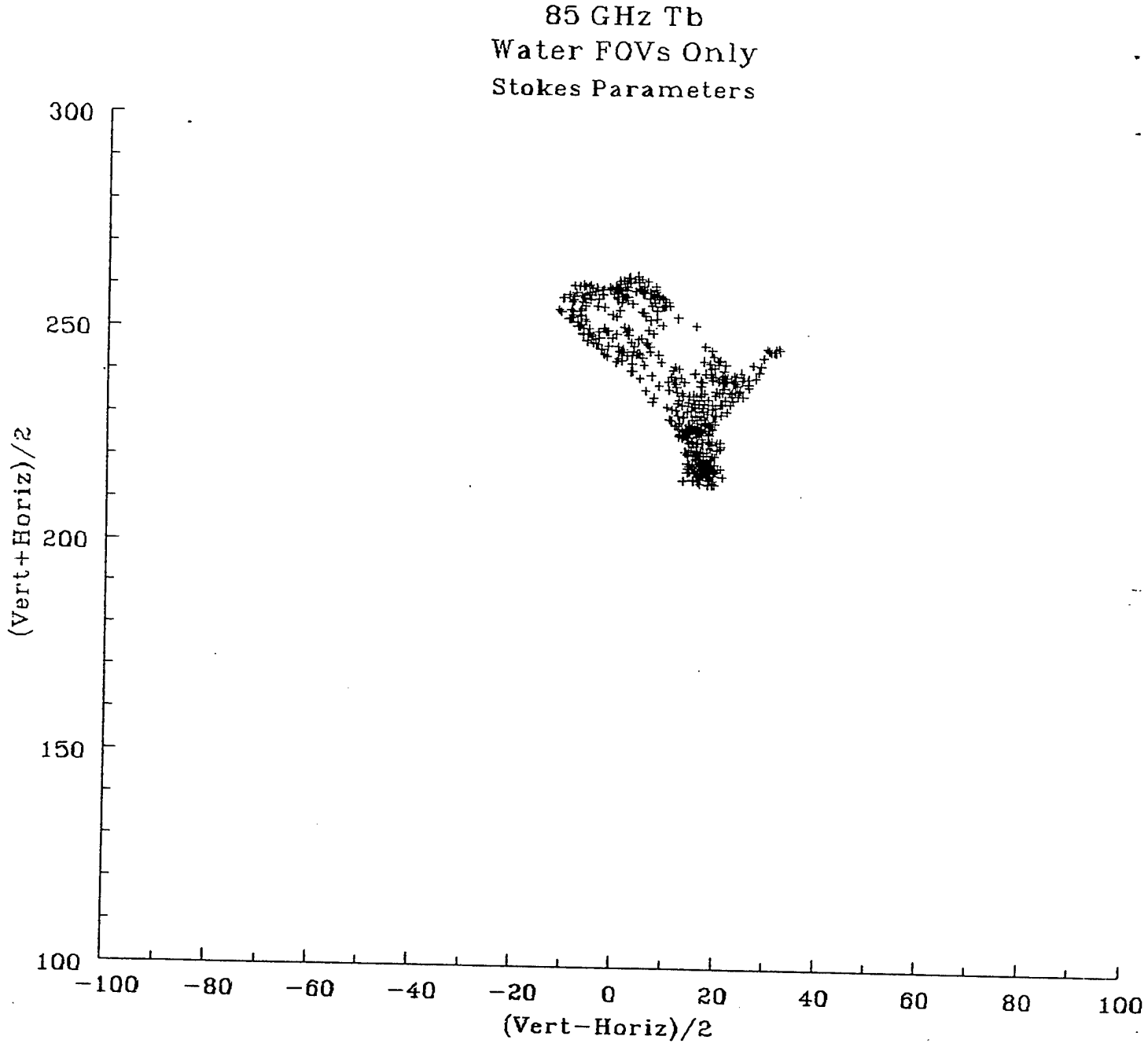

(c)

Figure 66. (continued) Two of the Stokes parameters ([V+H]/2 and [V-H]/2) for the AMPR data measured over water taken during the CAMEX and TOGA-COARE flights. Three of the AMPR channels are displayed: a) 19 GHz, b) 37 GHz and c) 85 GHz. V represents the vertically polarized T_bs (measured at 45° left of nadir) and H represents the horizontally polarized T_bs (measured at 45° right of nadir). Only data measured when the aircraft was at an altitude of at least 19 km and in level flight were used.

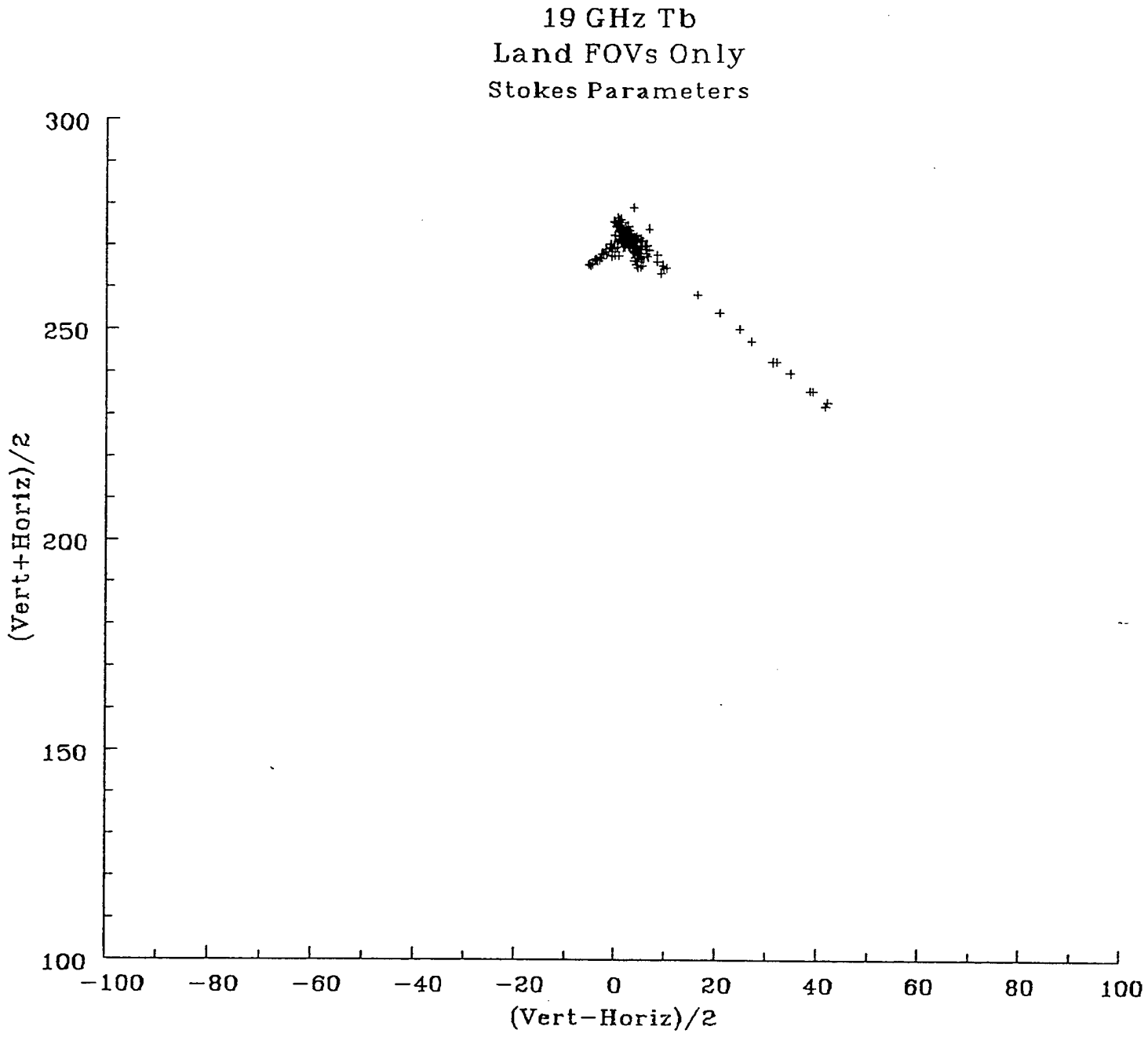

(a)

Figure 67. Two of the Stokes parameters ([V+H]/2 and [V-H]/2) for the AMPR data measured over land taken during the CAMEX and TOGA-COARE flights. Three of the AMPR channels are displayed: a) 19 GHz, b) 37 GHz and c) 85 GHz. V represents the vertically polarized T_bs (measured at 45° left of nadir) and H represents the horizontally polarized T_bs (measured at 45° right of nadir). Only data measured when the aircraft was at an altitude of at least 19 km and in level flight were used.

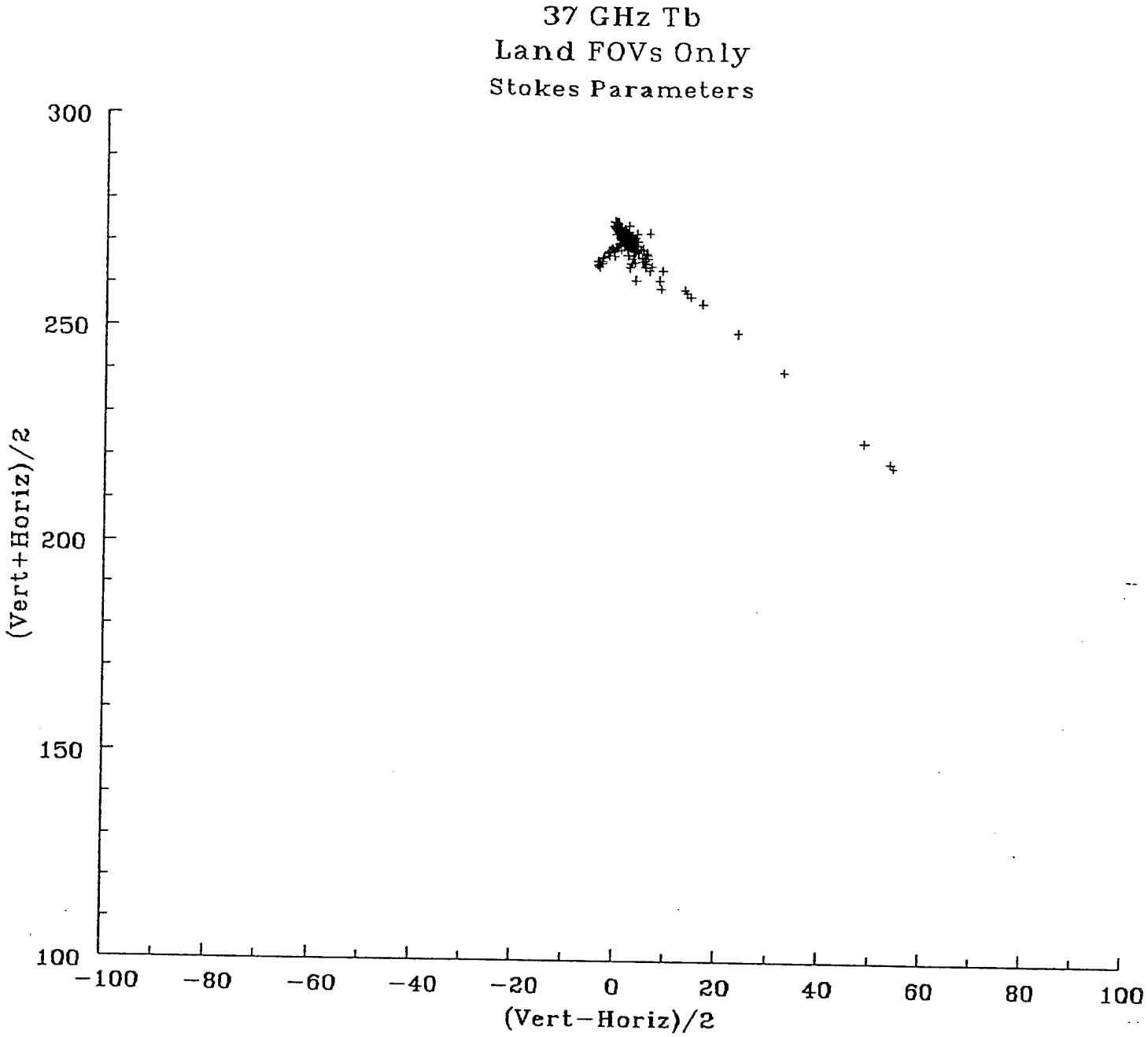

(b)

Figure 67. (continued) Two of the Stokes parameters ([V+H]/2 and [V-H]/2) for the AMPR data measured over land taken during the CAMEX and TOGA-COARE flights. Three of the AMPR channels are displayed: a) 19 GHz, b) 37 GHz and c) 85 GHz. V represents the vertically polarized T_bs (measured at 45° left of nadir) and H represents the horizontally polarized T_bs (measured at 45° right of nadir). Only data measured when the aircraft was at an altitude of at least 19 km and in level flight were used.

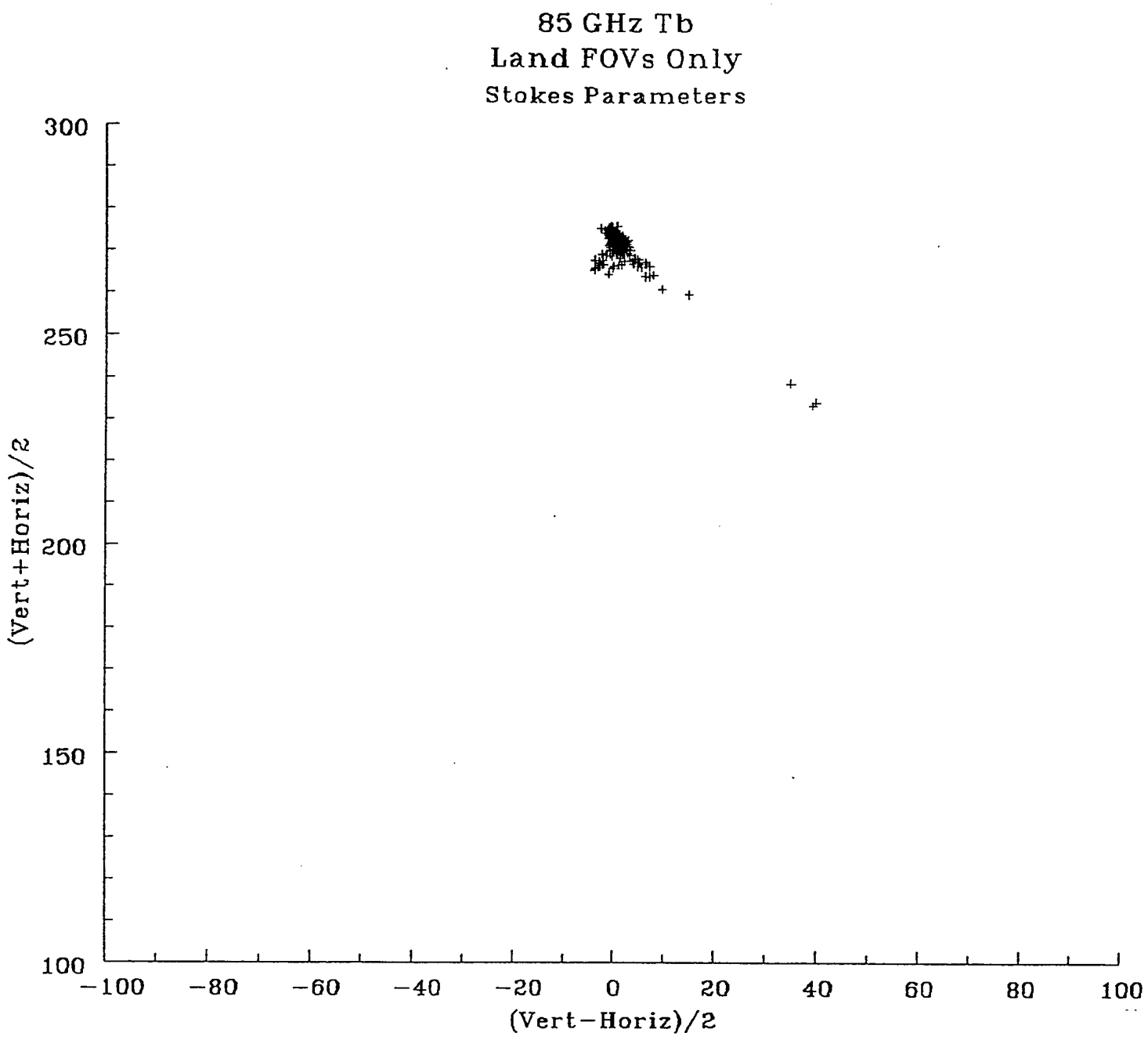

(c)

Figure 67. (continued) Two of the Stokes parameters ([V+H]/2 and [V-H]/2) for the AMPR data measured over land taken during the CAMEX and TOGA-COARE flights. Three of the AMPR channels are displayed: a) 19 GHz, b) 37 GHz and c) 85 GHz. V represents the vertically polarized T_bs (measured at 45° left of nadir) and H represents the horizontally polarized T_bs (measured at 45° right of nadir). Only data measured when the aircraft was at an altitude of at least 19 km and in level flight were used.

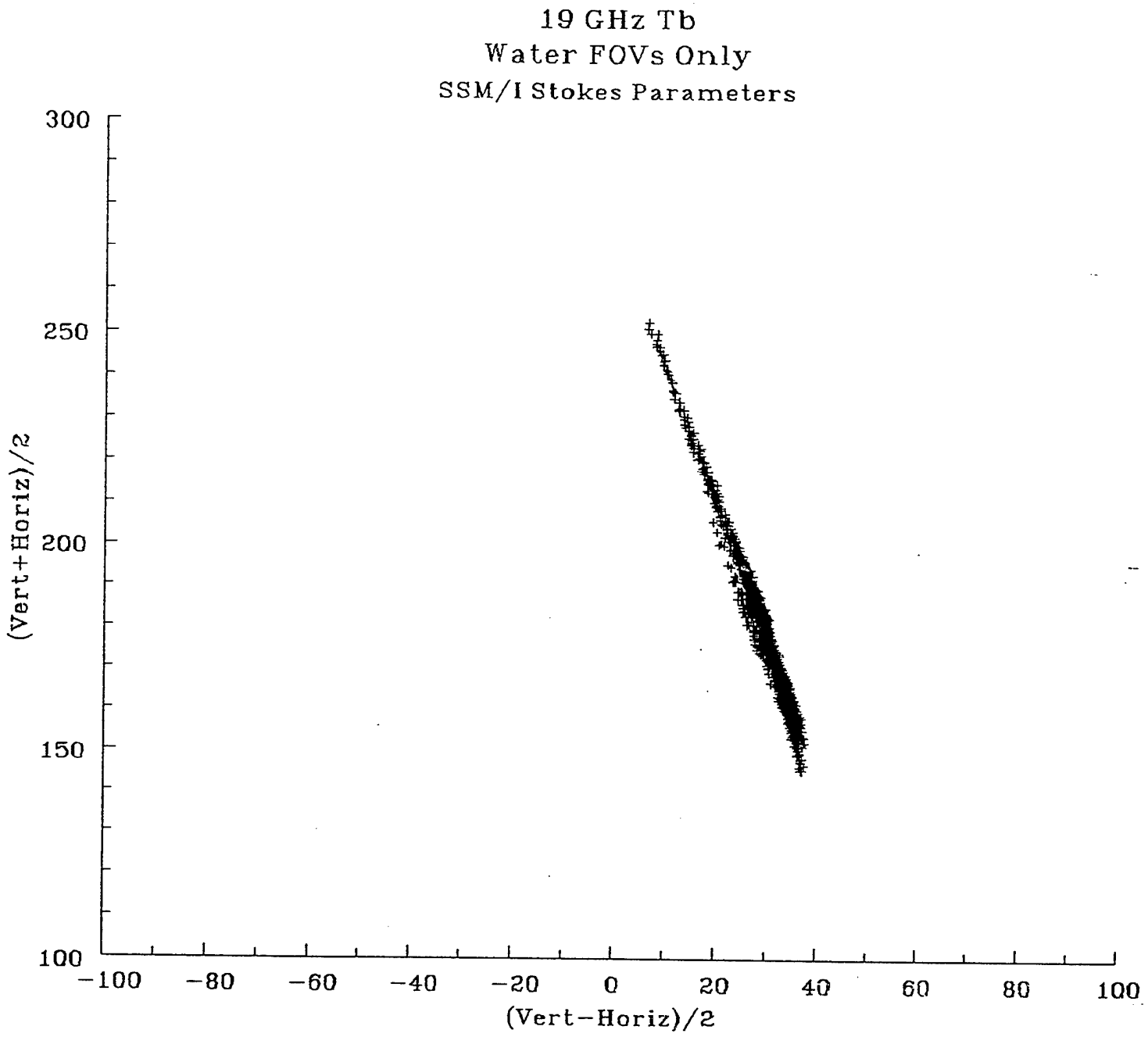

(a)

Figure 68. Two of the Stokes parameters ([V+H]/2 and [V-H]/2) for the SSM/I data over water observed within the region of the aircraft flights during the CAMEX and TOGA-COARE experiments. Three pairs of the SSM/I channels are displayed: a) 19 GHz, b) 37 GHz and c) 85 GHz. V represents the vertically polarized T_bs and H represents the horizontally polarized T_bs.

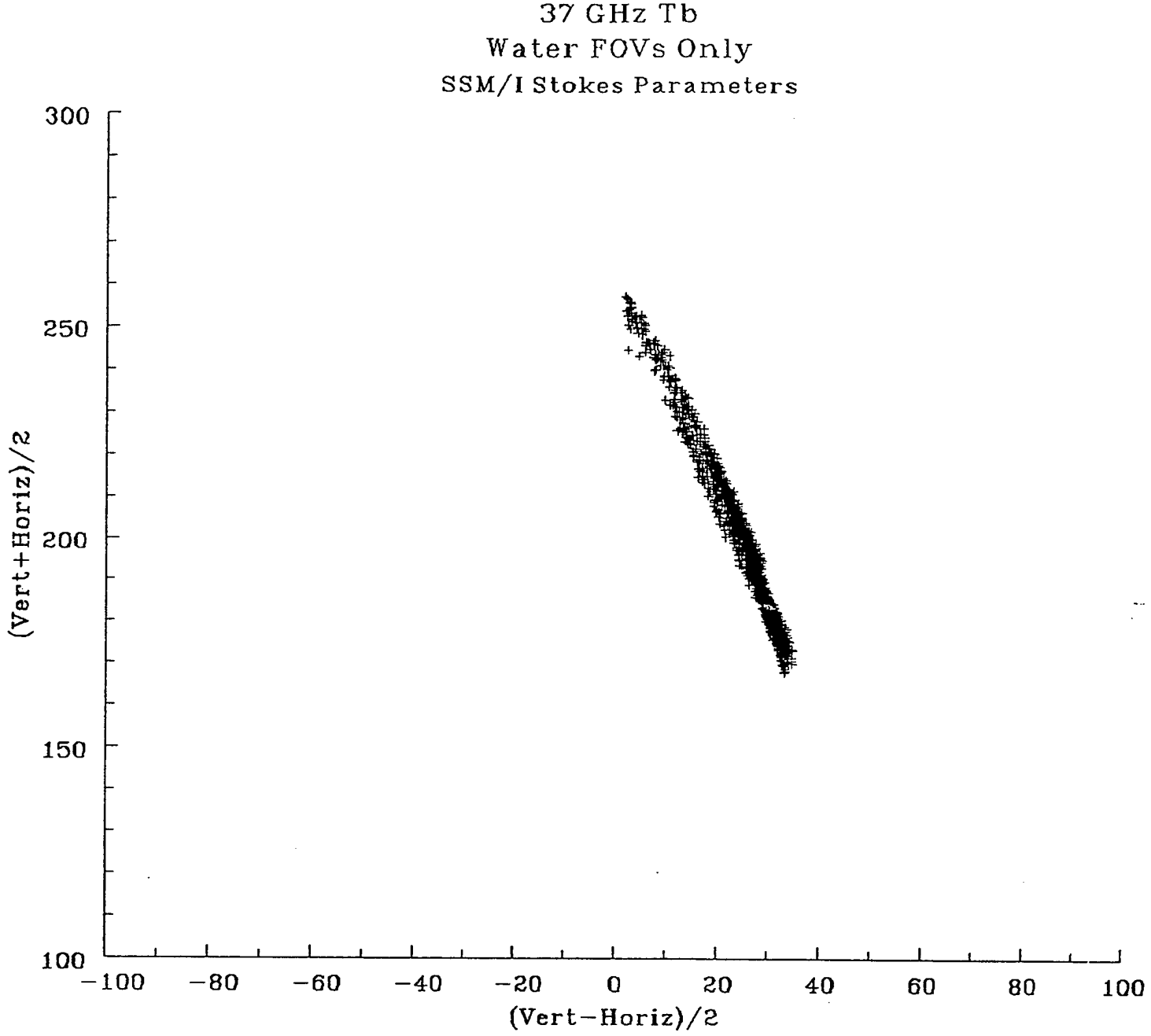

(b)

Figure 68. (continued) Two of the Stokes parameters ([V+H]/2 and [V-H]/2) for the SSM/I data over water observed within the region of the aircraft flights during the CAMEX and TOGA-COARE experiments. Three pairs of the SSM/I channels are displayed: a) 19 GHz, b) 37 GHz and c) 85 GHz. V represents the vertically polarized T_bs and H represents the horizontally polarized T_bs.

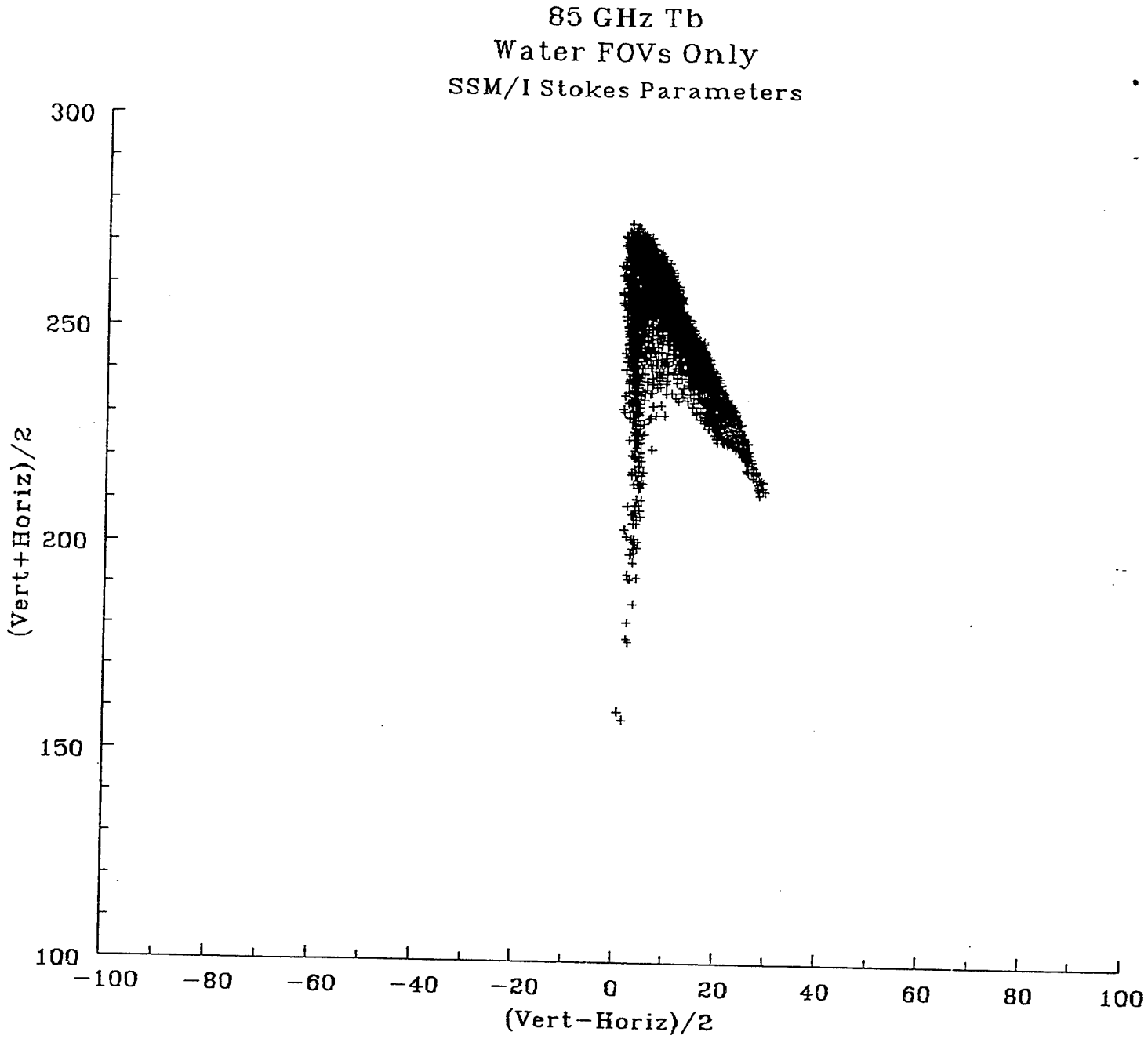

(c)

Figure 68. (continued) Two of the Stokes parameters ([V+H]/2 and [V-H]/2) for the SSM/I data over water observed within the region of the aircraft flights during the CAMEX and TOGA-COARE experiments. Three pairs of the SSM/I channels are displayed: a) 19 GHz, b) 37 GHz and c) 85 GHz. V represents the vertically polarized T_bs and H represents the horizontally polarized T_bs.

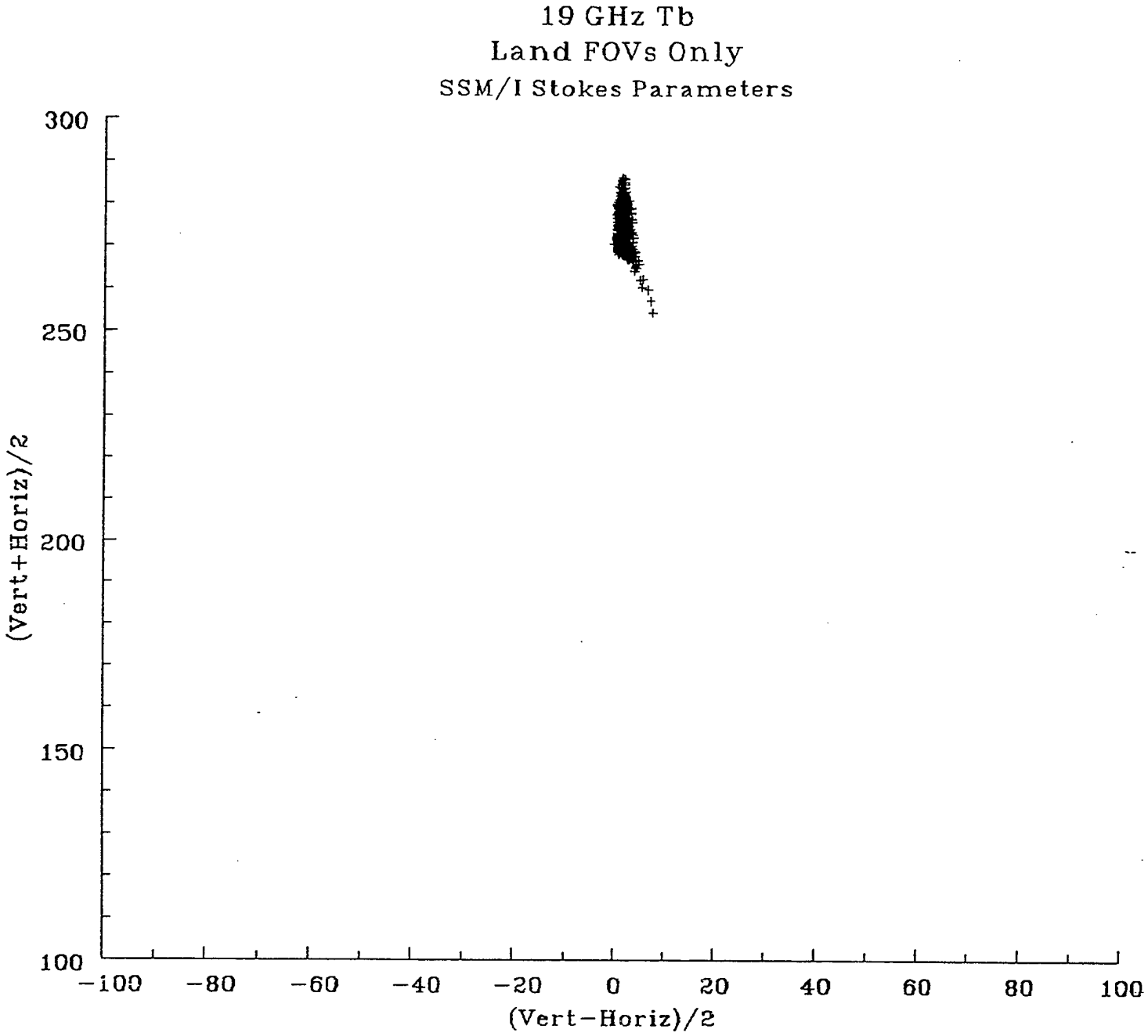

(a)

Figure 69. Two of the Stokes parameters ([V+H]/2 and [V-H]/2) for the SSM/I data over land observed within the region of the aircraft flights during the CAMEX and TOGA-COARE experiments. Three pairs of the SSM/I channels are displayed: a) 19 GHz, b) 37 GHz and c) 85 GHz. V represents the vertically polarized T_bs and H represents the horizontally polarized T_bs.

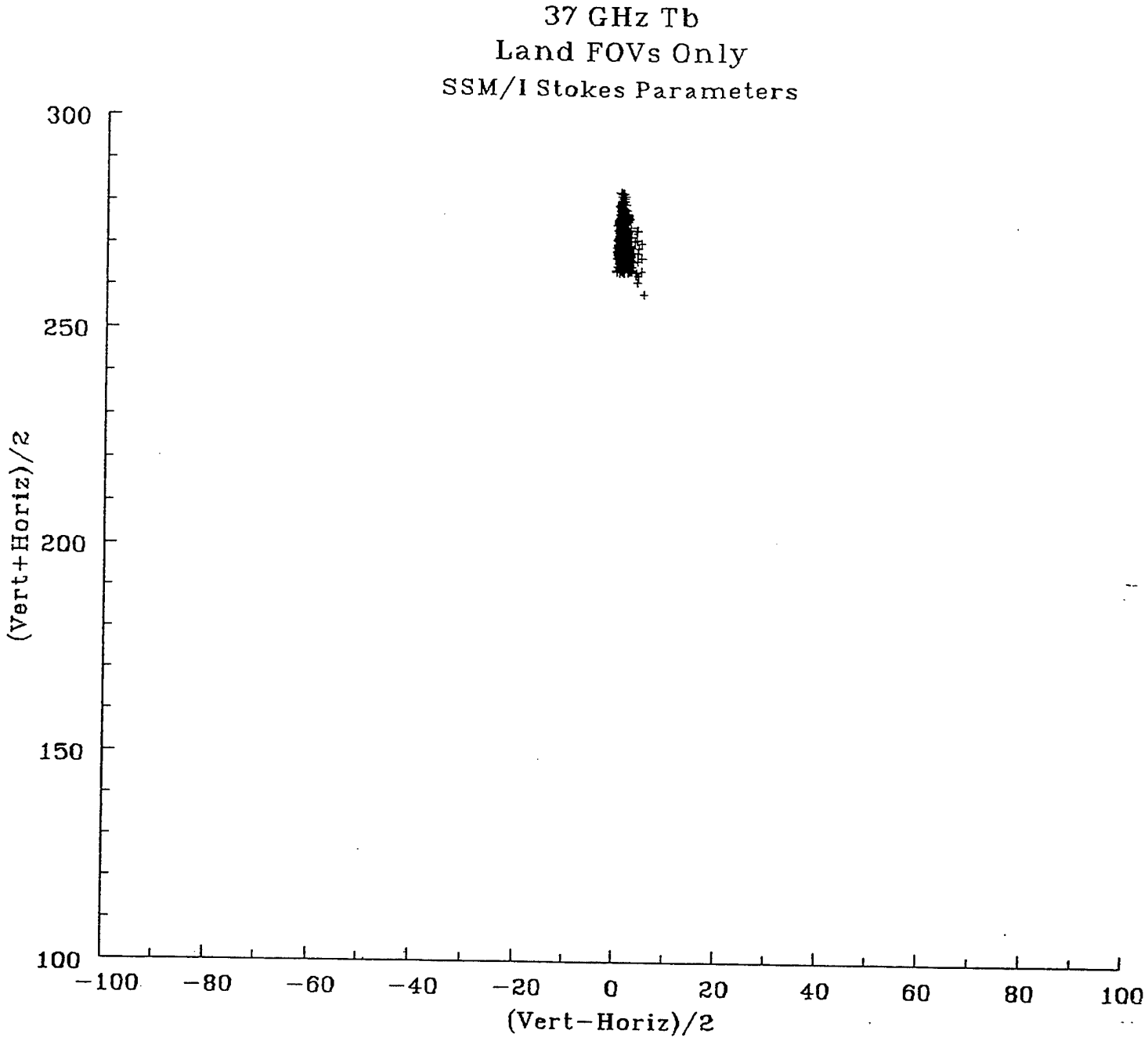

(b)

Figure 69. (continued) Two of the Stokes parameters ([V+H]/2 and [V-H]/2) for the SSM/I data over land observed within the region of the aircraft flights during the CAMEX and TOGA-COARE experiments. Three pairs of the SSM/I channels are displayed: a) 19 GHz, b) 37 GHz and c) 85 GHz. V represents the vertically polarized T_bs and H represents the horizontally polarized T_bs.

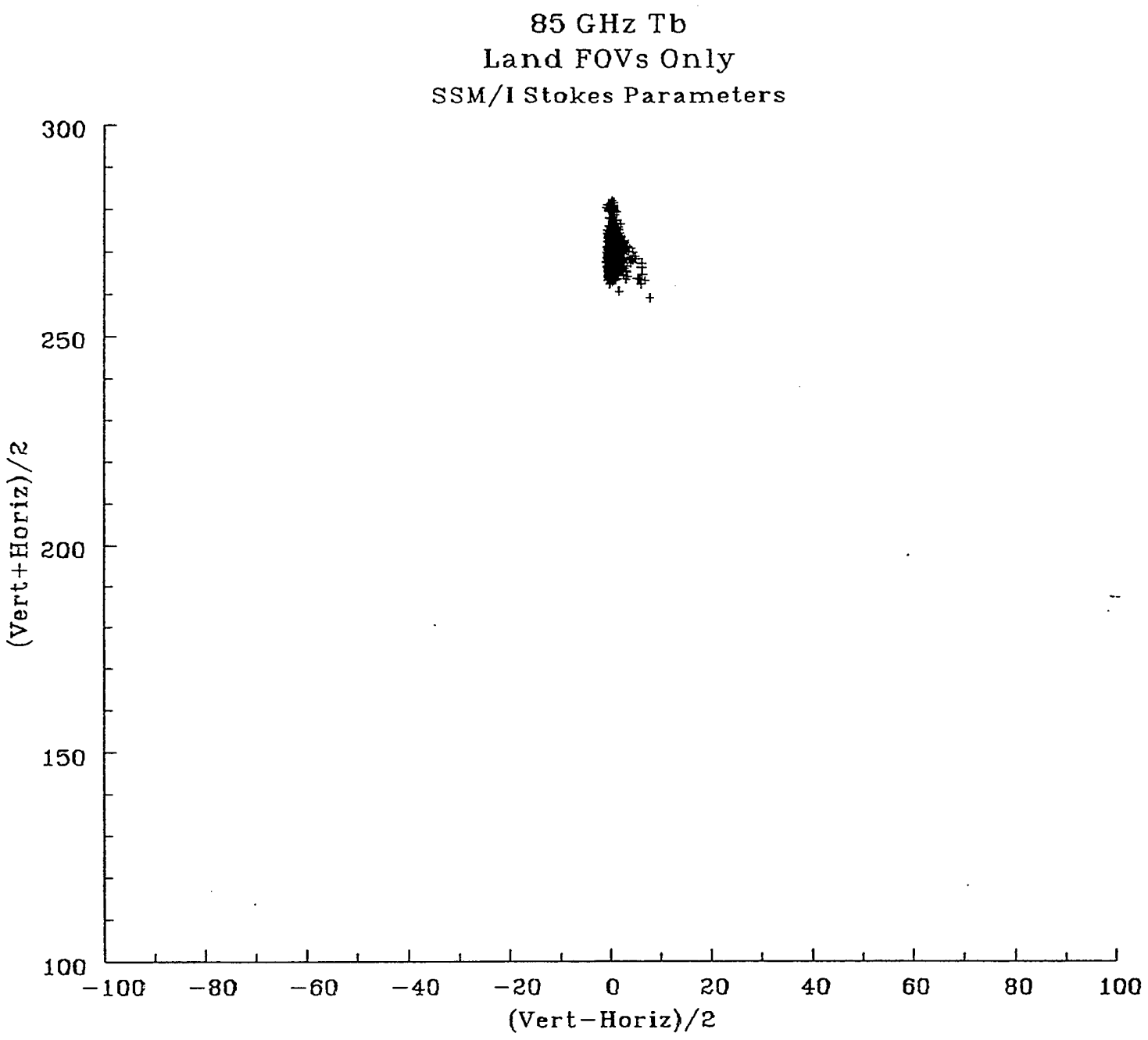

(c)

Figure 69. (continued) Two of the Stokes parameters ([V+H]/2 and [V-H]/2) for the SSM/I data over land observed within the region of the aircraft flights during the CAMEX and TOGA-COARE experiments. Three pairs of the SSM/I channels are displayed: a) 19 GHz, b) 37 GHz and c) 85 GHz. V represents the vertically polarized T_bs and H represents the horizontally polarized T_bs.

10. HIGH INCIDENCE ANGLE VIEWING

The MIR and AMPR data provided a chance to examine the effects of viewing angle along a swath width of roughly 50 km, versus over 1700 km of the T-2. The MIR results were presented in Section 4.3.1.

During the September 30, 1993 CAMEX flight, the ER-2 performed a near constant-roll figure eight maneuver over the ocean (Figure 4) in order to test the effects of high angle viewing on both the T-2 (MIR) and SSM/I (AMPR) frequencies. The results for the MIR were not different from those observed for the previous flights. Since the polarization was changing continuously across the swath, the AMPR data was examined by plots of only the vertically and horizontally polarized T_b at the corrected viewing angles (Figure 70). The 10 GHz plot is not included. All four channels showed the vertically polarized T_b to be greater than the horizontal; however, as the frequency increased, the horizontal T_b's viewing angle dependence decreased. Also, the 85 GHz channel displayed large variability compared to the other frequencies.

11. SUMMARY

The CALVAL study was undertaken to determine the accuracy of T-2 water vapor sounder T_bs by independent comparison with co-located aircraft measurements. Thirteen underflights of the T-2 were made by the NASA ER-2 research aircraft which carried the MIR, an instrument with similar channels and scan characteristics to the T-2 and a stated accuracy of 1 K. The flights occurred on both coasts of the U.S. and the equatorial Pacific Ocean with both water and land surfaces targeted for measurements. Comparisons of the T-2 and MIR 183 GHz measurements over water FOVs, which provided the most accurate estimate of the true instrument bias, displayed RMS differences of 0.9 to 1.6 K, roughly within the accuracy limits of the calibrating MIR instrument. Larger differences occurred for regions where surface emissivity variations are significant (up to 11 K for coast and land FOVs). The overall conclusion was that the T-2 suffered no significant bias in its calibration. The difference between the mean MIR T_bs and colocated T-2 T_bs was considerably larger for precipitation than for non-precipitating conditions.

One concern of a CALVAL effort was that the data be representative of the global conditions that will be measured by the sensor. The east and west coast calibration sites were biased toward mid-latitude climates collected during the spring and summer seasons over both land and ocean surfaces; the TOGA-COARE data represent tropical conditions predominantly over ocean. The radiosonde data were strongly weighted toward land sites. The means, standard deviations and ranges differed markedly between these two CALVAL data sets. For example, the mean T_b for 91 GHz was much cooler than that observed for the land-biased radiosonde data set. The overall ranges for the orbital data set (global data) were much larger than the data measured by the field test sites, which suggest that the range of the calibration sites could be extended to improve the representativeness to global conditions.

RT modeling was also employed to test the calibration of the satellite sensor. RT models simulated observed T-2 T_bs using co-located upper air temperature and moisture soundings. Atmospheric transmission was computed using both the enhanced RADTRAN line-by-line computer code and a rapid algorithm based on Eyre and Woolf (1988). Intercomparison indicated that observations and RT calculations agreed to within a few degrees for the spectrally opaque channels (i.e. no surface emissivity). The RMS between forward-calculated and satellite measured 183 ± 3 and 1 GHz T_bs were 5.7 and 6.5 K, respectively.

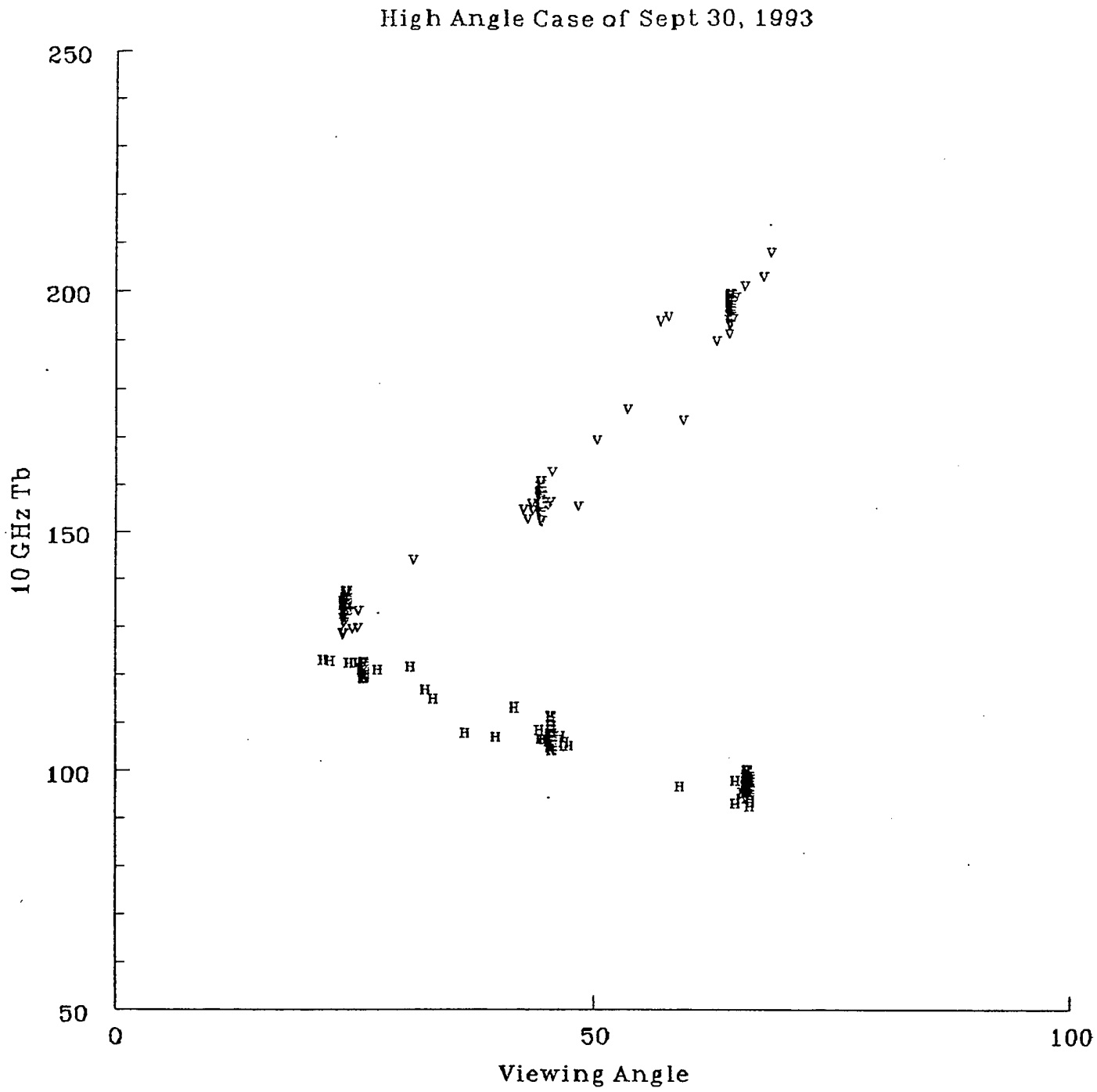

(a)

Figure 70. AMPR T_bs plotted versus scan angles across the 50 km swath during the CAMEX September 30, 1993 east coast where the aircraft performed a figure eight maneuver.

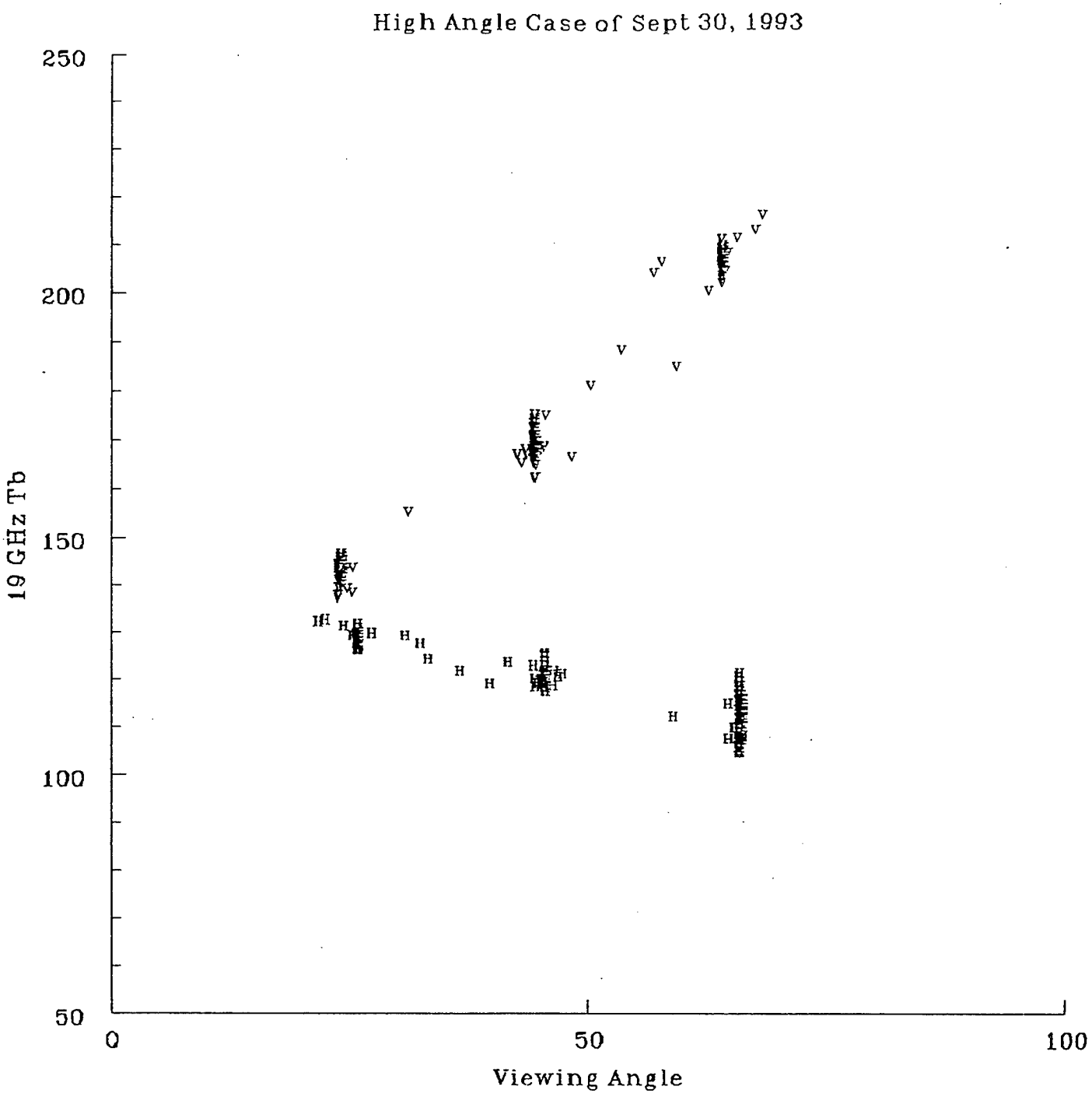

(b)

Figure 70. (continued) AMPR T_bs plotted versus scan angles across the 50 km swath during the CAMEX September 30, 1993 east coast where the aircraft performed a figure eight maneuver.

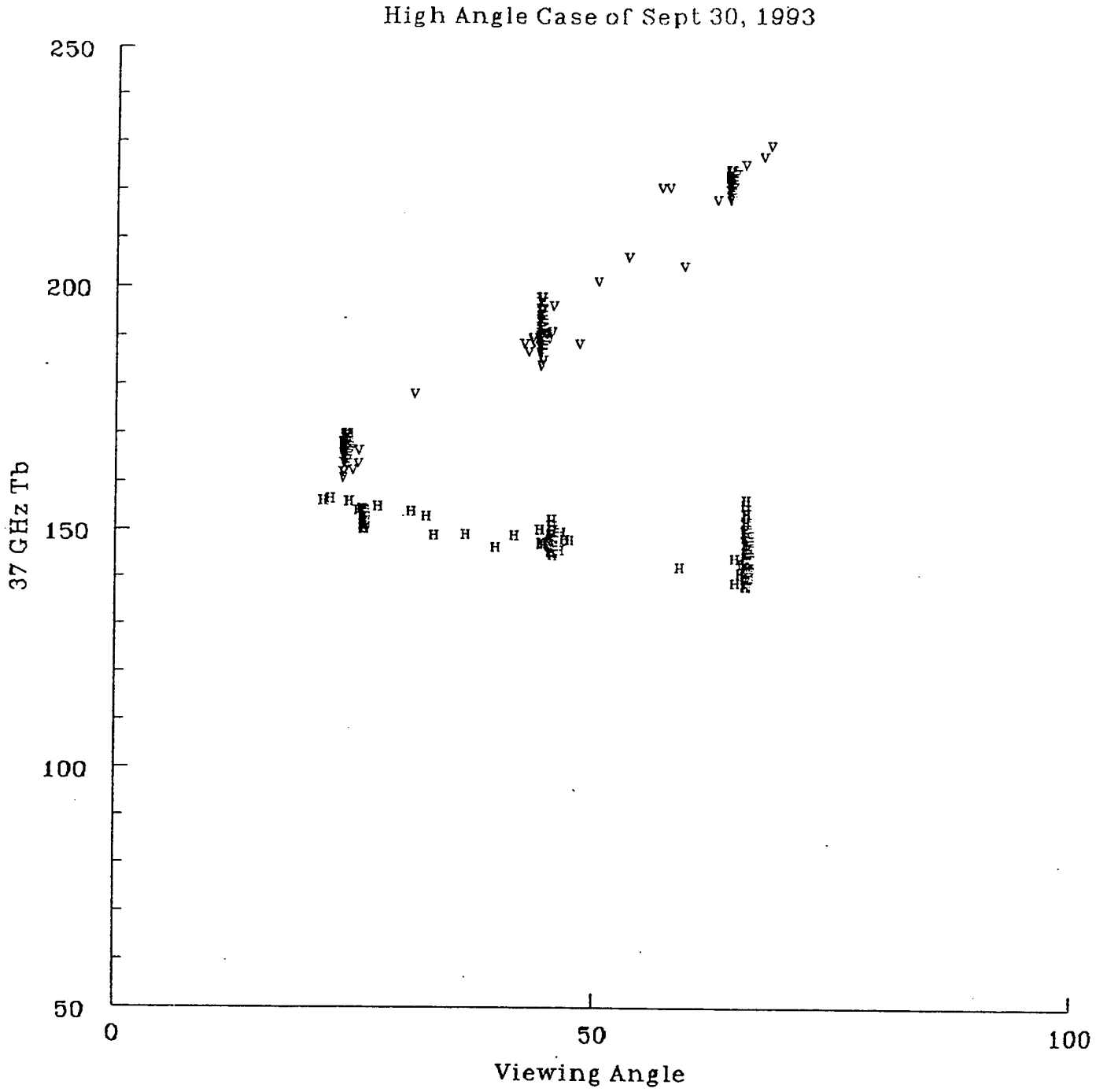

(c)

Figure 70. (continued) AMPR T_bs plotted versus scan angles across the 50 km swath during the CAMEX September 30, 1993 east coast where the aircraft performed a figure eight maneuver.

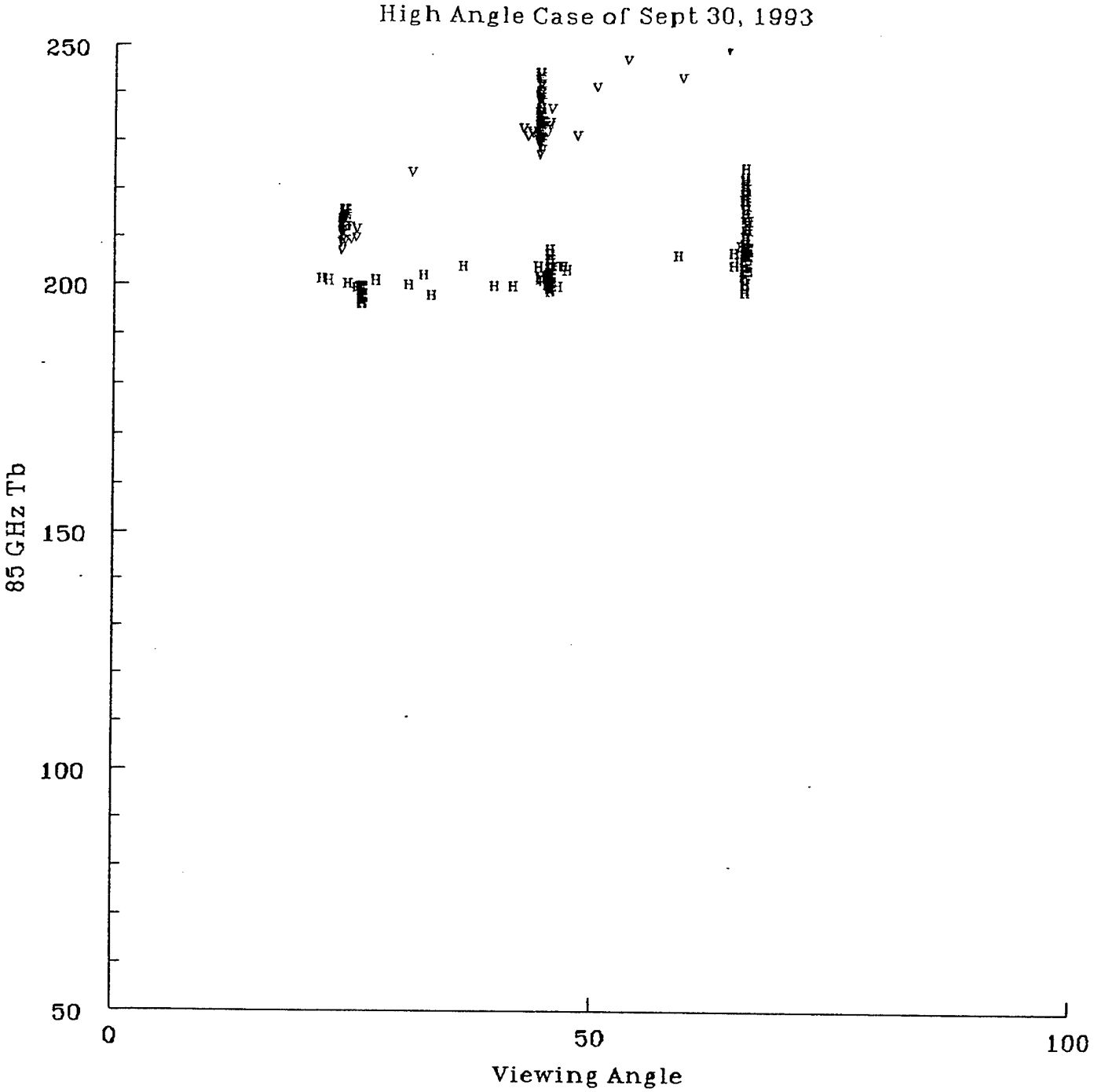

(d)

Figure 70. (continued) AMPR T_bs plotted versus scan angles across the 50 km swath during the CAMEX September 30, 1993 east coast where the aircraft performed a figure eight maneuver.

To calculate the uncertainties in retrieved moisture values due to the accuracy limits of the T-2 sensor, a RT model was used with a global set of radiosonde temperature and moisture profiles to relate the modification of moisture profiles to changes in forward-calculated T_bs. For 183±3 GHz, the channel least likely to be affected by uncertain upper-air moisture measurements and by surface radiation, a 1 K fluctuation in T_b, which was within the range of the accuracy limits of the 183 GHz channels, was obtained by changing the moisture profile by 12.1%. This could be said to be the limit of accuracy of the retrieved waster vapor profiles since any RMS RH error values below that value would be equivalent to a T_b error value less than 1 K (in the noise). Any RMS value greater than 12% would indicate inefficiencies in the retrieval algorithm.

RT models were used to examine the sensitivity of the T-2 channels to atmospheric moisture and temperature, surface emissivity and temperature, and satellite viewing angle. The general premise was to hold all but one of the variables constant and examine the change in the RT-model-generated T_bs with respect to the TPWs of the original sounding profiles. The atmospheric and surface emission contributions were quite sensitive to changes in the moisture profiles. The atmospheric channels were more sensitive when the sounding moisture content was low, and the window channels were more sensitive when the TPW was large. These components tended to counter one another, producing nominal sensitivity of the overall T_b. In general, when a channel sensed predominantly surface radiation, as with the window channels (91 and 150 GHz), there was a positive correlation between moisture and T_b changes. When a channel sensed predominantly atmospheric moisture contributions (the 183 GHz channels), there was a negative trend. A non-monotonic relationship occurred when the channel sensed significant contributions from both the surface and the atmosphere; as the moisture content was decreased, the channel behaved as a window channel, and when the moisture was increased, it became an atmospheric channel. Even the 183±1 GHz channel sensed the surface when the terrain was mountainous and/or the atmosphere extremely dry. Conversely, window channels had a significant atmospheric contribution when the profile was very moist, i.e. in the tropics, and/or for large viewing angles.

When a channel sensed predominantly surface radiation, there was decreased sensitivity between temperature and T_b changes. As the channel sensed a greater proportion of atmospheric moisture, there was a greater sensitivity to the atmospheric temperature change. For dry profiles, only the 183±3 and 1 GHz channel produced a greater amount of change in T_b compared to the change in temperature profile. For moister environments, all the atmospheric channels produced a larger change in T_b than was used in the temperature profile modification. The sensitivities for the 91 and 150 GHz displayed a gradual increase with increasing TPW while the 183 GHz channels became constant by 10 kg/m^2, showing no appreciable increase for larger TPWs. The sensitivities of the atmospheric channels were bounded.

As satellite viewing angle increased, the atmospheric path lengthened. For relatively dry atmospheric profiles, limb-cooling occurred for the 183±7, 3, and 1 GHz channels as a result of the increased atmospheric path causing the weighting function to shift to higher, cooler altitudes. Limb-warming was noted for the two window channels, 91 and 150 GHz since the majority of the weighting function was beneath the earth's surface; therefore, the additional atmospheric contribution, which was warmer than the contribution coming from the surface, increased the forward-calculated T_b. For moist atmospheric profiles, only the 91 GHz channel experienced limb-warming and at a much lower rate than that observed in the drier case. The 150 and 183 GHz channels displayed limb-cooling in moist atmospheres. Limb-warming for the 91 GHz channel occurred for all 1601 atmospheres, regardless of TPW; however, the amount of limb-warming peaked near a TPW of 23 kg/m^2 and decreased for larger TPWs. For the 150 GHz channel, limb-warming occurred in the drier atmospheres (almost always when the TPW was less than 19 kg/m^2 and possibly when between 19 and 38 kg/m^2). Limb-cooling occurred almost exclusively when the TPW was greater than 38 kg/m^2. Limb-warming occurred for the 183 GHz channels only for very dry atmospheres; limb-cooling was the predominant response for the

atmospheric channels. The mean (and minimum) amount of limb-cooling observed from 0 to 40.5° scan angle for the 183±7, 3, and 1 GHz was -3 (-5), -4 (-6), and -5 (-10) K, respectively.

Channels sensing predominantly surface radiation were sensitive to ground temperature. All T-2 channels became less sensitive to ground temperature as TPW increased. Similar results were observed with surface emissivity. Even the 183±1 GHz channel sensed the surface radiation when the moisture profile was dry. Surface emission was the dominant factor in determining T_b sensitivity; overriding the decrease in the surface reflectance.

Only 10% of the weighting functions for 91 GHz peaked above the earth's surface. This result led to the near constant pressure levels of the peak of the weighting function despite increasing TPW and the pressure levels of the 25th, 50th, and 75th percentiles of the weighting functions being at consistently lower values compared to the weighting functions for 150 GHz. However, the percent contributions from the surface emissions to the 91 GHz T_b decreased steadily as TPW increased. The trends observed for the other 4 T-2 channels were similar: weighting functions shifted to lower pressures and less of the surface and more of the atmosphere was sensed as TPW increased. As TPW increased, the weighting functions of the 183 GHz channels sensed a smaller band of the atmosphere and the overlap of the weighting functions decreased.

The variation and range of MIR T_bs within each of the colocated T-2 FOVs were due to variation of moisture, temperature, ground temperature, surface emissivity, viewing angle and the presence of cloud and precipitation. Examining the 183±3 and 1 GHz results minimized the surface effects. The average range of MIR T_bs within T-2 FOVs with less than 20% non-precipitating cloud cover was greater for 183±1 GHz (6-7 K) than for 183±3 GHz (4-5 K). Both frequencies displayed quite a large average range of brightness temperature within the 183 GHz FOV implying the variance of water vapor was quite large. Therefore, the precision of using the point-values of a radiosonde to calibrate and validate satellite sensors that have relatively large volume or areal sensing dimensions was quite limited. Note that the RMS between forward-calculated and satellite measured 183±3 and 1 GHz T_bs were 5.7 and 6.5 K, respectively.

Since the failure of the 150 GHz sensor of the T-2 instrument on board the F-11 satellite in June 1993, a multiple regression technique was developed to simulate T_bs. Since the T-2 channels sensed overlapping vertical segments of the atmosphere, relationships between the T_bs for various atmospheric and topographic conditions (clouds, rain, ice, ocean, land, etc.) were examined using CALVAL data gathered before the failure of the 150 GHz sensor. It was observed that a majority of observed T_b sets had similar relationships between channels and that individual T_bs were bounded by ranges of temperature, especially for clear sky conditions. Therefore a multiple regression technique was developed. Testing of the multiple regression technique on the independent data resulted in the following overall results:

Mean difference = 0.23 K,
Standard Deviation = 2.94 K,
Minimum difference = -29.0 K,
Maximum difference = 18.9K,
Number of Cases = 91,186.

With the premature loss of the 150 GHz channel in the summer of 1993, the T-2 instrument went under increased scrutiny. It was confirmed that cross-track anomalies existed for the 183±3 GHz channel at specific beam positions. These anomalies were found to occur as far back as the earliest available T-2 data; however, they do not significantly impact the final water vapor retrieval product since the magnitudes are on the order of 0.5 K at beam positions 14 and 16 (smaller deviations at other beam positions). These anomalies are below the determined 1 K accuracy limit of the T-2 channels.

There were T-2 T_b signatures for distinct atmospheric/surface environments. Using the colocated SSM/I and GOES data, rain produced noticeably different signatures compared to non-precipitating clouds over water. Light rain cases with rain filling less than 80% of the T-2 FOV produced the warmest T_bs at 150 GHz rather than 183±7 GHz. At 100% light precipitation within the FOV, two populations were present: one with peak T_bs at 150 GHz and one with peak T_bs at 91 GHz. As the rain rate increased, the first population decreased so that only those cases with peak T_bs at 91 GHz were observed. For this population, the minimum T_bs were typically at 183±7 GHz. As expected, the T_b signature over relatively cloud-free FOVs over land were markedly different compared to over water. The surface and near surface channel T_bs were much warmer over land with the warmest T_bs occurring at 150 GHz. The ranges of 183±3 and 1 GHz T_bs were similar for land and water FOVs. There were too few cloud-filled land FOVs to determine if distinct trends or differences occurred as the amount of clouds increased in the FOV. However, there did not appear to be noticeable differences in T_b signatures as the amount of cloud increased in the FOV over land. Using the global revolutions of T-2 T_bs, an interesting observation was noted: the cases with the warmest T_b at 183±1 GHz were confined to the poles and Greenland. Also, when the effects of TPW over land were examined using the colocated radiosonde database, the very dry profiles (TPWs ranging from 0 to 5 kg/m^2) had similar polar signatures. These radiosonde profiles were from northerly stations.

Griffin et al. (1994) showed a clear difference between T-2 T_b signatures for clear and cloud-filled FOVs over ocean; however, there was not an apparent signal over land. Griffin et al. (1994) also showed a clear T_b signature of heavy precipitation (a developing typhoon in the western South Pacific Ocean). The number and variety of precipitation cases were expanded, as were the data used to verify precipitation (MDR data were incorporated with SSM/I data). Two approaches were undertaken to examine the effects of precipitation: case studies and "bulk" data analysis. It was noticed from case studies that the majority of precipitation cases were quite identifiable with T-2 data; however, there were certain types of precipitation, possibly when ice was not associated with the rain, that had very little if any signature in the T-2 T_b fields.

Two techniques were developed to identify precipitation based on T-2 T_bs. One technique was based on thresholds of T-2 T_bs and buddy differences. Depth of convection was estimated based on whether anomalous values were present in the channels sensing higher in the atmosphere. For example, precipitation would be considered shallow if anomalies were seen in the 183±7 GHz T_bs and not the 183±3 and 183±1 GHz T_bs. Also, the confidence in the precipitation identification was determined by checking to see if the anomalies were present in the channels that sense lower in the atmosphere than the channel that first identified precipitation.

A technique was developed to generate fields of upper-tropospheric humidity (UTH) using 183±1 GHz T_bs and temperature profiles from radiosondes. The basic idea was to iteratively calculate the constant relative humidity profile necessary to produce the colocated T_b using a known temperature profile in the modified Eyre RT model. Because radiosondes were used as the source of the temperature profiles, the T-2 data were limited to be near 00 and 12 UTC (the time of radiosonde data). Testing of this technique with the 1601 colocated radiosonde/T_b data set indicated that the RMS difference between the constant relative humidity profiles and the averaged relative humidity between the 75th and 25th percentiles of the 183±1 GHz weighting function was 18%. If only unsaturated profiles were used (assumed to minimized the chance of clouds within the T-2 FOV), then the RMS was reduced to 14%. This technique was expanded to generate fields of UTH. Generated UTH fields were coherent in gradients, roughly paralleling the 183±1 GHz T_b field, and may be useful in identifying upper-tropospheric clouds, especially deep convective systems. Even in very dry conditions, when relatively large contributions of the T_b came from the surface, the UTH values appeared coherent in distribution.

AMPR data was quite difficult to use for this study since the AMPR only measured the vertical (horizontal) at the 45° left (right) of nadir, all other measurements across the scan were a combination of both polarizations. Due to these differences the Stokes parameters ([V+H]/2 and [V-H]/2) for both sensors were drastically different with the AMPR data creating trapezoidal shapes and the SSM/I creating linear shapes, except for the 85 GHz channel. Land and ocean masks were created, and the relationships between the Stokes parameters were reexamined. The trapezoidal shapes observed previously for the AMPR data nearly disappeared, suggesting that the coastal scenes were the source of the large scatter, e.g. one side of the swath (say the vertically polarized T_b) was seeing land and the other (horizontally polarized T_b) was viewing water. Another source of scatter would have been the presence of cloud boundaries across the scan. As expected, the two sensors produced similar T_bs for the land FOVs since polarization is minimal (i.e. [V-H]/2 ~ 0). Over water, [V+H]/2 were comparable for both sensors; however, the SSM/I's [V-H]/2 was greater by 10-15 K. One source for this difference is that the local viewing angles for AMPR and SSM/I are 45° and 53.1°, respectively.

Whenever the NASA ER-2 aircraft banked, the MIR sensor scanned beyond the normal limits (±48°), which allowed the effects of high-incidence viewing to be examined. MIR data taken during banked turns were gathered from seven of the T-2 CALVAL flights; 2 from the west coast of the United States, 3 from the east coast of the United States and 2 from the TOGA-COARE experiment. Each group of flight data was examined separately due to the drastically different TPW characteristics of all three regions. The swath data of the 91 GHz T_bs from generally showed a population displaying limb warming, agreeing with the RT model results described above. Limb-cooling was observed for the other four T-2 channels which also agreed with the model results. Viewing at higher angles did not create unexpected results.

12. CONCLUSIONS

This work provided many insights for future calibration efforts of satellites, in particular, the necessity of aircraft in the calibration of satellite sensors. In addition, this work showed the incredible wealth of information collected during a CALVAL effort, ranging from the value of various scales of measurements (aircraft, satellite and radiosonde), geographic variability, and the incredible variety of atmospheric/weather phenomena. The insights gained from these data sets were invaluable in understanding how the sensor behaved in various conditions and the limitations of the sensor as well. Work in examining T_b responses, signatures, climatology and related accuracy/limits are essential to users of the satellite information. Techniques developed in this calibration study should be considered in future calibrations of the AMSU and MHS sensors.

13. REFERENCES

Alishouse, J., S. Snyder, J. Vongsathorn, and R. Ferraro, 1990: Determination of Oceanic Total Precipitable Water from the SSM/I, IEEE TRANS. *Geosci. Remote Sensing*, *28*, 5, 811-816.

Brousaides, F. J., and J. F. Morrissey, 1974: Residual temperature-induced humidity errors in the National Weather Service radiosonde, Final Report, AFCRL-TR-74-0111, Instrumentation Papers, No. 215, Air Force Cambridge Research Laboratories, Mass., 40 pp., AD780643.

Eyre, J. and H. Woolf, 1988: Transmittance of atmospheric gases in the microwave region: a fast model. *Applied Optics, 27*, 15, 3244-3249.

Falcone, V.J., L.W. Abreu, and E.P. Shettle, 1979: Atmospheric attenuation of millimeter and submillimeter waves: Models and computer code, *AFGL-TR-79-0253.* [NTIS AD A084485].

Falcone, V.J., L.W. Abreu, and E.P. Shettle, 1982: Atmospheric attenuation in the 30-300 GHz region using RADTRAN and MWTRAN. *Proc. Soc. Photo Opt. Instrum. Eng., 337*, 62-66.

Falcone, V. J., M. K. Griffin, R. G. Isaacs, J. D. Pickle, J. F. Morrissey, A. J. Jackson, A. Bussey, R. Kakar, J. Wang, P. Racette, D. J. Boucher, B. H. Thomas, A. M. Kishi, 1992: SSM/T-2 Calibration and Validation Data Analysis, *PL-TR-92-2293*, Environmental Research Paper No. 1111, 432 pp., ADA265817.

Falcone, V. J., M. K. Griffin, R. G. Isaacs, J. D. Pickle, J. F. Morrissey, J. Wang, 1996: Millimeter wave moisture sounder (SSM/T-2) calibration/validation program. SSM/T-2 calibration and validation data analysis during TOGA-COARE. Volume II. PL-TR-95-XXXX.

Fleming, H. and L. McMillin, 1977: Atmospheric transmittance of an absorbing gas. 2: A computationally fast and accurate transmittance model for slant paths at different zenith angles. *Applied Optics, 16*, 5, 1366-1606.

Garand, L., C. Grassotti, J. Hallé, and G.L. Klein, 1992: On differences in radiosonde humidity-reporting practices and their implications for numerical weather prediction and remote sensing. *Bulletin American Meteorological Society, 73*, 9, 1417-1423.

Griffin, M. K., V. J. Falcone, J. F. Morrissey, R.G. Isaacs, J. D. Pickle, R. Kakar, J. Wang, P. Racette, 1993: The Special Sensor Microwave Water Vapor Sounder(T-2): Calibration Study, *Preprints, Eighth Symposium on Meteorological Observations and Instrumentation*, AMS, Anaheim CA.

Griffin, M.K., V.J. Falcone, J.D. Pickle, and R.G. Isaacs, 1994: T-2 Brightness Temperature Signatures, *AMS 7th Conference on Satellite Meteorology and Oceanography Proceedings*, Monterey, CA.

Hollinger, J. P., 1991: DMSP Special Sensor Microwave Calibration/Validation, Final Report, Volume II; Naval Research Laboratory, Washington, D. C.

Hollinger, J., R. Lo, G. Poe, R. Savage, and J. Peirce, 1987: Special Sensor Microwave/Imager User's Guide. Naval Research Laboratory, Washington, D.C.

Hollinger J.P. and the DMSP SSM/I CALVAL Team, 1991: DMSP Special Sensor Microwave/ Imager Calibration/Validation, Final Report. Naval Research Laboratory, 1, Washington, D.C.

Isaacs, R.G., R.D. Worsham, B.L. Lindner, 1989: Characterizing Microwave Propagation Using the AFGL Microwave Attenuation/Transmittance/Brightness Temperature Code. *GL-TR-89-0188*, Air Force Geophysics Laboratory, Hanscom AFB, MA, 01731, ADA220248.

Kiess, R. B., and W. Cox, 1988: The AFGWC Automated Real-time Cloud Analysis Model. *AFGWC Technical Note 88/001*, Air Force Global Weather Central, Offutt AFB, NE, 82 pp.

Nash, J., and F. J. Schmidlin, 1987: WMO International Radiosonde Comparison, Final Report. *World Meteorological Organization Instruments and Observing Methods Report No. 30*, WMO/TD-No. 195, 103 pp.

Oltmans, S.J., 1985: Measurements of Water Vapor in the Stratosphere with a Frost-Point Hygrometer, *International Symposium on Moisture and Humidity Proceedings*, pp. 251-258, Instrument Society of America, Research Triangle Park, North Carolina.

Pickle, J. D. and R. G. Isaacs, 1993: Development of Experimental Protocols for the Calibration of SSM/T-2 Millimeter Wave Moisture Sounder Data, *Annual Status Report No. 1*, Phillips Laboratory, Directorate of Geophysics, Hanscom AFB, MA.

Pickle, J. D., R, G, Isaacs, 1994, Retrieved Surface Emissivities using Radiative Transfer Models and Co-Located SSM/T-2 Brightness Temperatures and Radiosonde Profiles, Phillips Laboratory, Directorate of Geophysics, Hanscom Air Force Base, MA

Pickle, J. D. and R. G. Isaacs, 1994: Development of Experimental Protocols for the Calibration of SSM/T-2 Millimeter Wave Moisture Sounder Data, *Annual Status Report No. 2,* Phillips Laboratory, Directorate of Geophysics.

Pickle, J. D. and R. G. Isaacs, 1995: Development of Experimental Protocols for the Calibration of SSM/T-2 Millimeter Wave Moisture Sounder Data, *Annual Status Report No. 3*, Phillips Laboratory, Directorate of Geophysics, Hanscom AFB, MA.

Pickle, J. D., R. G. Isaacs, M. K. Griffin, V. J. Falcone, J. F. Morrissey, R. Kakar, J. R. Wang, 1993: Comparison of Co-located T-2 and MIR measurements; Results from the Calibration study. *SPIE proceedings*, vol 1935, Orlando, Florida.

Rosenkranz, P. W., M. J. Komichak, and D. H. Staelin, 1982: A method for estimation of atmospheric water vapor profiles by microwave radiometry. *Journal of Applied Meteorology, 21,* p. 1364-1370.

Schmidlin, F. J., 1988: WMO International Radiosonde Intercomparison Phase II, 1985. *World Meteorological Organization Instruments and Observing Methods Report No. 29*, WMO/TD-No. 312, 113 pp.

Spencer, R.W., R.E. Hood, F.J. LaFontaine, E.A. Smith, R. Platt, J. Galliano, V.L. Griffin, and E. Lobl, 1993: High Resolution Imaging of Rain Systems with the Advanced Microwave Precipitation Radiometer, submitted to AMS Journal of Atmospheric and Oceanic Technology.

Wu, X., and C.M. Hayden, 1994: Upper Troposphere Water Vapor from Geostationary Satellite Data, AGU Chapman Conference on Water Vapor in the Climate System, Jekyll Island, GA.

Appendix A - Meetings Attended

A.1. April 6, 1992 Meeting at Phillips Laboratory

Attendees: Vincent Falcone (PL/GPAS), Mike Griffin (PL/GPAS), Jim Morrissey (PL/GPAS), Ed LeFebvre (PL/GPAS), Ron Isaacs (AER) and John Pickle (AER)

The timeline of the data sources as well as PL's and AER's responsibility for the calibration effort were discussed. Aerospace is responsible for the validation study.

For planning purposes for the ER-2 under flight on the west coast, a satellite orbital program (TRACKSAT) was obtained to determine the track and timing of the F-11 satellite. Possible flight plans of the ER-2 aircraft were analyzed with the premise that the ER-2 should fly over as much varied terrain as possible during the flight. Options for weather support were explored. So far, the only weather that would cancel the flight would be a frontal system in the area.

The amount of co-located RAOB data and T-2 data using the late January to early March data saved by Aerospace were presented. Due to tape problems and software problems at AFGWC, there were roughly four days of useful data. Three parameters were used to define co-located points: distance from the center of the satellite footprint to the location of the radiosonde release, the time difference from the balloon release time to satellite overpass time, and the satellite viewing angle.

The group discussed the upcoming presentation of the T-2 calibration presentation at the Conference on DMSP Retrieval Products, held in Washington D.C. on 14-15 April, 1992, plus set the proposed the agenda for the CALVAL meeting with Aerospace during this conference.

A.2. April 15, 1992 Meeting at the NOAA Science Center, Washington D.C.

Attendees: John Alishouse (NOAA/NESDIS), Vin Falcone, Jim Morrissey, Mike Griffin, and John Pickle

Discussed John Alishouse's experiences with the SSM/I CALVAL and asked for his advice. He recommended using one SDR per co-located RAOB. Their co-location criteria was the closest "hit" within +/- 1 hour and +/- 100 km. He stated that the main source of error in the RAOB moisture profiles occurred when the default values were used when the relative humidity went below 20%. Plus, there is a 4% variance (noise) of radiosonde relative humidity values when two sondes are released on the same balloon. Another source of error were the varying radiosonde instruments used globally to measure atmospheric moisture. Although there are (and were) differences in the type of radiosondes used by different countries to sense water vapor, which would lead to different sensitivities in the calculated moisture profiles, the SSM/I CALVAL did not take this into account. It is believed that most radiosondes were Vaisala. Plus, he warned us to beware of AFGWC's QC of radiosondes - some island stations passed their QC program despite having missing lower level values, and that we should use only island stations with land areas less than 10% of the satellite's field of view. Finally, the SSM/T-2 needs to take into account the scan angle and the cross-polarization at the earth's surface.

A.3. April 15, 1992 Meeting at the NOAA Science Center, Washington D.C.

Attendees: Don Boucher, Bruce Thomas, Vin Falcone, Jim Morrissey, Mike Griffin, Ron Isaacs, and John Pickle

Discussed T-2 calibration/validation concerns. Some of the problem areas discussed:
Problems with T-2 EDR calculation - the D-Matrix over the oceans is faulty.
Thinning of satellite data south of 50 S.
Solar shield contamination on the edge of SSM/T-1 and T-2 SDR data (only on one side of the swath).
Time and procedural constraints and considerations for saving data within the AFGWC operational processing.

A.4. April 21, 1992 Meeting at Phillips Laboratory

Attendees: Vin Falcone, Mike Griffin, Artie Jackson (PL/GPAS), Jim Morrissey, Ron Isaacs and John Pickle

Discussed schedule for the upcoming ER-2 flights on the west coast. Weather support will be from Ames and from PL (Artie Jackson). Instrument integration flight will occur sometime between April 27 and 5 May. The flights occur between 5 and 16 May. Discussed the limitations of the aircraft and flight procedures, e.g. the aircraft is restricted to flying up to 200 miles from land. Requesting special radiosonde releases from Pt. Magoo, Vandenburg AFB and San Nicolas Island. Discussed TRACKSAT results and determined the best flight days were May 5 and 6 in the morning. But we determined other days that were acceptable. Discussed the merits of various flight plans for the ER-2 to fly during the F-11 overpass.

A.5. May 20, 1992 Meeting at NASA/Goddard Flight Center, Greenbelt, MD

Attendees: Vin Falcone and John Pickle

Met with Dr. James Wang (NASA/GODDARD) to review the data collected by the ER-2 during the May 15 and 16 at roughly 00Z along the West Coast. Discussed the data that was going to be given to PL and AER for the comparison with the T-2 data. Since the T-2 data is 28 pixels per swath (+/- 40.5 degrees), Dr. Wang will average the high resolution ER-2 data to appear similar in viewing angle as the T-2 data. Discussed computer capabilities and decided that we should exchange floppy disks to one another.

Also met with Dr. Harvey Melfi (NASA/GODDARD) to discuss the capabilities of the Raman lidar system for measuring water vapor in the lower 10 km of the atmosphere. He presented results and provided a tour of the lidar instrument and data collection/analysis systems.

A.6. June 3, 1992 Meeting at Phillips Laboratory

Attendees: Vincent Falcone, Jim Morrissey, Alan Bussey, Ron Isaacs and John Pickle

Discussed which model do we want to use. We have tested three RT models (RADTRAN, enhanced RADTRAN and the Eyre model). Discussed the strengths and weaknesses of all three models.

A.7. June 25, 1992 Meeting at NASA/GODDARD Flight Center

The trip was made with Vincent Falcone (PL/GPAS), Jim Morrissey (PL/GPAS) and John Pickle (AER). There were two primary objectives: to exchange ER-2 and T-2 data with Dr. Jim Wang (NASA/GODDARD) and to discuss possible flight patterns of the ER-2 for the upcoming East Coast flights out of Wallops Island with Jim Wang and Dr. Harvey Melfi (NASA/GODDARD).

Provided Jim Wang with diskettes of data to Jim Wang that contained the data from the 15 and 16th of May at 00Z. This corresponds to the time of the ER-2 flights. The T-2 SDRs bounded by 40-25 N and 110-135 W, the global network of radiosondes, the special radiosonde releases from San Nicolas and Point Magoo, and service-A and synoptic surface observations for the California stations (data was recovered from the AIMS system) were provided. Besides the diskettes, two graphics of the T-2 orbits at 00Z on both days were provided as were programs used to create and manipulate the data. Also, we copied the T-2 data description sheets that were given to us by Bruce Thomas of Aerospace.

Jim Wang gave the CALVAL group 10 diskettes of ER-2 West Coast data (90; 150; 183 +/- 1, 3, 7; and 220 GHz). He has smoothed the data to be more compatible with the T-2 data. He has provided 32 values for each swath ranging from +/- 48 degrees (the T-2 data ranges from +/- 40.5 degrees with 28 positions) were each value has been averaged over 3 degrees (+/- 1.5 degrees) along the swath, not along the aircraft line of flight. Jim Wang also gave us four mag tapes of the cloud cover along both day's flight paths.

Meeting with Jim Wang and Harvey Melfi, we discussed what instrumentation will be available during the mid- to late July east coast ER-2 flights. Harvey Melfi will set up his Raman lidar to examine a 2-dimensional sector of the atmosphere's moisture. In addition, there will be a wind profiler available as well as special radiosondes that will be released every 3 hours during a twelve hour period. These radiosondes will carry three raobs - one Vaisala, one VIZ and one AIR. This will allow a comparison of the strengths and weaknesses of the three raobs in measuring water vapor. We would like the raobs released at an hour and a half before and after the F-11 overpass (so we would end up with soundings -3, -1.5, 0, +1.5 and +3.0 hours of the T-2 data). There was agreement that the ER-2 should spend at least an hour flying an east-west track over Wallops Island, where most of the land-based instrumentation is located. Possible flight paths were discussed.

A.8 October 7, 1992 Meeting at Phillips Laboratory

Attendees: Capt. Mike Lapointe, Don Boucher, Vin Falcone, Mike Griffin and John Pickle

First, reviewed text of Phase 1 Final Report on the CALVAL work. Also reviewed Don Boucher's T-2 imagery comparison to HIRAS fields and his computerized T-2 imagery of Hurricane Andrew. Discussed what weaknesses of the calibration effort:
Only mid-latitude scenarios for calibration - really need to have some calibration flights in the tropics during the TOGA-COARE project in Jan.-Feb., 1993.
Have not examined calibration of the "wings" of the T-2 subtrack (between 40.5 and 28.5 degrees).
Better weather analysis/comparison on the calibration efforts.
Possibly average the MIR scan line along the flight track (since the MIR is only averaged along the scan line).
Need to study high altitude moisture in the Eyre model.

Curious about 183 GHz channels MIR - T-2 difference over land (Mt. Whitney region in particular).

A.9. November 10, 1993 Meeting at Phillips Laboratory

Attendees: Capt. Mike LaPointe, Ron Isaacs, Vin Falcone, Jim Morrissey and John Pickle

Reviewed calibration results as well as discussed the pros and cons of physical retrievals and D-matrix retrievals. Discussed AER's latest RT work.

A.10. November 13, 1992 Meeting at NOAA/NESDIS, Washington D.C.

Attendees: Capt. Mike LaPointe, Vin Falcone (speaker), Don Boucher (speaker), Mike Griffin, Jim Morrissey, Bruce Thomas and John Pickle

Capt. Mike LaPointe's opening comments at the meeting discussed future work, which included physical retrievals.

Don Boucher's talk: Suggested strongly that the 150 GHz is not modeled correctly - one possible reason is that dimers may be contributing unknown effects. And if the 150 GHz channel was not modeled correctly, then Aerojet could not produce an adequate D-matrix. He stated that there are differences between 6.7 and 183 GHz - like multiple scattering and ice clouds. He stressed the question, what are you seeing with 183 GHz? A question brought out was that although there was no spatial difference in the validation results, there was no test for temporal effects. A comment from the audience was that the overall RMS for relative humidity were quite low compared to the retrievals for AMSU. Also, Boucher discussed T-2 EDR imagery data and its possible uses. Stated in talk and agreed by the audience that specific humidity should be used and not relative humidity since RH needs temperature retrievals from SSM/T-1. As for cloud determination, it was pointed out that visible OLS imagery is not useful since the F-11 is flying the terminator. It was brought up that the Geophysics Directorate will pursue a cloud flag over land using TACNEPH technology.

Afternoon discussions about radiosondes: Paul Julian provided a discussion of NMC's radiosonde QC (hydrostatic check, buddy checks, forecast background checks and corrections using Schmidlin's 3 thermistor test which checks sonde type and solar elevation angle - there really isn't a good QC for the moisture measurements). China and the new Soviet states also appear to radiosonde QC problems. Dian Gaffen stated that above 500 hPa, moisture measurements are very suspect at best for climatology studies. Note that the 183 +/- 1 GHz channel's weighting functions consistently peak at pressures below 500 hPa. Don Boucher's ship data has a bimodal distribution: one where the ship radiosondes and EDRs agree quite well, the second where they are very different. Ship identification, which would have allowed tracking of each ship's performance, were not saved.

A.11. March 4, 1993 Meeting at Phillips Laboratory

Attendees: Vin Falcone, Mike Griffin, Ron Isaacs and John Pickle

Discussed the statistical variance of the global radiosonde data and how that related to the validation results. Basically, the variance of the radiosonde's relative humidity data was less than or equal to the D-matrix retrieval results of the T-2 validation study. This radiosonde

data set is similar but not exactly the same as that used by Aerospace; although the data came from the same radiosonde database collected by Aerospace for the CALVAL study.

In review of the statistical analysis computer code developed by the calibration group, the following restrictions were applied to the radiosonde database:

> Eliminated radiosondes when the pressure difference between successive reported levels was greater than 150 hPa; when less than 3 reported temperature observations; when no dewpoint depression observations; when dewpoint depressions of 0 K at levels below non-zero dewpoint depression data; and when a dewpoint depression of greater than or equal to 30 K.
>
> Suggestions were to calculate specific humidity, change the units of mixing ratio to [gm/kg], separate cases of saturation for unsaturated profiles, modify some of the elimination rules (for example, do not discard profiles with dewpoint depressions greater than or equal to 30 K, just terminate the profile at that level), and separate cases by instrument (VIZ for the United States and Canada and Vaisala for European stations).

Discussed how to assess the uncertainty of the T-2 SDRs to theoretical accuracy limits in the retrieved moisture values. In a sense, use what we have determined from the calibration study (that the instrument noise is 1 to 2 K) to provide limits of possible retrieved accuracy. This assumes that we can model the forward RT problem for clear sky cases accurately with either the Eyre code or Enhanced RADTRAN.

The Eyre code will be modified to use two different radiosonde modification schemes (one based on constant relative humidity and/or specific humidity modification with height and the second based on increasing modification to either the relative humidity and/or specific humidity with height based on Morrissey and Broussaides' work) to iteratively determine how much the radiosonde profiles must be modified to produce a 1 K and 2 K change in each of the 5 calculated T-2 brightness temperatures.

Incorporate code that will iteratively calculate the surface emissivity for each sounding.

Will not use any radiosonde that does not have measured moisture below 300 hPa; that has a dewpoint depression of less than or equal to 30 K; with a difference in pressure between successive reported levels was greater than 150 hPa; with less than 3 reported temperature observations or no dewpoint depression observations; and with dewpoint depressions of 0 K at levels below non-zero dewpoint depression data.

Will not iteratively modify the upper-air climatology required by the Eyre model.

Will compare the results with the statistics of the radiosonde database to determine if the data base currently collected is adequate for validation of the T-2 data.

Briefly discussed the calibration effort using the data collected during TOGA-COARE; one aspect being the high angle incidence study of the sensor.

Appendix B - Papers Presented

Falcone, V. J., M. K. Griffin, J. D. Pickle, R. G. Isaacs, and J. Wang, 1994, SSM/T-2 Brightness Temperature Signatures, International Symposium on Spectral Sensing Research '94 Proceedings, Dual Use Technologies, San Diego, CA.

Falcone, V. J., M. K. Griffin, J. D. Pickle, and R. G. Isaacs, 1994, SSM/T-2 Calibration Results, AMS 7th Conference on Satellite Meteorology and Oceanography Proceedings, Monterey, CA.

Falcone, V. J., M. K. Griffin, R. G. Isaacs, J. D. Pickle, J. F. Morrissey, A. Bussey, R. Kakar, J. Wang, and P. Racette, 1993, SSM/T-2 Calibration Data Analysis, IEEE proceedings, Combined Optical-Microwave Earth and Atmosphere Sensing Conference, Albuquerque, NM.

Falcone, V. J., M. K. Griffin, R. G. Isaacs, J. D. Pickle, J. F. Morrissey, A. J. Jackson, A. Bussey, R. Kakar, J. Wang, P. Racette, D. J. Boucher, B. H. Thomas, and A. M. Kishi, 1992, SSM/T-2 Calibration and Validation Data Analysis. *PL-TR-92-2293*, Hanscom AFB, MA, 432 pp., ADA265817.

Falcone, V. J., M. K. Griffin, R. G. Isaacs, J. D. Pickle, J. F. Morrissey, A. J. Jackson, A. Bussey, E. O. LeFebvre, R. Kakar, J. Wang, and P. Racette, 1992, SSM/T-2 Calibration West Coast Aircraft Preliminary Data Analysis, Phillips Laboratory Technical Report, Millimeter Wave Moisture Sounder (SSM/T-2) Calibration/Validation Program. Phillips Laboratory, Hanscom AFB, MA 01731.

Felde, G. W. and J. D. Pickle, 1994, Microwave Earth Surface Emissivities at 91 and 150 GHz, AMS 8th Conference on Atmospheric Radiation Proceedings, Nashville, TN.

Felde, G. W. and J. D. Pickle, 1995, Retrieval of 91 and 150 GHz Earth Surface Emissivities, Journal of Geophysical Research, v. 199, no. D10, p. 20855-20866.

Glass, M., M. K. Griffin, G. W. Felde, and J. D. Pickle, 1993, Comparison of SSM/T-2 and SSM/I Estimates of Total Precipitable Water, SPIE Proceedings, vol. 1935, Orlando, FL.

Griffin, M. K., V. J. Falcone, J. D. Pickle, 1996, Remote Sensing at High Frequencies in the Microwave, submitted to International Radiation Symposium, "Current Problems in Atmospheric Radiation", 19-24 August, 1996, Fairbanks, Alaska.

Griffin, M. K., and J. D. Pickle, 1996, Upper Tropospheric Humidity From SSM/T-2 Measurements, AMS Proceedings, Eighth Conference on Satellite Meteorology and Oceanography, Jan 28-Feb 2, 1996, Atlanta, GA, p. 10-14.

Griffin, M. K, V. J. Falcone, J. D. Pickle, R. G. Isaacs, 1995, SSM/T-2 Measurements: A Descriptive Overview, SPIE Proceedings, Synthetic Aperture Radar and Passive Microwave Sensing, Volume 2584, 25-28 September, 1995, Paris, France, p. 404-414.

Griffin, M. K., V. J. Falcone, J. D. Pickle, and R. G. Isaacs, 1994, SSM/T-2 Measurement Accuracy and Sensitivity to Atmospheric Moisture, submitted to AGU Chapman Conference, Water Vapor in the Climate System, Jekyll Island, GA.

Griffin, M. K., V. J. Falcone, J. D. Pickle, R. G. Isaacs, and J. Wang, 1994, Sensitivity of SSM/T-2 Channels to Water Vapor, International Symposium on Spectral Sensing Research '94 Proceedings, Dual Use Technologies, San Diego, CA.

Griffin, M. K., V. J. Falcone, J. D. Pickle, and R. G. Isaacs, 1994, SSM/T-2 Brightness Temperature Signatures, AMS 7th Conference on Satellite Meteorology and Oceanography Proceedings, Monterey, CA.

Griffin, M. K., V. J. Falcone, J. F. Morrissey, R.G. Isaacs, J. D. Pickle, R. Kakar, J. Wang, P. Racette, 1993, The Special Sensor Microwave Water Vapor Sounder (SSM/T-2): Calibration Study, AMS 8th Symposium on Meteorological Observations and Instrumentation Proceedings, Anaheim, CA.

Griffin, M.K., V.J. Falcone, J.D. Pickle, R.G. Isaacs, 1994, SSM/T-2 Accuracy and Sensitivity to Atmospheric Moisture, AGU Chapman Conference on Water Vapor in the Climate System Proceedings, Jekyll Island Georgia, October 25-28, 1994.

Morrissey, J. F., J. D. Pickle, and V. J. Falcone, 1993, Effects of Radiosonde Type on Satellite Derived Humidities, IEEE Proceedings, Combined Optical-Microwave Earth and Atmosphere Sensing Conference, Albuquerque, NM.

Pickle, J. D. R. G. Isaacs, V. Jakabhazy, M. K. Griffin, and V. J. Falcone, 1996, Detection of Precipitation using SSM/T-2 Measurements, AMS Proceedings, Eighth Conference on Satellite Meteorology and Oceanography, Jan. 28-Feb. 2, 1996, Atlanta, GA, p. 238-242.

Pickle, J. D. R. G. Isaacs, V. Jakabhazy, M. K. Griffin, and V. J. Falcone, 1995, Effects of Precipitation on SSM/T-2 Brightness Temperatures, SPIE Proceedings, Synthetic Aperture Radar and Passive Microwave Sensing, Volume 2584, 25-28 September, 1995, Paris, France, p. 415-425.

Pickle, J. D., R. G. Isaacs, V. J. Falcone, and M. K. Griffin, 1994, Sensitivity of SSM/T-2 Channels to Atmospheric and Surface Parameters, International Symposium on Spectral Sensing Research '94 Proceedings, Dual Use Technologies, San Diego, CA.

Pickle, J. D., R. G. Isaacs, V. J. Falcone, and M. K. Griffin, 1994, Sensitivity of SSM/T-2 Channels to Water Vapor, AMS 7th Conference on Satellite Meteorology and Oceanography Proceedings, Monterey, CA.

Pickle, J. D., R. G. Isaacs, M. K. Griffin, V. J. Falcone, J. F. Morrissey, R. Kakar, and J. R. Wang, 1993, Comparison of Co-located SSM/T-2 and MIR measurements; Results from the Calibration study. SPIE Proceedings, vol. 1935, Orlando, FL.